The bile-drug-excipient interplay

Dissertation zur Erlangung des naturwissenschaftlichen Doktorgrades der

Julius-Maximilians-Universität Würzburg

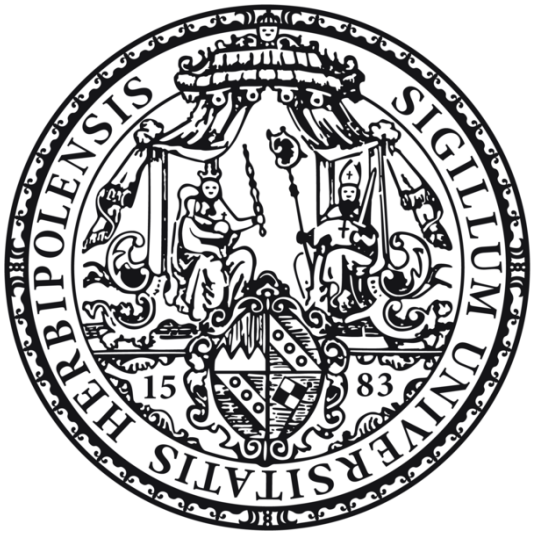

vorgelegt von

Jonas Schlauersbach

aus Nürnberg

Würzburg 2022

Eingereicht bei der Fakultät für Chemie und Pharmazie am

_____

Gutachter der schriftlichen Arbeit

1. Gutachter: _____

2. Gutachter: _____

Prüfer des öffentlichen Promotionskolloquiums

1. Prüfer: _____

2. Prüfer: _____

3. Prüfer: _____

Datum des öffentlichen Promotionskolloquiums

_____

Doktorurkunde ausgehändigt am

_____

Die vorliegende Arbeit wurde in der Zeit von Juni 2018 bis April 2022 am Institut für Pharmazie und Lebensmittelchemie der Bayerischen Julius-Maximilians-Universität Würzburg unter der Anleitung von Herrn Prof. Dr. Dr. Lorenz Meinel angefertigt.

Εί γαρ και τα μάλιστα τύχοι τετελεσμένον ειπών,
αυτός όμως ουκ οίδε· δόκος δ' έπί πάσι τέτυκται.

For even if one speaks the most perfect by pure chance, nevertheless he himself will not be aware of it. The assumption veils everything.
Xenophanes of Colophon c. 570- c. 470 BC

Table of contents

Summary 1

Zusammenfassung 5

Introduction 9

Chapter I: Predicting bile and lipid interaction for drug substances 27

Chapter II: Leveraging bile solubilization of poorly water-soluble drugs by rational polymer selection 69

Chapter III: Bile and excipient interactions directing drug pharmacokinetics in rats 137

Chapter IV: Harnessing bile for drug absorption through rational excipient selection 147

Appendix: Step by step guide for excipient screening with simulated intestinal fluids for drug substances 189

Conclusion and outlook 215

Abbreviations 222

Publications 225

Acknowledgements 227

Documentation of authorship 228

Summary

The bile system in vertebrates is an evolutionary conserved endogenous solubilization system for hydrophobic fats and poorly water-soluble vitamins.[1] Bile pours out from the gallbladder through the common bile duct into the duodenum triggered by cholecystokinin. Cholecystokinin is released from enteroendocrine cells after food intake. The small intestine is also the absorption site of many orally administered drugs. Most emerging drug candidates belong to the class of **p**oorly **w**ater-**s**oluble **d**rugs (**PWSDs**).[2, 3] Like hydrophobic vitamins, these PWSDs might as well be solubilized by bile.[4] Therefore, this natural system is of high interest for drug formulation strategies.[5] Simulated intestinal fluids containing bile salts (e.g., **t**auro**c**holate **TC**) and phospholipids (e.g., **l**ecithin **L**) have been widely applied over the last decade to approximate the behavior of PWSDs in the intestine.[6] Solubilization by bile can enhance the oral absorption of PWSDs being at least in part responsible for the positive "food effect".[7] The dissolution rate of PWSDs can be also enhanced by the presence of bile.[8] Furthermore, some PWSDs profit from supersaturation stabilization by bile salts.[9] Some excipients solubilizing PWSDs seemed to be promising candidates for drug formulation when investigated *in vitro* without bile.[10] When tested *in vivo*, these excipients reduced the bioavailability of drugs. However, these observations have been hardly examined on a molecular level and general links between bile interaction *in vitro* and bioavailability are still missing.

This thesis investigated the interplay of bile, PWSDs, and excipients on a molecular level, providing formulation scientists a blueprint for rational formulation design taking bile/PWSD/excipient/ interaction into account. The first chapter focus on an *in silico* ^{1}H **n**uclear **m**agnetic **r**esonance (**NMR**) spectroscopy-based algorithm for bile/drug interaction prediction. Chapter II to IV report the impact of excipients on bioavailability of PWSDs interacting with bile. At last, we summarized helpful *in vitro* methods for drug formulation excipient choice harnessing biopharmaceutic solubilization in chapter V.

Chapter I applies ^{1}H NMR studies with bile and drugs on a large scale for quantitative structure-property relationship analysis. 141 drugs were tested in simulated intestinal media by ^{1}H NMR. Drug aryl-proton signal shifts were correlated to *in silico* calculated molecular 2D descriptors. The probability of a drug interacting with bile was dependent on its polarizability and lipophilicity, whereas interaction with lipids in simulated intestinal media

components was dependent on molecular symmetry, lipophilicity, hydrogen bond acceptor capability, and aromaticity. The probability of a drug to interact with bile was predictive for a positive food effect. This algorithm might help in the future to identify a bile and lipid interacting drug *a priori*.

Chapter II investigates the impact of excipients on bile and free drug fraction. Three different interaction patterns for excipients were observed. The first pattern defined excipients that interacted with bile and irreversibly bound bile. Therefore, the free drug fraction of bile interacting drugs increased. The second pattern categorized excipients that formed new colloidal entities with bile which had a high affinity to bile interacting drugs. These colloids trapped the drug and decreased the free drug fraction. The last excipient pattern described excipients that formed supramolecular structures in coexistence with bile and had no impact on the free drug fraction. These effects were only observed for drugs interacting with bile (Perphenazine and Imatinib). Metoprolol's free drug fraction, a compound not interacting with bile, was unaffected by bile or bile/excipient interaction. We hypothesized that bile/excipient interactions may reduce the bioavailability of bile interacting drugs.

Chapter III addresses the hypothesis from chapter II. A pharmacokinetic study in rats revealed that the absorption of Perphenazine was reduced by bile interacting excipients due to bile/excipient interaction. The simultaneous administration of excipient patterns I and II did not further reduce or enhance Perphenazine absorption. Conversely, the absorption of Metoprolol was not impacted by excipients. This reinforced the hypothesis, that drugs interacting with bile should not be formulated with excipients also interacting with bile.

Chapter IV further elaborates which *in vitro* methods using simulated intestinal fluids are predictive for a drug's pharmacokinetic profile. The PWSD Naporafenib was analyzed *in vitro* with simulated intestinal fluids and in presence of excipients regarding solubility, supersaturation, and free drug fraction. Naporafenib showed a strong interaction with TC/L from simulated bile. Assays with TC/L, but not without identified one excipient as possibly bioavailability reducing, one as supersaturation destabilizing, and the last as bile not interacting and supersaturation stabilizing excipient. A pharmacokinetic study in beagle dogs outlined and confirmed the *in vitro* predictions.

The **Appendix** summarizes *in vivo* predictive methods as presented in chapter I to IV and rationalizes experimental design paving the way towards a biopharmaceutic excipient screening. The first presented preliminary decision tree is transformed into a step-by-step instruction. The presented decision matrix might serve as a blueprint for processes in early phase drug formulation development.

In summary, this thesis describes how a drug can be defined as bile interacting or non-interacting and gives a guide as well how to rate the impact of excipients on bile. We showed in two *in vivo* studies that bile/excipient interaction reduced the bioavailability of bile interacting drugs, while bile non-interacting drugs were not affected. We pointed out that the bile solubilization system must be incorporated during drug formulation design. Simulated gastrointestinal fluids offer a well-established platform studying the fate of drugs and excipients *in vivo*. Therefore, rational implementation of biopharmaceutic drug and excipient screening steers towards efficacy of oral PWSD formulation design.

References

1. Monte, M. J.; Marin, J. J.; Antelo, A.; Vazquez-Tato, J., Bile acids: chemistry, physiology, and pathophysiology. *World J. Gastroenterol.* **2009,** *15* (7), 804-16.
2. Lipinski, C., Poor aqueous solubility—an industry wide problem in drug discovery. *Am. Pharm. Rev.* **2002,** *5* (3), 82-85.
3. Waring, M. J.; Arrowsmith, J.; Leach, A. R.; Leeson, P. D.; Mandrell, S.; Owen, R. M.; Pairaudeau, G.; Pennie, W. D.; Pickett, S. D.; Wang, J.; Wallace, O.; Weir, A., An analysis of the attrition of drug candidates from four major pharmaceutical companies. *Nat. Rev. Drug Discovery* **2015,** *14* (7), 475-86.
4. Sun, F.; Jaspers, T. C.; van Hasselt, P. M.; Hennink, W. E.; van Nostrum, C. F., A Mixed Micelle Formulation for Oral Delivery of Vitamin K. *Pharm. Res.* **2016,** *33* (9), 2168-79.
5. Sugano, K.; Kataoka, M.; Mathews Cda, C.; Yamashita, S., Prediction of food effect by bile micelles on oral drug absorption considering free fraction in intestinal fluid. *Eur. J. Pharm. Sci.* **2010,** *40* (2), 118-24.
6. Riethorst, D.; Mols, R.; Duchateau, G.; Tack, J.; Brouwers, J.; Augustijns, P., Characterization of Human Duodenal Fluids in Fasted and Fed State Conditions. *J. Pharm. Sci.* **2016,** *105* (2), 673-681.
7. Kawai, Y.; Fujii, Y.; Tabata, F.; Ito, J.; Metsugi, Y.; Kameda, A.; Akimoto, K.; Takahashi, M., Profiling and Trend Analysis of Food Effects on Oral Drug Absorption Considering Micelle Interaction and Solubilization by Bile Micelles. *Drug Metab. Pharmacokinet.* **2011,** *26* (2), 180-191.
8. Sugano, K.; Okazaki, A.; Sugimoto, S.; Tavornvipas, S.; Omura, A.; Mano, T., Solubility and dissolution profile assessment in drug discovery. *Drug Metab. Pharmacokinet.* **2007,** *22* (4), 225-54.
9. Indulkar, A. S.; Gao, Y.; Raina, S. A.; Zhang, G. G. Z.; Taylor, L. S., Crystallization from Supersaturated Solutions: Role of Lecithin and Composite Simulated Intestinal Fluid. *Pharm. Res.* **2018,** *35* (8), 158.

10. Saal, W.; Wyttenbach, N.; Alsenz, J.; Kuentz, M., Interactions of dimethylaminoethyl methacrylate copolymer with non-acidic drugs demonstrated high solubilization in vitro and pronounced sustained release in vivo. *Eur. J. Pharm. Biopharm.* **2018,** *125*, 68-75.

Zusammenfassung

Das Gallensystem in Wirbeltieren ist ein evolutionär konserviertes endogenes Solubilisierungssystem für hydrophobe Fette und schwer wasserlösliche Vitamine.[1] Ausgelöst durch Cholecystokinin wird Galle aus der Gallenblase durch den Hauptgallengang in den Zwölffingerdarm ausgeschüttet. Cholecystokinin wird zum Beispiel nach der Nahrungsaufnahme aus enteroendokrinen Zellen freigesetzt. Der Dünndarm ist auch der Ort, an dem viele oral verabreichte Arzneimittel aufgenommen werden. Die meisten neuen Arzneimittelkandidaten gehören zur Klasse der schlecht wasserlöslichen Arzneimittel (poorly water-soluble drugs: PWSDs).[2, 3] Galle kann auch wie bei hydrophoben Vitaminen die Löslichkeit von PWSDs verbessern.[4] Daher ist dieses natürliche System von großem Interesse für Arzneimittelformulierungsstrategien.[5] Simulierte Darmflüssigkeiten, die Gallensalze (z.B. **T**auro**c**holat **TC**) und Phospholipide (**L**ecithin **L**) enthalten, wurden in den letzten Jahren häufig verwendet, um das Verhalten von PWSDs im Darm zu simulieren.[6] Die Löslichkeitsverbesserung durch Galle kann die orale Absorption von PWSDs erhöhen, was ein möglicher Grund für den sogenannten positiven "Nahrungsmitteleffekt" darstellt.[7] Auch die Auflösungsgeschwindigkeit von PWSD kann durch die Anwesenheit von Galle verbessert werden.[8] Darüber hinaus profitieren einige PWSDs von der Stabilisierung der Übersättigung durch Gallensalze.[9] Einige Hilfsstoffe, die die Löslichkeit von PWSDs stark erhöhten, schienen vielversprechende Kandidaten für die Arzneimittelformulierung zu sein, wenn sie *in vitro* ohne Galle untersucht wurden.[10] *In vivo* getestet, verringerten diese Hilfsstoffe jedoch die Bioverfügbarkeit. Diese Beobachtungen wurden bisher kaum auf molekularer Ebene untersucht, und allgemeine Zusammenhänge zwischen der Interaktion mit der Galle *in vitro* und der Bioverfügbarkeit fehlen bisher.

In dieser Arbeit wurde das Zusammenspiel von PWSD, Hilfsstoffen und Galle auf molekularer Ebene untersucht, um Formulierungswissenschaftlern einen Entwurf für ein rationales Formulierungsdesign zu liefern, das die Wechselwirkung zwischen PWSD, Hilfsstoffen und Galle berücksichtigt. Das erste Kapitel befasst sich mit einem auf ^{1}H-Kernspinresonanzspektroskopie (^{1}H **NMR**) basierenden *in-silico*-Algorithmus zur Vorhersage von Wechselwirkungen zwischen Galle und Arzneimittel. Die Kapitel II bis IV zeigen die Auswirkungen von Hilfsstoffen auf die Bioverfügbarkeit von PWSDs, die mit der Galle interagieren. Schließlich haben wir in Kapitel V hilfreiche *in-vitro*-Methoden für die

Auswahl von Hilfsstoffen in Arzneimittelformulierungen zusammengefasst, die die biopharmazeutische Solubilisierung nutzen.

In **Kapitel I** werden ^{1}H-NMR-Studien mit Galle und Arzneimitteln in großem Maßstab zur quantitativen Analyse der Struktur-Eigenschafts-Beziehung durchgeführt. 141 Arzneimittel wurden in simulierten Darmmedien mittels ^{1}H-NMR untersucht. Die Aryl-Proton-Signalverschiebungen der Arzneimittel wurden mit *in silico* berechneten molekularen Deskriptoren korreliert. Die Wahrscheinlichkeit, dass ein Arzneimittel mit Galle interagiert, hing von seiner Polarisierbarkeit und Lipophilie ab, während die Interaktion mit Lipiden in simulierten Darmmedienkomponenten von der molekularen Symmetrie, Lipophilie, der Fähigkeit Wasserstoffbrückenbindungen einzugehen, und der Aromatizität abhing. Die Wahrscheinlichkeit, dass ein Arzneimittel mit Galle interagiert, war prädiktiv für einen positiven Nahrungsmitteleffekt. Dieser Algorithmus könnte in Zukunft dabei helfen, ein mit Galle und Lipiden interagierendes Arzneimittel *a priori* zu identifizieren.

In **Kapitel II** wird der Einfluss von Hilfsstoffen auf die Galle und den Anteil des freien Arzneimittels untersucht. Es wurden drei verschiedene Interaktionsmuster für Hilfsstoffe beobachtet. Das erste Muster interagiert mit der Galle und bindet die Galle irreversibel. Dadurch erhöhte sich der Anteil des freien Wirkstoffs. Das zweite Muster von Hilfsstoffen bildete mit der Galle neue kolloidale Strukturen, die eine hohe Affinität zum Arzneimittel hatten. Diese Kolloide schlossen den Wirkstoff ein und verringerten den Anteil des freien Wirkstoffs. Das letzte Hilfsstoffmuster bildete supramolekulare Strukturen in Koexistenz mit der Galle und hatte keinen Einfluss auf den Anteil des freien Arzneistoffes. Diese Auswirkungen wurden nur bei Arzneimitteln beobachtet, die mit der Galle interagieren (Perphenazin und Imatinib). Der Anteil des freien Wirkstoffs Metoprolol, der nicht mit der Galle interagiert, wurde durch die Interaktion von Galle oder Galle/Hilfsstoff nicht beeinflusst. Wir stellten die Hypothese auf, dass Wechselwirkungen zwischen Galle und Hilfsstoffen die Bioverfügbarkeit von Arzneimitteln, die mit der Galle interagieren, verringern können.

Kapitel III befasst sich mit der Hypothese aus Kapitel II. Eine pharmakokinetische Studie an Ratten ergab, dass die Absorption von Perphenazin durch mit der Galle interagierende Hilfsstoffe aufgrund einer Wechselwirkung zwischen Galle und Hilfsstoff verringert wurde. Die gleichzeitige Verabreichung der Hilfsstoffmuster I und II führte nicht zu einer weiteren Verringerung oder Erhöhung der Perphenazin-Resorption. Umgekehrt wurde die Absorption

von Metoprolol durch die Hilfsstoffe nicht beeinträchtigt. Dies bestätigt die Hypothese, dass Arzneimittel, die mit Galle interagieren, nicht mit Hilfsstoffen formuliert werden sollten, die ebenfalls mit Galle interagieren.

In **Kapitel IV** wird näher erläutert, welche *in-vitro*-Methoden für das pharmakokinetische Profil eines Arzneimittels aussagekräftig sind. Das PWSD Naporafenib wurde *in vitro* mit simulierten Darmflüssigkeiten und in Gegenwart von Hilfsstoffen hinsichtlich Löslichkeit, Übersättigung und freiem Wirkstoffanteil analysiert. Naporafenib zeigte eine starke Wechselwirkung mit TC/L aus simulierter Galle. Bei Untersuchungen mit TC/L, aber nicht ohne TC/L, wurde ein Hilfsstoff als möglicherweise bioverfügbarkeitsvermindernd, ein Hilfsstoff als die Übersättigung destabilisierend und der letzte als nicht mit der Galle interagierender und die Übersättigung stabilisierender Hilfsstoff identifiziert. In einer pharmakokinetischen Studie an Beagle-Hunden wurden die *in-vitro*-Vorhersagen bestätigt.

Der **Anhang** fasst die in den Kapiteln I bis IV vorgestellten *in-vivo*-Vorhersagemethoden zusammen und rationalisiert die Versuchsplanung, die den Weg für ein biopharmazeutisches Hilfsstoffscreening ebnet. Der vorgestellte vorläufige Entscheidungsbaum wird in eine Schritt-für-Schritt-Anleitung umgewandelt. Die vorgestellte Entscheidungsmatrix soll in den Prozess der frühen Phase der Entwicklung von Arzneimittelformulierungen implementiert werden können.

Zusammenfassend wird in dieser Arbeit beschrieben, wie ein Arzneimittel als Galle interagierend oder nicht interagierend definiert werden kann, und es wird ein Leitfaden für die Bewertung der Auswirkungen von Hilfsstoffen auf Galle gegeben. Wir haben in zwei In-vivo-Studien gezeigt, dass die Interaktion zwischen Galle und Hilfsstoff die Bioverfügbarkeit von Arzneistoffen, die mit der Galle interagieren, verringert, während Arzneistoffe, die nicht mit der Galle interagieren, davon nicht betroffen waren. Wir wiesen darauf hin, dass das Solubilisierungssystem der Galle bei der Entwicklung von Arzneimittelformulierungen berücksichtigt werden muss. Simulierte gastrointestinale Flüssigkeiten bieten eine gut etablierte Plattform zur Untersuchung von Arzneistoffen und Hilfsstoffen *in vivo*. Die rationelle Umsetzung des biopharmazeutischen Screenings von Arzneimitteln und Hilfsstoffen führt daher zu einem wirksamen Formulierungsdesign von oralen, schwer wasserlöslichen Arzneistoffen.

Referenzen

1. Monte, M. J.; Marin, J. J.; Antelo, A.; Vazquez-Tato, J., Bile acids: chemistry, physiology, and pathophysiology. *World J. Gastroenterol.* **2009,** *15* (7), 804-16.
2. Lipinski, C., Poor aqueous solubility—an industry wide problem in drug discovery. *Am. Pharm. Rev.* **2002,** *5* (3), 82-85.
3. Waring, M. J.; Arrowsmith, J.; Leach, A. R.; Leeson, P. D.; Mandrell, S.; Owen, R. M.; Pairaudeau, G.; Pennie, W. D.; Pickett, S. D.; Wang, J.; Wallace, O.; Weir, A., An analysis of the attrition of drug candidates from four major pharmaceutical companies. *Nat. Rev. Drug Discovery* **2015,** *14* (7), 475-86.
4. Sun, F.; Jaspers, T. C.; van Hasselt, P. M.; Hennink, W. E.; van Nostrum, C. F., A Mixed Micelle Formulation for Oral Delivery of Vitamin K. *Pharm. Res.* **2016,** *33* (9), 2168-79.
5. Sugano, K.; Kataoka, M.; Mathews Cda, C.; Yamashita, S., Prediction of food effect by bile micelles on oral drug absorption considering free fraction in intestinal fluid. *Eur. J. Pharm. Sci.* **2010,** *40* (2), 118-24.
6. Riethorst, D.; Mols, R.; Duchateau, G.; Tack, J.; Brouwers, J.; Augustijns, P., Characterization of Human Duodenal Fluids in Fasted and Fed State Conditions. *J. Pharm. Sci.* **2016,** *105* (2), 673-681.
7. Kawai, Y.; Fujii, Y.; Tabata, F.; Ito, J.; Metsugi, Y.; Kameda, A.; Akimoto, K.; Takahashi, M., Profiling and Trend Analysis of Food Effects on Oral Drug Absorption Considering Micelle Interaction and Solubilization by Bile Micelles. *Drug Metab. Pharmacokinet.* **2011,** *26* (2), 180-191.
8. Sugano, K.; Okazaki, A.; Sugimoto, S.; Tavornvipas, S.; Omura, A.; Mano, T., Solubility and dissolution profile assessment in drug discovery. *Drug Metab. Pharmacokinet.* **2007,** *22* (4), 225-54.
9. Indulkar, A. S.; Gao, Y.; Raina, S. A.; Zhang, G. G. Z.; Taylor, L. S., Crystallization from Supersaturated Solutions: Role of Lecithin and Composite Simulated Intestinal Fluid. *Pharm. Res.* **2018,** *35* (8), 158.
10. Saal, W.; Wyttenbach, N.; Alsenz, J.; Kuentz, M., Interactions of dimethylaminoethyl methacrylate copolymer with non-acidic drugs demonstrated high solubilization in vitro and pronounced sustained release in vivo. *Eur. J. Pharm. Biopharm.* **2018,** *125*, 68-75.

Introduction

Early phase drug formulation development

Nowadays, up to 75% of drug candidates in development belong to the class of **p**oorly-**w**ater-**s**oluble **d**rug**s** (**PWSDs**).[1-4] The reasons for this trend are multi-faceted, e.g., recent advances in synthetic chemistry,[5] more complex high-throughput biological screening assays,[6] and challenging biologic target structures including lipophilic and sterically demanding binding pockets.[7] All these factors created the phenomenon of "molecular obesity" identifying hydrophobic molecules with a high molecular weight and subsequent poor water-solubility as potential drug candidates.[8] The rule of five, defined by Lipinski et al., set up a theoretical design space for the developability of a drug in terms of lipophilicity, molecular weight, and hydrogen bond acceptor/donator moieties.[9] Small, but quite lipophilic molecules are better absorbed compared to big hydrophilic or nonpolar drugs. Furthermore, in case of "obese" molecules it was postulated that drugs with a molecular weight greater than 400 Dalton and/or a clog *P* value greater than 4 are more probable to result in poor pharmacokinetic profiles with low drug bioavailability.[10] Recent research modeling the quantitative structure-property relationship using 2D molecular descriptors found that a high clog P value, which correlates with lipophilicity, was more detrimental to developability than a high molecular weight.[5] However, this trend in drug development requires an expansion of its "space" and efficient methods to address the challenges associated with "molecular obesity". The oral route of drug administration in the form of solid dosage forms is the most common and popular, as administration is simple and solid dosage forms have a better shelf life compared to, for example, solutions.[11] The formulation development of PWSDs is more time and cost intensive, as drug formulation requires various strategies resulting in acceptable pharmacokinetic profiles and bioavailability.[12] Yet, to avoid hit generation of undevelopable drug candidates medicinal chemistry implies "property based design" to provide drug candidates with favorable biologic and chemical properties.[13, 14] Therefore, molecular design by medicinal chemists steers the success for drug development not only by generating high potent drugs, but also by modifying its physical and structural properties prior to formulation development. But chemical modification of a drug molecule by molecular modifications is limited. Afterwards, pharmaceutical technology strategies must be implemented at an early stage of formulation development to guarantee market success of a new drug substance.[15] Moreover, selection of the right PWSD formulation

strategy is not straightforward and requires precise information about a drug's physicochemical properties as well as the desired clinical relevant drug dose.[16] In early phases of drug formulation development, a formulation scientist is basically interested in generating first in animal formulations and to assess physicochemical drug properties which are later relevant for more advanced formulation strategies.[17] Enhancing drug solubility is necessary for first toxicological and pharmacokinetic animal studies. Choosing the right salt form or polymorph of a molecule can on the one hand enhance a drug's dissolution rate, achievable solubility, and on the other hand guarantee dosage form stability.[18, 19] Summarized, before starting considerations about formulation strategies for a PWSD, the most stable and/or soluble salt or polymorph drug form should be chosen for further development.

Thermodynamic drug solubility

As mentioned above, drug water solubility is a critical parameter during drug formulation development. Drugs with a critical water solubility with regard to their desired dosing range are more challenging to be released into market compared to corresponding water-soluble drugs.[20] Traditionally, formulation development aims to improve the thermodynamic solubility of a drug to maximize its absorption.[21] Thermodynamic solubility is defined as the equilibrium drug concentration in the water phase of a solid, crystalline drug form under defined conditions (temperature, pH, buffer composition of water phase).[22] Hereby, drug in its solid form is suspended in water and shaken for at least 24 hours. Then, remaining solid drug is removed by either centrifugation or filtration and the drug concentration in the supernatant is determined. The term "thermodynamic solubility" includes different definitions. The first solubility term is the intrinsic solubility and describes the solubility of a drug in its uncharged form.[23, 24] Intrinsic solubility can be an interesting parameter when comparing different drug candidates, but if the drug is naturally charged at physiological pH values, this parameter may become useless as a predictor of drug absorption. The pH-dependent solubility of drugs is a more valuable information. For neutral drugs, intrinsic and pH-dependent solubility coincide. For basic drugs, solubility at low pH is expected to be higher than for acidic drugs and vice versa. Knowledge of solubility at physiologic relevant pH values is imperative to estimate the importance of solubility for drug absorption.

Amorphous drug solubility

Exceeding thermodynamic solubility of a drug results in supersaturated solutions.[25] In this case, the chemical potential of the solute is higher than the potential of the solute in the supernatant of the most stable crystalline drug form.[26] Therefore, supersaturation is kinetically stabilized, but drugs tend to convert into their most thermodynamically stable form. The higher the supersaturation of the drug, the more likely the drug will precipitate quickly. Intermediate polymorphic or amorphous precipitation is also possible. Amorphous drug forms are thermodynamically unstable, and they will convert to their most stable crystalline form. The occurrence and conversion to the most stable crystalline drug form is dependent on physicochemical drug properties and experimental conditions.[27] Nevertheless, drug amorphization is a good option to increase solubility of drugs beyond their thermodynamic solubility.

Exceeding the maximum supersaturation of a drug results in phase separation. This concentration is defined as amorphous drug solubility. Phase separated drug can appear as an emulsion like phase separation (**l**iquid-**l**iquid **p**hase **s**eparation; **LLPS**) or as an amorphous precipitate (**l**iquid-**g**lass **p**hase **s**eparation; **LGPS**). From a thermodynamic point of view, the amorphous solubility can be described as follows (Eq.1):[28]

$$C_{amorphous} = C_{eq} \cdot e^{-I(a_2)} \cdot e^{\frac{\Delta Gc \rightarrow a}{R \cdot T}} \quad \text{(Eq. 1)}$$

$C_{amorphous}$ is the amorphous solubility of a drug, C_{eq} is the thermodynamic solubility of the crystalline drug form, $\Delta G_{c \rightarrow a}$ describes the free energy difference between the crystal and amorphous form. $-I(a_2)$ resembles the activity of amorphous drug saturated with water. R is the gas constant and T the absolute temperature. Drugs with high a supersaturation ratio (Eq. 2) have a promising potential to show improved bioavailability when applied as a supersaturated formulation.

$$supersaturation\ ratio = \frac{C_{amorphous}}{C_{eq}} \quad \text{(Eq. 2)}$$

From this theoretical perspective, drugs with a high melting point and subsequent larger chemical potential difference between crystalline and amorphous form at physiological relevant temperatures will show a high supersaturation ratio. This high supersaturation ratio leads to higher oral bioavailability of drugs when amorphous solubility is achieved in the

intestine. This has been reported exemplarily for the PWSDs Ritonavir and Telepravir.[29, 30] Nevertheless, the activity of amorphous drug saturated with water might be an important factor to consider. A low activity of drug when saturated with water results in a lower supersaturation ratio. Ideally the drug's activity would be held at the highest possible value (amorphous solubility) until the drug is completely absorbed. Phase separated drug can serve as a "reservoir" for maintaining amorphous drug solubility by replenishing the water phase with drug molecules. This was shown for clotrimazole nanodroplets, where the amorphous solubility remains at its maximum even when significant amount of drug diffuses through membranes.[31] High absolute supersaturation of a drug could be problematic. Highly supersaturated systems tend to fast drug precipitation. Once precipitation of the drug and subsequent conversion of the drug to its most stable form occurs, the supersaturation decreases, and the drug concentration approaches its respective thermodynamic solubility. Some drugs show rapid crystallization and are therefore entitled as "fast crystallizers". For example, 50 drug substances were found to crystallize within 2.5 min after generation of supersaturated solutions in aqueous media by solvent shift technique.[32] Supersaturated drug states with slow crystallization are of particular interest for PWSDs as drug absorption *in vivo* increases.[33] In case of fast crystallizing drugs, crystallization inhibiting excipients might be applied to pharmaceutically harness drug supersaturation.

Pharmaceutical technologies enhancing drug solubility and dissolution rate

The simplest method to maximize a drug's water solubility is to pre-dissolve the PWSD in the formulation. When the formulation is added to water, high drug concentrations or even supersaturated solutions can be achieved, as no drug dissolution is required. This can be achieved by using Co-solvents or surfactants.[34-36] Unfortunately, the use of those is limited due to safety and tolerability as well as unfavorable stability from the technological point of view.[37-39] Therefore, other methods must be applied increasing the dissolution rate of a PWSD. The mathematical basis for solubility-promoting processes in solid dosage forms is the Whitney-Noyes equation with the Nernst-Brunner diffusion model, which describes the dissolution of drugs (Eq. 3).[26]

$$\frac{dM}{dt} = \frac{DA}{h} \cdot (C_{eq} - C) \qquad \text{(Eq. 3)}$$

M describes the amount of dissolved drug, dM/dt resembles the dissolution rate, D is the drug specific diffusion coefficient, A is the surface area, h is the diffusion layer thickness, C_{eq} is the thermodynamic solubility of the crystalline drug form in solution, and C the concentration of drug in solution. The diffusion layer thickness and diffusion coefficient are dedicated to the physiology of the gastrointestinal system and the molecule itself.[40] But a formulation scientist can modify the drug to medium surface area and solubility of the PWSD. The first can be achieved by, e.g., special milling techniques or reducing particle size to the nanoscale.[41, 42] These methods might be applicable for compounds with a poor dissolution rate or bad wetting properties. Solubility enhancement/dissolution rate can furthermore be reached by the addition of solubilizing excipients (surfactants[36, 43], polymers[44-46], cyclodextrins[47-49]), salt formation[22, 50], co-crystallization[51-53], and drug amorphization including **a**morphous **s**olid **d**ispersion**s** (**ASDs**).[54, 55] ASDs are applied to generate supersaturated drug solutions *in situ* and consist of a PWSD molecularly dissolved within a polymer matrix. Some ASDs are now on the market underlining the emerging potency of these systems for PWSD delivery.[56-58] Upon gastrointestinal dissolution of ASDs or other enabling formulation approaches, supersaturated drug solutions are generated *in situ*. Furthermore LLPS/GLPS might occur ideally driving drug absorption. Surfactants and polymers were proven to prevent the agglomeration and coalescence of LLPS nanodroplets.[59] Polymeric excipients can effectively prevent drug crystallization,[55, 60] while surfactants either prevent[61, 62] or promote[47, 63] crystallization in a drug and surfactant specific manner. Another way to generate supersaturated drug solutions *in situ* is to use the natural pH switch from the stomach to the small intestine, which for example leverages the absorption of the PWSD Albendazole.[64] It is a weak base and hence more soluble in the acidic environment of the stomach. When the drug is released into the duodenum having a higher pH, Albendazole supersaturates, which steers the drug's absorption. Thus, beside considerations of PWSD solubility and methods enhancing it, the gastrointestinal system exhibits a tremendous impact on drug absorption and needs to be further elucidated.

The human gastrointestinal system

After swallowing an oral dosage form, it is confronted with a complex environment from which the drug must be released and absorbed into the bloodstream.[65] Some dosage forms like Oro-dispersible films dissolve in the mouth caveat and drug is readily absorbed.[66] This brings some advantages, such as more accurate dosing, faster onset of action, or even higher

bioavailability for some drugs.[67-69] The maximum amount of administrable drug is unfortunately limited, manufacturing is expensive and special packing is required for those dosage forms.[67] Therefore, they appear to be more rare and exotic than commonly manufactured tablets. The next intestinal compartment is the stomach. The acidic pH of the stomach has a high inter and intra-individual variability.[70] Some drugs profit from this acidic milieu and their solubility increases (as mentioned for Albendazole).[64, 71] Especially poorly water-soluble basic drugs can therefore benefit from enhanced solubility in the stomach generating supersaturated concentrations in the small intestine after pyloric passage.[72] Other drug substances like Omeprazole need to be protected from the acidic gastric milieu as cleavage occurs inactivating the drug.[73] Drugs sensitive to acidic catalysed cleavage are usually coated with polymers that dissolve in the small intestine but not in the stomach. Nevertheless, the stomach surface is small compared to the intestine and plays a minor role in drug absorption.[74, 75] Food intake can upregulate the pH (1.6 – 2.2 fasted vs. 4.7 -5.3 fed) and increase the mean residence time of a drug in the stomach, which must be considered.[70, 75] After the stomach, the drug is released into the small intestine. The main absorption of drugs takes place in the duodenum and jejunum, which have a common surface area of roughly 200 m².[76] Here. food and digestion products, gastrointestinal enzymes and microbiota may impact the liberation, and absorption of a drug.[65] Lipids from food for example might rise the solubility of lipophilic drugs or impact the wetting of solid dosage forms.[77] Another main component of intestinal fluid is bile, which is a natural system for poorly water-soluble fat and vitamin solubilization.[78, 79] The pH in the small intestine is higher (pH 5.2 – 6.1, fasted) compared to the stomach.[70] In the following intestinal compartments (Ileum, Colon) the pH value becomes almost neutral with a low liquid volume and surface area of only 1.3 m².[76, 80] The large intestine usually plays a minor role in drug absorption.[74] But dosage forms can be also designed to release a drug in the colon, which is significant for the therapy of, e.g., inflammatory bowel diseases or colonic cancer.[74] The colonic microflora expressing specific enzymes, for example, can be utilized for controlled drug release.[81, 82]

Focusing now on drug delivery of PWSDs in the small intestine, solubilization of drugs by bile salts might be a considerable aspect for drug formulation.[83] Bile salts are amphiphilic molecules from the cholesterol metabolism produced by the liver, stored in the gallbladder, and released by cholecystokinin after food intake into the duodenum through the common bile duct.[84] In humans and higher vertebrates, the C24 bile acids consist of a steroid scaffold

and are conjugated to either glycine (70% of bile salts) or taurine (30%), which increases their water solubility.[85, 86] Bile salts have a unique molecular structure with a hydrophilic and a hydrophobic surface contrasting classic detergents, where hydrophobic and lipophilic structures are spatially separated from each other.[87] This explains in part the complex aggregation behaviour of bile salts in water including no clear critical micellar concentration.[88, 89] Bile furthermore contains cholesterol and phospholipids. All together they spontaneously form intestinal mixed micelles, which play an important role in digestion of lipids and fat-soluble vitamins.[78, 79] Lack of bile salts causes nutrient malabsorption.[90, 91] Gallbladder stones result from a unfavorable ratio of cholesterol to bile salts.[92] Vitamin K uptake has been shown to be reduced in neonates with cholestasis.[93] This versatile and essential natural solubilization system could also increase the solubility and bioavailability of PWSDs.[40, 83] Therefore, knowledge of how PWSDs are solubilized by bile is of great interest to scientists involved in drug formulation.

Simulated intestinal fluids

Simulated intestinal fluids have been developed to mimic and predict the behavior of drugs in the small intestine and are widely applied in the pharmaceutical industry.[94] Nowadays, simulated intestinal fluids are prepared from commercially available ready-to-use powders making preparation easy and fast.[95] As mentioned earlier, bile is a mixture of various bile salts, phospholipids, and cholesterol. Simulated intestinal fluids usually consist of a buffer that resembles the osmolality and pH of the small intestine in the fasted or fed state.[96] Different buffer types have been described (phosphate buffered saline based, acetic acid/acetate buffer based, or maleic acid buffer based).[97] The most common bile salt used in simulated intestinal fluids is taurocholic acid due to its frequent occurrence in human collected intestinal fluids and higher solubility at low pH values compared to the most abundant bile salt glycocholic acid.[98] Moreover, phospholipids from egg or soy lecithin are used for simulated intestinal fluid preparation. Bile salts and phospholipids mimic the intestinal solubilization capacity through mixed micelle formation. In general, collected human intestinal fluid is considered more accurate for in *vitro/in vivo* portability compared to simulated intestinal fluids.[86, 99, 100] In addition to intestinal solubilization, other parameters such as stabilization of the supersaturated drug state may depend on the actual bile salt composition and lecithin content.[101] Unfortunately, the accessibility of human intestinal fluid for research is limited. Nevertheless, simulated intestinal fluids have been shown to

accurately predict the solubility of poorly water-soluble drugs in most cases.[102] Recently, more complex simulated intestinal fluids containing 5 different bile salts have been proposed.[103] In summary, simulated intestinal fluids offer a well-established and easy tool to approximate the *in vivo* solubility, dissolution rate, and duration of supersaturated drug states for drug formulation design.

Drug permeability

Another key parameter during drug formulation development is the drug substance's permeability through biologic membranes.[9] Drug bioavailability is not only governed by a drugs solubility in the intestine, but moreover determined by the drug's ability to cross the intestinal wall. Passive absorption is the main route for PWSD absorption. The rate of diffusion of a solute can be expressed by Fick's first law (Eq. 4).[104]

$$\frac{dM}{dt} = -DA \cdot \frac{dC}{dh} \qquad \text{(Eq. 4)}$$

dM/dt is the mass of diffusion solute per time across an area (A) following a concentration gradient (dC/dh). The diffusion coefficient D for spherical particles can be further described by the stokes-Einstein equation (Eq. 5).[105]

$$D = \frac{R \cdot T}{6 \cdot \eta \cdot r \cdot N_a} \qquad \text{(Eq. 5)}$$

R is the gas constant, T is the absolute temperature, η is the dynamic viscosity of the medium, r is the radius of spherical particles, and N_a the Avogadro's constant. Fick's fist law can be modified to describe a drug's absorption *in vivo*. The amount of absorbed drug dM/dt (mass/time) depends on the effective permeability (P_{eff}), the intestinal surface Area (A), and the concentration of drug in the small intestine ($C_{intestine}$). It is theoretically dependent on the concentration in the blood as well (C_{blood}), but concentration in blood becomes negligible due to higher luminal compared to systemic drug concentrations ($C_{lumen} >> C_{blood}$) (Eq. 6).

$$\frac{dM}{dt} = A \cdot P_{eff} \cdot (C_{intestine} - C_{blood}) = A \cdot P_{eff} \cdot C_{intestine} \qquad \text{(Eq. 6)}$$

Passive drug absorption can occur transcellular, paracellular through tight junctions, or paracellular through direct fluid effect (solvent drag). The two latter absorption routes play a minor role for PWSD absorption in humans.[106, 107] These routes are more important for small hydrophilic drugs. After dissolution of a drug form (Eq. 3), the drug substance must

be transported through an aqueous layer to the membrane including an unstirred water layer and the mucin layer above intestinal cell surfaces. After diffusion through the apical cell membrane, the drug needs to diffuse through the cytosol, basolateral cell membrane, interstitial fluid, and capillary wall to the blood stream. However, passive transcellular permeability can be described by the following *in vivo* factors (Eq. 7).[108]

$$P_{eff} = K \cdot \frac{D_m}{\lambda} \qquad \text{(Eq. 7)}$$

K is the drug specific membrane-aqueous partition coefficient, D_m is the diffusion coefficient of the drug in the membrane, and λ describes the thickness of the diffusion limiting barrier. Several *in vitro* or *ex vivo* methods approach *in vivo* drug permeability either using cell lines, excised tissue, or artificial membranes. Another possible route of drug absorption is active transport by transport proteins. This phenomenon is less common but plays a role in the uptake of amino acids, oligopeptides, and bile acids.[109] Active efflux of drugs by P-glycoprotein on the other side is more frequent and may impact the absorption of drugs. One model described as the gold standard to study intestinal drug permeability *in vitro* is the human colorectal adenocarcinoma (Caco-2) monolayer setup.[110] Here, cells are cultivated on 96-well plate filter supports. This generates two separated chambers, one apical and one basolateral side. After establishing a cell monolayer, permeation experiments may be conducted. Drug is introduced as stock solution in the apical part and drug concentration is measured in the basolateral compartment over time. An advantage of these cell line-based permeability measurements compared to permeability tests with artificial membranes is that transport proteins and some metabolizing enzymes are also expressed. Beside Caco-2 cells, lung cancer epithelial (Calu-3) cell lines mimicking airway epithelium have been established,[111] or Caco-2 cell co-cultures with mucus-secreting cells[112] have been described. Disadvantages of cell-based permeation studies include long incubation times, challenging handling, and limited medium compatibility of cell lines. Simulated intestinal fluids, food components, and certain pharmaceutical excipients for example show limited compatibility with Caco-2 cell lines.[113-116] Other *ex vivo* setups use excised tissue like rat, pig, or even human intestine to assess *in vivo* drug permeability.[117] The "Ussing-chamber" is a setup using excised tissue mounted between two chambers having oxygenated buffers.[118] The tissue must be freshly excised, so active transporter activity is maintained throughout the experiment. Drug solution is added to the apical side and concentration in the donor side is measured over time. In contrast to cell-based setups, a more *in vivo* relevant absorption

surface is provided with a big variety of different cells including mucin secreting cells or absorptive enterocytes.[119] One disadvantage of *ex vivo* methods are the relatively low experimental throughput and challenging tissue preparation. Furthermore, excised rat ileum was reported to be incompatible with simulated intestinal fluids as well.[120]

In addition to cell-based or *ex vivo* systems, artificial membranes have emerged as rapid, high-throughput compatible, and reliable alternatives for drug permeability testing. They can generally be divided into two groups: (i) barriers including phospholipids mimicking biological membranes, or (ii) dialysis membranes.[116] One example for the first group is the **p**arallel **a**rtificial **m**embrane **p**ermeation **a**ssay (**PAMPA**).[121] It consists of a filter (e.g., **p**oly**v**inyli**d**ene fluoride (**PVDF**)) impregnated with phospholipids in organic solvent (e.g., egg lecithin in n-dodecane). The acceptor compartment contains a sink buffer (e.g., sodium dodecyl sulfate, Tween 80, or Vitamin E - TPGS) maintaining sink conditions during permeation studies. Drug permeability measured by PAMPA is correlated with drug absorption in humans.[121] It is also possible to perform PAMPA like Caco-2 permeation studies on microtiter plates using, e.g., "Transwell" setups. Over the years, several modifications of PAMPA have been proposed using more bio-mimetic membrane compositions or additive mucus layers.[122, 123] Nevertheless, active or paracellular transport, drug retention in biologic membranes is not predictable with PAMPA. Additionally, membrane components may be emulsified into medium altering the solubilization capacity in the donor compartment. One attempt to avoid this phenomenon was to put the phospholipids between two supportive layers composed of regenerated cellulose creating the "Permeapad" membrane.[124] According to the manufacturers, phospholipid bilayers form within the support sheets after swelling, creating biomimetic membranes. The permeability coefficient correlation was like Caco-2 cells.[124] Membrane setups with dialysis membranes use regenerated cellulose membranes with a typical cutoff between 2-14 kda.[125] They are easy to handle and show a good correlation with Caco-2 cell determined permeability. Moreover, the membrane is compatible with food components, simulated intestinal fluids, solubilizers and pharmaceutically used excipients. In general, this compatibility with all kinds of additives is a big advantage compared to *ex vivo* and cell-based permeation tools.[126] Artificial cellulose membranes are robust in term of membrane leakages and medium pH.[125] As mentioned earlier PWSDs need additive solubilizers/excipients for formulations. Therefore, their impact on drug permeability is interesting for drug formulation development. The amount of permeating drug in setups using artificial membranes is

dependent on the concentration of free drug in solution. Exceeding the amorphous solubility of a drug does not lead to further increase in permeated drug amount over time. Additives or bile salts may solubilize drugs by micellar solubilization. Therefore, there is an equilibrium between the concentration of drug in solution (C_w) and micellar bound drug (C_m) defined as micellar partition coefficient K_m (Eq. 7).[127]

$$K_m = \frac{C_m}{C_w} \quad \text{(Eq. 7)}$$

The total drug solubility S_{tot} is composed of the solubility of crystalline drug in water S_w and K_m (Eq. 8).[128]

$$S_{tot} = S_w + K_m \cdot S_w \quad \text{(Eq. 8)}$$

Only free drug molecules drive permeation of drugs and their solubilization will decrease permeation kinetics.[129] Hence, in the presence of micelles, erroneous predictions of drug permeability may occur if calculations are made using the total drug concentration rather than the free drug concentration. Another drawback of cellulose membranes is that they represent hydrophilic barriers and lipid membrane partitioning or affinity of drugs to lipid membranes could not be predicted with this setup. In summary, combination of cell-based and cell-free permeation studies might give formulation scientists the most accurate view on *in vivo* drug absorption.

Predicting a drug's bio performance by *in silico* tools

Recent research has focused on *in silico* tools predicting liberation, absorption, distribution, metabolization, and excretion of drugs.[130] Several tools have been developed to help formulation scientists simulate drug solubility, and permeability and other biopharmaceutical parameters.[131] Nevertheless, this research area is emerging and aims to replace costly and time-consuming laboratory work in favor of computer simulations using, for example, algorithms, artificial neural networks, and molecular dynamic simulations.[131, 132] Large-scale dataset generation remains the biggest challenge, as experimental procedures differ across laboratories and datasets may not be comparable. We investigated the ^{1}H nuclear magnetic resonance shifts of 141 drugs in presence of simulated bile and lipids establishing a predictive algorithm for drug-bile and lipid interaction. Our procedure is described in Chapter 1.

References

1. Waring, M. J.; Arrowsmith, J.; Leach, A. R.; Leeson, P. D.; Mandrell, S.; Owen, R. M.; Pairaudeau, G.; Pennie, W. D.; Pickett, S. D.; Wang, J.; Wallace, O.; Weir, A., An analysis of the attrition of drug candidates from four major pharmaceutical companies. *Nat. Rev. Drug Discovery* **2015,** *14* (7), 475-86.
2. Ghadi, R.; Dand, N., BCS class IV drugs: Highly notorious candidates for formulation development. *J. Control. Release* **2017,** *248*, 71-95.
3. Lipinski, C., Poor aqueous solubility—an industry wide problem in drug discovery. *Am. Pharm. Rev.* **2002,** *5* (3), 82-85.
4. Di, L.; Fish, P. V.; Mano, T., Bridging solubility between drug discovery and development. *Drug Discovery Tod.* **2012,** *17* (9-10), 486-95.
5. Ritchie, T. J.; Macdonald, S. J. F.; Peace, S.; Pickett, S. D.; Luscombe, C. N., Increasing small molecule drug developability in sub-optimal chemical space. *MedChemComm* **2013,** *4* (4).
6. Rocke, D. M., Design and analysis of experiments with high throughput biological assay data. *Semin. Cell. Dev. Biol.* **2004,** *15* (6), 703-13.
7. Zhao, H., Lead optimization in the nondrug-like space. *Drug Discovery Tod.* **2011,** *16* (3-4), 158-63.
8. Hann, M. M., Molecular obesity, potency and other addictions in drug discovery. *MedChemComm* **2011,** *2* (5), 349-355.
9. Lipinski, C. A.; Lombardo, F.; Dominy, B. W.; Feeney, P. J., Experimental and computational approaches to estimate solubility and permeability in drug discovery and development settings. *Adv. Drug Delivery Rev.* **1997,** *23* (1-3), 3-25.
10. Gleeson, M. P., Generation of a set of simple, interpretable ADMET rules of thumb. *J. Med. Chem.* **2008,** *51* (4), 817-34.
11. York, P., The design of dosage forms. *Pharmaceutics: the science of dosage form design* **2013**, 1-12.
12. Fridgeirsdottir, G. A.; Harris, R.; Fischer, P. M.; Roberts, C. J., Support Tools in Formulation Development for Poorly Soluble Drugs. *J. Pharm. Sci.* **2016,** *105* (8), 2260-9.
13. van De Waterbeemd, H.; Smith, D. A.; Beaumont, K.; Walker, D. K., Property-based design: optimization of drug absorption and pharmacokinetics. *J. Med. Chem.* **2001,** *44* (9), 1313-33.
14. Di, L.; Kerns, E., *Drug-like properties: concepts, structure design and methods from ADME to toxicity optimization*. Academic press: 2015.
15. Denora, N.; Trapani, A.; Laquintana, V.; Lopedota, A.; Trapani, G., Recent advances in medicinal chemistry and pharmaceutical technology--strategies for drug delivery to the brain. *Cur. Top. Med. Chem.* **2009,** *9* (2), 182-96.
16. Palucki, M.; Higgins, J. D.; Kwong, E.; Templeton, A. C., Strategies at the interface of drug discovery and development: early optimization of the solid state phase and preclinical toxicology formulation for potential drug candidates. *J. Med. Chem.* **2010,** *53* (16), 5897-905.
17. Maas, J.; Kamm, W.; Hauck, G., An integrated early formulation strategy--from hit evaluation to preclinical candidate profiling. *Eur. J. Pharm. Biopharm.* **2007,** *66* (1), 1-10.
18. Pudipeddi, M.; Serajuddin, A. T., Trends in solubility of polymorphs. *J. Pharm. Sci.* **2005,** *94* (5), 929-39.
19. Serajuddin, A. T.; Thakur, A. B.; Ghoshal, R. N.; Fakes, M. G.; Ranadive, S. A.; Morris, K. R.; Varia, S. A., Selection of solid dosage form composition through drug-excipient compatibility testing. *J. Pharm. Sci.* **1999,** *88* (7), 696-704.
20. Alsenz, J.; Kansy, M., High throughput solubility measurement in drug discovery and development. *Adv. Drug Delivery Rev.* **2007,** *59* (7), 546-67.
21. Zane, P.; Gieschen, H.; Kersten, E.; Mathias, N.; Ollier, C.; Johansson, P.; Van den Bergh, A.; Van Hemelryck, S.; Reichel, A.; Rotgeri, A.; Schafer, K.; Mullertz, A.;

Langguth, P., In vivo models and decision trees for formulation development in early drug development: A review of current practices and recommendations for biopharmaceutical development. *Eur. J. Pharm. Biopharm.* **2019,** *142*, 222-231.
22. Dittert, L. W.; Higuchi, T.; Reese, D. R., Phase Solubility Technique in Studying the Formation of Complex Salts of Triamterene. *J. Pharm. Sci.* **1964,** *53*, 1325-8.
23. Avdeef, A., pH-metric solubility. 1. Solubility-pH profiles from Bjerrum plots. Gibbs buffer and pKa in the solid state. *Pharm. Pharmacol. Com.* **1998,** *4* (3), 165-178.
24. Stuart, M.; Box, K., Chasing equilibrium: measuring the intrinsic solubility of weak acids and bases. *Anal. Chem.* **2005,** *77* (4), 983-90.
25. Paus, R.; Ji, Y.; Vahle, L.; Sadowski, G., Predicting the Solubility Advantage of Amorphous Pharmaceuticals: A Novel Thermodynamic Approach. *Mol. Pharmaceutics* **2015,** *12* (8), 2823-33.
26. Taylor, L. S.; Zhang, G. G. Z., Physical chemistry of supersaturated solutions and implications for oral absorption. *Adv. Drug Delivery Rev.* **2016,** *101*, 122-142.
27. Babu, N. J.; Nangia, A., Solubility advantage of amorphous drugs and pharmaceutical cocrystals. *Cryst. Growth Des.* **2011,** *11* (7), 2662-2679.
28. Murdande, S. B.; Pikal, M. J.; Shanker, R. M.; Bogner, R. H., Solubility advantage of amorphous pharmaceuticals: I. A thermodynamic analysis. *J. Pharm. Sci.* **2010,** *99* (3), 1254-64.
29. Mosquera-Giraldo, L. I.; Taylor, L. S., Glass-liquid phase separation in highly supersaturated aqueous solutions of telaprevir. *Mol. Pharmaceutics* **2015,** *12* (2), 496-503.
30. Ilevbare, G. A.; Taylor, L. S., Liquid–Liquid Phase Separation in Highly Supersaturated Aqueous Solutions of Poorly Water-Soluble Drugs: Implications for Solubility Enhancing Formulations. *Cryst. Growth Des.* **2013,** *13* (4), 1497-1509.
31. Indulkar, A. S.; Gao, Y.; Raina, S. A.; Zhang, G. G.; Taylor, L. S., Exploiting the Phenomenon of Liquid-Liquid Phase Separation for Enhanced and Sustained Membrane Transport of a Poorly Water-Soluble Drug. *Mol. Pharmaceutics* **2016,** *13* (6), 2059-69.
32. Van Eerdenbrugh, B.; Raina, S.; Hsieh, Y. L.; Augustijns, P.; Taylor, L. S., Classification of the crystallization behavior of amorphous active pharmaceutical ingredients in aqueous environments. *Pharm. Res.* **2014,** *31* (4), 969-82.
33. Guzman, H. R.; Tawa, M.; Zhang, Z.; Ratanabanangkoon, P.; Shaw, P.; Gardner, C. R.; Chen, H.; Moreau, J. P.; Almarsson, O.; Remenar, J. F., Combined use of crystalline salt forms and precipitation inhibitors to improve oral absorption of celecoxib from solid oral formulations. *J. Pharm. Sci.* **2007,** *96* (10), 2686-702.
34. Mukerjee, P., Solubilization in Aqueous Micellar Systems. In *Solution Chemistry of Surfactants*, Mittal, K. L., Ed. Springer New York: Boston, MA, 1979; Vol. 1, pp 153-174.
35. Serajuddin, A. T.; Sheen, P. C.; Mufson, D.; Bernstein, D. F.; Augustine, M. A., Physicochemical basis of increased bioavailability of a poorly water-soluble drug following oral administration as organic solutions. *J. Pharm. Sci.* **1988,** *77* (4), 325-9.
36. Porter, C. J.; Pouton, C. W.; Cuine, J. F.; Charman, W. N., Enhancing intestinal drug solubilisation using lipid-based delivery systems. *Adv. Drug Delivery Rev.* **2008,** *60* (6), 673-91.
37. Azeem, A.; Rizwan, M.; Ahmad, F. J.; Iqbal, Z.; Khar, R. K.; Aqil, M.; Talegaonkar, S., Nanoemulsion components screening and selection: a technical note. *AAPS PharmSciTech* **2009,** *10* (1), 69-76.
38. Aungst, B. J., Optimizing Oral Bioavailability in Drug Discovery: An Overview of Design and Testing Strategies and Formulation Options. *J. Pharm. Sci.* **2017,** *106* (4), 921-929.
39. Jacobs, C.; Kayser, O.; Müller, R. H., Nanosuspensions as a new approach for the formulation for the poorly soluble drug tarazepide. *Int. J. Pharm.* **2000,** *196* (2), 161-164.
40. Sugano, K.; Kataoka, M.; Mathews Cda, C.; Yamashita, S., Prediction of food effect by bile micelles on oral drug absorption considering free fraction in intestinal fluid. *Eur. J. Pharm. Sci.* **2010,** *40* (2), 118-24.

41. Dolenc, A.; Kristl, J.; Baumgartner, S.; Planinsek, O., Advantages of celecoxib nanosuspension formulation and transformation into tablets. *Int. J. Pharm.* **2009,** *376* (1-2), 204-12.
42. Tsinman, K.; Tsinman, O.; Riebesehl, B.; Grandeury, A.; Juhnke, M., In situ method for monitoring free drug concentration released from nanoparticles. *Poster Present AAPS Annu Meet Expo Oct* **2012**, 14-18.
43. Feeney, O. M.; Crum, M. F.; McEvoy, C. L.; Trevaskis, N. L.; Williams, H. D.; Pouton, C. W.; Charman, W. N.; Bergstrom, C. A. S.; Porter, C. J. H., 50years of oral lipid-based formulations: Provenance, progress and future perspectives. *Adv. Drug Delivery Rev.* **2016,** *101*, 167-194.
44. Pignatello, R.; Corsaro, R., Polymeric Nanomicelles of Soluplus® as a Strategy for Enhancing the Solubility, Bioavailability and Efficacy of Poorly Soluble Active Compounds. *Curr. Nanomed.* **2019,** *9* (3), 184-197.
45. Lakshman, D.; Chegireddy, M.; Hanegave, G. K.; Sree, K. N.; Kumar, N.; Lewis, S. A.; Dengale, S. J., Investigation of drug-polymer miscibility, biorelevant dissolution, and bioavailability improvement of Dolutegravir-polyvinyl caprolactam-polyvinyl acetate-polyethylene glycol graft copolymer solid dispersions. *Eur. J. Pharm. Sci.* **2020,** *142*, 105137.
46. Fine-Shamir, N.; Dahan, A., Methacrylate-Copolymer Eudragit EPO as a Solubility-Enabling Excipient for Anionic Drugs: Investigation of Drug Solubility, Intestinal Permeability, and Their Interplay. *Mol. Pharmaceutics* **2019,** *16* (7), 2884-2891.
47. Brewster, M. E.; Vandecruys, R.; Peeters, J.; Neeskens, P.; Verreck, G.; Loftsson, T., Comparative interaction of 2-hydroxypropyl-beta-cyclodextrin and sulfobutylether-beta-cyclodextrin with itraconazole: phase-solubility behavior and stabilization of supersaturated drug solutions. *Eur. J. Pharm. Sci.* **2008,** *34* (2-3), 94-103.
48. Tang, P.; Wang, L.; Ma, X.; Xu, K.; Xiong, X.; Liao, X.; Li, H., Characterization and In Vitro Evaluation of the Complexes of Posaconazole with β- and 2,6-di-O-methyl-β-cyclodextrin. *AAPS PharmSciTech* **2017,** *18* (1), 104-114.
49. Jansook, P.; Ogawa, N.; Loftsson, T., Cyclodextrins: structure, physicochemical properties and pharmaceutical applications. *Int. J. Pharm.* **2018,** *535* (1-2), 272-284.
50. Samie, A.; Desiraju, G. R.; Banik, M., Salts and Cocrystals of the Antidiabetic Drugs Gliclazide, Tolbutamide, and Glipizide: Solubility Enhancements through Drug–Coformer Interactions. *Cryst. Growth Des.* **2017,** *17* (5), 2406-2417.
51. Balk, A.; Widmer, T.; Wiest, J.; Bruhn, H.; Rybak, J. C.; Matthes, P.; Muller-Buschbaum, K.; Sakalis, A.; Luhmann, T.; Berghausen, J.; Holzgrabe, U.; Galli, B.; Meinel, L., Ionic liquid versus prodrug strategy to address formulation challenges. *Pharm. Res.* **2015,** *32* (6), 2154-67.
52. Balk, A.; Wiest, J.; Widmer, T.; Galli, B.; Holzgrabe, U.; Meinel, L., Transformation of acidic poorly water soluble drugs into ionic liquids. *Eur. J. Pharm. Biopharm.* **2015,** *94*, 73-82.
53. Reggane, M.; Wiest, J.; Saedtler, M.; Harlacher, C.; Gutmann, M.; Zottnick, S. H.; Piechon, P.; Dix, I.; Muller-Buschbaum, K.; Holzgrabe, U.; Meinel, L.; Galli, B., Bioinspired co-crystals of Imatinib providing enhanced kinetic solubility. *Eur. J. Pharm. Biopharm.* **2018,** *128*, 290-299.
54. Iyer, R.; Petrovska Jovanovska, V.; Berginc, K.; Jaklic, M.; Fabiani, F.; Harlacher, C.; Huzjak, T.; Sanchez-Felix, M. V., Amorphous Solid Dispersions (ASDs): The Influence of Material Properties, Manufacturing Processes and Analytical Technologies in Drug Product Development. *Pharmaceutics* **2021,** *13* (10).
55. Alonzo, D. E.; Gao, Y.; Zhou, D.; Mo, H.; Zhang, G. G. Z.; Taylor, L. S., Dissolution and precipitation behavior of amorphous solid dispersions. *J. Pharm. Sci.* **2011,** *100* (8), 3316-3331.
56. Brough, C.; Williams, R. O., 3rd, Amorphous solid dispersions and nano-crystal technologies for poorly water-soluble drug delivery. *Int. J. Pharm.* **2013,** *453* (1), 157-66.

57. Kwong, A. D.; Kauffman, R. S.; Hurter, P.; Mueller, P., Discovery and development of telaprevir: an NS3-4A protease inhibitor for treating genotype 1 chronic hepatitis C virus. *Nat. Biotechnol.* **2011,** *29* (11), 993-1003.
58. Shah, N.; Iyer, R. M.; Mair, H. J.; Choi, D. S.; Tian, H.; Diodone, R.; Fahnrich, K.; Pabst-Ravot, A.; Tang, K.; Scheubel, E.; Grippo, J. F.; Moreira, S. A.; Go, Z.; Mouskountakis, J.; Louie, T.; Ibrahim, P. N.; Sandhu, H.; Rubia, L.; Chokshi, H.; Singhal, D.; Malick, W., Improved human bioavailability of vemurafenib, a practically insoluble drug, using an amorphous polymer-stabilized solid dispersion prepared by a solvent-controlled coprecipitation process. *J. Pharm. Sci.* **2013,** *102* (3), 967-81.
59. Ilevbare, G. A.; Liu, H.; Pereira, J.; Edgar, K. J.; Taylor, L. S., Influence of additives on the properties of nanodroplets formed in highly supersaturated aqueous solutions of ritonavir. *Mol. Pharmaceutics* **2013,** *10* (9), 3392-403.
60. Bachmaier, R. D.; Monschke, M.; Faber, T.; Krome, A. K.; Pellequer, Y.; Stoyanov, E.; Lamprecht, A.; Wagner, K. G., In vitro and in vivo assessment of hydroxypropyl cellulose as functional additive for enabling formulations containing itraconazole. *Int. J. Pharm. X* **2021,** *3*, 100076.
61. Chen, J.; Mosquera-Giraldo, L. I.; Ormes, J. D.; Higgins, J. D.; Taylor, L. S., Bile Salts as Crystallization Inhibitors of Supersaturated Solutions of Poorly Water-Soluble Compounds. *Cryst. Growth Des.* **2015,** *15* (6), 2593-2597.
62. Indulkar, A. S.; Gao, Y.; Raina, S. A.; Zhang, G. G. Z.; Taylor, L. S., Impact of Monomeric versus Micellar Surfactant and Surfactant–Polymer Interactions on Nucleation–Induction Times of Atazanavir from Supersaturated Solutions. *Cryst. Growth Des.* **2019,** *20* (1), 62-72.
63. Davis, A. F.; Hadgraft, J., Effect of supersaturation on membrane transport: 1. Hydrocortisone acetate. *Int. J. Pharm.* **1991,** *76* (1-2), 1-8.
64. Nagy, J.; Schipper, H. G.; Koopmans, R. P.; Butter, J. J.; Van Boxtel, C. J.; Kager, P. A., Effect of grapefruit juice or cimetidine coadministration on albendazole bioavailability. *Am. J. Tropical Med. Hygiene* **2002,** *66* (3), 260-3.
65. Basit, A. W.; Madla, C. M.; Gavins, F. K. H., Robotic screening of intestinal drug absorption. *Nat. Biomed. Eng.* **2020,** *4* (5), 485-486.
66. Dixit, R. P.; Puthli, S. P., Oral strip technology: overview and future potential. *J. Control. Release* **2009,** *139* (2), 94-107.
67. Thakur, N.; Bansal, M.; Sharma, N.; Yadav, G.; Khare, P., Overview "a novel approach of fast dissolving films and their patients". *Adv. Biol. Res.* **2013,** *7* (2), 50-58.
68. Ghodake, P. P.; Karande, K. M.; Osmani, R. A.; Bhosale, R. R.; Harkare, B. R.; Kale, B. B., Mouth dissolving films: Innovative vehicle for oral drug delivery. *Polymer* **2013,** *9*, 20.
69. Kathpalia, H.; Gupte, A., An introduction to fast dissolving oral thin film drug delivery systems: a review. *Curr. Drug Delivery* **2013,** *10* (6), 667-684.
70. Abuhelwa, A. Y.; Foster, D. J. R.; Upton, R. N., A Quantitative Review and Meta-Models of the Variability and Factors Affecting Oral Drug Absorption—Part I: Gastrointestinal pH. *AAPS J.* **2016,** *18* (5), 1309-1321.
71. Dressman, J. B.; Vertzoni, M.; Goumas, K.; Reppas, C., Estimating drug solubility in the gastrointestinal tract. *Adv. Drug Deliery. Rev.* **2007,** *59* (7), 591-602.
72. Mitra, A.; Kesisoglou, F., Impaired drug absorption due to high stomach pH: a review of strategies for mitigation of such effect to enable pharmaceutical product development. *Mol. Pharmaceutics* **2013,** *10* (11), 3970-9.
73. Chakravarthy, K. K.; Younus, M.; Shaik, S.; Pisipati, S. V. V., Formulation and evaluation of enteric coated pellets of omeprazole. *Int. J. Drug Dev. Res.* **2012,** *4* (4), 0-0.
74. Basit, A. W., Advances in colonic drug delivery. *Drugs* **2005,** *65* (14), 1991-2007.
75. Levine, R. R., Factors affecting gastrointestinal absorption of drugs. *Americ. J. Dig. Dis.* **1970,** *15* (2), 171-188.
76. Faigle, J., Drug metabolism in the colon wall and lumen. *Drugs Pharm. Sci.* **1993,** *60*, 29-54.

77. Koziolek, M.; Carrière, F.; Porter, C. J. H., Lipids in the Stomach – Implications for the Evaluation of Food Effects on Oral Drug Absorption. *Pharm. Res.* **2018,** *35* (3), 55.
78. Westergaard, H.; Dietschy, J. M., The mechanism whereby bile acid micelles increase the rate of fatty acid and cholesterol uptake into the intestinal mucosal cell. *J. Clin. Invest.* **1976,** *58* (1), 97-108.
79. Coleman, R., Bile salts and biliary lipids. *Biochem. Soc. Transactions* **1987,** *15*, 68S-80S.
80. Evans, D.; Pye, G.; Bramley, R.; Clark, A.; Dyson, T.; Hardcastle, J., Measurement of gastrointestinal pH profiles in normal ambulant human subjects. *Gut* **1988,** *29* (8), 1035-1041.
81. Svartz, N., Sulfasalazine: II. Some notes on the discovery and development of salazopyrin. *Am. J. gastroenterolog.* **1988,** *83* (5), 497-503.
82. Carrette, O.; Favier, C.; Mizon, C.; Neut, C.; Cortot, A.; Colombel, J.; Mizon, J., Bacterial enzymes used for colon-specific drug delivery are decreased in active Crohn's disease. *Dig. Dis. Sci.* **1995,** *40* (12), 2641-2646.
83. Holm, R.; Mullertz, A.; Mu, H., Bile salts and their importance for drug absorption. *Int. J. Pharm.* **2013,** *453* (1), 44-55.
84. Monte, M. J.; Marin, J. J.; Antelo, A.; Vazquez-Tato, J., Bile acids: chemistry, physiology, and pathophysiology. *World J. Gastroenterol.* **2009,** *15* (7), 804-16.
85. Hofmann, A. F.; Sjövall, J.; Kurz, G.; Radominska, A.; Schteingart, C. D.; Tint, G. S.; Vlahcevic, Z. R.; Setchell, K. D., A proposed nomenclature for bile acids. *J. Lipid. Res.* **1992,** *33* (4), 599-604.
86. Riethorst, D.; Mols, R.; Duchateau, G.; Tack, J.; Brouwers, J.; Augustijns, P., Characterization of Human Duodenal Fluids in Fasted and Fed State Conditions. *J. Pharm. Sci.* **2016,** *105* (2), 673-681.
87. Mukerjee, P.; Moroi, Y.; Murata, M.; Yang, A. Y., Bile salts as atypical surfactants and solubilizers. *Hepatology (Hoboken, NJ, U. S.)* **1984,** *4* (5 Suppl), 61S-65S.
88. Hanio, S.; Schlauersbach, J.; Lenz, B.; Spiegel, F.; Bockmann, R. A.; Schweins, R.; Nischang, I.; Schubert, U. S.; Endres, S.; Poppler, A. C.; Brandl, F. P.; Smit, T. M.; Kolter, K.; Meinel, L., Drug-Induced Dynamics of Bile Colloids. *Langmuir* **2021,** *37* (8), 2543-2551.
89. Madenci, D.; Egelhaaf, S. U., Self-assembly in aqueous bile salt solutions. *Curr. Opin. Colloid Interface Sci.* **2010,** *15* (1-2), 109-115.
90. Signer, E.; Murphy, G.; Edkins, S.; Anderson, C. M., Role of bile salts in fat malabsorption of premature infants. *Arch. Dis Child.* **1974,** *49* (3), 174-180.
91. Sanyal, A. J.; Hirsch, J. I.; Moore, E. W., Premicellar taurocholate enhances calcium uptake from all regions of rat small intestine. *Gastroenterology* **1994,** *106* (4), 866-874.
92. Paumgartner, G.; Sauerbruch, T., Gallstones: pathogenesis. *The Lancet* **1991,** *338* (8775), 1117-1121.
93. Schubiger, G.; Stocker, C.; Banziger, O.; Laubscher, B.; Zimmermann, H., Oral vitamin K1 prophylaxis for newborns with a new mixed-micellar preparation of phylloquinone: 3 years experience in Switzerland. *Eur. J. Pediatr.* **1999,** *158* (7), 599-602.
94. Kostewicz, E. S.; Brauns, U.; Becker, R.; Dressman, J. B., Forecasting the oral absorption behavior of poorly soluble weak bases using solubility and dissolution studies in biorelevant media. *Pharm. Res.* **2002,** *19* (3), 345-349.
95. Kloefer, B.; van Hoogevest, P.; Moloney, R.; Kuentz, M.; Leigh, M. L. S.; Dressman, J., Study of a Standardized Taurocholate– Lecithin Powder for Preparing the Biorelevant Media FeSSIF and FaSSIF. *Diss. Technol.* **2010,** *17* (3), 6-13.
96. Galia, E.; Nicolaides, E.; Hörter, D.; Löbenberg, R.; Reppas, C.; Dressman, J. B., Evaluation of various dissolution media for predicting in vivo performance of class I and II drugs. *Pharm. Res.* **1998,** *15* (5), 698-705.
97. Leigh, M.; Kloefer, B.; Schaich, M., Comparison of the Solubility and Dissolution of Drugs in FastedState Biorelevant Media (FaSSIF and FaSSIF-V2). *Dissolut. Technol.* **2013,** *20* (3), 44-50.

98. Sun, F.; Jaspers, T. C.; van Hasselt, P. M.; Hennink, W. E.; van Nostrum, C. F., A Mixed Micelle Formulation for Oral Delivery of Vitamin K. *Pharm. Res.* **2016,** *33* (9), 2168-79.
99. Perez de la Cruz Moreno, M.; Oth, M.; Deferme, S.; Lammert, F.; Tack, J.; Dressman, J.; Augustijns, P., Characterization of fasted-state human intestinal fluids collected from duodenum and jejunum. *J. Pharm. Pharmacol.* **2006,** *58* (8), 1079-89.
100. Riethorst, D.; Brouwers, J.; Motmans, J.; Augustijns, P., Human intestinal fluid factors affecting intestinal drug permeation in vitro. *Eur. J. Pharm. Sci.* **2018,** *121*, 338-346.
101. Indulkar, A. S.; Gao, Y.; Raina, S. A.; Zhang, G. G. Z.; Taylor, L. S., Crystallization from Supersaturated Solutions: Role of Lecithin and Composite Simulated Intestinal Fluid. *Pharm. Res.* **2018,** *35* (8), 158.
102. Dahlgren, D.; Venczel, M.; Ridoux, J. P.; Skjold, C.; Mullertz, A.; Holm, R.; Augustijns, P.; Hellstrom, P. M.; Lennernas, H., Fasted and fed state human duodenal fluids: Characterization, drug solubility, and comparison to simulated fluids and with human bioavailability. *Eur. J. Pharm. Biopharm.* **2021,** *163*, 240-251.
103. Fuchs, A.; Leigh, M.; Kloefer, B.; Dressman, J. B., Advances in the design of fasted state simulating intestinal fluids: FaSSIF-V3. *Eur. J. Pharm. Biopharm.* **2015,** *94*, 229-40.
104. Flynn, G.; Yalkowsky, S. H.; Roseman, T., Mass transport phenomena and models: theoretical concepts. *J. Pharm. Sci.* **1974,** *63* (4), 479-510.
105. Camenisch, G.; Folkers, G.; van de Waterbeemd, H., Review of theoretical passive drug absorption models: historical background, recent developments and limitations. *Pharm. Act. Helv.* **1996,** *71* (5), 309-327.
106. Stenberg, P.; Luthman, K.; Artursson, P., Virtual screening of intestinal drug permeability. *J. Controlled Release* **2000,** *65* (1-2), 231-243.
107. Mandagere, A. K.; Thompson, T. N.; Hwang, K. K., Graphical model for estimating oral bioavailability of drugs in humans and other species from their Caco-2 permeability and in vitro liver enzyme metabolic stability rates. *J. Med. Chem.* **2002,** *45* (2), 304-11.
108. Stein, W., *Transport and diffusion across cell membranes*. Elsevier: 2012.
109. Ayrton, A.; Morgan, P., Role of transport proteins in drug absorption, distribution and excretion. *Xenobiotica* **2001,** *31* (8-9), 469-497.
110. Artursson, P.; Palm, K.; Luthman, K., Caco-2 monolayers in experimental and theoretical predictions of drug transport. *Adv. Drug Delivery Rev.* **2001,** *46* (1-3), 27-43.
111. Florea, B. I.; Cassara, M. L.; Junginger, H. E.; Borchard, G., Drug transport and metabolism characteristics of the human airway epithelial cell line Calu-3. *J. Controlled Release* **2003,** *87* (1-3), 131-138.
112. Nollevaux, G.; Devillé, C.; El Moualij, B.; Zorzi, W.; Deloyer, P.; Schneider, Y.-J.; Peulen, O.; Dandrifosse, G., Development of a serum-free co-culture of human intestinal epithelium cell-lines (Caco-2/HT29-5M21). *BMC Cell Biology* **2006,** *7* (1), 1-11.
113. Ingels, F.; Deferme, S.; Destexhe, E.; Oth, M.; Van den Mooter, G.; Augustijns, P., Simulated intestinal fluid as transport medium in the Caco-2 cell culture model. *Int. J. Pharm.* **2002,** *232* (1-2), 183-192.
114. Ingels, F.; Beck, B.; Oth, M.; Augustijns, P., Effect of simulated intestinal fluid on drug permeability estimation across Caco-2 monolayers. *Int. J. Pharm.* **2004,** *274* (1-2), 221-32.
115. Wuyts, B.; Riethorst, D.; Brouwers, J.; Tack, J.; Annaert, P.; Augustijns, P., Evaluation of fasted state human intestinal fluid as apical solvent system in the Caco-2 absorption model and comparison with FaSSIF. *Eur. J. Pharm. Sci.* **2015,** *67*, 126-135.
116. Berben, P.; Bauer-Brandl, A.; Brandl, M.; Faller, B.; Flaten, G. E.; Jacobsen, A. C.; Brouwers, J.; Augustijns, P., Drug permeability profiling using cell-free permeation tools: Overview and applications. *Eur. J. Pharm. Sci.* **2018,** *119*, 219-233.
117. Neirinckx, E.; Vervaet, C.; Michiels, J.; De Smet, S.; Van den Broeck, W.; Remon, J. P.; De Backer, P.; Croubels, S., Feasibility of the Ussing chamber technique for the determination of in vitro jejunal permeability of passively absorbed compounds in different animal species. *J. Vet. Pharmacol. Ther.* **2011,** *34* (3), 290-7.

118. Bohets, H.; Annaert, P.; Mannens, G.; Anciaux, K.; Verboven, P.; Meuldermans, W.; Lavrijsen, K., Strategies for absorption screening in drug discovery and development. *Curr. Topics Med. Chem.* **2001,** *1* (5), 367-383.
119. Westerhout, J.; Wortelboer, H.; Verhoeckx, K., Ussing chamber. *Impact Food Bioact. Health* **2015**, 263-273.
120. Patel, N.; Forbes, B.; Eskola, S.; Murray, J., Use of simulated intestinal fluids with Caco-2 cells and rat ileum. *Drug Dev. Ind. Pharm.* **2006,** *32* (2), 151-161.
121. Kansy, M.; Senner, F.; Gubernator, K., Physicochemical high throughput screening: parallel artificial membrane permeation assay in the description of passive absorption processes. *J. Med. Chem.* **1998,** *41* (7), 1007-10.
122. Falavigna, M.; Klitgaard, M.; Brase, C.; Ternullo, S.; Skalko-Basnet, N.; Flaten, G. E., Mucus-PVPA (mucus Phospholipid Vesicle-based Permeation Assay): An artificial permeability tool for drug screening and formulation development. *Int. J. Pharm.* **2018,** *537* (1-2), 213-222.
123. Naderkhani, E.; Vasskog, T.; Flaten, G. E., Biomimetic PVPA in vitro model for estimation of the intestinal drug permeability using fasted and fed state simulated intestinal fluids. *Eur. J. Pharm. Sci.* **2015,** *73*, 64-71.
124. di Cagno, M.; Bibi, H. A.; Bauer-Brandl, A., New biomimetic barrier Permeapad for efficient investigation of passive permeability of drugs. *Eur. J. Pharm. Sci.* **2015,** *73*, 29-34.
125. Berben, P.; Brouwers, J.; Augustijns, P., The artificial membrane insert system as predictive tool for formulation performance evaluation. *Int. J. Pharm.* **2018,** *537* (1-2), 22-29.
126. Flaten, G. E.; Luthman, K.; Vasskog, T.; Brandl, M., Drug permeability across a phospholipid vesicle-based barrier 4. The effect of tensides, co-solvents and pH changes on barrier integrity and on drug permeability. *Eur. J. Pharm. Sci.* **2008,** *34* (2-3), 173-80.
127. Yalkowsky, S. H., *Solubility and solubilization in aqueous media*. American Chemical Society: 1999.
128. Katneni, K.; Charman, S. A.; Porter, C. J., Permeability assessment of poorly water-soluble compounds under solubilizing conditions: the reciprocal permeability approach. *J. Pharm. Sci.* **2006,** *95* (10), 2170-85.
129. Poelma, F. G. J.; Breäs, R.; Tukker, J. J.; Crommelin, D. J. A., Intestinal Absorption of Drugs. The Influence of Mixed Micelles on on the Disappearance Kinetics of Drugs from the Small Intestine of the Rat. *J. Pharm. Pharmacol.* **2011,** *43* (5), 317-324.
130. Bergström, C. A. S.; Charman, W. N.; Porter, C. J. H., Computational prediction of formulation strategies for beyond-rule-of-5 compounds. *Adv. Drug Delivery Rev.* **2016,** *101*, 6-21.
131. Casalini, T., Not only in silico drug discovery: Molecular modeling towards in silico drug delivery formulations. *J. Controlled Release* **2021,** *332*, 390-417.
132. Mullard, A., New drugs cost US $2.6 billion to develop. *Nat. Rev. Drug Discovery* **2014,** *13* (12), 877.

Chapter I: Predicting bile and lipid interaction for drug substances

Jonas Schlauersbach[1, #], Josef Kehrein[1, #], Simon Hanio[1], Bruno Galli[2], Cornelius Harlacher[2], Christopher Heidenreich[1], Bettina Lenz[1], Christoph Sotriffer[1], Lorenz Meinel[1,3, *]

[1] Institute for Pharmacy and Food Chemistry, University of Wuerzburg, Am Hubland, DE-97074 Wuerzburg, Germany

[2] Novartis Pharma AG, Lichtstrasse 35, CH-4056 Basel, Switzerland

[3] Helmholtz Institute for RNA-based Infection Biology (HIRI), Josef-Schneider-Straße 2/D15, DE-97080 Wuerzburg, Germany

[#] These authors contributed equally to this work.

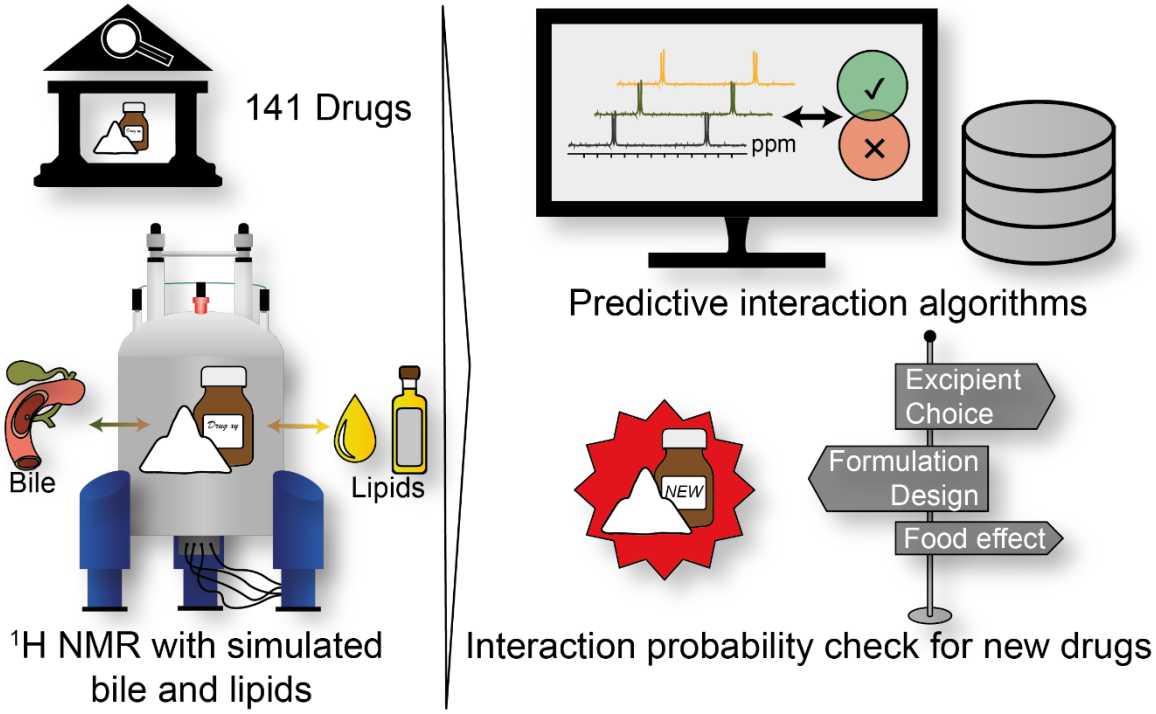

This chapter was originally published in Molecular Pharmaceutics. Reprinted with permission from Schlauersbach, J.; Kehrein, J. et. al. "Predicting Bile and Lipid Interaction for Drug Substances." *Molecular Pharmaceutics* **2022,** 19 (8), 2868-2876. Copyright 2022 American Chemical Society

*Corresponding author: Prof. Dr. Dr. Lorenz Meinel, Institute for Pharmacy and Food Chemistry, University of Wuerzburg, Am Hubland, DE-97074 Wuerzburg, Germany, E-Mail: lorenz.meinel@uni-wuerzburg.de

Abstract

Predicting biopharmaceutical characteristics and food effects for drug substances may substantially leverage rational formulation outcomes. We established a bile and lipid interaction prediction model for new drug substances and further explored the model for the prediction of bile-related food effects. 141 drugs were categorized as bile and/or lipid interacting and non-interacting drugs, respectively, using ^{1}H **n**uclear **m**agnetic **r**esonance (**NMR**) spectroscopy. **Q**uantitative **s**tructure-**p**roperty **r**elationship (**QSPR**) modeling with 2D molecular descriptors was applied to predict a drug's interaction with bile and/or lipids. Bile interaction, for example, was indicated by two descriptors characterizing polarity and lipophilicity with high balanced accuracy of 0.8. Furthermore, predicted bile interaction correlated with a positive food effect. Reliable prediction of drug substance interaction with lipids required four molecular descriptors with a balanced accuracy of 0.7. These described a drug's shape, lipophilicity, aromaticity, and hydrogen bond acceptor capability. In conclusion, reliable models might be found through drug libraries characterized for bile interaction by NMR. Furthermore, there is potential for predicting bile-related positive food effects.

Introduction

In silico molecular modeling may substantially leverage formulation development by providing *a priori* working hypotheses.[1, 2] Thereby, a trial and error approach may be replaced by rational development schemes following predicted avenues to success.[3, 4] One way of building such models is by generalizing molecular interactions seen for many drug substances with relevant biopharmaceutical input parameters, including bile.[5-7] The complexity of bile is approximated by surrogate media, including **fa**sted and **fe**d **s**tate **s**imulating **i**ntestinal **f**luids (**FaSSIF/FeSSIF**) containing **t**auro**c**holate (**TC**), **l**ecithin (**L**), and lipids.[8-10] Some poorly water-soluble drugs and vitamins rely on solubilization with bile, such as apparent solubility improvement or transport across mucus.[11, 12] Impairing bile-solubilization by pharmaceutical excipients including frequently chosen polymers may reduce bioavailability.[13, 14]

Furthermore, bile-driven increase of apparent solubility was linked to a positive food effect.[15, 16] Therefore, reliable prediction of drug-bile interactions is valuable for development. In general, high lipophilicity, charge, structural flexibility, and molecular weight favor bile interaction.[17, 18] One software predicts drug solubility in FaSSIF, but neither the source data nor the selected molecular descriptors are disclosed.[19-21] Other studies predicted solubility enhancement by bile using **q**uantitative **s**tructure-**p**roperty **r**elationships (**QSPR**) with molecular descriptors, as done in this study, or Abraham solvation descriptors.[22, 23] These studies generally relied on published solubility data.[24, 25]

The overall aim of our study was a dataset classifying drugs into bile and lipid interacting or non-interacting drugs and correlating the interactions with QSPR models. Therefore, ^{1}H NMR drug signal shift patterns of 141 drugs were collected in **p**hosphate-**b**uffered **s**aline pH 6.5 (**PBS**), PBS with TC/L, and PBS with TC/L and lipids. All drugs were systematically classified as bile or lipid interacting or non-interacting, respectively, using the ^{1}H NMR shifts of Metoprolol for reference. Metoprolol was previously characterized as not interacting with TC/L or lipids.[13, 26] The classification led to molecular descriptors and models for predicting TC/L and lipid interaction. The bile interaction model was further tested for predicting bile-related food effects.

Materials and methods

Materials

Drugs used in the study were purchased or gifted as listed in the supplementary information (**Table S1, S2**). Hexadeuterodimethyl sulfoxide (DMSO-d_6, 99.8 % D) was purchased from Euriso-top (Saarbrücken, Germany) and deuterated water (D_2O, 99.9 % D) from Deutero GmbH (Kastellaun, Germany). Deuterated water (D_2O, 99.9 % D) containing 0.05% 3-(trimethylsilyl)-propionic-2,2,3,3-d_4 sodium salt (TSP-d_4), 40 % sodium deuteroxide in deuterated water (NaOD, 99 % D), 35% deuterium chloride in deuterated water (DCl, 99 % D), sodium chloride (99 %), monobasic sodium phosphate monohydrate (99 %), were purchased from Sigma-Aldrich (Schnelldorf, Germany). Coaxial insert tubes and NMR tubes (5 mm, clear glass) were purchased from Norell (Landisville, PA, USA). Fasted state simulating intestinal fluid, fed state simulating intestinal fluid (FaSSIF/FeSSIF) V1 and FeSSIF V2 powder were purchased from biorelevant.com Ltd (London, UK). All other standard chemicals and laboratory consumables, if not stated otherwise, were purchased from either VWR International GmbH (Ismaning, Germany) or Sigma-Aldrich.

Methods

Media preparation

Modified PBS pH 6.5 was prepared in deuterated water following the manufacturer's protocol (biorelevant.com). This buffer, from now on referred to as PBS, was used for biorelevant media preparation (**Table 1**). A 1.5-fold higher concentration for FeSSIF-V2 than described by the manufacturer was chosen to align the **t**auro**c**holate (**TC**) concentration between FeSSIF-V1 and FeSSIF-V2. For pH adjustment in deuterated water a correction factor was used adjusting pD to 6.91 using DCl and NaOD.[27]

Table 1: Composition and definition of simulated intestinal media used within the study.

Component	Purpose	Modified FeSSIF-V1 "TC/L" [mmol/l]	Modified FeSSIF-V2 "TC/L with lipids" [mmol/l]
Sodium **t**auro**c**holate (**TC**)	natural bile salt	15	15
Lecithin (**L**)	natural surfactant	3.75	3
Sodium oleate	digestive product ("lipid")	-	1.2
Glycerol monooleate	digestive product ("lipid")	-	6.5

^{1}H nuclear magnetic resonance spectroscopy

For ^{1}H NMR measurements, a 0.1 mol/l DMSO-d_6 drug stock solution was prepared. Drug stock solution was added to the respective media resulting in 1 mmol/l nominal drug concentration. The amount of DMSO-d_6 did not exceed 1% (V/V). Samples were vortexed (VTX-3000L, LMSCO. LTD., Tokyo, Japan) for 30 s and filled into NMR tubes with coaxial inserts containing 0.05% TSP-d_4 in D_2O. ^{1}H NMR spectra were recorded on a Bruker Avance 400 MHz spectrometer (Bruker BioSpin GmbH, Karlsruhe, Germany) operating at 400.13 MHz with a BBI BB-H 5 mm probe head at a temperature of 300 K as previously described [13]. In brief, the acquisition parameters were set to 256 scans, flip angle of 30°, a broad spectral width of 20.55 ppm to record all possible signals, and a transmitter offset of 6.175 ppm. The acquisition time was 3.985 seconds, followed by a relaxation delay of 1.0 seconds with collection of 64 000 data points at a sample spinning frequency of 20 Hz to ensure proper signal resolution (no spinning sidebands were observed). One NMR measurement lasted 21 min. Spectra were processed using TopSpin 4.0.6 (Bruker BioSpin). Automatic baseline correction and manual phasing were applied. The chemical shifts were referenced to the external standard of TSP-d_4. ^{1}H NMR spectra were rescaled with a fixed receiver gain of 128, 254 scans, and 9 ms pulse length. Drug aryl-proton signal shifts and intensity alterations within the media were manually evaluated. The drug/medium mixture with the highest drug-aryl proton signal intensity was identified. Drug aryl-proton signal shifts in PBS to PBS with TC/L and PBS with TC/L to TC/L with lipids were characterized. The absolute mean shift value of detectable drug aryl-proton signals was used for characterization. If a drug had no aryl-protons, signals separated from TC/L signals were used for analysis. For Atovaquone, Itraconazole, and Trametinib which had no evaluable proton signals, a mean shift of TC protons (TC H7, H12, H18, H21, and H18) greater than 0.003 ppm as seen for Metoprolol was set as threshold indicating TC interaction.

Model generation

Out of the 141 drugs characterized by ^{1}H NMR, 13 compounds possessing a pKa value of 6.5 ± 0.7 according to literature were withdrawn for model generation, as protonation states were considered ambiguous in these cases (**Figure 1A, Table S1**). Furthermore, butylscopolammonium bromide and neostigmine bromide were withdrawn, as QikProp descriptors cannot be calculated for quaternary ammonium groups.[28] The remaining 126 drugs were classified into TC/L interacting and TC/L non-interacting, corresponding to the

^{1}H NMR classification (*vide supra*). Furthermore, drugs were classified into lipid interacting and lipid non-interacting. Protonation at pH 6.5 and subsequent energy minimization of 3D conformers of these drugs using the MMFF94x force field were performed with **M**olecular **O**perating **E**nvironment (**MOE**) 2020.09 with manual validity inspection.[29, 30] Racemic mixtures were modeled by one enantiomer. 2366 2D and 3D descriptors available within MOE, QikProp, and the PaDEL-Descriptor software were calculated.[31] A subset of 796 parameters describing ADME properties, lipophilicity, molecule composition, charge, and shape was created. During each model building process, descriptors with non-unique or missing values for any molecule were removed. Highly correlated descriptors (intercorrelation limit: 0.99) and variables with near-zero variance were removed. 18 drugs were randomly selected as an external **h**oldout **s**et (**HS**) for subsequent validation (**Table S1**).

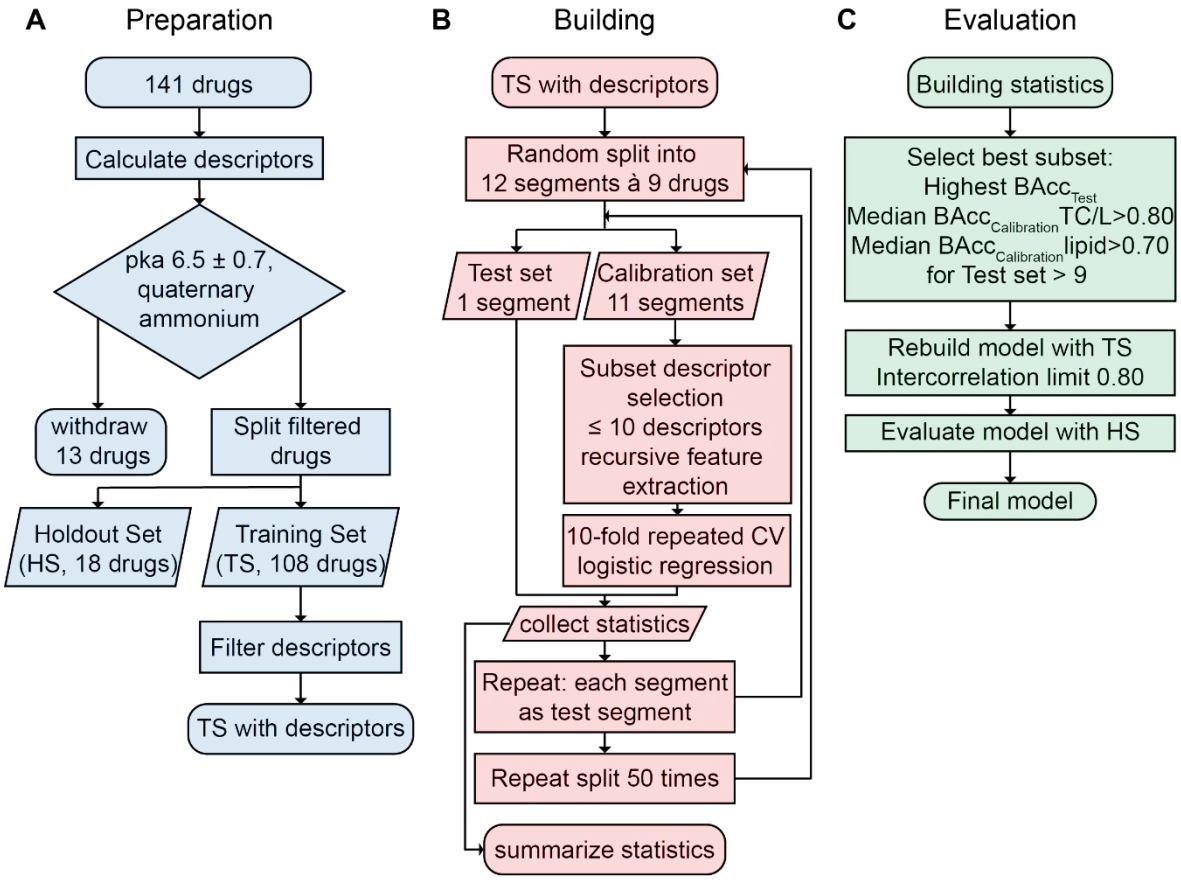

Figure 1: Schematic model building flowchart. (A) Drug and descriptor set was prepared, (B) models were generated, and (C) evaluated.

The remaining 108 drugs were deployed as **t**raining **s**et (**TS**). The whole descriptor set and the descriptor subset prediction models for TC/L and lipid interaction were generated

(**Figure 1B**). Binomial logistic regression models were developed, relying on a repeated double **c**ross-**v**alidation (**CV**) method to determine important descriptor subsets [32]. The TS was randomly split into 12 segments (each consisting of 9 molecules). One segment was used as a test set. The remaining 11 training segments (referred to as the calibration set) together were subjected to 50 runs of **r**ecursive **f**eature **e**xtraction (**RFE**).[33] The maximum number of selected descriptors was limited to 10. Logistic regression models were generated for all descriptor subsets selected by the RFE approach, based on the calibration set, applying a 10-fold repeated CV using the caret R package 6.0-84.[34] Data were centered and scaled. Model performance was examined with each training segment as test segment (12 inner loops). Afterwards, the TS was reordered into 12 new segments. This process was repeated 50 times. Training and test segment statistics were collected in each run. Finally, the parameter subset with the highest median value of **ba**lanced **ac**curacy (**BAcc**, Eq. 1) for all test segments was selected, provided that at least 10 test segments were tested with the subset and a median $BAcc_{Calibration}$ value of at least 0.80 for TC/L interaction models and 0.70 for lipid interaction models was retrieved (**Figure 1C**, **S1**).

$$BAcc = \frac{(specificity+selectivity)}{2} \quad \text{(Eq. 1)}$$

Parameters with a high correlation (intercorrelation limit: 0.70) within the final subset were subsequently removed. Then, a final logistic regression model was generated based on the whole TS. All models were validated with the external HS. The balanced accuracies and **a**reas **u**nder the receiver operating characteristic **c**urves (**AUC**) were calculated. At last, the probability p of a drug to interact with TC/L or lipids ranging between a value of 0 and 1 was calculated using the following equation (Eq. 2).[35]

$$p = \frac{1}{1+e^{-(\beta_0+\beta_1 x_1+\cdots+\beta_i x_i)}} \quad \text{(Eq. 2)}$$

wherein β_0 was the intercept and β_i were the coefficients of the scaled descriptor values x_i of a model with i descriptors. Before model generation, data was transformed by centering and scaling. Thus, the descriptor x_i can be described using TS mean and standard deviation of the descriptor value (Eq. 3).

$$x_i = \frac{(Original\ descriptor\ value - Mean\ descriptor\ value\ of\ TS)}{Standard\ deviation\ for\ the\ descriptor\ values\ of\ TS} \quad \text{(Eq. 3)}$$

Results

Drug classification by ^{1}H nuclear magnetic resonance spectroscopy

We referenced all drugs to the ^{1}H-NMR signal shifts seen for Metoprolol's aryl-proton signals. Metoprolol is a bile non-interacting and lipid non-interacting molecule.[13, 26] Based on these Metoprolol experiments, a drug's mean aryl-proton signal shift exceeding 8 Hz in the presence and absence of TC/L, respectively, classified it as bile-interacting (**Table 2**). Drugs with no signals in PBS (e.g., solubility constraints; signal to noise ratio < 10) but in TC/L were classified as bile-interacting. The threshold for drug-lipid interaction was also based on Metoprolol pilot experiments. Lipid interaction was postulated when the drug mean aryl-proton signal shift exceeded 8 Hz in TC/L with lipids compared to TC/L without lipids and for drugs leading to intensity increases with TC/L with lipids compared to TC/L without lipids. Furthermore, the medium with the highest relative signal intensity was determined. We defined the following six patterns (**Figure 2**, **Table 2**, **S1**).

Table 2: Drug classification by ^{1}H NMR aryl-proton signal shift pattern analysis.

Pattern	Medium with highest signal intensity	Mean shift in TC/L*	Mean shift in TC/L with lipids*	TC/L interaction	Lipid interaction	Number of drugs
1	PBS	< 8 Hz	<8 Hz	No	No	51
2	PBS	>8 Hz	<8 Hz	Yes	No	25
3	PBS	>8 Hz	>8 Hz	Yes	Yes	21
4	TC/L	>8 Hz	<8 Hz	Yes	No	19
5	TC/L with lipids	<8 Hz	>8 Hz	No	Yes	5
6	TC/L or TC/L with lipids	>8 Hz	>8 Hz	Yes	Yes	20

*Compared to without TC/L

Pattern 1 (all shifts < 8 Hz) was seen for 51 drugs, as shown for Sulfamethoxazole (**Figure 2A**). Drugs were assigned to pattern 2 if they interacted with TC/L but not with lipids and had the highest signal intensity in PBS. Ciprofloxacin is one of the 25 examples within this pattern (**Figure 2B**). Domperidone, and further 20 drugs, indicated pattern 3 showing interaction with TC/L and lipids and having the highest relative signal intensity in PBS (**Figure 2C**). 19 drugs manifested type 4 patterns (interaction with TC/L but not with lipids and highest signal intensity with TC/L), as shown for Amiodarone (**Figure 2D**). 5 drugs had pattern 5 (interaction with lipids but not TC/L and with the highest signal intensity in TC/L with lipids), as shown for Menadione (**Figure 2E**). 20 drugs imitated pattern 6, TC/L and

lipid interacting and with the highest signal intensity in either TC/L or TC/L with lipids, as shown for Glibenclamide (**Figure 2F**).

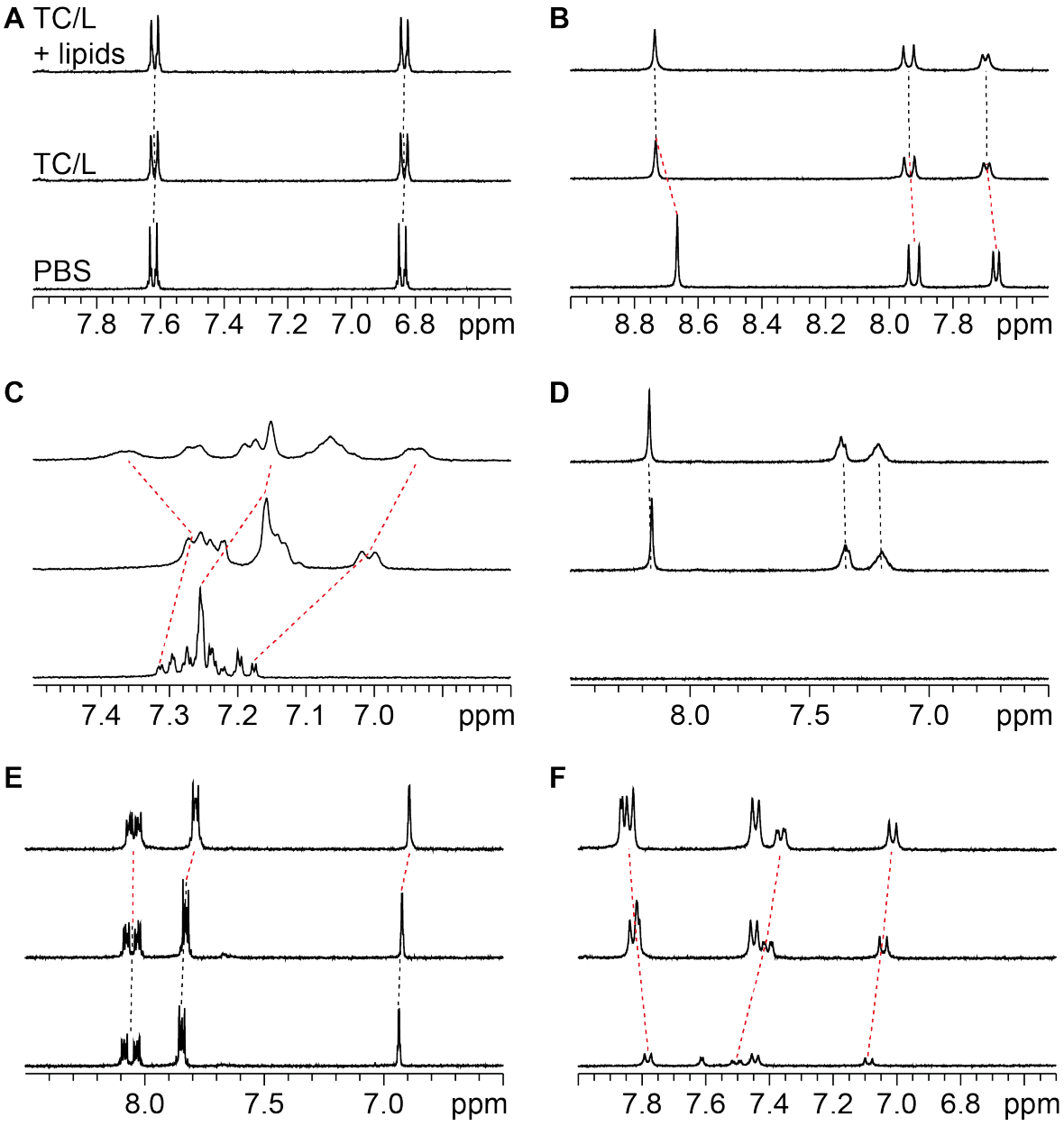

Figure 2: Drug aryl-proton signal patterns as observed by ^{1}H-NMR. Aryl-proton regions are shown in PBS (bottom), with TC/L (middle), and with TC/L and lipids (top). Shifts greater than 8 Hz are indicated with red dotted lines. Shifts below 8 Hz are marked with black dotted lines. (A) Sulfamethoxazole spectra extracts are shown as an example for pattern 1, (B) Ciprofloxacin for pattern 2, (C) Domperidone for pattern 3, (D) Amiodarone for pattern 4, (E) Menadione for pattern 5, and (F) Glibenclamide for pattern 6, respectively. The spectra intensity scaling was kept constant in all panels.

Prediction models

We calculated **ba**lanced **ac**curacies (**BAcc**) and **a**reas **u**nder the receiver operating characteristic **c**urves (**AUC**) for the **t**raining **s**et (**TS**) and **h**oldout **s**et (**HS**) of the final classification models using either the whole descriptor set, or the descriptor subset (**Table 3, 4**). Furthermore, **r**eceiver **o**perating **c**haracteristic (**ROC**) curves were computed for the TS and the HS (**Figure S2**). The threshold for interaction assertion was $p \geq 0.5$. TC/L interaction prediction models 1 and 2 showed a BAcc for the TS of 0.86 and 0.84, respectively. The AUC_{TS} was 0.93 and 0.90. Lipid interaction models 3 and 4 had a BAcc for the TS of 0.73 and 0.68, and an AUC_{TS} of 0.81 and 0.80. Models 2 and 3 had a substantially higher BAcc and AUC for the HS compared to models 1 and 4, respectively.

Table 3: Training set (TS) and holdout set (HS) balanced accuracies (BAcc) and areas under the receiver operating characteristic curves (AUC) of the final prediction models for TC/L interaction (models 1 and 2) and lipid interaction (models 3 and 4).

Metric	**Model 1** **TC/L interaction** **Whole descriptor set**	**Model 2** **TC/L interaction** **Descriptor subset**	**Model 3** **Lipid interaction** **Whole descriptor set**	**Model 4** **Lipid interaction** **Descriptor subset**
	Model 1	**Model 2**	**Model 3**	**Model 4**
$BAcc_{TS}$	0.86	0.84	0.73	0.68
AUC_{TS}	0.93	0.90	0.81	0.80
$BAcc_{HS}$	0.67	0.83	0.75	0.59
AUC_{HS}	0.83	0.93	0.83	0.74
Descriptors	3	2	4	7

Two molecular descriptors, Crippen's molar refractivity (CrippenMR[36]) and the octanol/water distribution coefficient at pH 7 (h_logD[37]), predicted the experimentally observed drug-bile interaction in model 2 (**Figure 3**). The prediction of drug-lipid interaction required 4 descriptors using model 3 (the average coefficient sum of the last eigenvector from detour matrix (VE2_Dt[38]), the sum of Kier-Hall electro-topological states for weak hydrogen bond acceptors (SwHBa[39]), the octanol/water partition coefficient (SlogP[36]), and the Hückel theory-based sum of *log (1 + π bond order)* for all bonds (h_log_pbo[40]); **Table S3**).

Table 4: Descriptors used for models 1-4. Descriptor software, regression coefficients for scaled data, mean value ± SD for TS of the unscaled data, and the definition of the descriptors are shown. Calculated model intercept β_0 is also defined.

Model	Descriptor	Software	Regression coefficient β_i	Mean ± SD for TS	Definition
1	CrippenLogP(o/w)	PaDEL	1.182	2.05 ± 2.25	Crippen's LogP[36]
1	SpMin1_Bhi	PaDEL	1.500	1.85 ± 0.11	Smallest absolute eigenvalue of Burden modified matrix - n 1 / weighted by relative first ionization potential[41]
1	MDEC 23	PaDEL	1.255	15.73 ± 8.80	Molecular distance edge between all secondary and tertiary carbons[37]
Intercept β_0 model 1: 0.405					
2	CrippenMR	PaDEL	1.976	90.81 ± 35.30	Crippen's molar refractivity[36]
2	h_logD	MOE	1.163	2.01 ± 1.88	The octanol/water distribution coefficient at pH 7, calculated as a state average: log sum ($10^{h\_logP_i - pC_i}$). h_logP_i and pC_i are the calculated logP value and the log concentration (normalized to a sum of 1) of protonation state i [30]
Intercept β_0 model 2: 0.800					
3	VE2_Dt	PaDEL	-0.782	0.01 ± 0.01	Average coefficient sum of the last eigenvector from detour matrix[38]
3	SwHBa	PaDEL	0.624	12.85 ± 8.96	Sum of Kier-Hall E-states for weak hydrogen bond acceptors [39]
3	SlogP	MOE	0.474	2.10 ± 1.99	Log octanol/water partition coefficient [36]
3	h_log_pbo	MOE	0.036	7.12 ± 3.35	Sum of log (1 + π bond order) for all bonds (Hückel theory descriptor)[40]
Intercept β_0 model 3: -8.088					
4	A_aro	MOE	0.237	9.66 ± 5.99	Number of aromatic atoms[30]
4	ASA+	MOE	0.724	193.93 ± 72.60	Solvent-accessible surface area of atoms with positive partial charge using a probe radius of 1.4 Å[30]
4	ETA_Eta_F_L	PaDEL	-1.422	5.05 ± 2.10	Extended topochemical atom (ETA) index: local functionality contribution EtaF_local[42]
4	nwHBa	PaDEL	1.403	10.91 ± 5.21	Count of E-States for weak hydrogenbond acceptors[39]
4	SHother	PaDEL	0.225	2.91 ± 1.83	Sum of atom-type H E-State: H on aaCH, dCH2 or dsCH[39]
4	SlogP	MOE	0.761	2.10 ± 1.99	Log octanol/water partition coefficient[36]
4	SwHBa	PaDEL	-0.637	12.85 ± 8.96	Sum of Kier-Hall E-states for weak hydrogen bond acceptors[39]
Intercept β_0 model 4: -0.755					

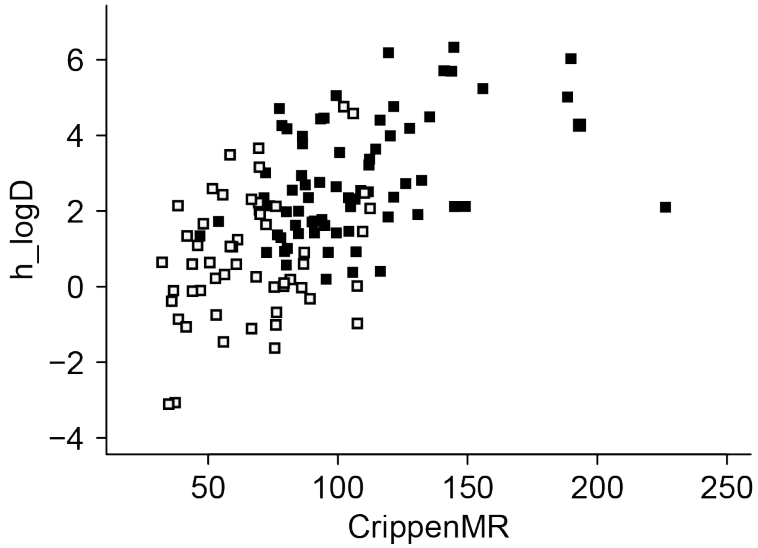

Figure 3: Visualization of descriptors used in model 2 (TC/L interaction). The X-axis shows the calculated CrippenMR value, the Y-axis the drug's h_logD. TS and HS drugs were included. Black boxes indicate drugs interacting with TC/L, and empty boxes indicate TC/L non-interacting drugs determined by ^{1}H NMR.

Model evaluation to ^{1}H nuclear magnetic resonance signal shifts

The respective measured drugs' mean aryl-proton signal shift was plotted against the calculated probability of TC/L interaction (**Figure 4A**, model 2) and interaction with lipids (**Figure 4B,** model 3). Type II error (false positive prediction) was seen for drugs with a signal shift below the threshold of 8 Hz, and a calculated probability of interaction of at least 0.5.

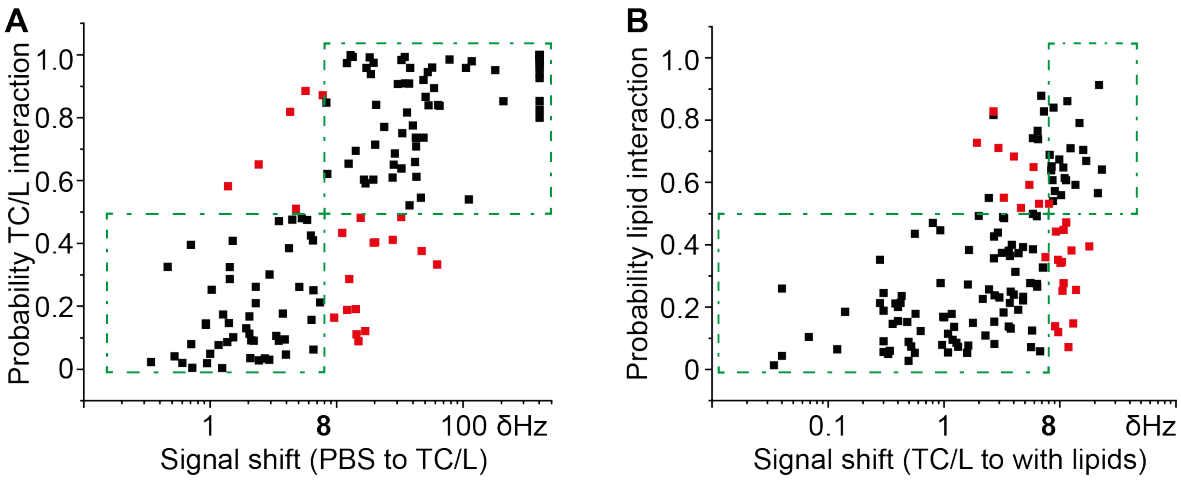

Figure 4: Mean drug aryl-proton signal shifts (experimentally assessed data) plotted against respective probability to interact with (A) TC/L and (B) lipids (calculated by respective model). All analyzed drugs were included and are represented as boxes. Black boxes were drugs with matching signal shift and interaction probability. Green dashed borders show correctly asserted data spaces. Black boxed drugs beyond the green dashed border represent drugs which were identified as lipid interacting by highest signal intensity in TC/L with lipids (**Table S1**). Red boxes were falsely predicted drugs (Type I and II error).

Drugs with a signal shift exceeding 8 Hz and a computed probability below 0.5 reflected a type I error (false negative prediction). These falsely asserted drugs represent the inaccuracy of our generated models.

Model evaluation to predict bile dependent food effects

TC/L interaction probabilities were calculated using model 2 for 38 drugs, previously reported regarding a bile-dependent food effect (**Figure 5**).[15] There the authors calculated the dose number using the orally administered standard dose and determined its solubility in FaSSIF (Eq. 4).

$$Dose\ number = \frac{Dose\ [mg]}{Solublity(FaSSIF)\left[\frac{mg}{ml}\right] \cdot 250\ [ml]} \qquad \text{(Eq. 4)}$$

The solubility ratio (FeSSIF/FaSSIF) was computed using shake flask solubility of respective drugs in media (Eq. 5). Drugs with a high solubility ratio showed high bile-dependent solubilization.

$$Solubility\ ratio = \frac{Solublity(FeSSIF)}{Solublity(FaSSIF)} \qquad \text{(Eq. 5)}$$

The clinical food effect obtained from literature was divided into positive (ratio AUC fed/AUC fasted larger than 1.1, yellow), no effect (ratio 1.1-0.9, blue), and negative (ratio smaller than 0.9, red). Drugs with a positive food effect were found at a solubility ratio of at least 1.5 and a dose number exceeding 2 (**Figure 5A**).

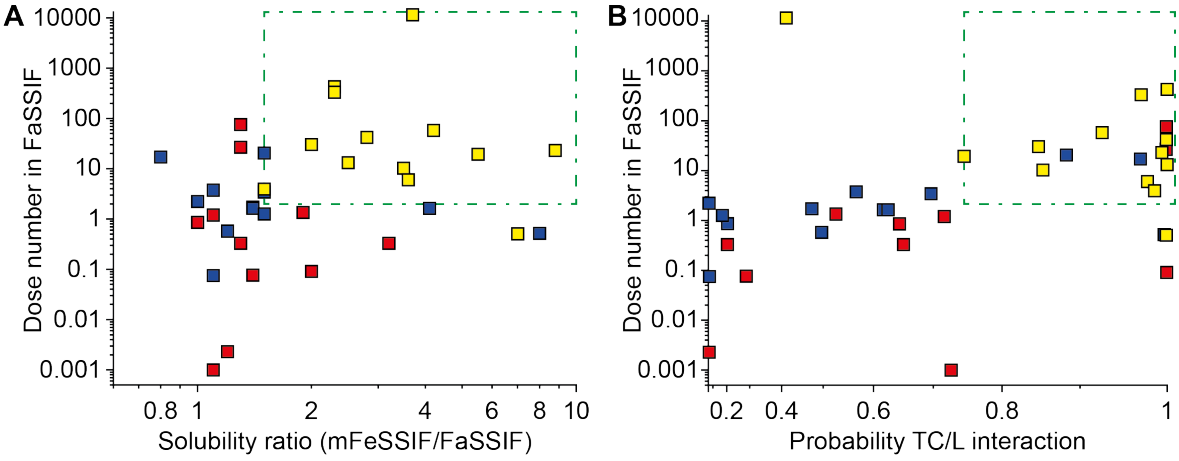

Figure 5: (A) Visualization of bile-dependent food effect described in literature [15]. Green dashed border represents drugs with solubility ratio ≥ 1.5 and dose number over 2. (B) Correlation of dose number with TC/L interaction probability calculated by model 2. Green dashed border represents drugs with a likelihood for TC/L interaction of ≥ 0.75 and dose number over 2. One outlier (Albendazole) was asterisked. Yellow boxes indicate drugs with positive, blue with no effect, and red with negative food effect, respectively.

We now plotted the dose number of these drugs against their calculated probability to interact with TC/L using model 2 (**Figure 5B**). Drugs had a likelihood for a positive food effect for probabilities of TC/L interaction of at least 0.75 and a dose number exceeding 2. Thereby, all drugs with positive food effects were within these limits, except for Albendazole and Azelnidipine.

Discussion

^{1}H NMR signal shifts and intensity changes were analyzed for 141 drugs in PBS, in the presence of TC/L, and TC/L with lipids, and six patterns were differentiated classifying drugs into TC/L and lipid interacting (**Figure 2, Table S1, Table 2**).[13, 26, 43] Within patterns 4 and 6, mainly poorly-water soluble class II and IV drugs according to the biopharmaceutical classification system were found (**Figure S3, S4**). **Q**uantitative **s**tructure-**p**roperty **r**elationship (**QSPR**) models using molecular descriptors decoded the molecular requirements for drugs interacting with TC/L and lipids (**Figure 1, 3, Table S3**), and prediction models were developed (**Table 3, 4, Figure 4**). The study further predicted potential positive food effects of 38 drugs (**Figure 5**). ^{1}H NMR signal shifts in the presence of TC/L were used as surrogates to postulate drug affinity to bile or lipids. Bile and lipid interaction has previously been linked to the preferential selection of non-bile interacting polymers for formulation.[13, 44] Likewise, an identified interaction with lipids suggests the potential for developing stable lipid-based formulations.[45-47] This study aimed to complement experimental needs for identifying bile and lipid interaction by calculating predictive models from molecular descriptors.

Prediction models for TC/L and lipid interaction were generated based on experimentally characterized drugs. Balanced accuracy distributions for calibration sets and test segments differed, as new models within each loop during the building process were trained on the former and subsequently validated against the latter **(Figure 1, S1).** This cross-validation process was used to assess the initial modeling performance of various possible descriptor selections. $BAcc_{Calibration}$ and $BAcc_{Test}$ distributions for descriptor selections with the highest median $BAcc_{Test}$ values indicated a good overall performance **(Figure S1)**. In agreement with these statistics, results for the final models regarding training and holdout sets **(Figure S2; Table 3)** were overall better for TC/L interaction models, compared to lipid interaction models. Models 2 and 3 showed a high predictive performance on new drug substances of

the external holdout set. In comparison, greater differences between statistics of the training and holdout sets in case of models 1 and 4 signalled a more limited external predictivity. Conclusively, our final TC/L and lipid interaction models 2 and 3 predicted a drug's interaction with bile and lipids (**Figure 4, S2; Table 3, S3**). Furthermore, we and others hypothesized that bile interaction might be linked to positive food effects, a piece of relevant information that might substantially reduce the risk in early drug development, including the setup of early clinical trials.[15, 16, 19, 20, 48-50] For example, a recently published study correlated food effect of drugs with their dose number and solubility ratio (solubility in FeSSIF compared to solubility in FaSSIF) and a positive food effect correlated with a high dose number and solubility ratio (**Figure 5A**).[15] We calculated the TC/L interaction probability for the same drug set and plotted the probability against the dose number (**Figure 5B**), as well as solubility ratio (**Figure S3**). Our models were also able to correlate a positive food effect using TC/L interaction prediction instead of FeSSIF/FaSSIF solubility ratio. The solubility ratio plotted against TC/L interaction probability was as well predictive (**Figure S3**). We also observed some drugs deviating from this relationship. For example, Albendazole has a positive food effect, and a low predicted TC/L interaction probability of 0.4 (**Figure 5**). Previous studies confirmed the difficulty of predicting Albendazole patterns to bile interaction, a drug marginally benefitting from the presence of higher concentrations of TC/L and lipids (FaSSIF 1.8 µg/ml vs. FeSSIF 6.6 µg/ml) while being used at relatively high doses (5200 mg/day).[15] Albendazole's positive food effect was linked to CYP3A4 inhibition in the intestinal epithelium and delayed gastric emptying, pharmacokinetic and (patho-) physiologic parameters, which cannot be captured by our bile-derived models.[51] Therefore, Albendazole outcome nicely indicated the boundaries of our models. Our models were predictive only for bile related food effects. Expanding these by patient-centric aspects such as delayed gastric emptying will be an exciting task for the future.

Previously, more complex models were developed to predict drug-bile interaction reflecting lipophilicity, charge, flexibility, and molecular weight.[17, 18, 22, 23] This study expanded off these outcomes in that as few as 2 descriptors, resulting from atom-based contributions (h_logD, CrippenMR; model 2)[30, 36], might be sufficient for the prediction of TC/L interaction. The h_logD is a well-known descriptor that categorizes drugs by lipophilicity. CrippenMR is a predictor for the molar refractivity of a substance. The latter can be derived by the Lorentz-Lorenz equation and essentially depends on the molecular size and dispersive interactions, hence molecular polarizability.[52-54] Therefore, lipophilic drugs with higher

molecular weight *and* simultaneous ability to acquire an electric dipole moment (e.g., possessing aromatic rings and halogen atoms) are more likely to interact with TC/L. The situation is slightly more complex for interaction with lipids. We identified 4 descriptors leading to meaningful prediction, some of which being rather abstract. For example, the descriptor VE2_Dt represents the average coefficient sum of the last eigenvector from the detour matrix. The latter is a matrix describing all distances between atoms of a molecule. Topological indices based on such matrices were previously used to model structure-boiling point relationships. More branched alkanes showed smaller values than linear isomers for such indices.[38] In our data set, we noticed that symmetric molecules (e.g., Bisacodyl or Diphenhydramine) showed small VE2_Dt values and, thus, a high probability of lipid interaction. Other descriptors positively correlated with lipid interaction were the electronegativity of hydrogen bond acceptors (SwHBa),[39] the octanol/water partition coefficient (SlogP)[36], and the molecular aromaticity (h_log_pbo).[40] Based on intrinsic values for 35 different atom groups, Kier-Hall electro-topological states, determining the value of the descriptor SwHBa, describe the amount of valence and sigma electrons of atoms taking their surrounding chemical environment into account.[39] The descriptor h_log_pbo represents a summation of all π bond orders of the molecule calculated according to Hückel theory. Hence, unsaturated systems seem to be favored for lipid interactions.[40] These results confirmed previous findings. A drug's potential for interaction with lipids cannot reliably predicted by logP alone.[55, 56]

Conclusion

We successfully generated interpretable QSPR-based models for TC/L and lipid interaction using NMR data with acceptable balanced accuracies (0.8 and 0.7, respectively). Only 2 descriptors were needed for the TC/L interaction model describing polarizability and lipophilicity of a molecule. 4 descriptors were integrated into a lipid interaction model using descriptors of molecule shape, hydrogen bond acceptor capability, lipophilicity, and aromaticity. Furthermore, high TC/L interaction probability correlated with a positive food effect. *A priori* knowledge about these interactions might flag drug substances for bile interaction and possibly bile-related positive food effects in the future. This may reduce the need for iterative preclinical study cycle during early development and may drive life-cycle management towards high quality formulations. However, the food effect is complex with multiple pharmacokinetics and pharmacodynamic causes. What is presented here fails to

predict bile-independent positive food effects (e.g., efflux pumps). Further studies are needed along these lines, possibly integrating this or similar models into one larger, overarching one available in the future.

Acknowledgements

We gratefully acknowledge the financial support by Novartis Pharma AG for JS and BASF SE for SH. This research was supported by the German Ministry of Education and Research (grant number 13XP5049B, Next-PEG). C.H. is a full-time associate of Novartis Pharma. L.M. and B.G. are former associates of Novartis Pharma.

References

1. Mullard, A., New drugs cost US $2.6 billion to develop. *Nat. Rev. Drug Discovery* **2014,** *13* (12), 877.
2. Casalini, T., Not only in silico drug discovery: Molecular modeling towards in silico drug delivery formulations. *J. Controlled Release* **2021,** *332*, 390-417.
3. Siepmann, J.; Siepmann, F., Mathematical modeling of drug dissolution. *Int. J. Pharm.* **2013,** *453* (1), 12-24.
4. Siepmann, J.; Siepmann, F., Mathematical modeling of drug delivery. *Int. J. Pharm.* **2008,** *364* (2), 328-43.
5. Yu, L. X.; Amidon, G.; Khan, M. A.; Hoag, S. W.; Polli, J.; Raju, G. K.; Woodcock, J., Understanding Pharmaceutical Quality by Design. *AAPS J.* **2014,** *16* (4), 771-783.
6. Casalini, T.; Limongelli, V.; Schmutz, M.; Som, C.; Jordan, O.; Wick, P.; Borchard, G.; Perale, G., Molecular Modeling for Nanomaterial-Biology Interactions: Opportunities, Challenges, and Perspectives. *Front. Bioeng. Biotechnol.* **2019,** *7*, 268.
7. Jones, H. M.; Parrott, N.; Ohlenbusch, G.; Lave, T., Predicting pharmacokinetic food effects using biorelevant solubility media and physiologically based modelling. *Clin. Pharmacokinet.* **2006,** *45* (12), 1213-26.
8. Riethorst, D.; Mols, R.; Duchateau, G.; Tack, J.; Brouwers, J.; Augustijns, P., Characterization of Human Duodenal Fluids in Fasted and Fed State Conditions. *J. Pharm. Sci.* **2016,** *105* (2), 673-681.
9. Dahlgren, D.; Venczel, M.; Ridoux, J. P.; Skjold, C.; Mullertz, A.; Holm, R.; Augustijns, P.; Hellstrom, P. M.; Lennernas, H., Fasted and fed state human duodenal fluids: Characterization, drug solubility, and comparison to simulated fluids and with human bioavailability. *Eur. J. Pharm. Biopharm.* **2021,** *163*, 240-251.
10. Brouwers, J.; Brewster, M. E.; Augustijns, P., Supersaturating drug delivery systems: the answer to solubility-limited oral bioavailability? *J. Pharm. Sci.* **2009,** *98* (8), 2549-72.
11. Sun, F.; Jaspers, T. C.; van Hasselt, P. M.; Hennink, W. E.; van Nostrum, C. F., A Mixed Micelle Formulation for Oral Delivery of Vitamin K. *Pharm. Res.* **2016,** *33* (9), 2168-79.
12. Meaney, C.; O'Driscoll, C., Mucus as a barrier to the permeability of hydrophilic and lipophilic compounds in the absence and presence of sodium taurocholate micellar systems using cell culture models. *Eur. J. Pharm. Sci.* **1999,** *8* (3), 167-175.
13. Schlauersbach, J.; Hanio, S.; Lenz, B.; Vemulapalli, S. P. B.; Griesinger, C.; Poppler, A. C.; Harlacher, C.; Galli, B.; Meinel, L., Leveraging bile solubilization of poorly water-soluble drugs by rational polymer selection. *J. Control. Release* **2021,** *330*, 36-48.

14. Saal, W.; Wyttenbach, N.; Alsenz, J.; Kuentz, M., Interactions of dimethylaminoethyl methacrylate copolymer with non-acidic drugs demonstrated high solubilization in vitro and pronounced sustained release in vivo. *Eur. J. Pharm. Biopharm.* **2018,** *125*, 68-75.
15. Kawai, Y.; Fujii, Y.; Tabata, F.; Ito, J.; Metsugi, Y.; Kameda, A.; Akimoto, K.; Takahashi, M., Profiling and Trend Analysis of Food Effects on Oral Drug Absorption Considering Micelle Interaction and Solubilization by Bile Micelles. *Drug Metab. Pharmacokinet.* **2011,** *26* (2), 180-191.
16. Sugano, K.; Kataoka, M.; Mathews Cda, C.; Yamashita, S., Prediction of food effect by bile micelles on oral drug absorption considering free fraction in intestinal fluid. *Eur. J. Pharm. Sci.* **2010,** *40* (2), 118-24.
17. Ottaviani, G.; Gosling, D. J.; Patissier, C.; Rodde, S.; Zhou, L.; Faller, B., What is modulating solubility in simulated intestinal fluids? *Eur. J. Pharm. Sci.* **2010,** *41* (3-4), 452-7.
18. Persson, E. M.; Gustafsson, A.-S.; Carlsson, A. S.; Nilsson, R. G.; Knutson, L.; Forsell, P.; Hanisch, G.; Lennernäs, H.; Abrahamsson, B., The Effects of Food on the Dissolution of Poorly Soluble Drugs in Human and in Model Small Intestinal Fluids. *Pharm. Res.* **2005,** *22* (12), 2141-2151.
19. Miller, N. A.; Reddy, M. B.; Heikkinen, A. T.; Lukacova, V.; Parrott, N., Physiologically Based Pharmacokinetic Modelling for First-In-Human Predictions: An Updated Model Building Strategy Illustrated with Challenging Industry Case Studies. *Clin. Pharmacokinet.* **2019,** *58* (6), 727-746.
20. Tistaert, C.; Heimbach, T.; Xia, B.; Parrott, N.; Samant, T. S.; Kesisoglou, F., Food effect projections via physiologically based pharmacokinetic modeling: predictive case studies. *J. Pharm. Sci.* **2019,** *108* (1), 592-602.
21. Bergstrom, C. A. S.; Larsson, P., Computational prediction of drug solubility in water-based systems: Qualitative and quantitative approaches used in the current drug discovery and development setting. *Int. J. Pharm.* **2018,** *540* (1-2), 185-193.
22. Fagerberg, J. H.; Karlsson, E.; Ulander, J.; Hanisch, G.; Bergstrom, C. A., Computational prediction of drug solubility in fasted simulated and aspirated human intestinal fluid. *Pharm. Res.* **2015,** *32* (2), 578-89.
23. Niederquell, A.; Kuentz, M., Biorelevant Drug Solubility Enhancement Modeled by a Linear Solvation Energy Relationship. *J. Pharm. Sci.* **2018,** *107* (1), 503-506.
24. Wei, M.; Zhang, X.; Pan, X.; Wang, B.; Ji, C.; Qi, Y.; Zhang, J. Z. H., HobPre: accurate prediction of human oral bioavailability for small molecules. *J. Cheminformatics* **2022,** *14* (1), 1.
25. Falcon-Cano, G.; Molina, C.; Cabrera-Perez, M. A., ADME Prediction with KNIME: Development and Validation of a Publicly Available Workflow for the Prediction of Human Oral Bioavailability. *J. Chem. Inf. Model.* **2020,** *60* (6), 2660-2667.
26. Hanio, S.; Schlauersbach, J.; Lenz, B.; Spiegel, F.; Bockmann, R. A.; Schweins, R.; Nischang, I.; Schubert, U. S.; Endres, S.; Poppler, A. C.; Brandl, F. P.; Smit, T. M.; Kolter, K.; Meinel, L., Drug-Induced Dynamics of Bile Colloids. *Langmuir* **2021,** *37* (8), 2543-2551.
27. Baucke, F. G. K., Further Insight into the Dissociation Mechanism of Glass Electrodes. The Response in Heavy Water. *J. Phys. Chem. B* **1998,** *102* (24), 4835-4841.
28. *Schrödinger Release 2021-2*, Schrödinger Release 2021-2; LLC: New York, 2021.
29. Halgren, T. A., Merck molecular force field. I. Basis, form, scope, parameterization, and performance of MMFF94. *J. Comput. Chem.* **1996,** *17* (5-6), 490-519.
30. *MOE. Molecular Operating Environment (MOE), 2019.01*, Chemical Computing Group ULC: 1010 Sherbooke St. West, Suite #910, Montreal, QC, Canada, 2019.
31. Yap, C. W., PaDEL-descriptor: an open source software to calculate molecular descriptors and fingerprints. *J. Comput. Chem.* **2011,** *32* (7), 1466-74.
32. Gurian, E.; Di Silvestre, A.; Mitri, E.; Pascut, D.; Tiribelli, C.; Giuffre, M.; Croce, L. S.; Sergo, V.; Bonifacio, A., Repeated double cross-validation applied to the PCA-LDA

classification of SERS spectra: a case study with serum samples from hepatocellular carcinoma patients. *Anal. Bioanal. Chem.* **2021,** *413* (5), 1303-1312.
33. Guyon, I.; Weston, J.; Barnhill, S.; Vapnik, V., Gene Selection for Cancer Classification using Support Vector Machines. *Machine Learning* **2002,** *46* (1/3), 389-422.
34. Kuhn, M., Building Predictive Models inRUsing thecaretPackage. *J. Stat. Software* **2008,** *28* (5), 1-26.
35. James, G.; Witten, D.; Hastie, T.; Tibshirani, R., *An introduction to statistical learning*. Springer: 2013; Vol. 112.
36. Wildman, S. A.; Crippen, G. M., Prediction of physicochemical parameters by atomic contributions. *J. Chem. Inf. Comput. Sci.* **1999,** *39* (5), 868-873.
37. Liu, S.; Cao, C.; Li, Z., Approach to estimation and prediction for normal boiling point (NBP) of alkanes based on a novel molecular distance-edge (MDE) vector, λ. *J. Chem. Inf. Comput. Sci.* **1998,** *38* (3), 387-394.
38. Trinajstić, N.; Nikolić, S.; Lučić, B.; Amić, D.; Mihalić, Z., The Detour Matrix in Chemistry. *J. Chem. Inf. Comput. Sci.* **1997,** *37* (4), 631-638.
39. Lowell H. Hall, L. B. K., *The Molecular Connectivity Chi Indexes and Kappa Shape Indexes in Structure-Property Modeling*. John Wiley & Sons, Inc., 2007: 1991.
40. Gerber, P. R.; Muller, K., MAB, a generally applicable molecular force field for structure modelling in medicinal chemistry. *J. Comput.-Aided Mol. Des.* **1995,** *9* (3), 251-68.
41. Todeschini, R.; Consonni, V., *Molecular descriptors for chemoinformatics. 1. Alphabetical listing*. Wiley-VCH: 2009.
42. Roy, K.; Ghosh, G., QSTR with extended topochemical atom indices. 2. Fish toxicity of substituted benzenes. *J. Chem. Inf. Comput. Sci.* **2004,** *44* (2), 559-567.
43. Wiest, J.; Saedtler, M.; Böttcher, B.; Grüne, M.; Reggane, M.; Galli, B.; Holzgrabe, U.; Meinel, L., Geometrical and Structural Dynamics of Imatinib within Biorelevant Colloids. *Mol. Pharmaceutics* **2018,** *15* (10), 4470-4480.
44. Fine-Shamir, N.; Dahan, A., Methacrylate-Copolymer Eudragit EPO as a Solubility-Enabling Excipient for Anionic Drugs: Investigation of Drug Solubility, Intestinal Permeability, and Their Interplay. *Mol. Pharmaceutics* **2019,** *16* (7), 2884-2891.
45. Charman, W. N., Lipids, Lipophilic Drugs, and Oral Drug Delivery—Some Emerging Concepts. *J. Pharm. Sci.* **2000,** *89* (8), 967-978.
46. Silva, L. A. D.; Cintra, E. R.; Alonso, E. C. P.; Alves, G. L.; Lima, E. M.; Taveira, S. F.; da Cunha-Filho, M. S. S.; Marreto, R. N., Selection of excipients for the development of carvedilol loaded lipid-based drug delivery systems. *J. Therm. Anal. Calorim.* **2017,** *130* (3), 1593-1604.
47. Ditzinger, F.; Price, D. J.; Ilie, A.-R.; Köhl, N. J.; Jankovic, S.; Tsakiridou, G.; Aleandri, S.; Kalantzi, L.; Holm, R.; Nair, A.; Saal, C.; Griffin, B.; Kuentz, M., Lipophilicity and hydrophobicity considerations in bio-enabling oral formulations approaches – a PEARRL review. *J. Pharm. Pharmacol.* **2018,** *71* (4), 464-482.
48. Cheng, L.; Wong, H., Food Effects on Oral Drug Absorption: Application of Physiologically-Based Pharmacokinetic Modeling as a Predictive Tool. *Pharmaceutics* **2020,** *12* (7), 672.
49. Lentz, K. A., Current Methods for Predicting Human Food Effect. *AAPS J.* **2008,** *10* (2), 282-8.
50. Bennett-Lenane, H.; Griffin, B. T.; O'Shea, J. P., Machine learning methods for prediction of food effects on bioavailability: A comparison of support vector machines and artificial neural networks. *Eur. J. Pharm. Sci.* **2022,** *168*, 106018.
51. Nagy, J.; Schipper, H. G.; Koopmans, R. P.; Butter, J. J.; Van Boxtel, C. J.; Kager, P. A., Effect of grapefruit juice or cimetidine coadministration on albendazole bioavailability. *Am. J. Tropical Med. Hygiene* **2002,** *66* (3), 260-3.
52. Aronsson, R.; Karawacki, E., Refractive Index and Molar Refractivity of Molten AgNO3. *Zeitschrift für Naturforschung A* **1980,** *35* (7), 694-696.

53. Ghose, A. K.; Crippen, G. M., Atomic Physicochemical Parameters for Three-Dimensional Structure-Directed Quantitative Structure-Activity Relationships I. Partition Coefficients as a Measure of Hydrophobicity. *J. Comp. Chem.* **1986,** *7* (4), 565-577.
54. Ghose, A. K.; Crippen, G. M., Atomic physicochemical parameters for three-dimensional-structure-directed quantitative structure-activity relationships. 2. Modeling dispersive and hydrophobic interactions. *J. Chem. In.f Comput. Sci.* **1987,** *27* (1), 21-35.
55. Rane, S. S.; Anderson, B. D., What determines drug solubility in lipid vehicles: Is it predictable? *Adv. Drug Delivery Rev.* **2008,** *60* (6), 638-656.
56. Ribeiro, M. M. B.; Melo, M. N.; Serrano, I. D.; Santos, N. C.; Castanho, M. A. R. B., Drug–lipid interaction evaluation: why a 19th century solution? *Trends Pharmacol. Sci.* **2010,** *31* (10), 449-454.

Supporting information

S1 Drug classification

Table 1: Analyzed drugs and their classification according to Table 1. Shift was calculated as mean of absolute shift values for detectable drug signal pattern. If signals appeared only with TC/L, the shift was set to theoretical value of 400.129 (operating frequency). Atovaquone, itraconazole, and Trametinib TC shift was higher compared to Metoprolol. They were classified as TC/L but not lipid interacting. Compounds classified as lipid interacting due to highest signal intensity in TC/L with lipids are marked with a star (*). Drugs were divided into two modeling sets: a training set (TS) and an external holdout set (HS) for validation. If the drug was filtered due to quaternary ammonium groups or pKa values from literature near pH = 6.5 the compound is marked as belonging to the filtered set (FS). In the last two columns, the predictions for models 2 and 3 are shown as probabilities (0 = no interaction, 1 = interaction).

#	Drug/ Manufacturer (Table S2)	Solubility in water defined by Ph. Eur. 10.0	BCS classification	Shift (PBS to TC/L) (Hz)	Shift (TC/L to TC/L with lipids) (Hz)	Pattern	Set	Probability TC/L interaction (model 2)	Probability Lipid interaction (model 3)
1	Acetazolamide[1]	very slightly soluble	IV[1]	0.600	0.080	1	HS	0.02	0.10
2	Acetylsalicylic acid[2]	slightly soluble	I[2]	1.360	0.440	1	TS	0.09	0.21
3	Afatinib[3]	practically insoluble	I/III[3]	178.978	8.703	3	TS	0.95	0.54
4	Allopurinol[4]	very slightly soluble	III[4]	0.960	0.400	1	TS	0.02	0.16
5	Alpelisib[5]	practically insoluble	II[5]	53.097	5.842	2	TS	0.84	0.39
6	Ambroxol[6]	sparingly soluble	I[6]	61.940	10.083	3	TS	0.33	0.34
7	Amiodarone[7]	very slightly soluble	II[7]	400.129	5.842	4	TS	1.00	0.50

#	Drug/ Manufacturer (Table S2)	Solubility in water defined by Ph. Eur. 10.0	BCS classification	Shift (PBS to TC/L) (Hz)	Shift (TC/L to TC/L with lipids) (Hz)	Pattern	Set	Probability TC/L interaction (model 2)	Probability Lipid interaction (model 3)
8	Amitriptyline[7]	freely soluble	I/II[1]	42.374	1.641	2	TS	0.71	0.38
9	Amlodipine[8]	slightly soluble	I[8]	42.014	2.281	2	TS	0.74	0.11
10	Amoxicillin[9]	slightly soluble	I[9]	1.440	0.160	1	TS	0.32	0.19
11	Asciminib[5]	practically insoluble	II[10]	52.257	5.442	2	TS	0.94	0.59
12	Atazanavir[10]	slightly soluble	II[11]	12.804	10.683	6	TS	1.00	0.65
13	Atenolol[11]	sparingly soluble	III[4]	1.921	0.320	1	TS	0.13	0.19
14	Atovaquone[7]	practically insoluble	II[12]	400.129	0.000	4	FS (pKa = 6.9)[13]	0.99	0.68
15	Atropine[6]	very soluble	I/III[4]	6.522	2.721	1	TS	0.25	0.15
16	Benzocaine[12]	very slightly soluble	N/A	14.325	6.722	2	TS	0.11	0.06
17	Bifonazole[7]	practically insoluble	IV[14]	400.129	11.564	6	FS (pKa = 6.29)[15]	0.98	0.86
18	Bisacodyl[12]	practically insoluble	N/A	17.166	7.282	6*	TS	0.96	0.83
19	Bromhexine[12]	very slightly soluble	II[16]	110.436	3.721	4	TS	0.54	0.36
20	Buspirone[7]	freely soluble	I[1]	4.281	4.842	1	TS	0.82	0.23
21	Butylscopolammonium bromide[6]	freely soluble	N/A	7.763	2.681	1	FS (quaternary)	0.87	0.36

#	Drug/ Manufacturer (Table S2)	Solubility in water defined by Ph. Eur. 10.0	BCS classification	Shift (PBS to TC/L) (Hz)	Shift (TC/L to TC/L with lipids) (Hz)	Pattern	Set	Probability TC/L interaction (model 2)	Probability Lipid interaction (model 3)
22	Candesartan cilexitil[7]	practically insoluble	II[17]	400.129	1.921	4	TS	0.94	0.73
23	Capmatinib[5]	practically insoluble	II/IV[18]	400.129	2.681	4	TS	0.98	0.43
24	Captopril[13]	soluble in water	III[4]	0.720	0.040	1	HS	0.08	0.04
25	Carbamazepine[14]	very slightly soluble	II[4]	16.845	10.763	3	TS	0.59	0.45
26	Carbimazole[15]	slightly soluble	I[19]	0.920	0.320	1	TS	0.14	0.09
27	Celecoxib[16]	practically insoluble	II[20]	400.129	2.441	6*	TS	0.85	0.55
28	Ceritinib[5]	practically insoluble	IV[21]	32.490	5.802	6*	TS	0.98	0.74
29	Cetirizine[8]	freely soluble	III[1]	23.648	8.603	3	TS	0.77	0.61
30	Chinidin[6]	sparingly soluble	I[22]	19.446	8.043	3	HS	0.60	0.53
31	Chinin[17]	very slightly soluble	I/II[23]	16.365	6.602	2	TS	0.60	0.53
32	Chloramphenicol[12]	slightly soluble	III[4]	5.282	1.601	1	TS	0.48	0.08
33	Chloroquine[8]	freely soluble	I[1]	32.330	9.083	3	TS	0.48	0.14
34	Chlorpromazine[7]	very soluble	II/IV[4]	48.336	2.921	2	TS	0.74	0.44
35	Chlorprothixene[7]	soluble	II[24]	32.971	4.601	2	TS	0.75	0.52

#	Drug/ Manufacturer (Table S2)	Solubility in water defined by Ph. Eur. 10.0	BCS classification	Shift (PBS to TC/L) (Hz)	Shift (TC/L to TC/L with lipids) (Hz)	Pattern	Set	Probability TC/L interaction (model 2)	Probability Lipid interaction (model 3)
36	Cimetidine[12]	slightly soluble	III[4]	2.921	1.080	1	FS (pKa = 6.80)[25]	0.03	0.05
37	Cinnarizine[7]	practically insoluble	II[26]	104.954	2.681	6*	TS	0.96	0.82
38	Ciprofloxacin[7]	practically insoluble	II/IV[4]	14.805	1.200	2	FS (pKa = 6.0)[27]	0.09	0.10
39	Clonidine[18]	soluble	III[28]	2.281	2.441	1	TS	0.21	0.26
40	Clopidogrel[8]	practically insoluble	II[29]	64.941	10.723	6	TS	0.84	0.28
41	Caffein[12]	sparingly soluble	I[30]	2.201	0.040	1	TS	0.09	0.26
42	Cortisone acetate[18]	practically insoluble	N/A	14.085	3.001	2	TS	0.70	0.23
43	Dabrafenib[5]	practically insoluble	II[31]	13.364	8.443	6	FS (pKa = 6.6)[32]	0.99	0.65
44	Danazol[16]	practically insoluble	II[33]	400.129	2.961	4	TS	0.93	0.71
45	Dexamethasone[19]	practically insoluble	I/III[4]	20.167	5.522	4	TS	0.71	0.28
46	Dextromethorphan[12]	sparingly soluble	II[34]	19.526	12.604	3	TS	0.40	0.38
47	Diclofenac[12]	sparingly soluble	II[35]	35.812	13.564	3	TS	0.82	0.59
48	Diltiazem[20]	freely soluble	I[1]	30.290	21.167	3	TS	0.91	0.57
49	Dimetindene[5]	slightly soluble	N/A	27.529	12.324	3	HS	0.61	0.71

#	Drug/ Manufacturer (Table S2)	Solubility in water defined by Ph. Eur. 10.0	BCS classification	Shift (PBS to TC/L) (Hz)	Shift (TC/L to TC/L with lipids) (Hz)	Pattern	Set	Probability TC/L interaction (model 2)	Probability Lipid interaction (model 3)
50	Diphenhydramine[12]	very soluble	I[36]	20.126	15.885	3	HS	0.40	0.70
51	Dipyridamole[7]	practically insoluble	II[37]	12.044	1.601	4	FS (pKa = 6.4)[38]	0.19	0.27
52	Domperidone[7]	practically insoluble	II[39]	37.292	22.927	3	TS	0.91	0.64
53	Doxepin[21]	freely soluble	I[1]	37.492	9.603	3	HS	0.52	0.35
54	Doxycycline[22]	very slightly soluble	I[4]	28.129	9.683	3	HS	0.65	0.12
55	Eltrombopag[5]	practically insoluble	N/A	400.129	8.123	6	TS	0.99	0.69
56	Etofylline[23]	freely soluble	N/A	1.520	0.400	1	HS	0.10	0.20
57	Fenofibrate[5]	practically insoluble	II[40]	56.778	7.482	6*	TS	0.96	0.36
58	Folic acid[12]	practically insoluble	II/IV[4]	3.481	0.480	1	TS	0.47	0.03
59	Furosemide[22]	practically insoluble	IV[1]	12.524	5.642	2	TS	0.29	0.07
60	Glibenclamide[4]	practically insoluble	II[41]	19.526	10.964	6	TS	0.98	0.61
61	Glimepiride[8]	practically insoluble	II[42]	400.129	3.241	4	TS	0.96	0.49
62	Haloperidol[8]	practically insoluble	II/IV[4]	20.447	8.403	6	TS	0.84	0.64
63	Hydrochlorothiazide[7]	very slightly soluble	III[4]	3.961	0.960	1	TS	0.05	0.08

#	Drug/ Manufacturer (Table S2)	Solubility in water defined by Ph. Eur. 10.0	BCS classification	Shift (PBS to TC/L) (Hz)	Shift (TC/L to TC/L with lipids) (Hz)	Pattern	Set	Probability TC/L interaction (model 2)	Probability Lipid interaction (model 3)
64	Hydrocortisone[17]	practically insoluble	I[43]	28.729	4.802	2	TS	0.69	0.22
65	Ibuprofen[16]	practically insoluble	II[4]	5.802	10.523	5	HS	0.48	0.25
66	Imatinib[5]	very slightly soluble	I/II[44]	116.718	14.725	3	TS	0.98	0.79
67	Imipramine[7]	freely soluble	I[1]	32.410	4.121	2	TS	0.64	0.31
68	Indometacin[24]	practically insoluble	II[1]	48.416	10.243	3	TS	0.92	0.56
69	Isoniazid[7]	freely soluble	I[1]	0.360	0.040	1	TS	0.02	0.01
70	Isoprenaline[6]	freely soluble	N/A	2.081	1.320	1	TS	0.04	0.07
71	Itraconazole[7]	practically insoluble	II[1]	400.129	0.000	4	TS	1.00	0.94
72	Ivermectine[7]	practically insoluble	II/IV[1]	400.129	3.281	4	TS	1.00	0.55
73	Ketoconazole[7]	practically insoluble	II[1]	34.371	6.482	6*	FS (pKa = 6.5)[45]	0.99	0.74
74	Ketoprofen[8]	practically insoluble	II[46]	1.400	2.721	1	TS	0.58	0.24
75	Lapatinib[7]	practically insoluble	IV[47]	400.129	21.687	6	TS	1.00	0.91
76	Lidocaine[7]	very soluble	I[7]	6.482	11.844	5	TS	0.41	0.07
77	Loperamide[25]	slightly soluble	II[48]	18.206	9.883	3	HS	0.99	0.67
78	Loratadine[26]	practically insoluble	II[49]	400.129	3.841	4	TS	0.96	0.40
79	LSZ-102[5]	practically insoluble	N/A	400.129	8.763	6	TS	0.99	0.84

#	Drug/ Manufacturer (Table S2)	Solubility in water defined by Ph. Eur. 10.0	BCS classification	Shift (PBS to TC/L) (Hz)	Shift (TC/L to TC/L with lipids) (Hz)	Pattern	Set	Probability TC/L interaction (model 2)	Probability Lipid interaction (model 3)
80	Maprotiline[27]	slightly soluble	I[24]	42.534	13.724	3	TS	0.61	0.26
81	Mefloquine[7]	very slightly soluble	II/IV[4]	46.215	4.001	2	TS	0.55	0.24
82	Menadione[7]	practically insoluble	N/A	5.042	11.324	5	TS	0.26	0.47
83	Mepivacaine[28]	freely soluble	N/A	4.201	17.886	5	TS	0.39	0.39
84	Metamizole[12]	very soluble	I[50]	0.720	1.601	1	TS	0.40	0.05
85	Metformin[8]	freely soluble	III[1]	0.720	0.360	1	TS	0.00	0.06
86	Metipranolol[29]	very slightly soluble	N/A	6.242	10.363	5	HS	0.43	0.35
87	Metoclopramide[12]	very soluble	I/III[4]	2.961	1.160	1	TS	0.30	0.18
88	Metoprolol[7]	very soluble	I[51]	7.362	3.681	1	TS	0.21	0.21
89	Metronidazole[12]	slightly soluble	I[4]	6.522	3.761	1	TS	0.06	0.13
90	Minocycline[4]	sparingly soluble	III[52]	39.813	13.004	3	TS	0.78	0.15
91	Naporafenib[5]	practically insoluble	II[53]	77.665	16.805	6	TS	0.99	0.67
92	Neostigmine bromide[29]	very soluble	III[4]	1.040	0.280	1	FS (quaternary)	0.25	0.35
93	Niclosamide[30]	practically insoluble	II/IV[4]	400.129	6.322	4	TS	0.83	0.49

#	Drug/ Manufacturer (Table S2)	Solubility in water defined by Ph. Eur. 10.0	BCS classification	Shift (PBS to TC/L) (Hz)	Shift (TC/L to TC/L with lipids) (Hz)	Pattern	Set	Probability TC/L interaction (model 2)	Probability Lipid interaction (model 3)
94	Nifedipine[30]	practically insoluble	II[54]	400.129	5.762	4	TS	0.80	0.13
95	Nilotinib[5]	practically insoluble	IV[55]	400.129	6.402	6*	HS	1.00	0.77
96	Nitrofurantoin[4]	very slightly soluble	II[4]	1.280	0.560	1	TS	0.17	0.18
97	Norfloxacin[8]	very slightly soluble	IV[56]	16.765	1.280	2	FS (pKa = 6.2)[57]	0.12	0.09
98	Ofloxacin[18]	slightly soluble	II[58]	9.523	1.240	2	FS (pKa = 6.0)[59]	0.16	0.14
99	Omeprazole[7]	very slightly soluble	I[60]	12.364	7.122	2	HS	0.65	0.33
100	p-aminosalicylic acid[7]	very slightly soluble	IV[61]	2.441	0.560	1	TS	0.03	0.05
101	Papaverine[7]	sparingly soluble	II[24]	34.611	9.003	6	TS	0.91	0.57
102	Paracetamol[12]	sparingly soluble	III[4]	2.121	0.120	1	TS	0.09	0.07
103	Penicillamine[18]	freely soluble	III[4]	1.240	0.320	1	TS	0.00	0.06
104	Penicillin V[18]	practically insoluble	I[4]	4.441	1.761	1	TS	0.48	0.15
105	Perphenazine[7]	practically insoluble	II[62]	58.659	3.601	2	TS	0.89	0.38
106	Phenacetin[12]	very slightly soluble	II[63]	14.125	6.322	2	HS	0.19	0.27
107	Phenazone[17]	very soluble	I[4]	1.440	0.360	1	TS	0.29	0.15
108	Phenprocoumon[31]	slightly soluble	II[4]	8.283	2.001	2	TS	0.85	0.49

#	Drug/ Manufacturer (Table S2)	Solubility in water defined by Ph. Eur. 10.0	BCS classification	Shift (PBS to TC/L) (Hz)	Shift (TC/L to TC/L with lipids) (Hz)	Pattern	Set	Probability TC/L interaction (model 2)	Probability Lipid interaction (model 3)
109	Phenytoin[1]	practically insoluble	II[4]	15.445	5.922	4	TS	0.48	0.65
110	Piroxicam[1]	practically insoluble	II[1]	4.762	0.800	1	HS	0.51	0.47
111	Posaconazole[7]	practically insoluble	II[64]	400.129	6.882	6*	TS	1.00	0.88
112	Prazosin[4]	very slightly soluble	I[65]	3.881	3.161	1	FS (pKa = 6.50)[66]	0.09	0.38
113	Prednisolone acetat[17]	practically insoluble	I[67]	207.187	4.361	4	TS	0.85	0.19
114	Procaine[18]	very soluble	N/A	3.761	0.520	1	TS	0.18	0.07
115	Promethazine[13]	very soluble	III[4]	41.533	3.761	2	TS	0.66	0.25
116	Propranolol[12]	soluble	I[4]	46.895	2.721	2	TS	0.38	0.08
117	Propyphenazone[12]	slightly soluble	N/A	2.401	1.080	1	TS	0.65	0.11
118	Proxiphylline[8]	very soluble	N/A	1.400	0.480	1	TS	0.15	0.15
119	Pyridoxine[16]	freely soluble	I[4]	0.520	0.400	1	HS	0.04	0.21
120	Quetiapine[7]	slightly soluble	II[68]	50.216	2.161	2	TS	0.87	0.23
121	Ramipril[8]	sparingly soluble	I/II[69, 70]	5.682	3.601	1	TS	0.89	0.14
122	Ranitidine[32]	freely soluble	III[1]	0.480	1.000	1	TS	0.33	0.17

#	Drug/ Manufacturer (Table S2)	Solubility in water defined by Ph. Eur. 10.0	BCS classification	Shift (PBS to TC/L) (Hz)	Shift (TC/L to TC/L with lipids) (Hz)	Pattern	Set	Probability TC/L interaction (model 2)	Probability Lipid interaction (model 3)
123	Rosigliatzone[7]	sparingly soluble	I[1]	63.220	11.284	3	FS (pKa = 6.8)[71]	0.84	0.61
124	Salbutamol[12]	sparingly soluble	I[4]	1.160	0.480	1	HS	0.08	0.09
125	Salicylic acid[17]	slightly soluble	N/A	2.681	0.320	1	TS	0.03	0.05
126	Sotuletinib[5]	practically insoluble	N/A	38.052	2.681	4	TS	0.90	0.53
127	Spironolactone[6]	practically insoluble	II/IV[1]	18.566	4.802	4	TS	0.94	0.39
128	Sulfadiazine[7]	practically insoluble	II/IV[4]	0.920	0.920	1	FS (pKa = 6.5)[72]	0.15	0.28
129	Sulfamethoxazole[7]	practically insoluble	II[4]	2.041	0.560	1	TS	0.17	0.44
130	Sulfathiazole[7]	practically insoluble	II[56]	3.321	0.920	1	FS (pKa = 7.1)[73]	0.11	0.45
131	Sumatriptan[8]	freely soluble	III[74]	3.481	0.440	1	TS	0.09	0.24
132	Taminadenant[5]	practically insoluble	II[75]	11.004	9.203	6	TS	0.43	0.44
133	Tetracaine[17]	very slightly soluble	N/A	27.609	6.362	3	TS	0.41	0.27
134	Tetracycline[12]	very slightly soluble	III[76]	8.403	0.640	2	TS	0.62	0.12
135	Theophylline[7]	slightly soluble	I[4]	1.000	0.280	1	TS	0.05	0.21
136	Tolbutamide[7]	practically insoluble	II[77]	1.520	1.000	1	TS	0.41	0.17

#	Drug/ Manufacturer (Table S2)	Solubility in water defined by Ph. Eur. 10.0	BCS classification	Shift (PBS to TC/L) (Hz)	Shift (TC/L to TC/L with lipids) (Hz)	Pattern	Set	Probability TC/L interaction (model 2)	Probability Lipid interaction (model 3)
137	Trametinib[5]	practically insoluble	IV[78]	400.129	0.000	4	TS	1.00	0.67
138	Triamterene[13]	very slightly soluble	II[79]	6.282	4.401	1	HS	0.16	0.37
139	Trimethoprim[12]	very slightly soluble	II[4]	2.281	3.281	1	TS	0.26	0.18
140	Valproic acid[33]	very slightly soluble	II[4]	2.041	0.320	1	TS	0.11	0.25
141	Verapamil[34]	soluble	I/II[4]	12.004	3.281	2	TS	0.97	0.49

Table S2: Manufacturer list of drugs according to Table S1.

Number	Manufacturer/Supplier	Company domicil
(1)	Pfizer Pharma GmbH	Berlin, Germany
(2)	Dr. Pfleger Arzneimittel GmbH	Bamberg, Germany
(3)	Advanced ChemBlock Inc.	Hayward, CA, USA
(4)	Heumann Pharma GmbH & Co. Generica KG	Nürnberg, Germany
(5)	Novartis AG	Basel, Switzerland
(6)	Boehringer Ingelheim Pharma GmbH & Co. KG	Ingelheim am Rhein, Germany
(7)	Sigma-Aldrich GmbH	Schnelldorf, Germany
(8)	TCI Deutschland GmbH	Eschborn, Germany
(9)	TAD Pharma GmbH	Cuxhaven, Germany
(10)	The United States Pharmacopeial Convention	Rockville, MD, USA
(11)	Aliud Pharma GmbH	Laichingen, Germany
(12)	Fagron GmbH & Co. KG	Glinde, Germany
(13)	UCB Pharma GmbH	Monheim, Germany
(14)	Alfa Aesar (Thermo Fischer GmbH)	Kandel, Germany
(15)	Henning Arzneimittel GmbH & Co. KG	Flörsheim am Main, Germany
(16)	BASF SE	Ludwigshafen am Rhein, Germany
(17)	Caesar & Loretz GmbH	Hilden, Germany
(18)	Sanofi-Aventis GmbH	Frankfurt, Germany
(19)	Dr. Winzer Pharma GmbH	Berlin, Germany
(20)	Mylan dura GmbH	Bad Homburg, Germany
(21)	Neuraxpharm Arneimittel GmbH	Langenfeld, Germany
(22)	Haupt Pharma AG	Berlin Germany
(23)	Südmedica GmbH	München, Germany
(24)	Euro OTC Pharma GmbH	Bönen, Germany
(25)	1A Pharma GmbH	Holzkirchen, Germany
(26)	STADAPHARM GmbH	Bad Vilbel
(27)	Dolorgiet GmbH & Co. KG	Sankt Augustin, Germany
(28)	Johnson & Johnson GmbH	Neuss, Germany
(29)	Roche Deutschland Holding GmbH	Grenzach-Wyhlen, Germany
(30)	Bayer AG	Leverkusen, Germany
(31)	Wörwag Pharma GmbH & Co. KG	Stuttgart, Germany
(32)	Alfred E. Tiefenbacher (GmbH & Co. KG)	Hamburg, Germany
(33)	Pharma Wernigerode GmbH	Wernigerode, Germany
(34)	WPG Pharma GmbH	Heidelberg, Germany

S2 Prediction models

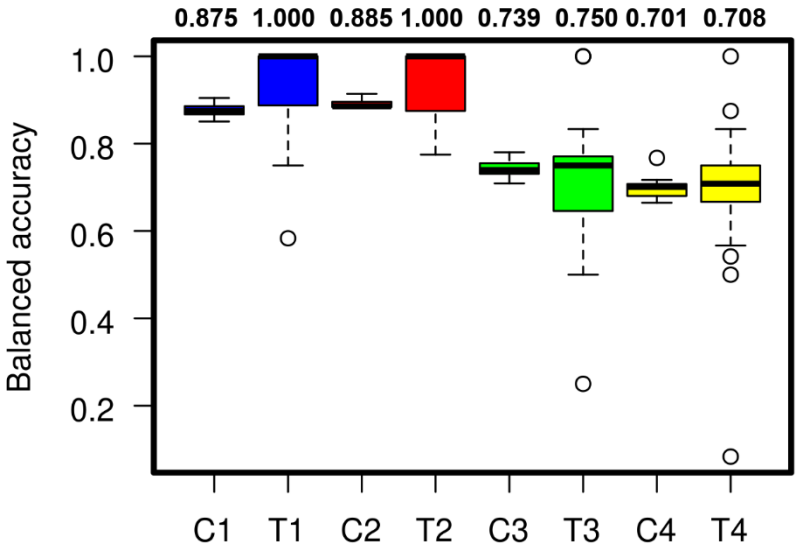

Figure S1: Distributions of balanced accuracies for all calibration sets (C) and test segments (T) that were used during the model generation process for the respective descriptor selection providing the overall highest median $BAcc_{Test}$ value. The median values are shown on top. The distributions are illustrated for all four modeling approaches (C1/T1: TC/L prediction with whole descriptor set (blue), resulting in model 1; C2/T2: TC/L prediction with descriptor subset (red), resulting in model 2; C3/T3: Lipid prediction with whole descriptor set (green), resulting in model 3; C4/T4: Lipid prediction with descriptor subset (yellow), resulting in model 4). Within each inner loop of the model building process (see Figure 1), a new model was trained on a different calibration set and subsequently tested on an external test segment, leading to a $BAcc_{Calibration}$ and a $BAcc_{Test}$ value respectively. Summed up for each tested selection of descriptors, this led to final distributions of $BAcc_{Calibration}$ and $BAcc_{Test}$ values, the latter serving as selection criteria for the overall best descriptor selection.

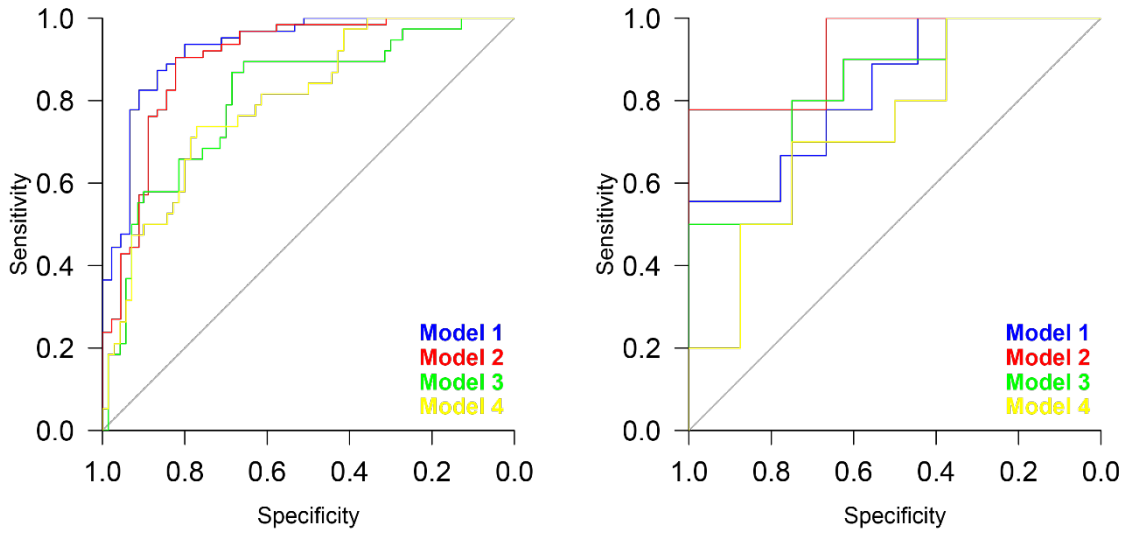

Figure S2: Receiver operating characteristic curves for models 1 – 4 regarding the training set (left) and the external validation set (right). The respective training set was used for building the final model, whereas the external set was subsequently used for validating it against new drug substances.

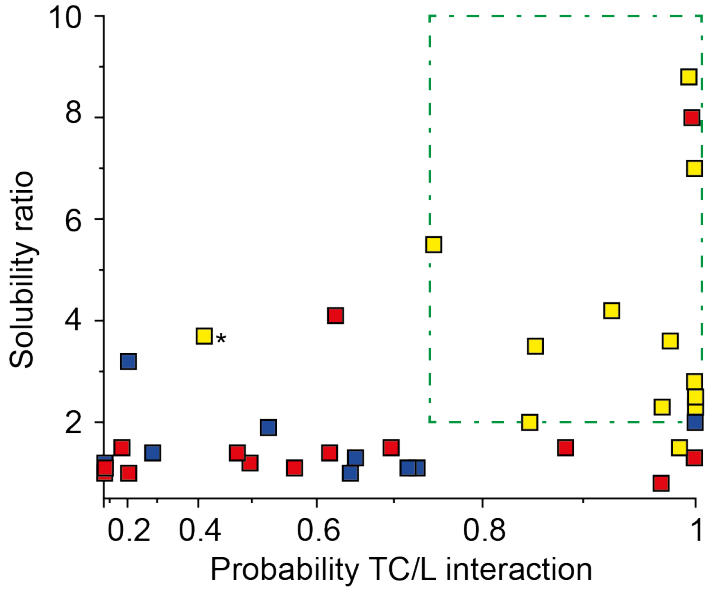

Figure S3: Correlation of solubility ratio with TC/L interaction probability calculated by model 2. Green dashed border represents drugs with a likelihood for TC/L interaction of ≥ 0.75 and solubility ratio over 2. One outlier (Albendazole) was asterisked. Yellow boxes indicate drugs with positive, blue with no effect, and red with negative food effect, respectively.

S3 Drug correlation to solubility and BCS classification

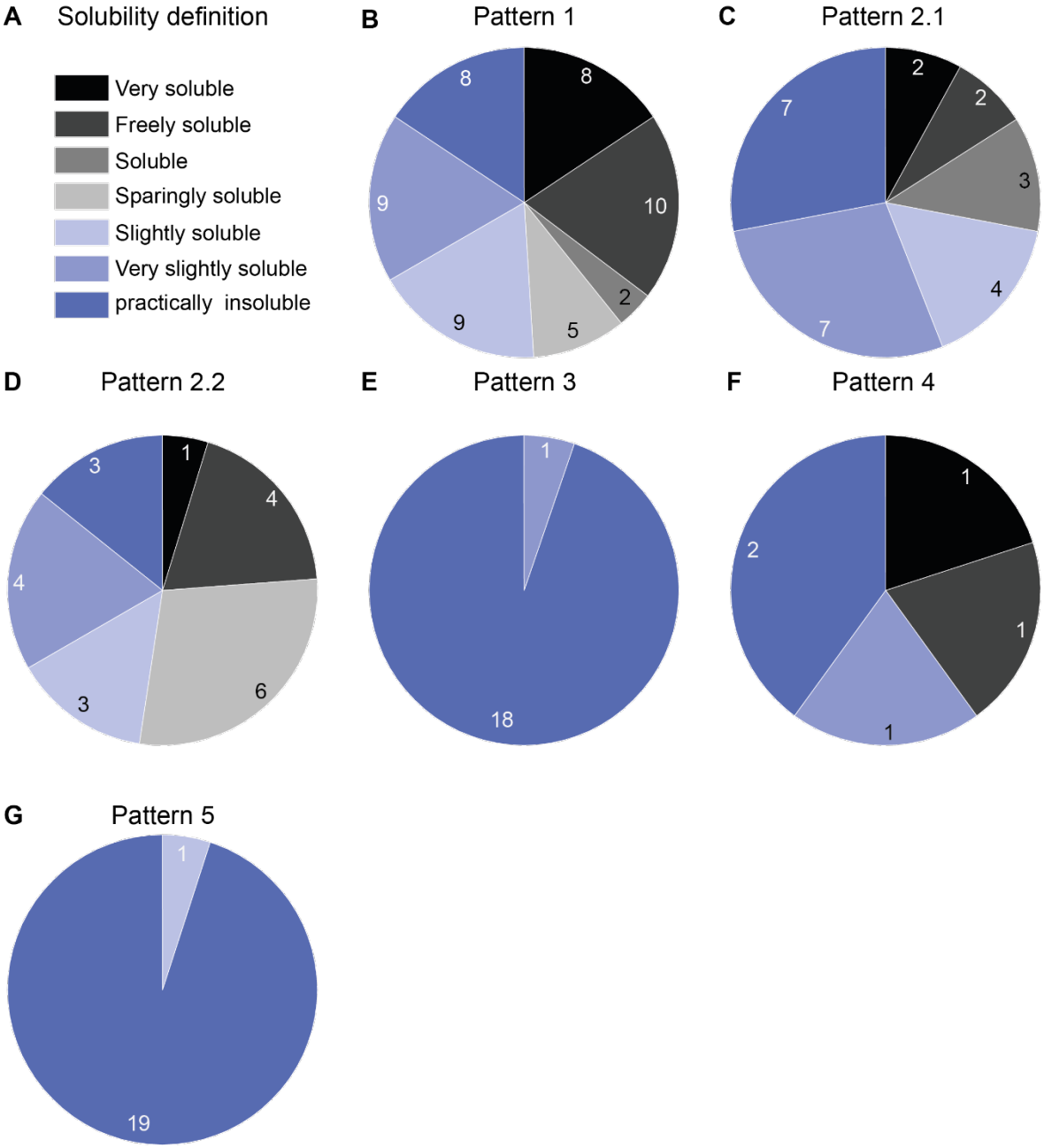

Figure S4: Solubilities of drugs within pattern analyzed by NMR according to table S1. (A) Drug solubility in water was defined by Ph. Eur. as very soluble (>1000 mg/ml; black), freely soluble (100-1000 mg/ml; dark grey), soluble (33-100 mg/ml; grey), sparingly soluble (10-33 mg/l; light grey), slightly soluble (1-10 mg/ml, light blue), very slightly soluble (0.1-1 mg/ml; blue), and practically insoluble (< 0.1 mg/ml; dark blue). (B, C, D, F) There was no correlation between solubility and NMR pattern 1, 2, 3, and 5. (E, G) Pattern 4 and 6 contained only slightly to practically insoluble drugs. The total amount of classified drugs is shown within pattern.

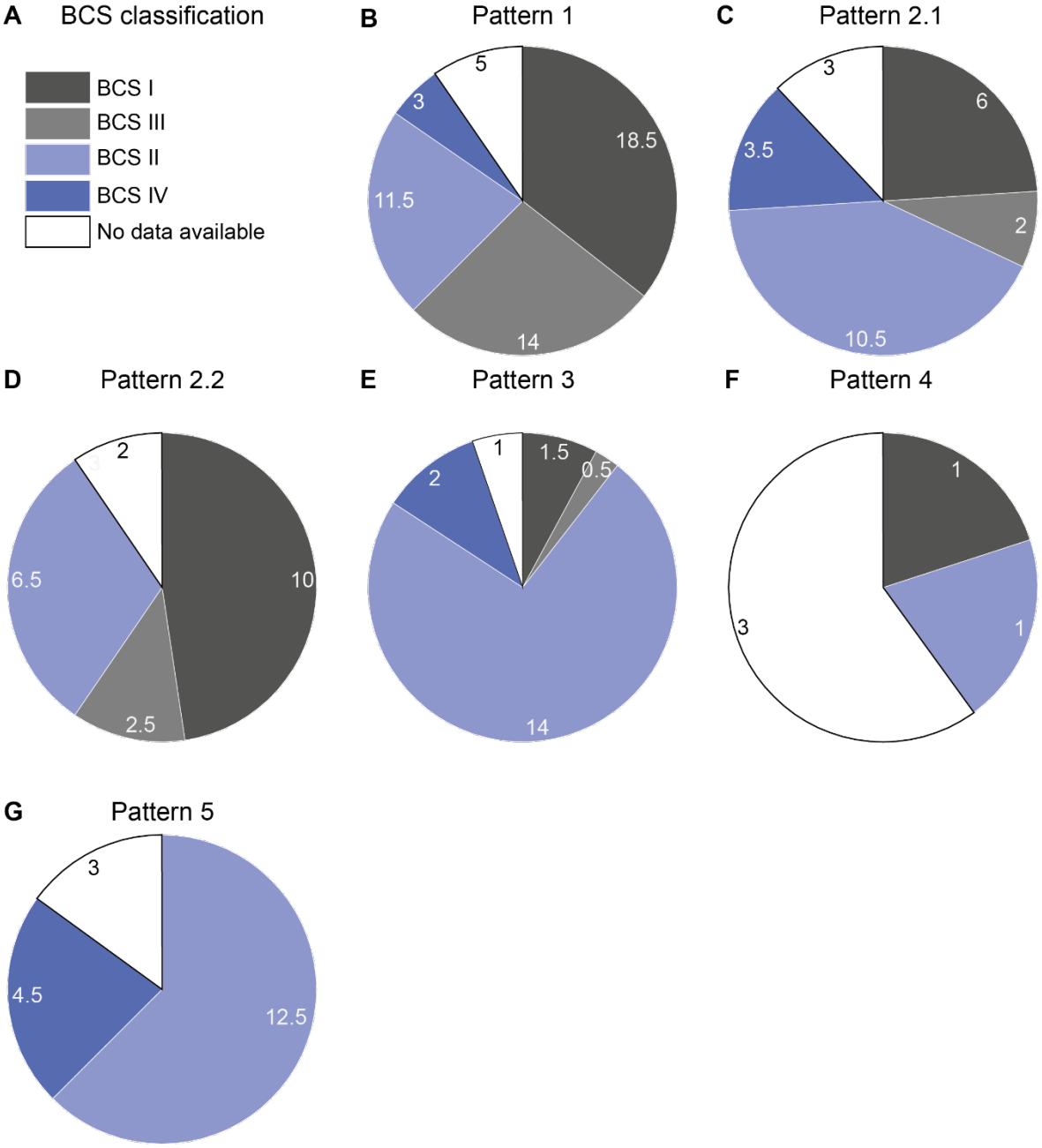

Figure S5: Biopharmaceutical classification (BCS) for drugs within NMR pattern according to table S1. (A) Drugs were classified into the BCS system, class I (grey), class III (light grey), class II (light blue), and class IV (blue) or marked as no available data (white). (B, C, D, F) There was no correlation between BCS and NMR 1, 2, 3, and 5. (E, G) Pattern 4 and 6 contained mostly BCS II and IV drugs. The total amount of classified drugs is shown within pattern. A drug was counted as 0.5 for a respective BCS class, if 2 groups were mentioned in literature.

References

1. Wu, C. Y.; Benet, L. Z., Predicting drug disposition via application of BCS: transport/absorption/ elimination interplay and development of a biopharmaceutics drug disposition classification system. *Pharm. Res.* **2005,** *22* (1), 11-23.
2. Yazdanian, M.; Briggs, K.; Jankovsky, C.; Hawi, A., The "high solubility" definition of the current FDA Guidance on Biopharmaceutical Classification System may be too strict for acidic drugs. *Pharm. Res.* **2004,** *21* (2), 293-9.

3. Wind, S.; Schnell, D.; Ebner, T.; Freiwald, M.; Stopfer, P., Clinical Pharmacokinetics and Pharmacodynamics of Afatinib. *Clin. Pharmacokinet.* **2017,** *56* (3), 235-250.
4. Lindenberg, M.; Kopp, S.; Dressman, J. B., Classification of orally administered drugs on the World Health Organization Model list of Essential Medicines according to the biopharmaceutics classification system. *Eur. J. Pharm. Biopharm.* **2004,** *58* (2), 265-78.
5. Gajewska, M.; Blumenstein, L.; Kourentas, A.; Mueller-Zsigmondy, M.; Lorenzo, S.; Sinn, A.; Velinova, M.; Heimbach, T., Physiologically Based Pharmacokinetic Modeling of Oral Absorption, pH, and Food Effect in Healthy Volunteers to Drive Alpelisib Formulation Selection. *AAPS J.* **2020,** *22* (6), 134.
6. Stetinova, V.; Smetanova, L.; Kholova, D.; Svoboda, Z.; Kvetina, J., Classification of the model drug (ambroxol hydrochloride) into the Biopharmaceutics Classification System (BCS) and prediction of the intestinal transport using Caco-2 cells. *Toxicol. Lett.* **2009,** *189*.
7. Benet, L. Z., There are no useful CYP3A probes that quantitatively predict the in vivo kinetics of other CYP3A substrates and no expectation that one will be found. *Mol. Interventions* **2005,** *5* (2), 79-83.
8. Williams, H. D.; Ford, L.; Lim, S.; Han, S.; Baumann, J.; Sullivan, H.; Vodak, D.; Igonin, A.; Benameur, H.; Pouton, C. W.; Scammells, P. J.; Porter, C. J. H., Transformation of Biopharmaceutical Classification System Class I and III Drugs Into Ionic Liquids and Lipophilic Salts for Enhanced Developability Using Lipid Formulations. *J. Pharm. Sci.* **2018,** *107* (1), 203-216.
9. Thambavita, D.; Galappatthy, P.; Mannapperuma, U.; Jayakody, L.; Cristofoletti, R.; Abrahamsson, B.; Groot, D. W.; Langguth, P.; Mehta, M.; Parr, A.; Polli, J. E.; Shah, V. P.; Dressman, J., Biowaiver Monograph for Immediate-Release Solid Oral Dosage Forms: Amoxicillin Trihydrate. *J. Pharm. Sci.* **2017,** *106* (10), 2930-2945.
10. Hoch, M.; Zack, J.; Quinlan, M.; Huth, F.; Forte, S.; Dodd, S.; Aimone, P.; Hourcade-Potelleret, F., Pharmacokinetics of Asciminib When Taken With Imatinib or With Food. *Clin. Pharmacol. Drug Dev.* **2021**.
11. Benet, L. Z.; Broccatelli, F.; Oprea, T. I., BDDCS applied to over 900 drugs. *AAPS J.* **2011,** *13* (4), 519-47.
12. Kathpalia, H.; Juvekar, S.; Shidhaye, S., Design and In Vitro Evaluation of Atovaquone Nanosuspension Prepared by pH Based and Anti-solvent Based Precipitation Method. *Colloid Interface Sci. Commun.* **2019,** *29*, 26-32.
13. Birth, D.; Kao, W.-C.; Hunte, C., Structural analysis of atovaquone-inhibited cytochrome bc 1 complex reveals the molecular basis of antimalarial drug action. *Nat. Commun.* **2014,** *5* (1), 1-11.
14. Patel, D.; Patel, D.; Prajapati, J.; Patel, U.; Patel, V., Formulation of thermoresponsive and buccal adhesive in situ gel for treatment of oral thrush containing poorly water soluble drug bifonazole. *J. Pharm. Bioallied Sci.* **2012,** *4* (Suppl 1), S116-7.
15. Suñer-Carbó, J.; Calpena-Campmany, A.; Halbaut-Bellowa, L.; Clares-Naveros, B.; Rodriguez-Lagunas, M. J.; Barbolini, E.; Zamarbide-Losada, J.; Boix-Montañés, A., Biopharmaceutical development of a bifonazole multiple emulsion for enhanced epidermal delivery. *Pharmaceutics* **2019,** *11* (2), 66.
16. Reza, M. S.; Islam, Z.; Limpa, S. I., Comparative Evaluation of Bromhexine HCl Mucoadhesive Microspheres Prepared by Anionic, Cationic and Nonionic Polymers. *Bangladesh Pharm. J.* **2020,** *23* (2), 117-124.
17. Figueroa-Campos, A.; Sanchez-Dengra, B.; Merino, V.; Dahan, A.; Gonzalez-Alvarez, I.; Garcia-Arieta, A.; Gonzalez-Alvarez, M.; Bermejo, M., Candesartan Cilexetil In Vitro-In Vivo Correlation: Predictive Dissolution as a Development Tool. *Pharmaceutics* **2020,** *12* (7).
18. Hughes, D. L., Review of Synthetic Routes and Crystalline Forms of the Oncology Drugs Capmatinib, Selpercatinib, and Pralsetinib. *Org. Process Res. Dev.* **2021,** *25* (10), 2192-2204.

19. Hosey, C. M.; Chan, R.; Benet, L. Z., BDDCS Predictions, Self-Correcting Aspects of BDDCS Assignments, BDDCS Assignment Corrections, and Classification for more than 175 Additional Drugs. *AAPS J.* **2016,** *18* (1), 251-60.
20. Dolenc, A.; Kristl, J.; Baumgartner, S.; Planinsek, O., Advantages of celecoxib nanosuspension formulation and transformation into tablets. *Int. J. Pharm.* **2009,** *376* (1-2), 204-12.
21. Chennuru, R.; Koya, R. T.; Kommavarapu, P.; Narasayya, S. V.; Muthudoss, P.; Vishweshwar, P.; Babu, R. R. C.; Mahapatra, S., In Situ Metastable Form: A Route for the Generation of Hydrate and Anhydrous Forms of Ceritinib. *Cryst. Growth Des.* **2017,** *17* (12), 6341-6352.
22. Grube, S.; Langguth, P.; Junginger, H. E.; Kopp, S.; Midha, K. K.; Shah, V. P.; Stavchansky, S.; Dressman, J. B.; Barends, D. M., Biowaiver monographs for immediate release solid oral dosage forms: quinidine sulfate. *J. Pharm. Sci.* **2009,** *98* (7), 2238-51.
23. Strauch, S.; Dressman, J. B.; Shah, V. P.; Kopp, S.; Polli, J. E.; Barends, D. M., Biowaiver monographs for immediate-release solid oral dosage forms: quinine sulfate. *J. Pharm. Sci.* **2012,** *101* (2), 499-508.
24. Box, K. J.; Comer, J. E., Using measured pKa, LogP and solubility to investigate supersaturation and predict BCS class. *Curr. Drug Metab.* **2008,** *9* (9), 869-78.
25. Jantratid, E.; Prakongpan, S.; Dressman, J.; Amidon, G.; Junginger, H.; Midha, K.; Barends, D., Biowaiver monographs for immediate release solid oral dosage forms: Cimetidine. *J. Pharm. Sci.* **2006,** *95* (5), 974-984.
26. Christiansen, M. L.; Holm, R.; Abrahamsson, B.; Jacobsen, J.; Kristensen, J.; Andersen, J. R.; Mullertz, A., Effect of food intake and co-administration of placebo self-nanoemulsifying drug delivery systems on the absorption of cinnarizine in healthy human volunteers. *Eur. J. Pharm. Sci.* **2016,** *84*, 77-82.
27. Osonwa, U. E.; Ugochukwu, J. I.; Ajaegbu, E. E.; Chukwu, K. I.; Azevedo, R. B.; Esimone, C. O., Enhancement of antibacterial activity of ciprofloxacin hydrochloride by complexation with sodium cholate. *Bull. Faculty of Pharmacy (Cairo University)* **2017,** *55* (2), 233-237.
28. Hanning, S. M.; Orlu Gul, M.; Toni, I.; Neubert, A.; Tuleu, C.; CloSed, C., A mini-review of non-parenteral clonidine preparations for paediatric sedation. *J. Pharm. Pharmacol.* **2017,** *69* (4), 398-405.
29. Mora, M. J.; Onnainty, R.; Granero, G. E., Comparative Oral Drug Classification Systems: Acetazolamide, Azithromycin, Clopidogrel, and Efavirenz Case Studies. *Mol. Pharmaceutics* **2018,** *15* (8), 3187-3196.
30. Wagner-Hattler, L.; Schoelkopf, J.; Huwyler, J.; Puchkov, M., Stability investigation of FCC-based tablets for oral suspension with caffeine and oxantel pamoate as model drugs. *Drug Dev. Ind. Pharm.* **2019,** *45* (2), 222-230.
31. Ouellet, D.; Grossmann, K. F.; Limentani, G.; Nebot, N.; Lan, K.; Knowles, L.; Gordon, M. S.; Sharma, S.; Infante, J. R.; Lorusso, P. M.; Pande, G.; Krachey, E. C.; Blackman, S. C.; Carson, S. W., Effects of particle size, food, and capsule shell composition on the oral bioavailability of dabrafenib, a BRAF inhibitor, in patients with BRAF mutation-positive tumors. *J. Pharm. Sci.* **2013,** *102* (9), 3100-9.
32. Puszkiel, A.; Noé, G.; Bellesoeur, A.; Kramkimel, N.; Paludetto, M.-N.; Thomas-Schoemann, A.; Vidal, M.; Goldwasser, F.; Chatelut, E.; Blanchet, B., Clinical pharmacokinetics and pharmacodynamics of dabrafenib. *Clin. Pharmacokinet.* **2019,** *58* (4), 451-467.
33. Tsume, Y.; Igawa, N.; Drelich, A. J.; Ruan, H.; Amidon, G. E.; Amidon, G. L., The in vivo predictive dissolution for immediate release dosage of donepezil and danazol, BCS class IIc drugs, with the GIS and the USP II with biphasic dissolution apparatus. *J. Drug Delivery Sci. Technol.* **2020,** *56*.
34. Naqvi, R. F.; Khan, A.; Umer, M. F.; Malik, O.; Shahwani, N. A., Design and Optimization of Novel Taste-Masked Medicated Chocolates of Dextromethorphan with In vitro and In vivo Taste Evaluation. *J. Pharm. Innovation* **2020**.

35. Mirza, M. A., Solubility Enhancement of Diclofenac Using Solid Dispersions. *Int. J. Pharm. Pharmacol.* **2021,** *5* (1), 1-6.
36. Jyothi, S. A.; Mounika, P.; Vineesha, S.; Mehdia, S.; Dutt, N. A., Formulation Development and Evaluation of Oral Thin Films-Diphenhydramine HCl. *Int. J. Pharm. Sci. Res.* **2013,** *4* (9), 3484.
37. Tsume, Y.; Patel, S.; Wang, M.; Hermans, A.; Kesisoglou, F., The Introduction of a New Flexible In Vivo Predictive Dissolution Apparatus, GIS-Alpha (GIS-alpha), to Study Dissolution Profiles of BCS Class IIb Drugs, Dipyridamole and Ketoconazole. *J. Pharm. Sci.* **2020,** *109* (11), 3471-3479.
38. Mizoguchi, M.; Nakatsuji, M.; Takano, J.; Ishibashi, O.; Wada, K.; Inui, T., Development of pH-independent drug release formulation using lipocalin-type prostaglandin D synthase. *J. Pharm. Sci.* **2016,** *105* (9), 2735-2742.
39. Daihom, B. A.; Bendas, E. R.; Mohamed, M. I.; Badawi, A. A., Development and in vitro evaluation of domperidone/Dowex resinate embedded gastro-floatable emulgel and effervescent alginate beads. *J. Drug Delivery Sci. Technol.* **2020,** *59*, 101941.
40. Shelake, S. S.; Patil, S. V.; Patil, S. S., Formulation and Evaluation of Fenofibrate-loaded Nanoparticles by Precipitation Method. *J. Indian Pharm. Sci.* **2018,** *80* (3).
41. Bari, A.; Chella, N.; Sanka, K.; Shastri, N. R.; Diwan, P. V., Improved anti-diabetic activity of glibenclamide using oral self nano emulsifying powder. *J. Microencapsulation* **2015,** *32* (1), 54-60.
42. Tzankov, B.; Voycheva, C.; Aluani, D.; Yordanov, Y.; Avramova, K.; Tzankova, V.; Spassova, I.; Kovacheva, D.; Yoncheva, K., Improvement of dissolution of poorly soluble glimepiride by loading on two types of mesoporous silica carriers. *J. Solid State Chem.* **2019,** *271*, 253-259.
43. Lennernas, H.; Skrtic, S.; Johannsson, G., Replacement therapy of oral hydrocortisone in adrenal insufficiency: the influence of gastrointestinal factors. *Expert Opin. Drug Metab. Toxicol.* **2008,** *4* (6), 749-58.
44. Reggane, M.; Wiest, J.; Saedtler, M.; Harlacher, C.; Gutmann, M.; Zottnick, S. H.; Piechon, P.; Dix, I.; Muller-Buschbaum, K.; Holzgrabe, U.; Meinel, L.; Galli, B., Bioinspired co-crystals of Imatinib providing enhanced kinetic solubility. *Eur. J. Pharm. Biopharm.* **2018,** *128*, 290-299.
45. Tsume, Y.; Mudie, D. M.; Langguth, P.; Amidon, G. E.; Amidon, G. L., The Biopharmaceutics Classification System: subclasses for in vivo predictive dissolution (IPD) methodology and IVIVC. *Eur. J. Pharm. Sci.* **2014,** *57*, 152-163.
46. Shohin, I. E.; Kulinich, J. I.; Ramenskaya, G. V.; Vasilenko, G. F., Evaluation of In Vitro Equivalence for Drugs Containing BCS Class II Compound Ketoprofen. *Dissolution Technol.* **2011,** *18* (1), 26-29.
47. Koch, K. M.; Im, Y. H.; Kim, S. B.; Urruticoechea Ribate, A.; Stephenson, J.; Botbyl, J.; Cartee, L.; Holshouser, J.; Ridgway, D., Effects of Esomeprazole on the Pharmacokinetics of Lapatinib in Breast Cancer Patients. *Clin. Pharmacol. Drug Dev.* **2013,** *2* (4), 336-41.
48. Zaki, N. M.; Artursson, P.; Bergstrom, C. A., A modified physiological BCS for prediction of intestinal absorption in drug discovery. *Mol. Pharmaceutics* **2010,** *7* (5), 1478-87.
49. Wang, J.; Chang, R.; Zhao, Y.; Zhang, J.; Zhang, T.; Fu, Q.; Chang, C.; Zeng, A., Coamorphous Loratadine-Citric Acid System with Enhanced Physical Stability and Bioavailability. *AAPS PharmSciTech* **2017,** *18* (7), 2541-2550.
50. Nikolova, I.; Tencheva, J.; Voinikov, J.; Petkova, V.; Benbasat, N.; Danchev, N., Metamizole: A Review Profile of a Well-Known "Forgotten" Drug. Part I: Pharmaceutical and Nonclinical Profile. *Biotechnol. Biotechnological Equipment* **2014,** *26* (6), 3329-3337.
51. Basu, S.; Yang, H.; Fang, L.; Gonzalez-Sales, M.; Zhao, L.; Trame, M. N.; Lesko, L.; Schmidt, S., Physiologically Based Pharmacokinetic Modeling to Evaluate Formulation Factors Influencing Bioequivalence of Metoprolol Extended-Release Products. *J. Clin. Pharmacol.* **2019,** *59* (9), 1252-1263.

52. Papich, M. G.; Martinez, M. N., Applying Biopharmaceutical Classification System (BCS) Criteria to Predict Oral Absorption of Drugs in Dogs: Challenges and Pitfalls. *AAPS J.* **2015,** *17* (4), 948-64.
53. Ramurthy, S.; Taft, B. R.; Aversa, R. J.; Barsanti, P. A.; Burger, M. T.; Lou, Y.; Nishiguchi, G. A.; Rico, A.; Setti, L.; Smith, A.; Subramanian, S.; Tamez, V.; Tanner, H.; Wan, L.; Hu, C.; Appleton, B. A.; Mamo, M.; Tandeske, L.; Tellew, J. E.; Huang, S.; Yue, Q.; Chaudhary, A.; Tian, H.; Iyer, R.; Hassan, A. Q.; Mathews Griner, L. A.; La Bonte, L. R.; Cooke, V. G.; Van Abbema, A.; Merritt, H.; Gampa, K.; Feng, F.; Yuan, J.; Mishina, Y.; Wang, Y.; Haling, J. R.; Vaziri, S.; Hekmat-Nejad, M.; Polyakov, V.; Zang, R.; Sethuraman, V.; Amiri, P.; Singh, M.; Sellers, W. R.; Lees, E.; Shao, W.; Dillon, M. P.; Stuart, D. D., Design and Discovery of N-(3-(2-(2-Hydroxyethoxy)-6-morpholinopyridin-4-yl)-4-methylphenyl)-2-(trifluorom ethyl)isonicotinamide, a Selective, Efficacious, and Well-Tolerated RAF Inhibitor Targeting RAS Mutant Cancers: The Path to the Clinic. *J. Med. Chem.* **2020,** *63* (5), 2013-2027.
54. Nader, A. M.; Quinney, S. K.; Fadda, H. M.; Foster, D. R., Effect of Gastric Fluid Volume on the In Vitro Dissolution and In Vivo Absorption of BCS Class II Drugs: a Case Study with Nifedipine. *AAPS J.* **2016,** *18* (4), 981-8.
55. Budha, N. R.; Frymoyer, A.; Smelick, G. S.; Jin, J. Y.; Yago, M. R.; Dresser, M. J.; Holden, S. N.; Benet, L. Z.; Ware, J. A., Drug absorption interactions between oral targeted anticancer agents and PPIs: is pH-dependent solubility the Achilles heel of targeted therapy? *Clin. Pharmacol. Ther.* **2012,** *92* (2), 203-13.
56. Gopi, S. P.; Ganguly, S.; Desiraju, G. R., A Drug-Drug Salt Hydrate of Norfloxacin and Sulfathiazole: Enhancement of in Vitro Biological Properties via Improved Physicochemical Properties. *Mol. Pharmaceutics* **2016,** *13* (10), 3590-3594.
57. Gips, M.; Soback, S., Norfloxacin pharmacokinetics in lactating cows with sub-clinical and clinical mastitis. *J. Veterinary Pharmacol. Ther.* **1999,** *22* (3), 202-208.
58. Jagdale, S.; Pawar, S., Gellified Emulsion of Ofloxacin for Transdermal Drug Delivery System. *Adv. Pharm. Bull.* **2017,** *7* (2), 229-239.
59. Navaratnam, S.; Claridge, J., Primary Photophysical Properties of Ofloxacin¶. *Photochem. Photobiol.* **2000,** *72* (3), 283-290.
60. Ni, J.; Ouyang, H.; Seto, C.; Sakuma, T.; Ellis, R.; Rowe, J.; Acheampong, A.; Welty, D.; Szekely-Klepser, G., Sensitivity and proportionality assessment of metabolites from microdose to high dose in rats using LC-MS/MS. *Bioanalysis* **2010,** *2* (3), 407-19.
61. Smetanova, L.; Stetinova, V.; Kholova, D.; Kunes, M.; Nobilis, M.; Svoboda, Z.; Kvetina, J., Transintestinal transport mechanisms of 5-aminosalicylic acid (in situ rat intestine perfusion, Caco-2 cells) and Biopharmaceutics Classification System. *Gen. Physiol. Biophys.* **2013,** *32* (3), 361-9.
62. Mohammadi, P.; Mahjub, R.; Mohammadi, M.; Derakhshandeh, K.; Ghaleiha, A.; Mahboobian, M. M., Pharmacokinetics and brain distribution studies of perphenazine-loaded solid lipid nanoparticles. *Drug Dev. Ind. Pharm.* **2021,** *47* (1), 146-152.
63. Darwich, A. S.; Neuhoff, S.; Jamei, M.; Rostami-Hodjegan, A., Interplay of metabolism and transport in determining oral drug absorption and gut wall metabolism: a simulation assessment using the "Advanced Dissolution, Absorption, Metabolism (ADAM)" model. *Curr. Drug Metab.* **2010,** *11* (9), 716-29.
64. Hens, B.; Bermejo, M.; Tsume, Y.; Gonzalez-Alvarez, I.; Ruan, H.; Matsui, K.; Amidon, G. E.; Cavanagh, K. L.; Kuminek, G.; Benninghoff, G.; Fan, J.; Rodriguez-Hornedo, N.; Amidon, G. L., Evaluation and optimized selection of supersaturating drug delivery systems of posaconazole (BCS class 2b) in the gastrointestinal simulator (GIS): An in vitro-in silico-in vivo approach. *Eur. J. Pharm. Sci.* **2018,** *115*, 258-269.
65. Berginc, K.; Zakelj, S.; Kristl, A., In vitro interactions between aged garlic extract and drugs used for the treatment of cardiovascular and diabetic patients. *Eur. J. Nutr.* **2010,** *49* (6), 373-84.

66. Wei, X.; Yin, J.; Yang, G.; He, C.; Chen, Y., On-line solid-phase extraction with a monolithic weak cation-exchange column and simultaneous screening of α1-adrenergic receptor antagonists in human plasma. *J. Sep. Sci.* **2007,** *30* (17), 2851-2857.
67. Kasim, N. A.; Whitehouse, M.; Ramachandran, C.; Bermejo, M.; Lennernas, H.; Hussain, A. S.; Junginger, H. E.; Stavchansky, S. A.; Midha, K. K.; Shah, V. P.; Amidon, G. L., Molecular properties of WHO essential drugs and provisional biopharmaceutical classification. *Mol. Pharmaceutics* **2004,** *1* (1), 85-96.
68. DeVane, C. L.; Nemeroff, C. B., Clinical pharmacokinetics of quetiapine: an atypical antipsychotic. *Clin. Pharmacokinet.* **2001,** *40* (7), 509-22.
69. Ogawa, R.; Stachnik, J. M.; Echizen, H., Clinical pharmacokinetics of drugs in patients with heart failure: an update (part 2, drugs administered orally). *Clin. Pharmacokinet.* **2014,** *53* (12), 1083-114.
70. Alhasani, K. F.; Kazi, M.; Ibrahim, M. A.; Shahba, A. A.; Alanazi, F. K., Self-nanoemulsifying ramipril tablets: a novel delivery system for the enhancement of drug dissolution and stability. *Int. J. Nanomedicine* **2019,** *14*, 5435-5448.
71. Kamila, M. M.; Mondal, N.; Ghosh, L. K.; Gupta, B. K., Multiunit floating drug delivery system of rosiglitazone maleate: development, characterization, statistical optimization of drug release and in vivo evaluation. *AAPS PharmSciTech* **2009,** *10* (3), 887-899.
72. Hofmann, V.; Ringsdorf, H.; Schaumlöffel, E., Pharmakologisch-aktive polymere, 18. Körperverteilung und ausscheidungsverhalten von monomerem und polymerem sulfadiazinacrylamid. *Die Makromolekulare Chemie: Macromolecular Chemistry and Physics* **1979,** *180* (3), 595-602.
73. Velosa, A. C.; Nascimento, C. A., Evaluation of sulfathiazole degradation by persulfate in Milli-Q water and in effluent of a sewage treatment plant. *Environ. Sci. Pollut. Res.* **2017,** *24* (7), 6270-6277.
74. Chatzizacharia, K.; Hatziavramidis, D., New frames of reference for mapping drugs in the four classes of the BCS and BDDCS into regions with clear boundaries. *AIChE J.* **2015,** *61* (11), 3570-3579.
75. Ambuehl, M. F., Elvire; Fraichard, Amandine; Froidevaux, Sylvie; Geiseler, Oliver; Herrmann, Charlyse; Hubler, Francis; Murphy, Mark; Renneberg, Dorte; Stamm, Simon; Von Raumer, Markus Pharmaceutical composition compromising a tetrahydrozolopyrimidinone Compound. 2021.
76. de Oliveira, J. L. S.; Teles Júnior, G. A. C.; Bonfim, D. A.; Carvalho Júnior, C. M. R.; Santos, J. A.; Ferreira, M. S.; Santos Júnior, A. d. F., Effect of Medium pH on In Vitro Dissolution of Marketed Tetracyclines (Tetracycline and Doxycycline) Solid Oral Dosage Forms in Bahia, Brazil. *Dissolution Technol.* **2020,** *27* (2), 32-40.
77. Samie, A.; Desiraju, G. R.; Banik, M., Salts and Cocrystals of the Antidiabetic Drugs Gliclazide, Tolbutamide, and Glipizide: Solubility Enhancements through Drug–Coformer Interactions. *Cryst. Growth Des.* **2017,** *17* (5), 2406-2417.
78. de la Croix Ndong, J.; Stevens, D. M.; Vignaux, G.; Uppuganti, S.; Perrien, D. S.; Yang, X.; Nyman, J. S.; Harth, E.; Elefteriou, F., Combined MEK inhibition and BMP2 treatment promotes osteoblast differentiation and bone healing in Nf1Osx -/- mice. *J. Bone Miner. Res.* **2015,** *30* (1), 55-63.
79. Maeda, H.; Shiobara, R.; Tanaka, M.; Kajinami, A.; Nakayama, H., Effect of mechanochemical inclusion of triamterene into sulfobutylether-beta-cyclodextrin and its improved dissolution behavior. *Drug Dev. Ind. Pharm.* **2021,** *47* (4), 535-541.

Chapter II: Leveraging bile solubilization of poorly water-soluble drugs by rational polymer selection

Jonas Schlauersbach[1, #], Simon Hanio[1, #], Bettina Lenz[1],
Sahithya P. B. Vemulapalli[2], Christian Griesinger[2], Ann-Christin Pöppler[3],
Cornelius Harlacher[4], Bruno Galli[4], Lorenz Meinel[1,5*]

[1] Institute for Pharmacy and Food Chemistry, University of Wuerzburg, Am Hubland, DE-97074 Wuerzburg, Germany

[2] Max Planck Institute for Biophysical Chemistry, Am Faßberg 11, DE-37077 Goettingen, Germany

[3] Institute of Organic Chemistry, University of Wuerzburg, Am Hubland, DE-97074 Wuerzburg, Germany

[4] Novartis Pharma AG, Lichtstrasse 35, CH-4056 Basel, Switzerland

[5] Helmholtz Institute for RNA-based Infection Biology (HIRI), Josef-Schneider-Straße 2/D15, DE-97080 Wuerzburg, Germany

[#] These authors contributed equally to this work.

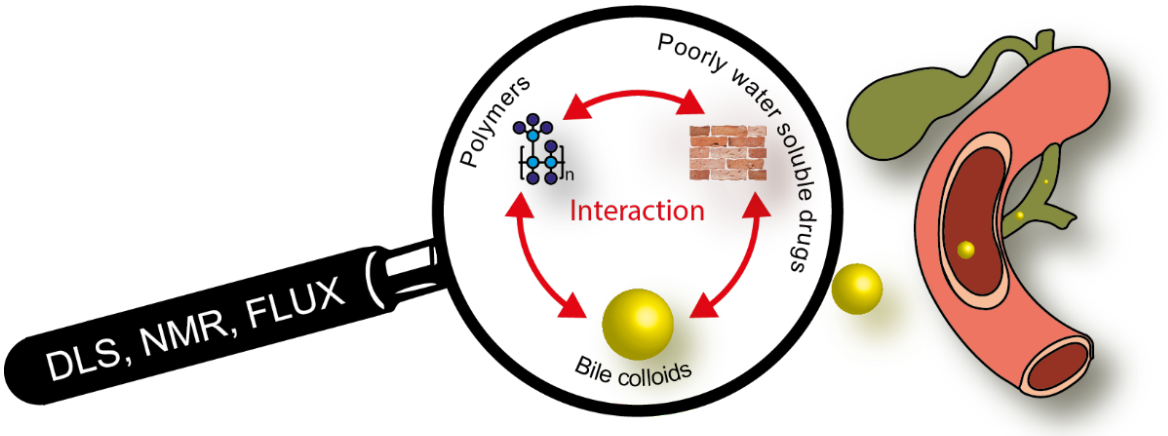

This chapter was originally published in Journal of Controlled Release. Reprinted with permission from Schlauersbach J., et al. Journal of controlled release, "Leveraging bile solubilization of poorly water-soluble drugs by rational polymer selection", vol. 330, pp. 36-48, 2021; DOI: 10.1016/j.jconrel.2020.12.016. Copyright © (2021) Elsevier. This manuscript version is made available under the CC-BY-NC-ND 4.0 license.

https://creativecommons.org/licenses/by-nc-nd/4.0/

*Corresponding author: Prof. Dr. Dr. Lorenz Meinel, Institute for Pharmacy and Food Chemistry, University of Wuerzburg, Am Hubland, DE-97074 Wuerzburg, Germany, E-Mail: lorenz.meinel@uni-wuerzburg.de

Abstract

Poorly water-soluble drugs frequently solubilize into bile colloids and this natural mechanism is key for efficient bioavailability. We tested the impact of pharmaceutical polymers on this solubilization interplay using proton nuclear magnetic resonance spectroscopy, dynamic light scattering, and by assessing the flux across model membranes. Eudragit E, Soluplus, and a therapeutically used model polymer, Colesevelam, impacted the bile-colloidal geometry and molecular interaction. These polymer-induced changes reduced the flux of poorly water-soluble and bile interacting drugs (Perphenazine, Imatinib) but did not impact the flux of bile non-interacting Metoprolol. Non-bile interacting polymers (Kollidon VA 64, HPMC-AS) neither impacted the flux of colloid-interacting nor colloid-non-interacting drugs. These insights into the drug substance/polymer/bile colloid interplay potentially point toward a practical optimization parameter steering formulations to efficient bile-solubilization by rational polymer selection.

Introduction

Long-lasting supersaturating systems and/or strategies increasing dissolution rates address pharmaceutical challenges of **p**oorly **w**ater-**s**oluble **d**rugs (**PWSD**),[1] including salt design,[2-7] nanoparticles[8, 9] and, **a**morphous **s**olid **d**ispersions (**ASD**)[10, 11] among other approaches[12-17] to obtain reproducible and adequate **p**harmaco**k**inetics (**PK**). Polymer excipients used for drug formulation were traditionally referred to as "inert"[18-20] in spite of a role in, e.g., drug transporter inhibition,[21] allergic reactions,[22] or physicochemical interactions.[23] Other reports highlighted the impact of these excipients on the natural solubilization systems[24, 25] and the current manuscript is within this context. Bile salts (including **t**auro**c**holate – **TC**), phospholipids (including **l**ecithin – **L**), cholesterol, and lipids pour out of the common bile duct into the duodenum and are largely reabsorbed in the ileum.[26] The resulting aqueous **t**auro**c**holate and **l**ecithin **mi**xed **m**icelles (denoted **TC/L MIM**) form the natural solubilization systems for poorly water-soluble vitamins and PWSDs.[27-30] For example, MIM solubilization is key for vitamin K absorption,[31] e.g., reflected by the fact that healthy neonates readily absorb orally given vitamin K,[29] while absorption occurs to a lesser extent in neonates with an obstructed bile duct/cholestasis.[32] For the most part, the focus of publications on pharmaceutical polymers detail aspects of drug dissolution and the impact on drug permeation across the gut epithelial barrier.[33-35] Selected examples along these lines are the use of **H**ydroxy**p**ropyl **m**ethyl**c**ellulose **a**cetate **s**uccinate (**HPMC-AS**) increasing the bioavailability of a PWSD,[36] while the amino methacrylate copolymer Eudragit E, though increasing the apparent drug solubility *in vitro*, resulted in delayed and reduced systemic availability as compared to control without polymer.[37] We hypothesize that reduced bioavailability for PWSDs in the presence of polymer excipients such as Eudragit E is in part due to polymer induced changes in the MIM colloidal structure, thereby impacting MIM solubilization of drugs. We used **Fa**sted **S**tate **S**imulated **I**ntestinal **F**luid (**FaSSIF**) as a model biological fluid containing TC/L MIM as seen in bile.[24, 27, 38] We characterized the impact of polymers (modified polyallylamine (Colesevelam), Eudragit E, polyvinyl caprolactam–polyvinyl acetate–polyethylene glycol graft copolymer (Soluplus), vinylpyrrolidone-vinyl acetate copolymer (Kollidon VA 64), and HPMC-AS) on the molecular interaction within TC/L MIM by **^{1}H n**uclear **m**agnetic **r**esonance (**^{1}H NMR**) and on changes on colloidal geometries by **d**ynamic **l**ight **s**cattering (**DLS**). Both methods combined provided the necessary granularity to assess geometries by hydrodynamic radii

and molecular interaction by ^{1}H NMR analysis. Throughout the manuscript we are using the terms "MIM interacting polymers" or "MIM *non*-interacting polymers" to indicate the interaction of *polymers* with TC/L MIM. Colesevelam was selected as a model polymer used therapeutically due to its bile acid/TC binding ability.[39] Eudragit E is a glazing agent used for taste masking in many pharmaceutical formulations[40, 41] and in ASD formulations.[42] Soluplus has also been used for ASDs.[43, 44] Kollidon VA 64 is a dry binder, granulating agent, and film forming agent,[45] HPMC-AS an enteric coating material,[46] and both polymers are used as solid dispersion carrier, or precipitation inhibitor.[47] Furthermore, we compared the polymer impact on the solubilization and flux across an artificial membrane for the poorly water soluble drugs Perphenazine and Imatinib with the water soluble and well permeable drug Metoprolol.[48] Throughout the manuscript we are using the terms "MIM interacting drugs" or "MIM *non*-interacting drugs" to indicate the interaction of *drugs* with TC/L MIM. The flux across these artificial membranes has been previously correlated to bioavailability.[49-51] The outcome of our experiments led to a preliminary decision tree by which drug substances are firstly categorized in those for which interaction with bile colloids is critical or not. Depending on this initial classification, secondly classes of pharmaceutical polymers are proposed for TC/L MIM solubilizing drug substances or for drug substance, which do not or marginally interact with TC/L MIM.

Materials and methods

Materials

Hydroxypropyl methylcellulose acetate succinate (HPMC-AS, grade LF) was obtained from Shin-Etsu Chemical Co Ltd. (Tokyo, Japan). Eudragit E PO was kindly provided by Evonik Nutrition and Care GmbH (Essen, Germany). Kollidon VA 64 and Soluplus were kindly provided by BASF SE (Ludwigshafen, Germany). Colesevelam was purchased from BOCSCI Inc. (New York, USA). Deionized, purified water (Millipore water) was generated by in-house Millipore purification system from Merck KGaA (Darmstadt, Germany). Hexadeuterodimethyl sulfoxide (DMSO-d_6, 99.8% D) was purchased from Euriso-top (Saarbrücken, Germany) and deuterated water (D_2O, 99.9% D) from Deutero GmbH (Kastellaun, Germany). Deuterated water (D_2O, 99.9% D) containing 0.05% 3-(trimethylsilyl)-propionic-2,2,3,3-d_4 sodium salt (TSP-d_4), 40% sodium deuteroxide in deuterated water (NaOD, 99% D), 35% deuterium chloride in deuterated water (DCl, 99%

D), sodium chloride (99%), monobasic sodium phosphate monohydrate (99%), D-α-Tocopherol polyethylene glycol 1000 succinate (Vitamin E TPGS), Perphenazine (99%), Metoprolol (99%) were purchased from Sigma-Aldrich (Schnelldorf, Germany). Imatinib free base was kindly provided by Novartis Pharma AG (Basel, Switzerland). Coaxial insert tubes and NMR tubes (5 mm, clear and amber glass) were purchased from Norell, Inc. (Landisville, PA USA). FaSSIF (FeSSIF/FaSSGF) powder was purchased from biorelevant.com Ltd. (London, UK). All other standard chemicals and laboratory consumables, if not stated otherwise, were purchased from either VWR International GmbH (Ismaning, Germany) or Sigma-Aldrich.

Methods

Dynamic light scattering

DLS was assessed by a Delsa Nano HC particle analyzer (Beckman Coulter Inc., Brea, California) with a backscattering angle of 165°. Modified **p**hosphate **b**uffered **s**aline pH 6.5 (**PBS**) and FaSSIF-V1 (hereinafter referred to as TC/L in PBS) with a concentration of 3 mmol/l TC and 0.75 mmol/l L were prepared according to the manufacturer's protocol (biorelevant.com). The respective polymer amount in medium (PBS or TC/L in PBS) was shaken for 2 h at 25 °C, 750 rpm on a Thermomixer F1.5 (Eppendorf AG, Hamburg, Germany). Unfiltered samples were measured in disposable 1.5 ml UV-Cuvettes (Brand GmbH & Co. KG, Wertheim, Germany) in triplicate with an accumulation of 70 scans in each run. Data was analyzed using the CUMULANT method. The Z-Average particle size was evaluated with a refractive index of 1.333 as determined for TC/L in PBS by an Abbe refractometer (Carl Zeiss AG, Oberkochen, Germany). The hydrodynamic diameter was adjusted by the dynamic viscosities of the respective solutions as read with a rolling-ball viscometer LOVIS 2000 M using capillary LOVIS 1.8 equipped with a steel ball at an inclination angle of 70° (diameter 1.5 mm, steel 1.4125, density 7.66 g/cm^3, Anton Paar GmbH, Graz, Austria). The temperature was set to 298 K for all experiments. Density was determined using an Anton Paar Density Meter DMA 4100 M. Samples with visible particles were excluded from statistical analysis.

^{1}H Nuclear Magnetic Resonance Spectroscopy

For ^{1}H NMR measurements a 0.1 mol/l DMSO-d_6 drug stock solution was prepared. Deuterated water was used for media preparation. Briefly, for pH adjustment in deuterated

water a correction factor was used adjusting pD to 6.91 using DCl and NaOD.[52] Perphenazine experiments were carried out under light protection. 1 mmol/l drug solutions were prepared by adding stock solution to the deuterated medium or polymer/medium mixtures, subsequently shaking for 2 h, 25 °C, and 750 rpm on a Thermomixer. ^{1}H NMR spectra were recorded on a Bruker Avance 400 MHz spectrometer (Bruker BioSpin GmbH, Karlsruhe, Germany) operating at 400.13 MHz with a BBI BB-H 5 mm probe head and at a temperature of 300 K. For ^{1}H NMR experiments the acquisition parameters were set to 256 scans with 56 dummy scans for sample equilibration, flip angle of 30°, a broad spectral width of 20.55 ppm to record all possible signals, and transmitter offset of 6.175 ppm. The acquisition time was 3.985 seconds followed by a relaxation delay of 1.0 second with collection of 64 000 data points at a sample spinning frequency of 20 Hz to ensure proper signal resolution (no spinning side bands were observed). The data were processed using TopSpin 4.0.6 (Bruker BioSpin). An exponential line broadening window function of 0.3 Hz was used (no difference in noise was seen at 0.5 Hz, data not shown). Automatic baseline correction and manual phasing were applied. The chemical shifts were referenced to the external standard of 0.05% TSP-d_4 in D_2O filled in a coaxial insert tube. Proton peaks from deuterated solvents such as DMSO-d_6 are denoted DMSO-d_5 which comprises all isotopomers of DMSO with at least one detectable proton. For ^{1}H **d**iffusion-**o**rdered **s**pectroscop**y** (DOSY) polymers and media compounds were dried (60 °C, 24 h) in a vacuum drier (Heraeus GmbH, Hanau, Germany). Samples in deuterated TC/L in PBS and PBS were prepared in a constantly nitrogen flushed Sekuroka glove box (Carl Roth GmbH & Co. KG, Karlsruhe, Germany). Signal assignment was done using ^{13}C, ^{1}H-^{1}H **co**rrelated **s**pectroscop**y** (COSY), and edited ^{1}H-^{13}C **h**eteronuclear **s**ingle **q**uantum **c**oherence (**HSQC**) spectra as described before [24]. DOSY spectra were recorded at 298 K on Bruker Avance Neo 600 MHz spectrometer (Bruker BioSpin) operating at 600.25 MHz for ^{1}H, equipped with a 5 mm TCI cryo-probe containing a z-axis gradient coil with a maximum gradient strength of 58.305 G cm^{-1}. A pulse sequence for diffusion measurement using double stimulated echo for convection compensation and longitudinal eddy current delay sequence with bipolar gradient pulses for diffusion and 3 spoil gradients was used (dstebpgp3s).[53, 54] A series of 16 spectra with a linear gradient ramp from 25 to 70% of the maximum gradient strength were recorded with an eddy current delay of 5 ms and a recycle delay of 5 s. The water (HDO) diffusion coefficients were obtained after data processing by fitting signal intensity at 4.703 ppm using dynamics center 2.6 (Bruker BioSpin) as a function of gradient strength (Eq. 1).

$$I(G) = I_0 \cdot e^{-\gamma^2 \cdot G^2 \cdot \delta^2 \cdot (\Delta - \frac{\delta}{3}) \cdot D} \quad \text{(Eq.1)}$$

Where *I(G)* is the gradient strength dependent signal intensity, I_0 initial signal intensity, γ gyromagnetic ratio of protons (4258 Hz/Gauss), G gradient strength, δ gradient length (2 ms), Δ diffusion time (50 ms), and D diffusion coefficient. The HDO signal decayed to below 5% of the initial signal intensity.

Flux

A side-by-side diffusion cell (PermeGear Inc., Hellertown, USA) was used (for assay workflow refer to **Figure S1**). The donor and receiver compartments (each with a filling volume of 10 ml) were separated by a regenerated cellulose membrane with an average pore size of 33 nm according to the manufacturer (innoME GmbH, Espelkamp, Germany). The orifice had a diameter of 15 mm resulting in a surface area of 1.77 cm². The five polymers were tested either in TC/L in PBS or in PBS (0.05% and 1%; % means weight per weight unless stated otherwise) and shaken on an orbital shaker Reax 20 for 2 h (Heidolph GmbH, Schwabach, Germany), and then transferred to the donor chamber. Eudragit E was additionally tested at a concentration of 0.01%. The receiver compartment was filled with PBS containing 0.2% Vitamin E TPGS. In all experiments, the maximum concentration in the receiver cell was less than one tenth of the amount added to the donor (sink condition). The temperature was held at 298 K using a Haake Fisons C1 water circulator (Thermo Fisher Scientific Inc., Karlsruhe, Germany) with a DLK 1002 cooling unit (FRYKA GmbH, Esslingen, Germany). The fluids in the cells were stirred continuously at 500 rpm on a H9-CB-02 stirring apparatus (SES GmbH, Bechenheim, Germany). At the beginning of the diffusion experiment, a 0.1 mol/l drug stock solution in DMSO was added to achieve a nominal starting concentration of 1 mmol/l. The total amount of DMSO never exceeded 1% (v/v). Perphenazine experiments were carried out under light protection. After 5-, 15-, 30-, 60-, 120-, 180-, and 240-minutes aliquots of 100 µl were taken from the receiver medium and replaced with fresh PBS containing 0.2% Vitamin E TPGS. Subsequently, the samples were diluted with 25 µl of **ac**eto**n**itrile (**ACN**) containing 0.1% **t**ri**f**luoro**a**cetic acid (**TFA**), vortexed for at least 30 seconds (VTX-3000L, LMSCO. LTD., Tokyo, Japan), and centrifuged with a MiniSpin centrifuge (Eppendorf) at 13000 rpm for 10 minutes.

High pressure liquid chromatography analysis

High **P**ressure **L**iquid **C**hromatography (**HPLC**) was used to determine the receiver compartment concentration change over time. The flux in nmol/min·cm² was obtained from the slope of the resulting concentration versus time profile using linear regression per permeated area. The amount of drug in the acceptor increased linearly showing a high coefficient of correlation ($R^2 > 0.996$). Experiments were carried out in triplicate. Samples were analyzed with an Agilent 1260 infinity II HPLC (Agilent Technologies Inc., Waldbronn, Germany) using a Synergi™ 4 µm Hydro-RP18 80 Å 150 x 4.6 mm LC column (Phenomenex LTD, Aschaffenburg, Germany). The device was equipped with a variable wavelength detector (G7114A, Agilent), an automatic vialsampler (G7129C, Agilent), flexible Pump (G7104C, Agilent), and multicolumn oven (G7116A, Agilent). Mobile phase A was 0.1% TFA in Millipore water. Mobile phase B was ACN with 0.1% TFA, flow was set to 1 ml/min, injection volume was 50 µl, and the wavelength of the detector was set to λ = 255 nm for Perphenazine, λ = 267 nm for Imatinib, and λ = 275 nm for Metoprolol. The gradient started at 20% B increasing to 100% within 6 minutes, held for 4 minutes, then back to 20% B within 1 minute, and held for 4 minutes. Quantification was done by calibration curves (**Figure S2**).

Statistical analysis

DLS and Metoprolol flux were statistically evaluated by one-way ANOVA followed by *post hoc* Dunnett's test for pairwise comparison with the control group. For flux, pairwise comparisons of all groups were done by *post hoc* Tukey test. Homogeneity of variance was tested by a Levene-test. A double-sided Grubb's test was used for outlier testing and excluded data points are always mentioned in the respective figure legend. Data was considered statistically significant at $p \leq 0.05$. OriginPro 2017 (OriginLab Corporation, Northampton, MA, USA) was used for statistical analysis.

Results

Drug interaction with taurocholate/lecithin mixed micelles

We analyzed the interaction of Perphenazine and Metoprolol with TC/L MIM by ^{1}H NMR spectroscopy. In the ^{1}H NMR spectrum, the TC/L signals appeared in the range 0.7 to 5.3 ppm which is in agreement with the previously reported measurement (**Figure 1A, S3, S4**).[24]

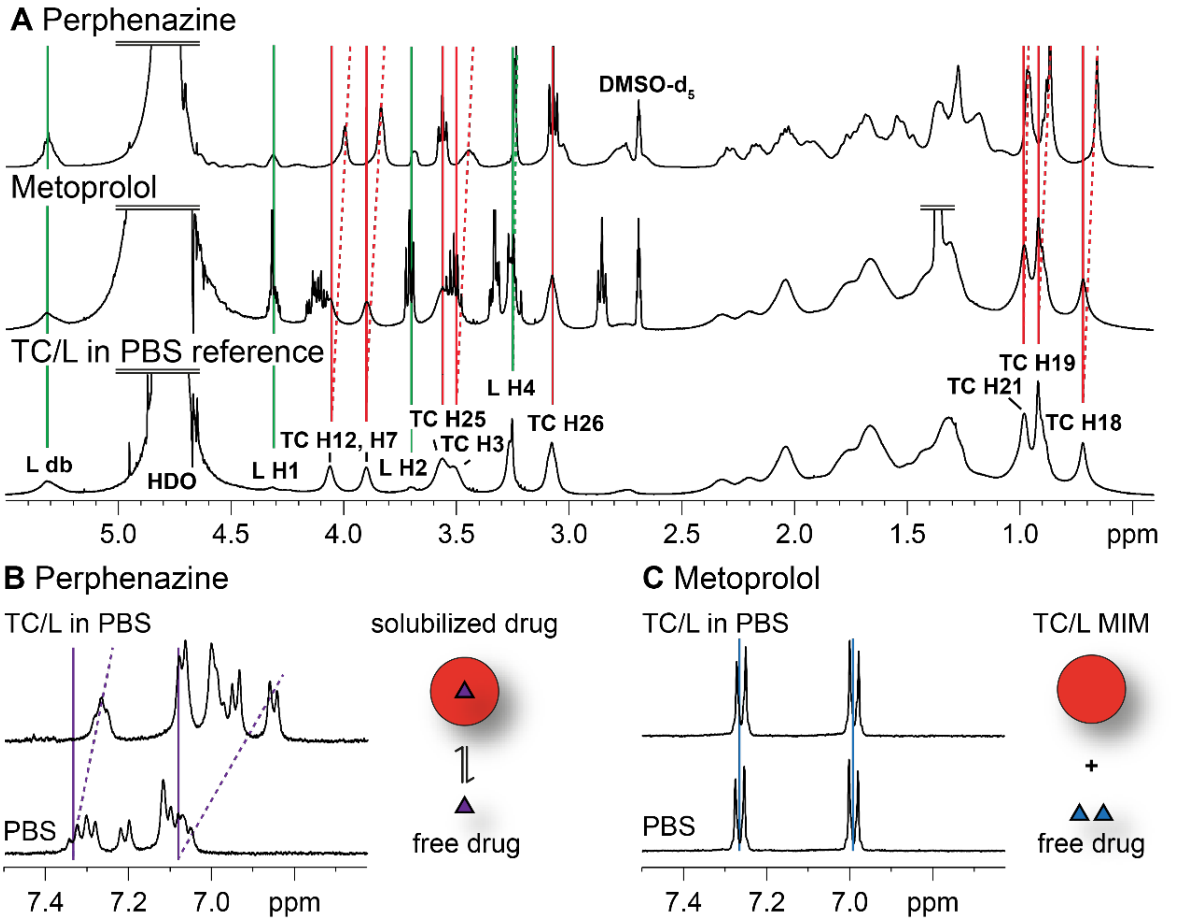

Figure 1: [1]H NMR spectra of Perphenazine – interacting with TC/L MIM - and Metoprolol - not interacting with TC/L MIM. (A) [1]H NMR spectra of TC/L in PBS as reference (bottom; green and red lines for L and TC signals, respectively), TC/L in PBS with Metoprolol (center), and TC/L in PBS with Perphenazine (top). [1]H NMR aryl-proton excerpt of (B) Perphenazine, and (C) Metoprolol in TC/L in PBS (top), and in PBS (bottom) including cartoons abstracting findings for the TC/L MIM interaction with (B) Perphenazine (purple triangle) and absence of interaction of (C) Metoprolol (blue triangles). Signal shifts are indicated by dotted lines.

TC H12, H7, H3, H21, H19, H18, and L H4 proton signals shifted to lower ppm in the presence of Perphenazine thereby indicating interaction of the drug substance with TC/L MIM. This was also reflected by Perphenazine's aryl-proton signals shifting to lower ppm in the presence of TC/L MIM (**Figure 1B**, **S4, S7**). In contrast, no chemical shift of TC/L signals were observed in the presence of Metoprolol including Metoprolol's aryl-proton resonances (**Figure 1A, 1C**), orthogonally confirming previous reports.[55] We refer to analogous studies for Imatinib, which is integrated into the assessment of drug substance/polymer/TC/L MIM interactions (*vide infra*).[24] Complete [1]H NMR spectra, chemical structures, and the approach of aryl-proton spectra interpretation is outlined in the supplementary information (**Figure S3-8**).

Polymer interaction with taurocholate/lecithin mixed micelles

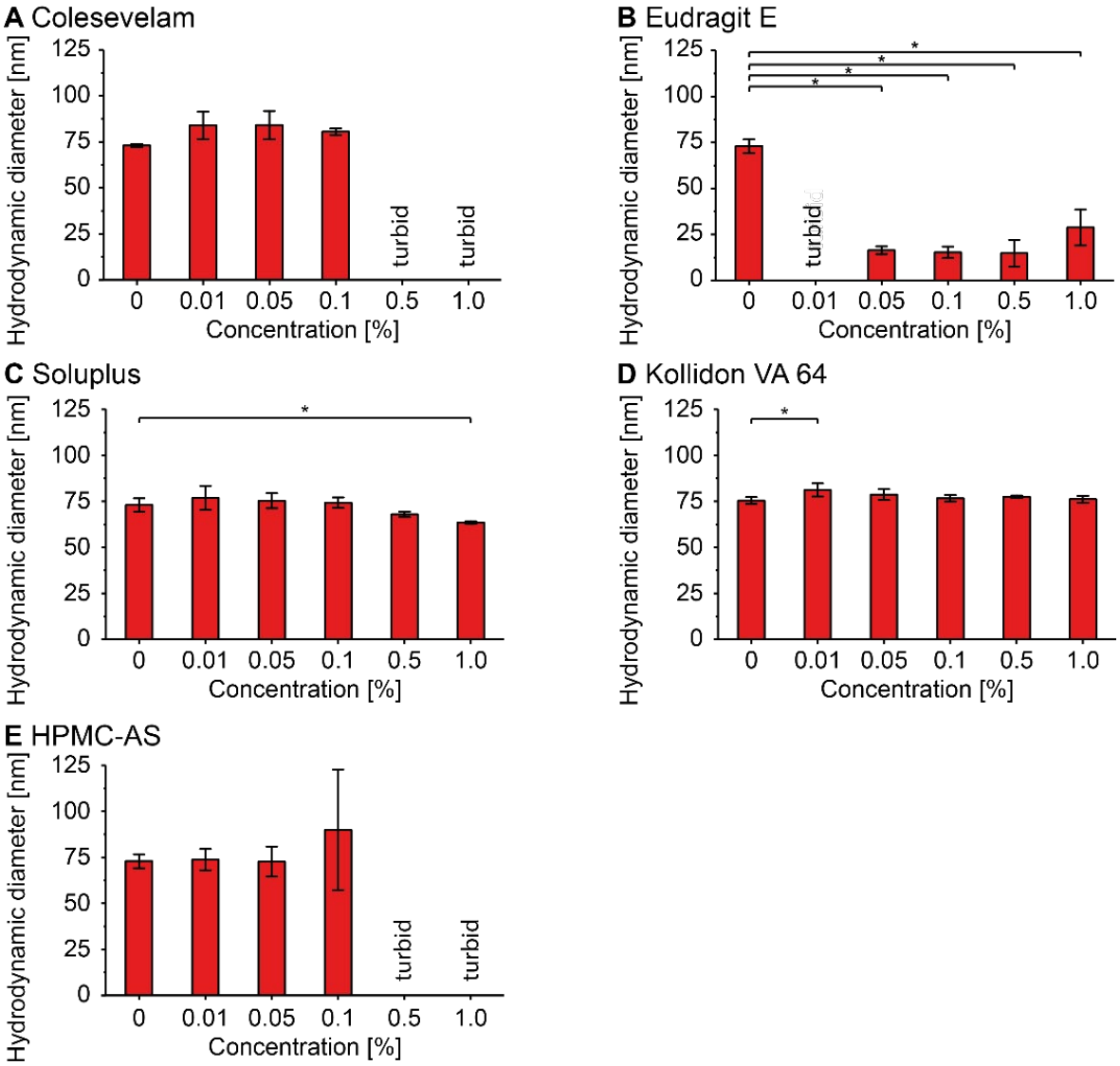

Figure 2: Hydrodynamic diameter of colloids in TC/L in PBS with (A) Colesevelam, (B) Eudragit E, (C) Soluplus, (D) Kollidon VA 64, and (E) HPMC-AS at concentrations as indicated measured by DLS. DLS outcome from turbid samples is qualitatively reported. Data shown as mean ± **s**tandard **d**eviation (**SD**), ANOVA considering $p \leq 0.05$ as statistically significant followed by Dunnett's *post-hoc* for pairwise comparison to the 0% polymer group (significant differences are shown by asterisks).

We characterized the polymers in PBS and their impact on TC/L in PBS concerning colloidal size change and molecular interaction by DLS and ^{1}H NMR spectroscopy, respectively. The hydrodynamic diameter of TC/L MIM was 73.0 ± 0.9 nm (**Figure 2A**). Colesevelam at 0.5 and 1% resulted in visually turbid samples (**Figure 2A**). Eudragit E - insoluble at 0.01% in TC/L in PBS – was visually turbid (**Figure 2B**). At ≥ 0.05% Eudragit E, particles were formed with 15 to 30 nm in diameter. Soluplus did not impact the size of the TC/L MIM other than at 1% (**Figure 2C**) nor did Kollidon VA 64 (**Figure 2D**), or HPMC-AS (**Figure**

2E). DLS results of the polymers in PBS are detailed in the supplementary information (**Figure S9, Table S1-3**). Furthermore, we analyzed polymers in TC/L in PBS and in PBS by ^{1}H NMR spectroscopy. No Colesevelam signals were seen in PBS and the TC/L signal intensities decreased in presence of this TC binding polymer (**Figure 3A**). Eudragit E reduced the intensity of the TC/L signals with signal broadening observed for TC protons in the range 0.5 to 1.2 ppm (**Figure 3B**).

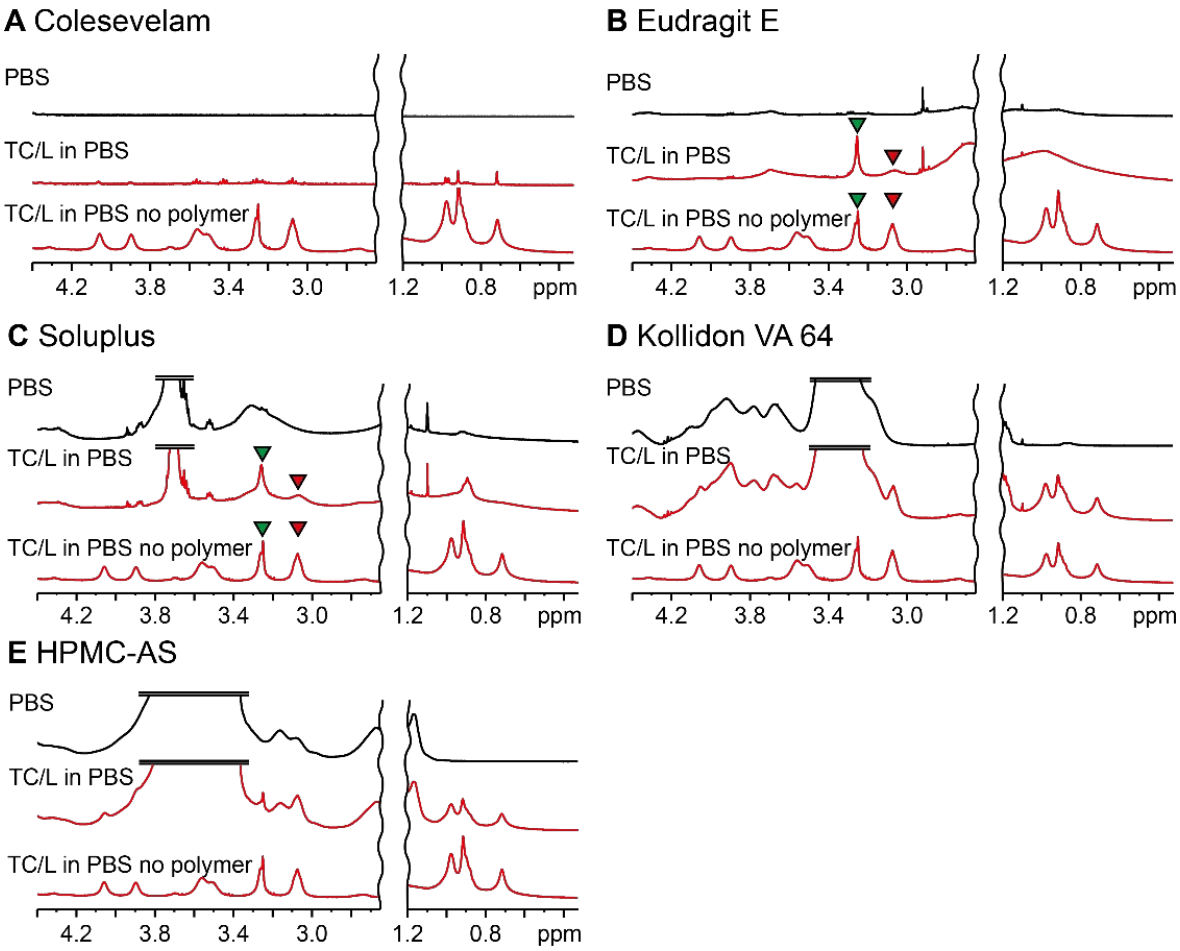

Figure 3: Extracts from ^{1}H NMR spectra of 1% (A) Colesevelam, (B) Eudragit E, (C) Soluplus, (D) Kollidon VA 64, and (E) HPMC-AS in PBS (top, black), in TC/L in PBS (center, red), and for comparison and identical across panels in TC/L in PBS without polymer as reference (bottom, red). L H4 (green triangle pointing at 3.25 ppm) and TC H26 (red triangle pointing at 3.1 ppm) are highlighted for the assessment of polymer/TC/L MIM interaction, which was seen for (A) Colesevelam, (B) Eudragit E, and (C) Soluplus but not (D) Kollidon VA 64, nor (E) HPMC-AS.

TC signals from 3.8 to 4.2 ppm were no longer observed, while L H4 at 3.25 ppm and TC H26 at 3.1 ppm remained detectable. Soluplus effects in TC/L in PBS were comparable to Eudragit E (**Figure 3C**). In contrast, neither the presence of Kollidon VA 64 (**Figure 3D**) nor HPMC-AS (**Figure 3E**) shifted TC/L signals. Concentration dependent polymer effects

on TC/L signals, polymer signals in PBS, chemical structures, and complete ^{1}H NMR spectra are detailed in the supplementary information (**Figure S10-S22**).

Impact of polymers on Perphenazine flux across and aryl-proton signals in presence and in absence of taurocholate/lecithin mixed micelles

Subsequently, we focused on the impact of the polymers on Perphenazine's flux in TC/L in PBS and in PBS across regenerated cellulose membranes, which were previously used in correlation studies of flux and bioavailability.[49-51] DLS studies indicated that aggregates did not permeate across the cellulose membrane (nominal pore size 33 nm according to the manufacturer), including aggregates bellow 33 nm as seen for Eudragit E (data not shown). Perphenazine's flux was reduced by 82% when solubilized into TC/L MIM as compared to PBS (**Figure 4**). Colesevelam increased the Perphenazine flux in TC/L in PBS in a concentration dependent manner contrasting observations in PBS (**Figure 4A**). Increased Perphenazine flux was recorded at low Eudragit E concentrations (0.01 and 0.05%) in TC/L in PBS but was reduced at 1% Eudragit E in TC/L in PBS and at all Eudragit E concentrations in PBS (**Figure 4B**). Soluplus resulted in a concentration dependent flux decrease in both TC/L in PBS and in PBS (**Figure 4C**). The flux did not change in TC/L in PBS when Kollidon VA 64 was added but decreased in PBS at 1% Kollidon VA 64 (**Figure 4D**). Similarly, HPMC-AS did not reduce the flux in TC/L in PBS, contrasting findings in PBS (**Figure 4E**). The lag time of Perphenazine increased at 1% Eudragit E in TC/L in PBS and in PBS as compared to without polymer (**Figure 4F**). Colesevelam reduced the lag time as a function of the polymer concentration in TC/L in PBS. 1% HPMC-AS increased the lag time in TC/L in PBS and in PBS (**Figure S44**). In addition to flux experiments, we analyzed Perphenazine's aryl-proton signals in TC/L in PBS in the presence of the polymers detailing the molecular interactions likely driving the flux effects.

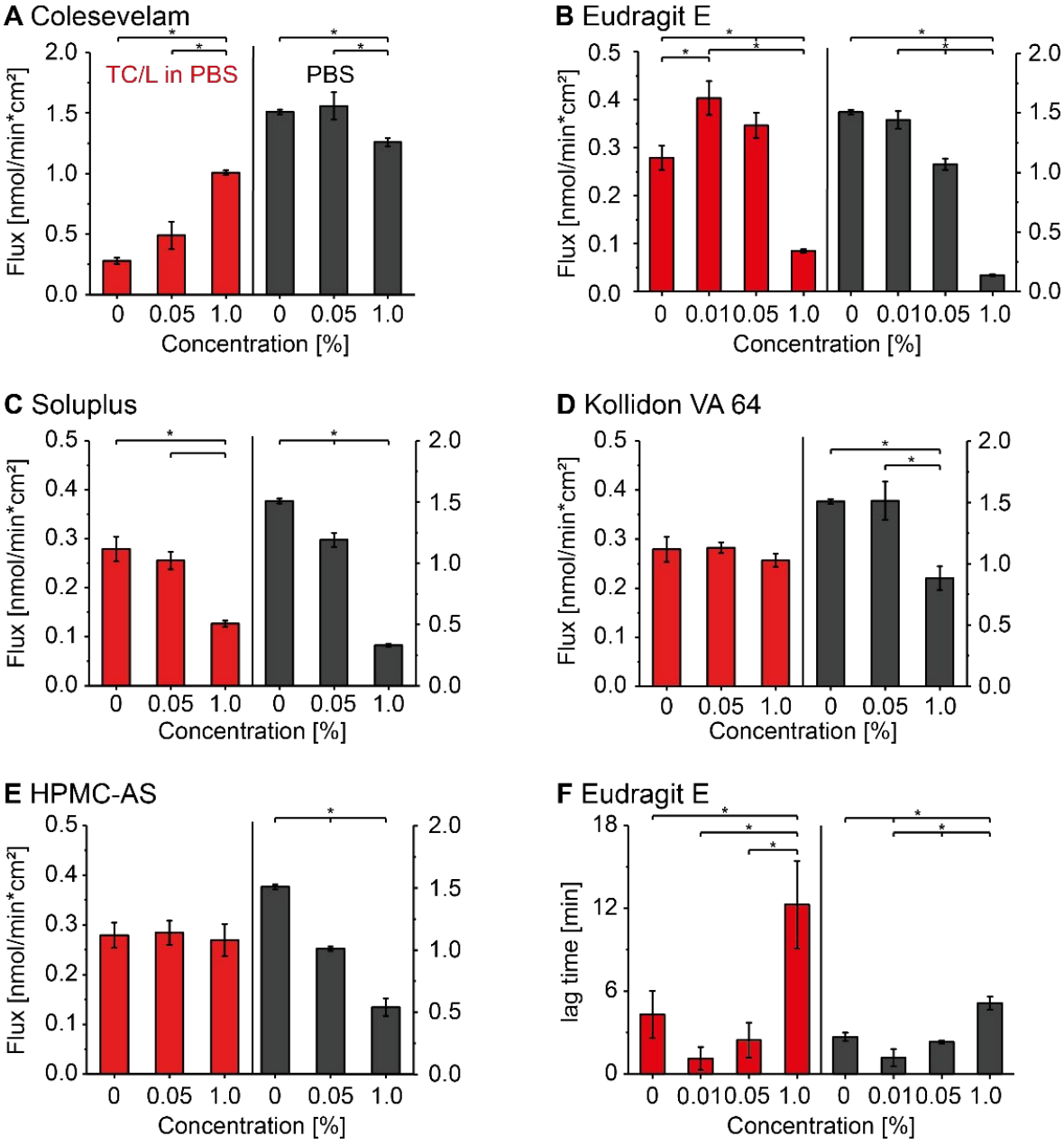

Figure 4: Perphenazine flux with (A) Colesevelam, (B) Eudragit E, (C) Soluplus, (D) Kollidon VA 64, and (E) HPMC-AS in TC/L in PBS (red) and in PBS (black) at concentrations as indicated. (F) Lag time with Eudragit E in TC/L in PBS (red) and in PBS (black) at concentrations as indicated. The left ordinate refers to data recorded in TC/L in PBS (red bars), the right ordinate to in PBS (black bars). Data at 0% polymer concentration are identical for all flux panels and given for comparison. Data shown as mean ± SD, ANOVA considering $p \leq 0.05$ as statistically significant followed by Tukey *post-hoc* test for pairwise comparison (significant differences are shown by asterisks).

Signals broadened and shifted to higher ppm at 1% Colesevelam as compared to Perphenazine in TC/L in PBS, while in PBS signal intensity decreased and signals broadened (**Figure 5A**). The aryl-proton signals shifted to higher ppm with increasing Eudragit E concentration, decreased in intensity, and disappeared at 1% Eudragit E in TC/L in PBS (**Figure 5B**).

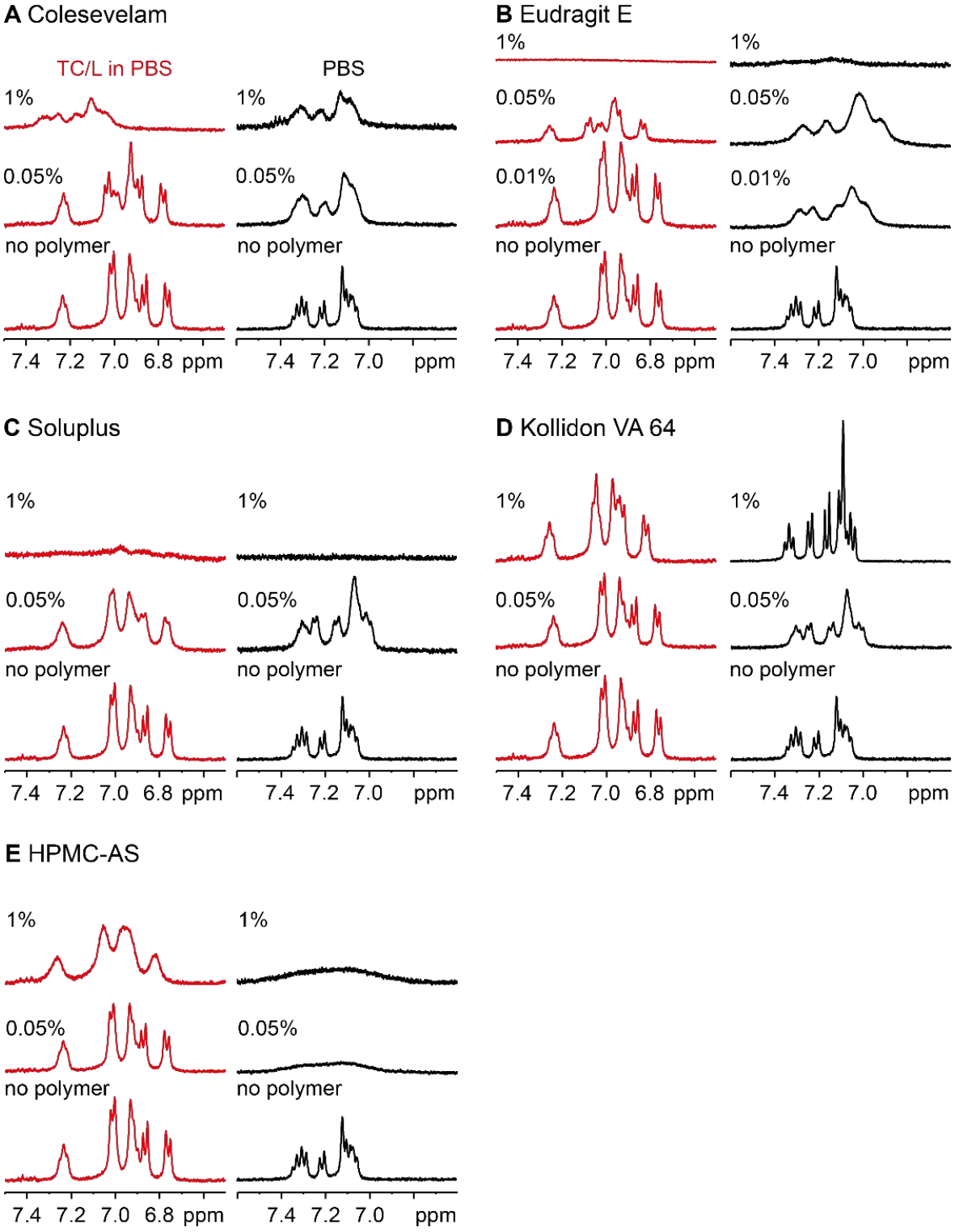

Figure 5: ^{1}H NMR excerpt of Perphenazine aryl-protons in TC/L in PBS (red) and in PBS (black) with (A) Colesevelam, (B) Eudragit E, (C) Soluplus, (D) Kollidon VA 64, and (E) HPMC-AS at concentrations as indicated. The reference spectrum of Perphenazine recorded in TC/L in PBS (red) and in PBS (black) is identical across panels and for comparison (no polymer).

In PBS, aryl-proton signals shifted with increasing Eudragit E concentration to lower ppm and broadened along with intensity decrease. Soluplus decreased Perphenazine's signal

intensity with increasing polymer concentration in TC/L in PBS and in PBS (**Figure 5C**). Additionally, broadening of the signals was observed. Kollidon VA 64 had no impact on the aryl-proton signals and only a slight shift to higher ppm was observed in TC/L in PBS (**Figure 5D**). In PBS signals sharpened and intensity increased as compared to Perphenazine in PBS. Perphenazine's aryl-proton signals broadened and shifted to higher ppm at 1% HPMC-AS with unchanged signal intensity in TC/L in PBS (**Figure 5E**). In PBS signals broadened and intensity decreased as a function of HPMC-AS concentration. Our interpretation of the aryl-proton spectra is outlined (**Figure S8**) and complete ^{1}H NMR spectra are provided in the supplementary information (**Figure S23-S27**).

Impact of polymers on Imatinib flux across and aryl-proton signals in presence and in absence of taurocholate/lecithin mixed micelles

In addition to Perphenazine, we analyzed the impact of the polymers on Imatinib's flux in TC/L in PBS and in PBS (**Figure 6**). Imatinib's interaction with TC/L MIM was previously described.[24] Imatinib's flux was reduced in TC/L in PBS as compared to in PBS. Adding Colesevelam to TC/L in PBS increased the flux as a function of Colesevelam concentration (**Figure 6A**). At 1% Colesevelam, the flux in TC/L in PBS was within the range of flux in PBS. At 0.05% Eudragit E, the flux increased in TC/L in PBS and decreased at 1% Eudragit E in TC/L in PBS and in PBS (**Figure 6B**). Soluplus reduced the flux in a concentration dependent manner in both, in TC/L in PBS and in PBS (**Figure 6C**). Kollidon VA 64 reduced Imatinib flux at 1% in TC/L in PBS (**Figure 6D**), as well as in PBS throughout the entire concentration range (**Figure 6D**). HPMC-AS also reduced the Imatinib flux at 1% in TC/L in PBS and in PBS (**Figure 6E**). The lag time was significantly increased in presence of 1% Eudragit E in TC/L in PBS but not in PBS (**Figure 6F**) and the other polymers had no impact on the lag time (**Figure S45**). We also analyzed Imatinib's aryl-proton signals in the presence of the polymers in TC/L in PBS and in PBS. Imatinib aryl-proton signals in TC/L in PBS sharpened and shifted at 1% Colesevelam as compared to Imatinib without polymer (**Figure 7A**). At 1% Colesevelam in PBS, Imatinib aryl-proton signals shifted to higher ppm as compared to without polymer. Eudragit E caused signal shifts and at 1% the signals broadened and their intensity decreased in TC/L in PBS and in PBS (**Figure 7B**). Broad signals were recorded at 1% Eudragit E in TC/L in PBS. With increasing Soluplus concentration the signal intensity decreased continuously and shifting to higher ppm. At 1% Soluplus all signals disappeared in TC/L in PBS and in PBS (**Figure 7C**).

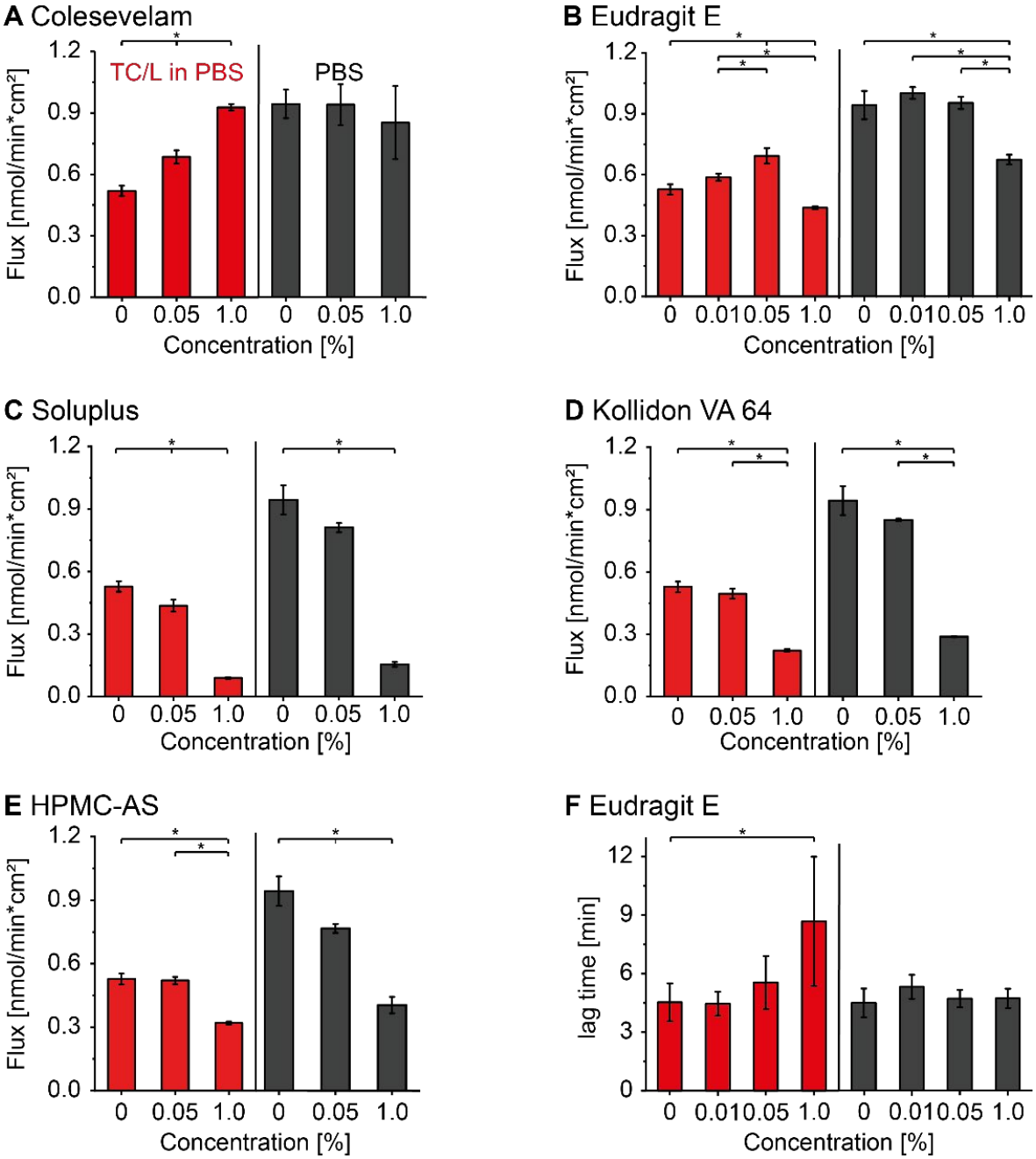

Figure 6: Imatinib flux with (A) Colesevelam, (B) Eudragit E, (C) Soluplus, (D) Kollidon VA 64, and (E) HPMC-AS in TC/L in PBS (red) and in PBS (black) at concentrations as indicated. (F) Lag time with Eudragit E in TC/L in PBS (red) and in PBS (black) at concentrations as indicated. The left ordinate refers to data recorded in TC/L in PBS (red bars), the right ordinate to in PBS (black bars). Data at 0% polymer concentration are identical for all panels and given for comparison. Data shown as mean ± SD, ANOVA considering $p \leq 0.05$ as statistically significant followed by Tukey *post-hoc* test for pairwise comparison (significant differences are shown by asterisks).

In the presence of Kollidon VA 64 signals shifted to higher ppm values as a function of concentration in TC/L in PBS and in PBS (**Figure 7D**). Increasing HPMC-AS concentration resulted in signal broadening along with intensity decrease in TC/L in PBS and in PBS

(**Figure 7E**). Broad signals were recorded at 1% HPMC-AS in PBS. All complete ^{1}H NMR spectra are detailed in the supplementary information (**Figure S28-S32**).

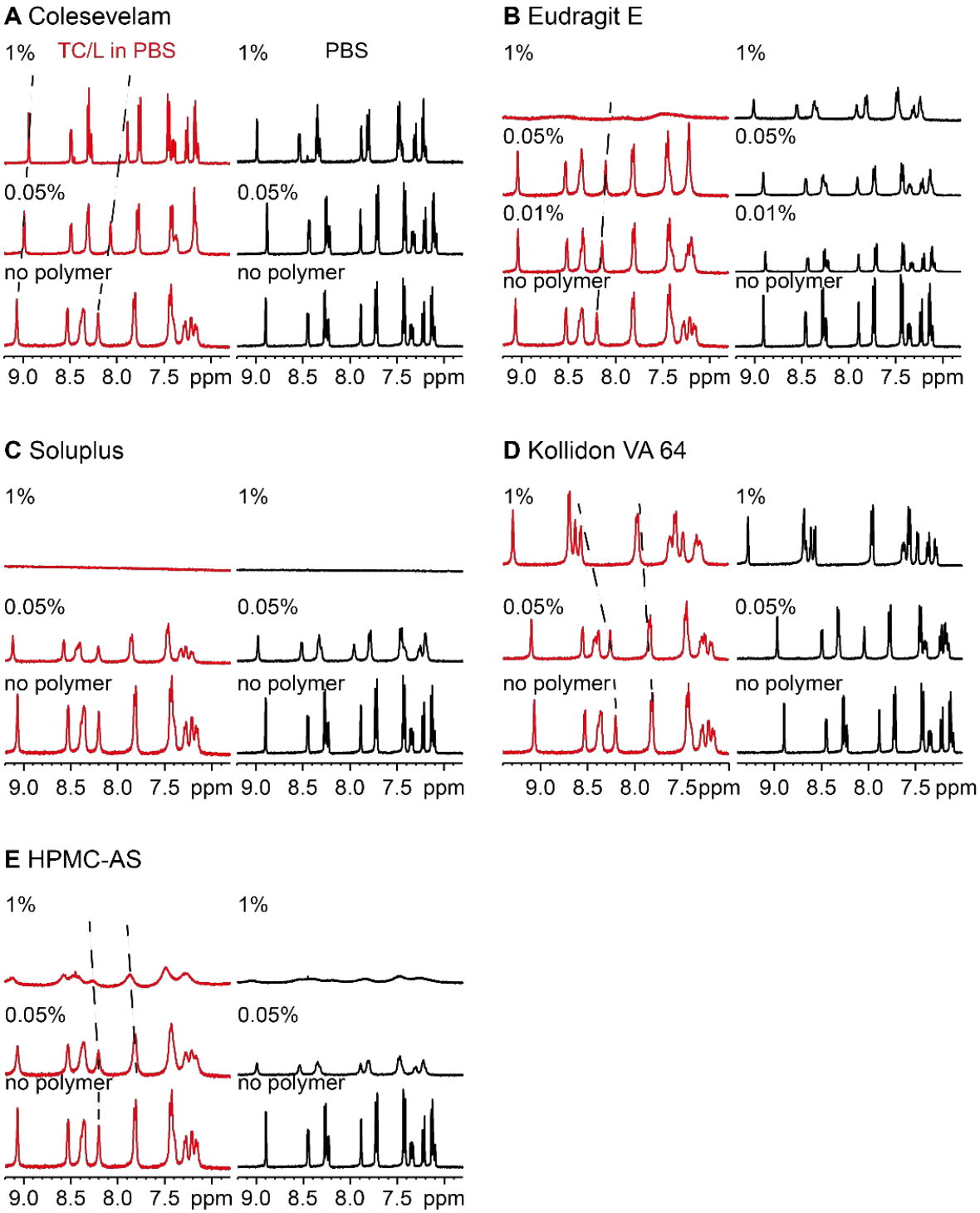

Figure 7: ^{1}H NMR excerpt of Imatinib aryl-protons in TC/L in PBS (red) and in PBS (black) with (A) Colesevelam, (B) Eudragit E, (C) Soluplus, (D) Kollidon VA 64, and (E) HPMC-AS at concentrations as indicated. The reference spectrum of Imatinib recorded in TC/L in PBS (red) and in PBS (black) is identical across panels and for comparison (no polymer). Signal shifts are indicated by dotted lines.

Impact of polymers on Metoprolol flux across and aryl-proton signals in presence and in absence of taurocholate/lecithin mixed micelles

The last studied drug was Metoprolol. The flux was reduced in TC/L in PBS as compared to in PBS (**Figure 8**). None of the polymers had an impact on Metoprolol flux in TC/L in PBS. Significant flux reduction was observed for 1% HPMC-AS in PBS as compared to in PBS. Except for Soluplus, Metoprolol aryl-proton signals were not impacted by the polymers in TC/L in PBS and in PBS (**Figure S33, S34**).

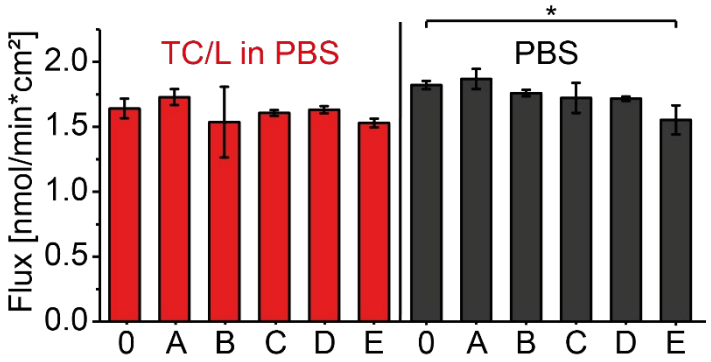

Figure 8: Metoprolol flux (0) in absence of polymer, with 1% (A) Colesevelam, (B) Eudragit E, (C) Soluplus, (D) Kollidon VA 64, and (E) HPMC-AS in TC/L in PBS (red) and in PBS (black). Data shown as mean ± SD, ANOVA considering $p \leq 0.05$ as statistically significant followed by Dunnett's *post-hoc* for pairwise comparison with the 0% polymer group (significant differences are shown by asterisks).

Diffusion coefficient of water in taurocholate/lecithin in PBS and the impact of polymer supplementation

At last, we determined diffusion coefficients of HDO in the presence of the polymers to assess the impact of diffusion on flux. The HDO diffusivity - in TC/L in PBS with Perphenazine - was $2.79 \cdot 10^{-9}$ m²/s (**Figure S35**) and was not impacted by the presence of any of the polymers at any concentration (**Table S4**).

Discussion

Colesevelam, Eudragit E, and Soluplus impacted TC/L MIM structure (referred to as "MIM interacting polymers") and Kollidon VA 64 or HPMC-AS did not ("MIM *non*-interacting polymers"; **Figure 2, 3**). These MIM *non*-interacting polymers formed supramolecular aggregates existing next to the TC/L MIM (**Figure S9**). Perphenazine was effectively solubilized into TC/L MIM (**Figure 1**). Similarly, Imatinib was integrated into TC/L MIM as previously described.[24] In the presence of MIM interacting polymers the molecular interaction of these drugs within the MIM and the resulting free drug fraction were

significantly impacted as compared to polymer-free conditions (**Figure 4**, **6**). Perphenazine shifts observed in presence of Colesevelam – used as a positive control among our polymers - were particularly striking, arguably reflecting the therapeutic use of this polymer in contrast to the other polymers which are used as excipients. In contrast, water soluble and well permeable Metoprolol did not interact with TC/L MIM (**Figure 1**) and its flux across membranes was barely or not affected by the MIM interacting polymers (**Figure 8**).

We hypothesized that MIM interacting polymers impact the molecular dynamics of TC/L MIM differently, as compared to MIM *non*-interacting polymers, and that these differences impact the flux of PWSDs across membranes. To address this hypothesis, we screened polymer concentrations from 0.01 to 1% - concentrations with possible clinical significance (**Section S6**).[41, 56-59] We started analyzing the impact of Colesevelam- an ion exchanging polymer used for bile salt binding[39] – on MIM structure and MIM molecular assembly hypothesizing and confirming that the polymer particularly impacted negatively charged TC (**Figure S3, S10, S12**). Colesevelam reduced the ^{1}H NMR signal intensity of TC and L in a Colesevelam-concentration dependent manner (**Figure 3, S12**), indicating that Colesevelam pushes TC/L from MIM into insoluble TC/L/Colesevelam particles and further reflected by the presence of aggregates (**Figure 2**). Consequently, we expected less TC/L MIM in presence of Colesevelam, hence reduced effects on crystallization inhibition, solubility, or dissolution rate of PWSDs, respectively, and as previously suggested.[60-62] Similarly, Eudragit E – frequently used in numerous formulations[41] - impacted the TC/L micellar system in a concentration dependent manner. Low Eudragit E concentrations resulted in *insoluble* aggregates containing TC/L with non-detectable ^{1}H NMR signals for L but still detectable TC signals suggesting efficient entrapment of L and to a lesser extent TC within these Eudragit E aggregates (**Figure 2, S14**). Furthermore, the lag time was significantly increased at 1% Eudragit E for both, Perphenazine and Imatinib (**Figure 4, 6**), whereas the other polymers had marginal lag time effects (**Figures S44, S45**). This may point to slower exchange kinetics of drug substance from Eudragit E structures as compared to the other polymers. Hence, Eudragit E's ability of integrating TC and L into its aggregates may critically jeopardize the solubilization of PWSD, findings which have previously suggested by others[63-65] and possibly causal to previously observed reductions in bioavailability of PWSD in presence of Eudragit E.[37, 66-68] At higher concentrations, these Eudragit E aggregates were not observed and *soluble* Eudragit E/TC/L MIM were formed. The ^{1}H NMR TC/L signals broadened and decreased in signal intensity indicating aggregates with high

molecular density and the colloids were smaller for the Eudragit E/TC/L MIM as compared to TC/L MIM (**Figure 2, 3, S8, S9**). This data confirmed previous studies reporting Eudragit E dynamics leading to either insoluble or soluble supramolecular aggregates as a function of polymer concentration.[27, 58] Similar to Eudragit E, Soluplus - an excipient enhancing the bioavailability of some PWSDs[68, 69] – interacted with TC/L MIM but in contrast to Eudragit E did not show polymer concentration effects on the formation of insoluble aggregates and soluble colloids (**Figure 3**). In alignment with previous reports, Soluplus impacted the size of TC/L MIM (**Figure 2, S8, S9**).[70, 71] Temperature effects in this range are particularly pronounced for Soluplus with a cloud point between 25 – 37 °C.[72] Kollidon VA 64 and similarly HMPC-AS at a concentration of up to 0.1% had no impact on TC/L MIM molecular structure or colloidal hydrodynamic diameters and our data indicated that pure polymer aggregates existed separate of the TC/L MIM (**Figure 2, 3**). HPMC-AS at a concentration of 0.5% and 1% generated insoluble aggregates in TC/L in PBS and in PBS resulting in turbid solutions (**Figure 2, S9**). Based on ^{1}H NMR we observed a coexistence of TC/L MIM and HPMC-AS supramolecular aggregates (**Figure 3, S20**). Soluplus had a minor impact on hydrodynamic diameters in DLS (**Figure 2**) but interacted with TC/L MIM (^{1}H NMR; **Figure 3, S25**). Future studies may further detail the resulting colloidal structures, particularly whether these structures are supramolecular or ionic. In summary, we categorized our polymers as MIM interacting (Colesevelam, Eudragit E, and Soluplus) or MIM *non*-interacting polymers (Kollidon VA 64, HPMC-AS).

We then proceeded to study the impact of either polymer category on the solubilization of drugs into TC/L MIM, and detailed the resulting supramolecular interaction of polymer, TC/L MIM, and flux. In analogy to the polymers (*vide supra*), we categorized drugs into those which interact with TC/L MIM and others that do not. Perphenazine and Imatinib interacted with TC/L MIM[24] whereas Metoprolol did not (**Figure 1**). Drug integration into the TC/L MIM - as observed for Perphenazine and Imatinib - reduced the flux across cellulose membranes (**Figure 4, 6**). These effects depended on the TC/L concentration with higher TC/L concentrations (simulating fed state) further reducing the flux (**Figure S36-S38**) and as described before.[73] Furthermore, flux depended on drug substance solubility which is why we selected a concentration (1 mmol/l) resulting in kinetically stable solutions throughout all experimental durations (**Figure S38-S43**). The flux was tested across cellulose membranes, which had previously been correlated to drug substance bioavailability.[49-51] This has been also shown for lipophilic membranes[74, 75] but we selected

cellulose membranes here to focus mostly on size exclusion. We confirmed efficient size exclusion by the absence of visible particles or DLS determined structures (data not shown). Thereby, the rate limiting step in our experiments were the events in the donor chamber and not in the diffusion layer (membrane and aqueous boundary layers) for all polymers as seen with Metoprolol (**Figure 8**). In addition, we excluded possible obstruction effects by the polymers in the donor compartment as demonstrated by comparable water (HDO) diffusion in solution among the experimental conditions (**Figure S35**).[76, 77] In conclusion, the absence of polymer obstruction effects on diffusion (**Figure S35**), absence of polymer impact on the diffusion across the diffusion layer as concluded from unaltered flux and lag time for Metoprolol (**Figure 8, S46**), we assigned the differences in flux as discussed below (**Figure 4, 6**) and lag times observed for Perphenazine and Imatinib (**Figure S44, S45**) directly to drug release phenomena from supramolecular structures including colloids being present in the donor chamber.

Starting off these findings, we studied the impact of MIM interacting polymers and MIM *non*-interacting polymers on these drugs in presence of TC/L MIM. This resulted in the differentiation of three distinct patterns. One pattern was seen with (i) Colesevelam or Eudragit E (at low concentrations) reducing the available TC/L for solubilization and consequently increasing the free drug fraction (^{1}H NMR signal shift) and flux of the MIM interacting drugs Perphenazine and Imatinib (**Figure 4-7**). An increase in free drug fraction of Perphenazine in presence of Colesevelam – as seen by higher flux (**Figure 4A**) – might also be reflected by the increased diffusion coefficient (**Table S5**). In contrast, the MIM *non*-interacting drug Metoprolol was not impacted by the presence of these polymers (**Figure 8, S33, and S34**). Metaphorically, both polymers push the drugs out of the TC/L MIM and into solution – obviously, a finding only relevant for drugs integrating into TC/L MIM. This might reduce bioavailability of drugs and fat-soluble vitamins relying on bile related solubilization.[32, 60-62] A contrasting pattern (ii) was observed for Eudragit E at higher concentration and Soluplus at any concentration. Both reduced the free drug fraction (^{1}H NMR signals shifted and decreased in intensity) and consequently the flux of MIM interacting but not MIM *non*-interacting drugs, respectively. This was in line with the formation of new colloidal structures combining all components, the polymer, the drug, and the TC/L MIM (**Figure 4-8**). Signals for Perphenazine (**Figure 5**) and Imatinib (**Figure 7**) shifted to higher ppm or lower ppm as compared to without polymer, phenomena detailed for guest-host cyclodextrin complexes before linking shifts to higher and lower ppm to

hydrophilic and hydrophobic interaction, respectively.[78-80] Lastly, a third (iii) pattern was observed for the polymers which did not substantially interact with TC/L MIM but formed separate aggregates (Kollidon VA 64 and HPMC-AS; **Figure 3**). These polymers did not (Perphenazine) or marginally (Imatinib) impact the flux of MIM interacting (**Figure 4, 6, Section S8**) or MIM *non*-interacting drugs (Metoprolol; **Figure 8**). For example, in spite of unaltered flux - hence unaltered free drug fraction - aryl-proton signal broadening of Perphenazine was observed at 1% as compared to 0.05% HPMC-AS (**Figure 5**). Because of concurrent Perphenazine flux reduction with HPMC-AS in PBS but not in TC/L in PBS, we attribute this signal broadening to drug-polymer but not MIM-polymer interaction, respectively, assuming that the MIM *non*-interacting character of the polymers does not change in presence of drug. This interpretation would also link to previous reports, reporting improved drug bioavailability with these MIM *non*-interacting polymers.[50, 81, 82] The three polymer patterns are summarized below (**Figure 9**) and potentially introduce a further optimization parameter in formulation design.

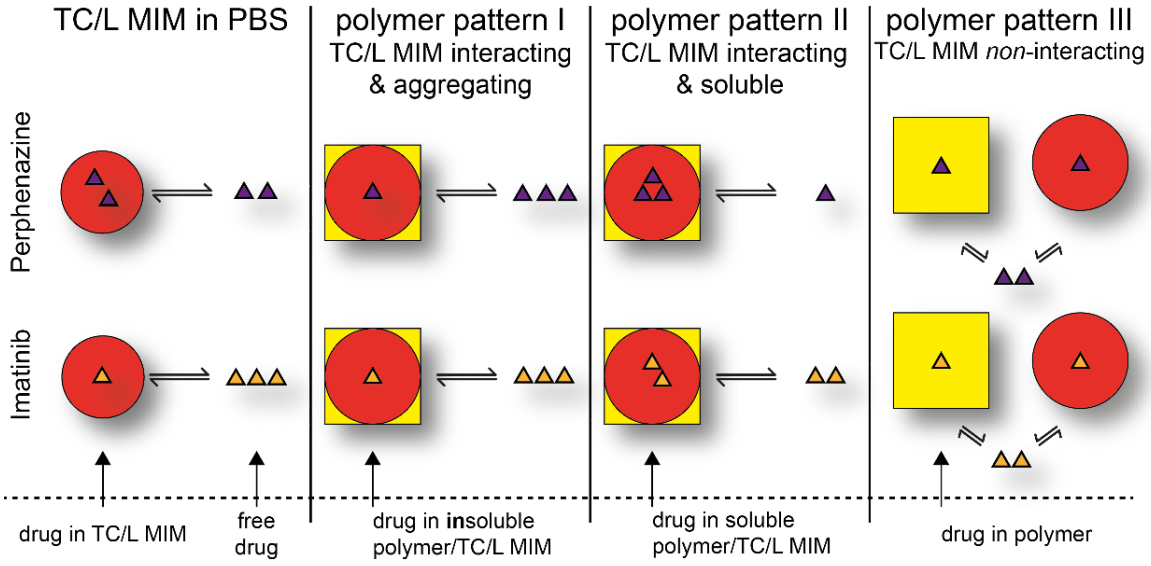

Figure 9: Illustration of interaction patterns seen for polymers (yellow squares) with TC/L MIM (red circle) with respective drugs. The cartoon abstracts Perphenazine's (purple triangle) and Imatinib's (orange triangle) relative partition into different structures formed by polymer and TC/L MIM as seen from the flux experiments.

Conclusion

Efficient solubilization by bile colloids is important for the bioavailability of many PWSD, hydrophobic vitamins or other essential components.[25, 32, 50] Hence, supporting this mechanism with properly selected polymers for formulation might offer advantages and lead

to better performing medication. Along these lines, we identified three patterns by which polymers impacted the molecular assembly and geometry of bile colloids and we linked these patterns to different flux rates of PWSD. Flux rates were previously correlated to bioavailability.[49-51] For those who wish to translate these findings into pharmaceutical application, we propose starting with the assessment whether a PWSD is solubilized by bile or not. If not (as for Metoprolol), polymer selection is rather uncritical even if the polymers affect TC/L molecular assembly and structure. However, if the PWSD interacts with the TC/L (as for Perphenazine and Imatinib), polymer selection is critical. Hence, this strategy integrates into polymer selection for maximizing the molecularly dissolved drug substance at resorption sites and extends these known strategies by taking polymer effects on bile solubilization into account. This and other exciting formulation strategies may unfold at this point. We summarize this approach in a preliminary decision tree (**Figure 10**).

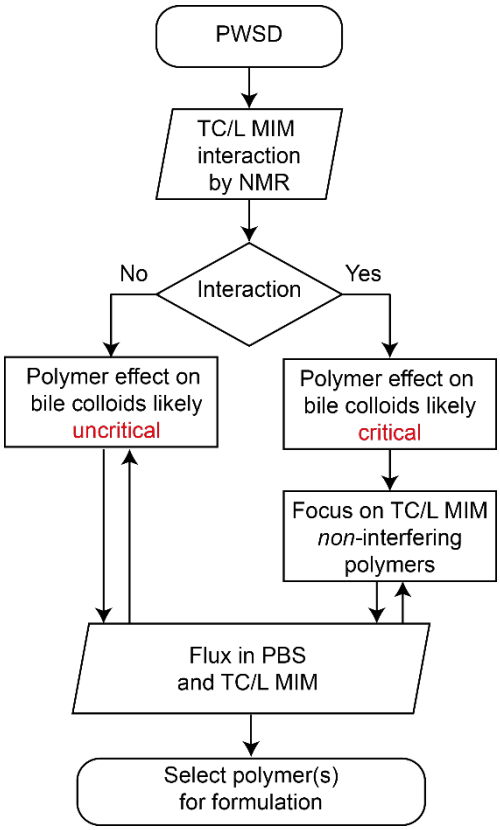

Figure 10: Preliminary decision tree for polymer selection. We classify Colesevelam, Eudragit E, and Soluplus as critical polymers in terms of TC/L MIM interaction, in contrast to uncritical polymers Kollidon VA 64 and HPMC-AS.

Possibly, future algorithms may allow prediction including performances in other fluids, e.g., fed state simulating gastrointestinal fluids and potentially biological aspirates.

Acknowledgements

We gratefully acknowledge the financial support by Novartis Pharma AG for JS. BG and CH are full time associated of Novartis and declare a possible conflict of interest. We also acknowledge the kind support by the Max Planck Gesellschaft. We would like to thank Christopher Heidenreich and Alexandra Mony for their great technical assistance.

References

1. Jiang, T.; Han, N.; Zhao, B.; Xie, Y.; Wang, S., Enhanced dissolution rate and oral bioavailability of simvastatin nanocrystal prepared by sonoprecipitation. *Drug Dev. Ind. Pharm.* **2012,** *38* (10), 1230-9.
2. Reggane, M.; Wiest, J.; Saedtler, M.; Harlacher, C.; Gutmann, M.; Zottnick, S. H.; Piechon, P.; Dix, I.; Muller-Buschbaum, K.; Holzgrabe, U.; Meinel, L.; Galli, B., Bioinspired co-crystals of Imatinib providing enhanced kinetic solubility. *Eur. J. Pharm. Biopharm.* **2018,** *128*, 290-299.
3. Balk, A.; Holzgrabe, U.; Meinel, L., 'Pro et contra' ionic liquid drugs - Challenges and opportunities for pharmaceutical translation. *Eur. J. Pharm. Biopharm.* **2015,** *94*, 291-304.
4. Balk, A.; Wiest, J.; Widmer, T.; Galli, B.; Holzgrabe, U.; Meinel, L., Transformation of acidic poorly water soluble drugs into ionic liquids. *Eur. J. Pharm. Biopharm.* **2015,** *94*, 73-82.
5. Balk, A.; Widmer, T.; Wiest, J.; Bruhn, H.; Rybak, J. C.; Matthes, P.; Muller-Buschbaum, K.; Sakalis, A.; Luhmann, T.; Berghausen, J.; Holzgrabe, U.; Galli, B.; Meinel, L., Ionic liquid versus prodrug strategy to address formulation challenges. *Pharm. Res.* **2015,** *32* (6), 2154-67.
6. Wiest, J.; Saedtler, M.; Balk, A.; Merget, B.; Widmer, T.; Bruhn, H.; Raccuglia, M.; Walid, E.; Picard, F.; Stopper, H.; Dekant, W.; Luhmann, T.; Sotriffer, C.; Galli, B.; Holzgrabe, U.; Meinel, L., Mapping the pharmaceutical design space by amorphous ionic liquid strategies. *J. Control. Release.* **2017,** *268*, 314-322.
7. Güntzel, P.; Schilling, K.; Hanio, S.; Schlauersbach, J.; Schollmayer, C.; Meinel, L.; Holzgrabe, U., Bioinspired Ion Pairs Transforming Papaverine into a Protic Ionic Liquid and Salts. *ACS Omega* **2020,** *5* (30), 19202-19209.
8. Horn, D.; Rieger, J., Organic Nanoparticles in the Aqueous Phase—Theory, Experiment, and Use. *Angew. Chem. Int. Ed.* **2001,** *40* (23).
9. Merisko-Liversidge, E. M.; Liversidge, G. G., Drug nanoparticles: formulating poorly water-soluble compounds. *Toxicol. Pathol.* **2008,** *36* (1), 43-8.
10. Six, K.; Daems, T.; de Hoon, J.; Van Hecken, A.; Depre, M.; Bouche, M. P.; Prinsen, P.; Verreck, G.; Peeters, J.; Brewster, M. E.; Van den Mooter, G., Clinical study of solid dispersions of itraconazole prepared by hot-stage extrusion. *Eur. J. Pharm. Sci.* **2005,** *24* (2-3), 179-86.
11. Pöppler, A. C.; Lübtow, M. M.; Schlauersbach, J.; Wiest, J.; Meinel, L.; Luxenhofer, R., Loading-Dependent Structural Model of Polymeric Micelles Encapsulating Curcumin by Solid-State NMR Spectroscopy. *Angew. Chem. Int. Ed. Engl.* **2019,** *58* (51), 18540-18546.
12. Porter, C. J.; Pouton, C. W.; Cuine, J. F.; Charman, W. N., Enhancing intestinal drug solubilisation using lipid-based delivery systems. *Adv. Drug Delivery Rev.* **2008,** *60* (6), 673-91.
13. Singh, D.; Bedi, N.; Tiwary, A. K., Enhancing solubility of poorly aqueous soluble drugs: critical appraisal of techniques. *J. Pharm. Investig.* **2017,** *48* (5), 509-526.

14. Bevernage, J.; Brouwers, J.; Brewster, M. E.; Augustijns, P., Evaluation of gastrointestinal drug supersaturation and precipitation: strategies and issues. *Int. J. Pharm.* **2013,** *453* (1), 25-35.
15. Rodriguez-Aller, M.; Guillarme, D.; Veuthey, J. L.; Gurny, R., Strategies for formulating and delivering poorly water-soluble drugs. *J. Drug Delivery Sci. Technol.* **2015,** *30*, 342-351.
16. Wiest, J.; Kehrein, J.; Saedtler, M.; Schilling, K.; Cataldi, E.; Sotriffer, C. A.; Holzgrabe, U.; Rasmussen, T.; Bottcher, B.; Cronin-Golomb, M.; Lehmann, M.; Jung, N.; Windbergs, M.; Meinel, L., Controlling Supramolecular Structures of Drugs by Light. *Mol Pharm* **2020,** *17* (12), 4704-4708.
17. Gamboa, A.; Schussler, N.; Soto-Bustamante, E.; Romero-Hasler, P.; Meinel, L.; Morales, J. O., Delivery of ionizable hydrophilic drugs based on pharmaceutical formulation of ion pairs and ionic liquids. *Eur. J. Pharm. Biopharm.* **2020,** *156*, 203-218.
18. Crowley, P.; Martini, L. G., Drug-excipient interactions. *Pharm. Technol.* **2001,** *4*, 7-12.
19. Pottel, J.; Armstrong, D.; Zou, L.; Fekete, A.; Huang, X. P.; Torosyan, H.; Bednarczyk, D.; Whitebread, S.; Bhhatarai, B.; Liang, G.; Jin, H.; Ghaemi, S. N.; Slocum, S.; Lukacs, K. V.; Irwin, J. J.; Berg, E. L.; Giacomini, K. M.; Roth, B. L.; Shoichet, B. K.; Urban, L., The activities of drug inactive ingredients on biological targets. *Science* **2020,** *369* (6502), 403-413.
20. Golightly, L.; Smolinske, S.; Bennett, M.; Sutherland, E. r.; Rumack, B., Pharmaceutical excipients. Adverse effects associated with inactive ingredients in drug products (Part I). *Med. Toxicol. Adv. Drug.* **1988 Mar-Apr,** *3(2)*, 128-65.
21. Werle, M., Natural and synthetic polymers as inhibitors of drug efflux pumps. *Pharm. Res.* **2008,** *25* (3), 500-511.
22. Reker, D.; Blum, S. M.; Steiger, C.; Anger, K. E.; Sommer, J. M.; Fanikos, J.; Traverso, G., "Inactive" ingredients in oral medications. *Sci. Transl. Med.* **2019,** *11* (483).
23. Borbas, E.; Tozser, P.; Tsinman, K.; Tsinman, O.; Takacs-Novak, K.; Volgyi, G.; Sinko, B.; Nagy, Z. K., Effect of Formulation Additives on Drug Transport through Size-Exclusion Membranes. *Mol. Pharm.* **2018,** *15* (8), 3308-3317.
24. Wiest, J.; Saedtler, M.; Böttcher, B.; Grüne, M.; Reggane, M.; Galli, B.; Holzgrabe, U.; Meinel, L., Geometrical and Structural Dynamics of Imatinib within Biorelevant Colloids. *Mol. Pharmaceutics* **2018,** *15* (10), 4470-4480.
25. Sugano, K.; Kataoka, M.; Mathews Cda, C.; Yamashita, S., Prediction of food effect by bile micelles on oral drug absorption considering free fraction in intestinal fluid. *Eur. J. Pharm. Sci.* **2010,** *40* (2), 118-24.
26. Hofmann, A. F., The enterohepatic circulation of bile acids in mammals: form and functions. *Front. Biosci.* **2009,** *14*, 2584-98.
27. Riethorst, D.; Baatsen, P.; Remijn, C.; Mitra, A.; Tack, J.; Brouwers, J.; Augustijns, P., An In-Depth View into Human Intestinal Fluid Colloids: Intersubject Variability in Relation to Composition. *Mol. Pharm.* **2016,** *13* (10), 3484-3493.
28. Riethorst, D.; Mols, R.; Duchateau, G.; Tack, J.; Brouwers, J.; Augustijns, P., Characterization of Human Duodenal Fluids in Fasted and Fed State Conditions. *J. Pharm. Sci.* **2016,** *105* (2), 673-681.
29. Schubiger, G.; Stocker, C.; Banziger, O.; Laubscher, B.; Zimmermann, H., Oral vitamin K1 prophylaxis for newborns with a new mixed-micellar preparation of phylloquinone: 3 years experience in Switzerland. *Eur. J. Pediatr.* **1999,** *158* (7), 599-602.
30. Augustijns, P.; Wuyts, B.; Hens, B.; Annaert, P.; Butler, J.; Brouwers, J., A review of drug solubility in human intestinal fluids: implications for the prediction of oral absorption. *Eur. J. Pharm. Sci.* **2014,** *57*, 322-32.
31. Shearer, M. J., Vitamin K in parenteral nutrition. *Gastroenterology* **2009,** *137* (5 Suppl), S105-18.
32. Sun, F.; Jaspers, T. C.; van Hasselt, P. M.; Hennink, W. E.; van Nostrum, C. F., A Mixed Micelle Formulation for Oral Delivery of Vitamin K. *Pharm. Res.* **2016,** *33* (9), 2168-79.
33. Schittny, A.; Huwyler, J.; Puchkov, M., Mechanisms of increased bioavailability through amorphous solid dispersions: a review. *Drug Delivery* **2020,** *27* (1), 110-127.

34. Karolewicz, B., A review of polymers as multifunctional excipients in drug dosage form technology. *Saudi Pharm. J.* **2016,** *24* (5), 525-536.
35. Liu, H.; Taylor, L. S.; Edgar, K. J., The role of polymers in oral bioavailability enhancement; a review. *Polymer* **2015,** *77*, 399-415.
36. Stewart, A. M.; Grass, M. E.; Brodeur, T. J.; Goodwin, A. K.; Morgen, M. M.; Friesen, D. T.; Vodak, D. T., Impact of Drug-Rich Colloids of Itraconazole and HPMCAS on Membrane Flux in Vitro and Oral Bioavailability in Rats. *Mol. Pharm.* **2017,** *14* (7), 2437-2449.
37. Saal, W.; Wyttenbach, N.; Alsenz, J.; Kuentz, M., Interactions of dimethylaminoethyl methacrylate copolymer with non-acidic drugs demonstrated high solubilization in vitro and pronounced sustained release in vivo. *Eur. J. Pharm. Biopharm.* **2018,** *125*, 68-75.
38. Vogtherr, M.; Marx, A.; Mieden, A. C.; Saal, C., Investigation of solubilising effects of bile salts on an active pharmaceutical ingredient with unusual pH dependent solubility by NMR spectroscopy. *Eur. J. Pharm. Biopharm.* **2015,** *92*, 32-41.
39. Davidson, M. H.; Dillon, M. A.; Gordon, B.; Jones, P.; Samuels, J.; Weiss, S.; Isaacsohn, J.; Toth, P.; Burke, S. K., Colesevelam hydrochloride (cholestagel): a new, potent bile acid sequestrant associated with a low incidence of gastrointestinal side effects. *Arch. Intern. Med.* **1999,** *159* (16), 1893-900.
40. Evonik Nutrition and Care GmbH, Eudragit Polymers for immediate release. https://healthcare.evonik.com/product/health-care/en/products/pharmaceutical-excipients/immediate-release/, 2020 (accessed 01 April 2020).
41. Medizinische Medien Informations GmbH, Gelbe Liste. https://www.gelbe-liste.de/, 2021 (accessed 15 December 2021).
42. Onoue, S.; Kojo, Y.; Aoki, Y.; Kawabata, Y.; Yamauchi, Y.; Yamada, S., Physicochemical and pharmacokinetic characterization of amorphous solid dispersion of tranilast with enhanced solubility in gastric fluid and improved oral bioavailability. *Drug Metab. Pharmacokinet.* **2012,** *27* (4), 379-87.
43. BASF SE, Technical information soluplus. https://documents.basf.com/d4806db3b7c1fd04c2fb8d78c37595a170986618?response-content-disposition=inline, 2019 (accessed 01 April 2020).
44. Linn, M.; Collnot, E. M.; Djuric, D.; Hempel, K.; Fabian, E.; Kolter, K.; Lehr, C. M., Soluplus(R) as an effective absorption enhancer of poorly soluble drugs in vitro and in vivo. *Eur. J. Pharm. Sci.* **2012,** *45* (3), 336-43.
45. BASF SE, Technical information Kollidon VA 64. https://documents.basf.com/54e50e670d2ea311a27b33287436dadc3d8373c1?response-content-disposition=inline, 2019 (accessed 01 April 2020).
46. Shin-Etsu Chemical Co. Ltd, information about Shin-Etsu AQOAT. https://www.shinetsupharmausa.com/en/pharma_excipients/Shin_etsu_aquoat/index.pmode , 2020 (accessed 01 April 2020). (01.04.2020).
47. Tanno, F.; Nishiyama, Y.; Kokubo, H.; Obara, S., Evaluation of hypromellose acetate succinate (HPMCAS) as a carrier in solid dispersions. *Drug Dev. Ind. Pharm.* **2004,** *30* (1), 9-17.
48. Yang, Y.; Faustino, P. J.; Volpe, D. A.; Ellison, C. D.; Lyon, R. C.; Yu, L. X., Biopharmaceutics Classification of Selected β-Blockers: Solubility and Permeability Class Membership. *Mol. Pharm.* **2007,** *4* (4), 608-14.
49. Berben, P.; Bauer-Brandl, A.; Brandl, M.; Faller, B.; Flaten, G. E.; Jacobsen, A. C.; Brouwers, J.; Augustijns, P., Drug permeability profiling using cell-free permeation tools: Overview and applications. *Eur. J. Pharm. Sci.* **2018,** *119*, 219-233.
50. Kawai, Y.; Fujii, Y.; Tabata, F.; Ito, J.; Metsugi, Y.; Kameda, A.; Akimoto, K.; Takahashi, M., Profiling and Trend Analysis of Food Effects on Oral Drug Absorption Considering Micelle Interaction and Solubilization by Bile Micelles. *Drug Metab. Pharmacokinet.* **2011,** *26* (2), 180-191.
51. Berben, P.; Brouwers, J.; Augustijns, P., The artificial membrane insert system as predictive tool for formulation performance evaluation. *Int. J. Pharm.* **2018,** *537* (1-2), 22-29.

52. Baucke, F. G. K., Further Insight into the Dissociation Mechanism of Glass Electrodes. The Response in Heavy Water. *J. Phys. Chem. B* **1998,** *102* (24), 4835-4841.
53. Jerschow, A.; Müller, N., 3D Diffusion-Ordered TOCSY for Slowly Diffusing Molecules. *J. Magn. Reson.* **1996,** *123* (2), 222-225.
54. Jerschow, A.; Müller, N., Suppression of Convection Artifacts in Stimulated-Echo Diffusion Experiments. Double-Stimulated-Echo Experiments. *J. Magn. Reson.* **1997,** *125* (2), 372-375.
55. Grosvenor, M. P.; Lofroth, J. E., Interaction between bile salts and beta-adrenoceptor antagonists. *Pharm. Res.* **1995,** *12* (5), 682-6.
56. Guthrie, B.; Makubate, B.; Hernandez-Santiago, V.; Dreischulte, T., The rising tide of polypharmacy and drug-drug interactions: population database analysis 1995-2010. *BMC Med.* **2015,** *13*, 74.
57. Charlesworth, C. J.; Smit, E.; Lee, D. S.; Alramadhan, F.; Odden, M. C., Polypharmacy Among Adults Aged 65 Years and Older in the United States: 1988-2010. *J. Gerontol. A Biol. Sci. Med. Sci.* **2015,** *70* (8), 989-95.
58. Schiller, C.; Fröhlich, C. P.; Giessmann, T.; Siegmund, W.; Monnikes, H.; Hosten, N.; Weitschies, W., Intestinal fluid volumes and transit of dosage forms as assessed by magnetic resonance imaging. *Aliment. Pharmacol. Ther.* **2005,** *22* (10), 971-9.
59. Koziolek, M.; Grimm, M.; Schneider, F.; Jedamzik, P.; Sager, M.; Kuhn, J. P.; Siegmund, W.; Weitschies, W., Navigating the human gastrointestinal tract for oral drug delivery: Uncharted waters and new frontiers. *Adv. Drug Delivery Rev.* **2016,** *101*, 75-88.
60. Bakatselou, V.; Oppenheim, R. C.; Dressman, J. B., Solubilization and wetting effects of bile salts on the dissolution of steroids. *Pharm. Res.* **1991,** *8* (12), 1461-9.
61. Mithani, S. D.; Bakatselou, V.; TenHoor, C. N.; Dressman, J. B., Estimation of the increase in solubility of drugs as a function of bile salt concentration. *Pharm. Res.* **1996,** *13* (1), 163-7.
62. Chen, J.; Mosquera-Giraldo, L. I.; Ormes, J. D.; Higgins, J. D.; Taylor, L. S., Bile Salts as Crystallization Inhibitors of Supersaturated Solutions of Poorly Water-Soluble Compounds. *Cryst. Growth Des.* **2015,** *15* (6), 2593-2597.
63. Serajuddin, A. T.; Sheen, P. C.; Mufson, D.; Bernstein, D. F.; Augustine, M. A., Physicochemical basis of increased bioavailability of a poorly water-soluble drug following oral administration as organic solutions. *J. Pharm. Sci.* **1988,** *77* (4), 325-9.
64. Hu, K.; Cao, S.; Hu, F.; Feng, J., Enhanced oral bioavailability of docetaxel by lecithin nanoparticles: preparation, in vitro, and in vivo evaluation. *Int. J. Nanomed.* **2012,** *7*, 3537-45.
65. Kumar, B. S.; Saraswathi, R.; Kumar, K. V.; Jha, S. K.; Venkates, D. P.; Dhanaraj, S. A., Development and characterization of lecithin stabilized glibenclamide nanocrystals for enhanced solubility and drug delivery. *Drug Delivery* **2014,** *21* (3), 173-84.
66. Sinha, V. R.; Kumria, R., Binders for colon specific drug delivery: an in vitro evaluation. *Int. J. Pharm.* **2002,** *249* (1-2), 23-31.
67. Moustafine, R. I.; Salachova, A. R.; Frolova, E. S.; Kemenova, V. A.; Van den Mooter, G., Interpolyelectrolyte complexes of Eudragit E PO with sodium alginate as potential carriers for colonic drug delivery: monitoring of structural transformation and composition changes during swellability and release evaluating. *Drug Dev. Ind. Pharm.* **2009,** *35* (12), 1439-51.
68. Yoshida, T.; Kurimoto, I.; Umejima, H.; Watanabe, S.; Sako, K.; Kikuchi, A., Effects of dissolved state of aminoalkyl methacrylate copolymer E/HCl on solubility enhancement effect for poorly water-soluble drugs. *Colloid Polym. Sci.* **2012,** *291* (5), 1191-1199.
69. Pignatello, R.; Corsaro, R., Polymeric Nanomicelles of Soluplus® as a Strategy for Enhancing the Solubility, Bioavailability and Efficacy of Poorly Soluble Active Compounds. *Curr. Nanomed.* **2019,** *9* (3), 184-197.
70. Pinto, J. M. O.; Rengifo, A. F. C.; Mendes, C.; Leao, A. F.; Parize, A. L.; Stulzer, H. K., Understanding the interaction between Soluplus(R) and biorelevant media components. *Colloids Surf. B* **2020,** *187*, 110673.

71. Thiry, J.; Broze, G.; Pestieau, A.; Tatton, A. S.; Baumans, F.; Damblon, C.; Krier, F.; Evrard, B., Investigation of a suitable in vitro dissolution test for itraconazole-based solid dispersions. *Eur. J. Pharm. Sci.* **2016,** *85*, 94-105.
72. Hughey, J. R.; Keen, J. M.; Miller, D. A.; Kolter, K.; Langley, N.; McGinity, J. W., The use of inorganic salts to improve the dissolution characteristics of tablets containing Soluplus(R)-based solid dispersions. *Eur. J. Pharm. Sci.* **2013,** *48* (4-5), 758-66.
73. Yano, K.; Masaoka, Y.; Kataoka, M.; Sakuma, S.; Yamashita, S., Mechanisms of membrane transport of poorly soluble drugs: role of micelles in oral absorption processes. *J. Pharm. Sci.* **2010,** *99* (3), 1336-45.
74. Dahan, A.; Miller, J. M., The solubility-permeability interplay and its implications in formulation design and development for poorly soluble drugs. *AAPS. J.* **2012,** *14* (2), 244-51.
75. Abdiche, Y. N.; Myszka, D. G., Probing the mechanism of drug/lipid membrane interactions using Biacore. *Anal. Biochem.* **2004,** *328* (2), 233-43.
76. Cvijic, S.; Parojcic, J.; Langguth, P., Viscosity-mediated negative food effect on oral absorption of poorly-permeable drugs with an absorption window in the proximal intestine: In vitro experimental simulation and computational verification. *Eur. J. Pharm. Sci.* **2014,** *61*, 40-53.
77. Gao, P.; Fagerness, P. E., Diffusion in HPMC gels. I. Determination of drug and water diffusivity by pulsed-field-gradient spin-echo NMR. *Pharm. Res.* **1995,** *12* (7), 955-64.
78. Eckenroad, K. W.; Manley, G. A.; Yehl, J. B.; Pirnie, R. T.; Strein, T. G.; Rovnyak, D., An Edge Selection Mechanism for Chirally Selective Solubilization of Binaphthyl Atropisomeric Guests by Cholate and Deoxycholate Micelles. *Chirality* **2016,** *28* (7), 525-33.
79. O'Farrell, C. M.; Hagan, K. A.; Wenzel, T. J., Water-Soluble Calix[4]Resorcinarenes as Chiral NMR Solvating Agents for Bicyclic Aromatic Compounds. *Chirality* **2009,** *21* (10), 911-921.
80. Smith, K. J.; Wilcox, J. D.; Mirick, G. E.; Wacker, L. S.; Ryan, N. S.; Vensel, D. A.; Readling, R.; Domush, H. L.; Amonoo, E. P.; Shariff, S. S.; Wenzel, T. J., Calix[4]arene, calix[4]resorcarene, and cyclodextrin derivatives and their lanthanide complexes as chiral NMR shift reagents. *Chirality* **2003,** *15 Suppl*, S150-8.
81. Pinto, J. M. O.; Leao, A. F.; Riekes, M. K.; Franca, M. T.; Stulzer, H. K., HPMCAS as an effective precipitation inhibitor in amorphous solid dispersions of the poorly soluble drug candesartan cilexetil. *Carbohydr. Polym.* **2018,** *184*, 199-206.
82. Chmiel, K.; Knapik-Kowalczuk, J.; Jurkiewicz, K.; Sawicki, W.; Jachowicz, R.; Paluch, M., A New Method To Identify Physically Stable Concentration of Amorphous Solid Dispersions (I): Case of Flutamide + Kollidon VA64. *Mol. Pharm.* **2017,** *14* (10), 3370-3380.

Supporting information

S1 Methods

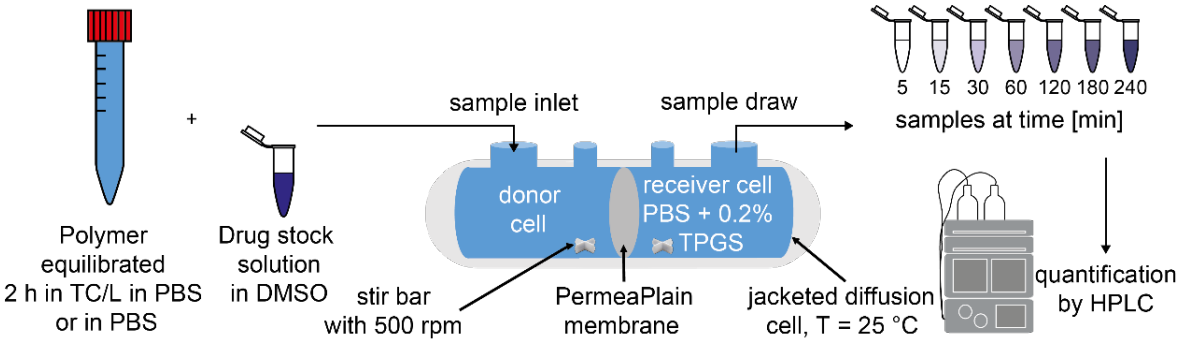

Figure S1: Flux assay as described in 2.2.3

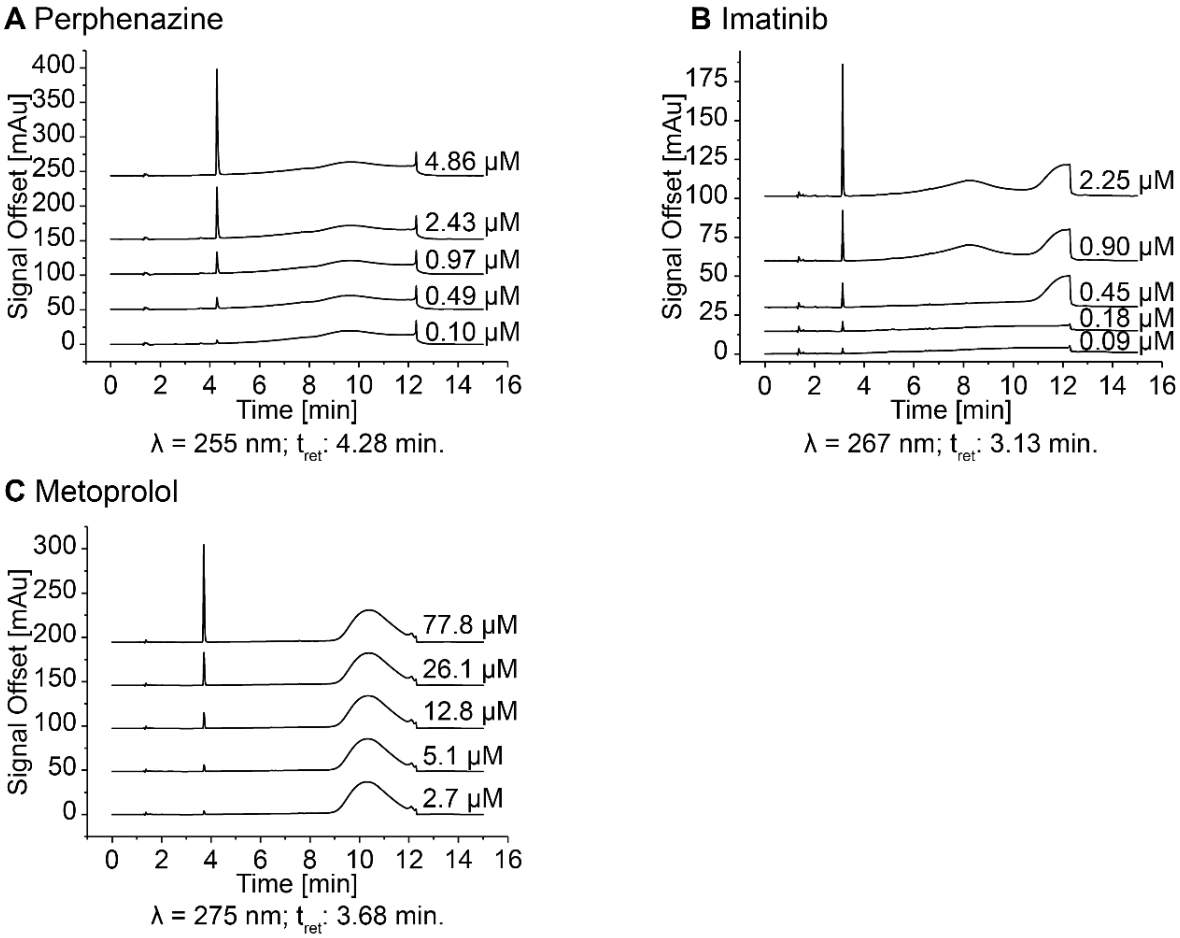

Figure S2: HPLC calibration spectra for (A) Perphenazine, (B) Imatinib, and (C) Metoprolol. Signal area under the curve (AUC) increased linearly with concentration. Respective nominal drug concentrations are shown on the right side of each spectrum. λ represents wavelength of detector and t_{ret} retention time of respective drug peak.

S2 [1]H nuclear magnetic resonance data interpretation

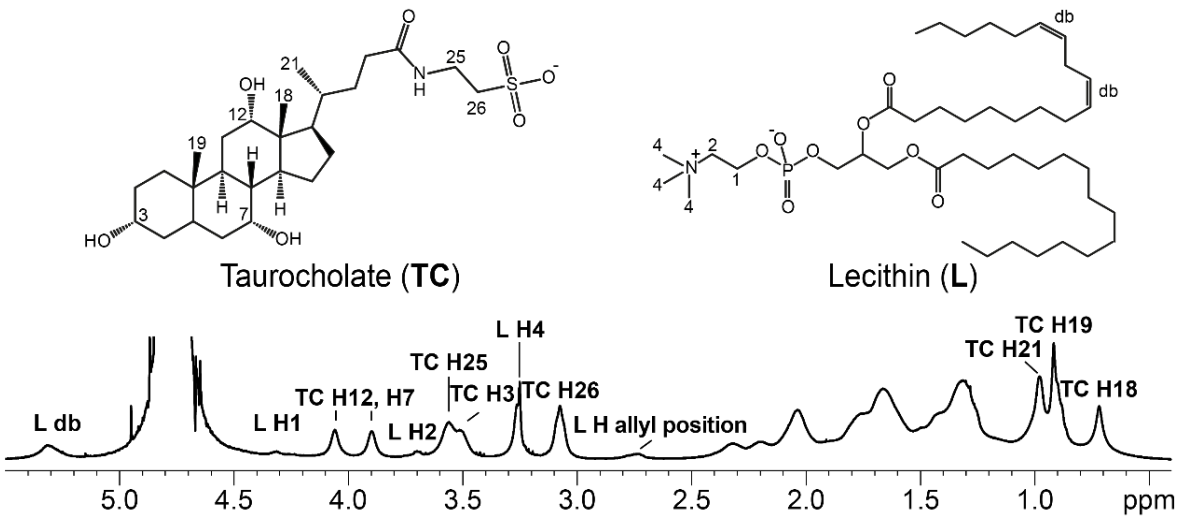

Figure S3: [1]H NMR signal assignment of **t**auro**c**holate (**TC**) and lecithin (**L**) based on.[1]

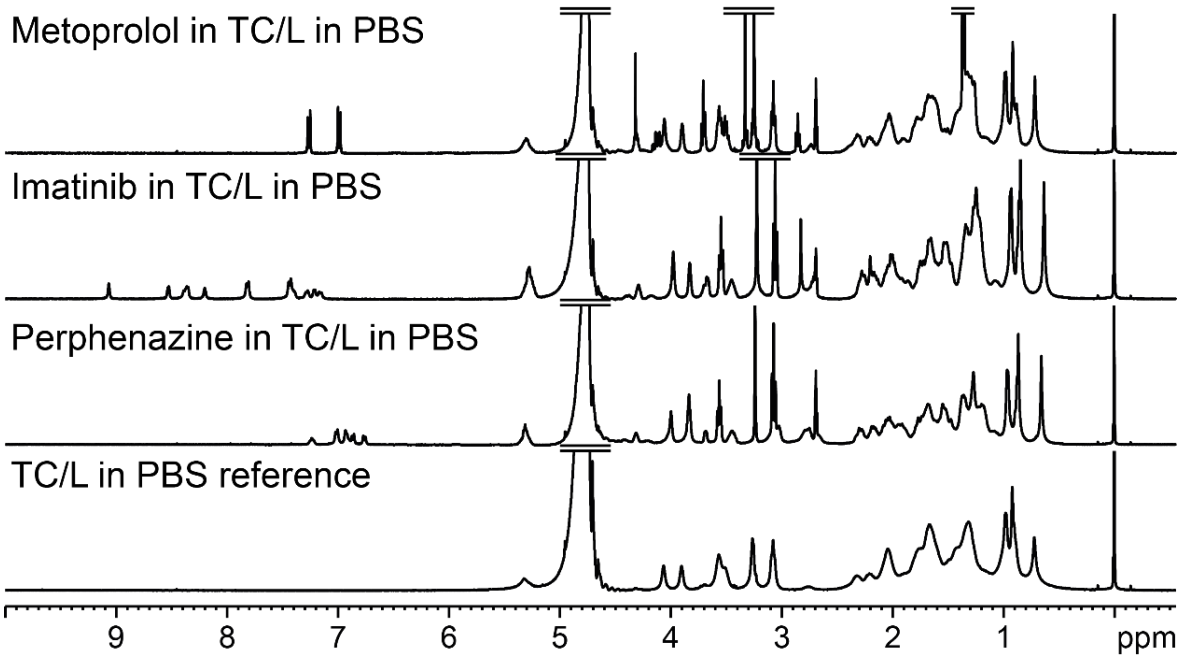

Figure S4: Complete [1]H NMR spectra of Metoprolol, Imatinib, and Perphenazine with TC/L. Bottom shows TC/L reference spectrum.

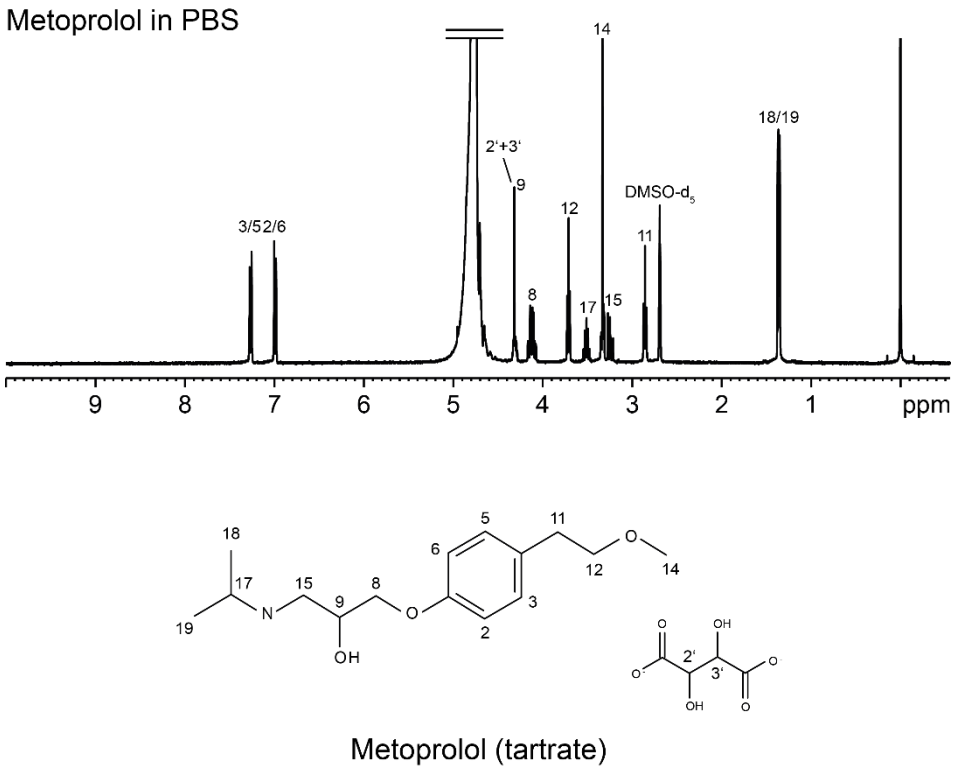

Figure S5: Complete ^{1}H NMR spectrum with signal assignment and respective molecular structure of Metoprolol in PBS. Standard 1D and 2D NMR techniques were applied for signal assignment.

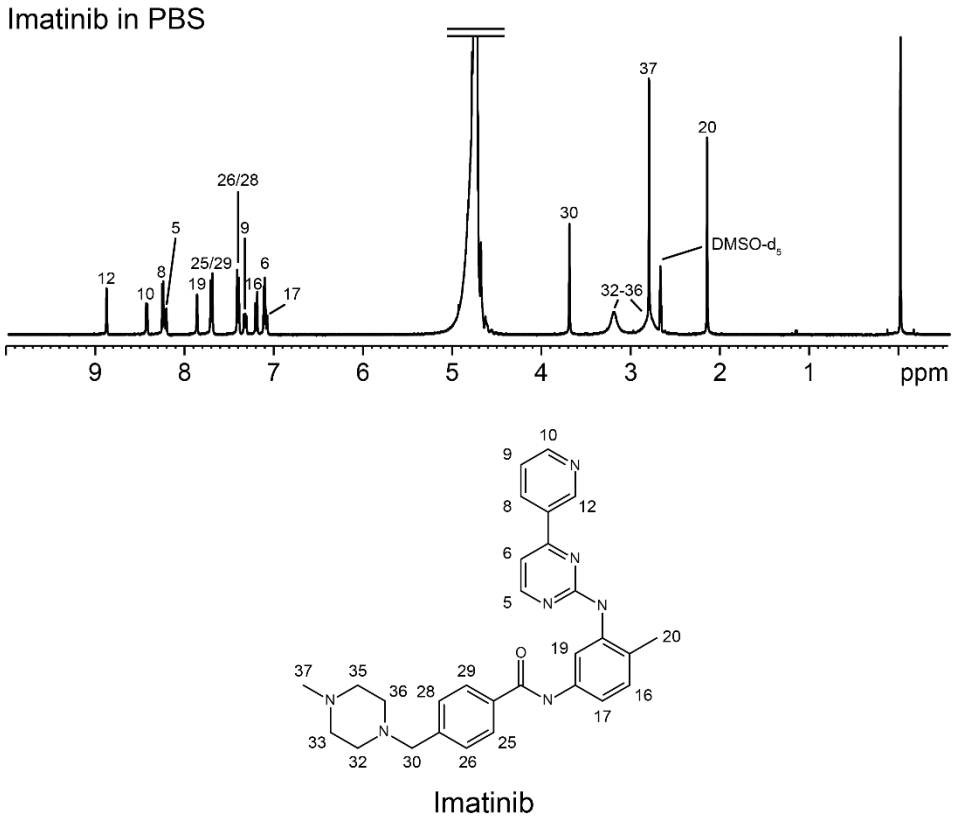

Figure S6: Complete ^{1}H NMR spectrum with signal assignment and respective molecular structure of Imatinib in PBS. Standard 1D and 2D NMR techniques were applied for signal assignment.

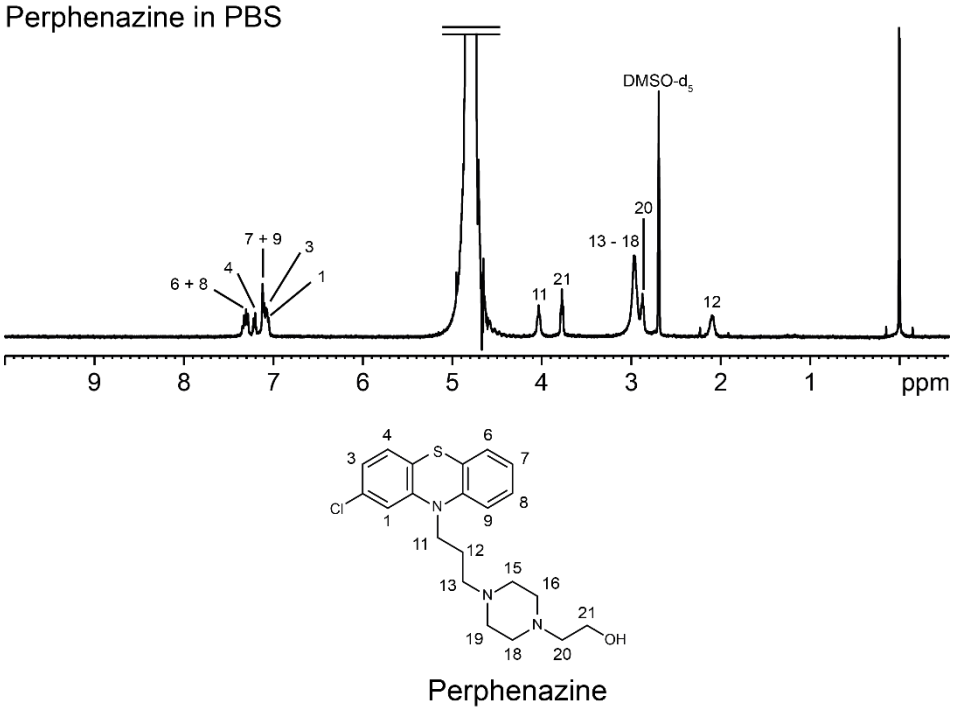

Figure S7: Complete ^{1}H NMR spectrum with signal assignment and respective molecular structure of Perphenazine in PBS. Standard 1D and 2D NMR techniques were applied for signal assignment.

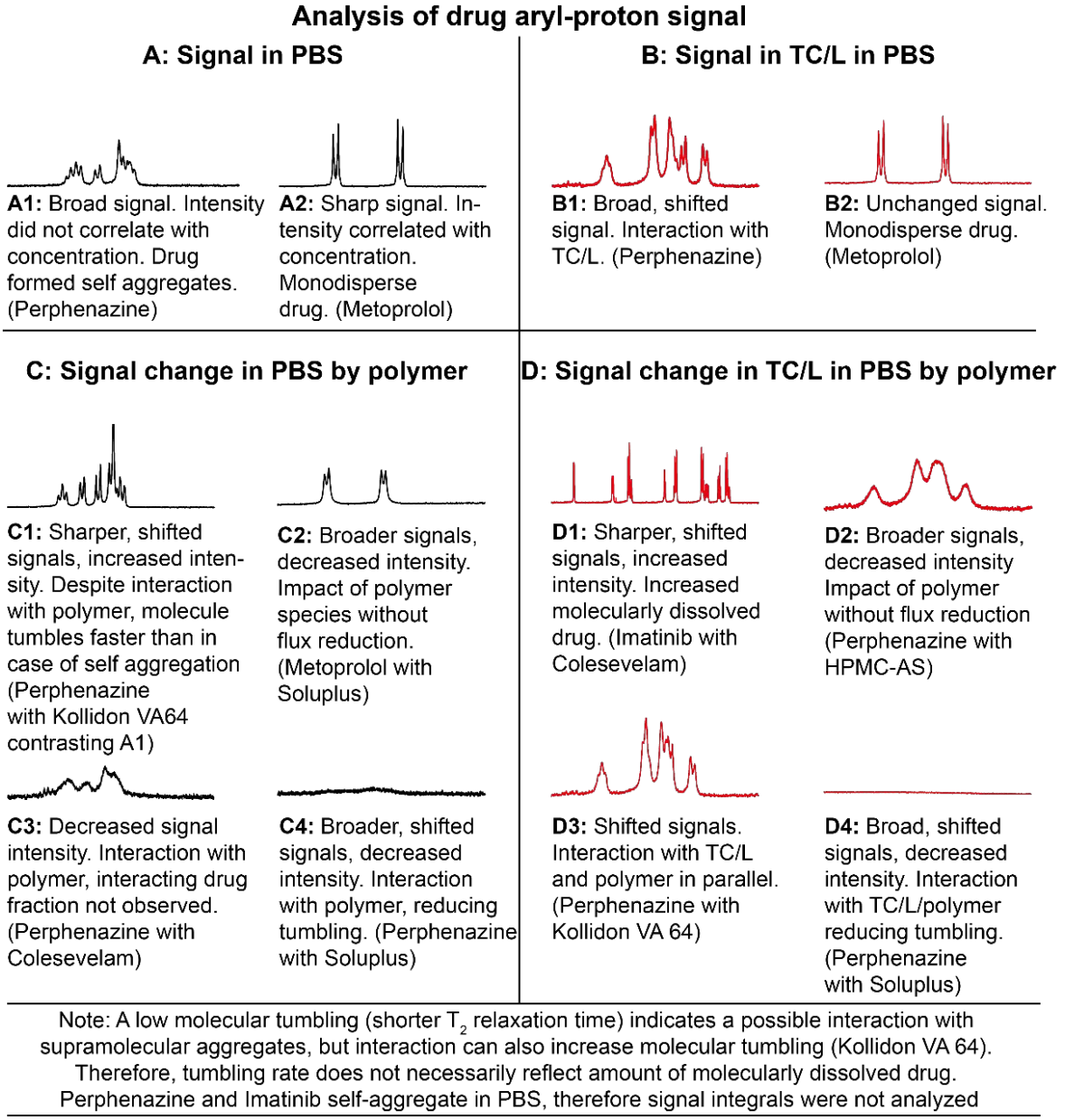

Figure S8: Interpretation of the NMR spectral patterns of the aryl-proton signals of drug molecules without polymer in PBS (A) and in TC/L in PBS (B) and with polymer in PBS (C) and in TC/L in PBS (D).

S3 Polymer characterization in TC/L in PBS and in PBS

S3.1 Particle size analysis in PBS by dynamic light scattering

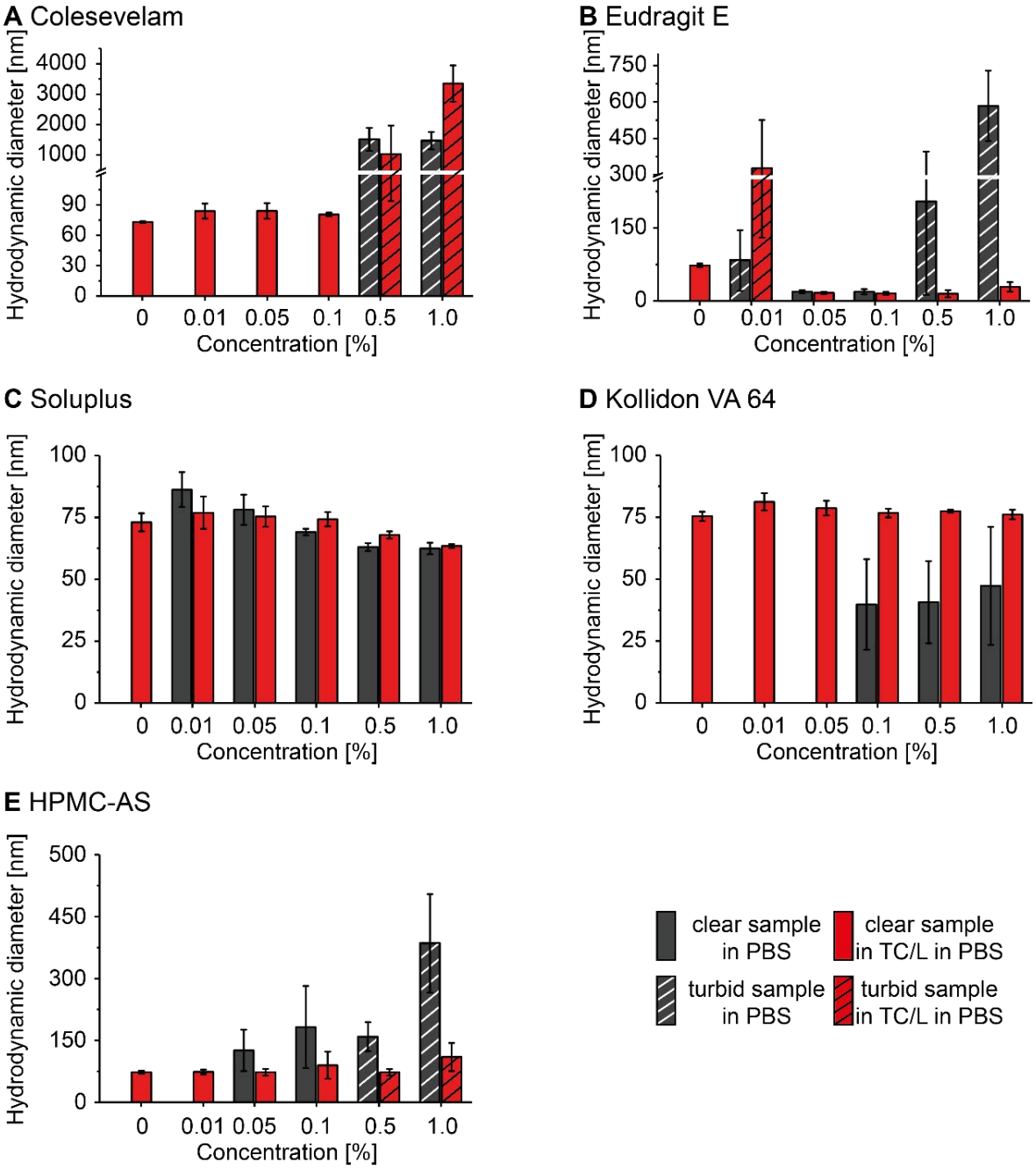

Figure S9: Mean hydrodynamic diameters of colloids in PBS (grey) and in TC/L in PBS (red) with (A) Colesevelam, (B) Eudragit E, (C) Soluplus, (D) Kollidon VA 64, and (E) HPMC-AS at different concentrations by DLS (mean ± SD). At ≥0.5% Colesevelam particles were detected (A grey). Turbidity was also observed for Eudragit E at 0.01, 0.5, and 1% (B, grey). At 0.05 and 0.1% Eudragit E formed colloids around 20 nm. Conversely, Eudragit E in TC/L in PBS formed colloids at ≥0.05% (B, red). Soluplus formed 60-90 nm particles in PBS (C, grey). At ≥0.1% Kollidon VA 64 particles around 40 nm were observed (D, grey). Hydrodynamic diameters of HPMC-AS ranged from 70 to 250 nm at 0.05 and 0.1% (E, grey). At ≥0.5% particle size up to 500 nm were observed along with turbidity.

Table S1: Polymer dynamic viscosities in TC/L in PBS and in PBS at 25 °C used for DLS data adjustment [mPa*s].

Concentration [%]	Colesevelam		Eudragit E		Soluplus		Kollidon VA 64		HPMC-AS	
	PBS	TC/L in PBS	PBS	TC/L in PBS	PBS	TC/L in PBS	PBS	TC/L in PBS	PBS	TC/L in PBS
0.01			0.9410	0.9457	0.9431	0.9312	N/A	0.9339	N/A	0.9488
0.05			0.9300	0.9258	0.9255	0.9400	N/A	0.9398	0.9540	0.9767
0.1	N/A	N/A	0.9337	0.9275	0.9269	0.9450	0.9527	0.9503	1.0014	1.0251
0.5			0.9689	0.9422	0.9572	0.9805	0.9866	1.0116	1.3985	1.3942
1			0.9366	0.9602	1.0014	1.0376	1.0685	1.0945	1.8190	1.4707
PBS	0.9104									
TC/L reference	0.9258									

Table S2: Mean polydispersity index (PDI) with standard deviation of colloids in TC/L in PBS.

Concentration [%]	Colesevelam		Eudragit E		Soluplus		Kollidon VA 64		HPMC-AS	
	PDI mean	PDI SD	PDI mean	PDI SD	PDI mean	PDI SD	PDI mean	PDI SD	PDI mean	PDI SD
0.01	0.075	0.036	0.23	0.12	0.108	0.007	0.143	0.032	0.083	0.049
0.05	0.050	0.030	0.180	0.088	0.099	0.018	0.086	0.020	0.060	0.015
0.1	0.095	0.015	0.19	0.10	0.077	0.033	0.097	0.012	0.107	0.078
0.5	0.40	0.24	0.13	0.13	0.066	0.024	0.104	0.032	0.126	0.044
1	0.933	0.070	0.249	0.029	0.062	0.013	0.127	0.025	0.173	0.014
TC/L reference	0.144	0.057	0.06	0.030	0.056	0.041	0.069	0.019	0.06	0.030

Table S3: Mean polydispersity index (PDI) with standard deviation of colloids in PBS.

Concentration [%]	Colesevelam		Eudragit E		Soluplus		Kollidon VA 64		HPMC-AS	
	PDI mean	PDI SD	PDI mean	PDI SD	PDI mean	PDI SD	PDI mean	PDI SD	PDI mean	PDI SD
0.01	N/A	N/A	0.32	0.26	0.14	0.02	N/A	N/A	N/A	N/A
0.05	N/A	N/A	0.20	0.13	0.088	0.023	N/A	N/A	0.30	0.09
0.1	N/A	N/A	0.27	0.01	0.059	0.013	0.40	0.03	0.21	0.07
0.5	0.52	0.15	0.23	0.08	0.051	0.018	0.24	0.04	0.23	0.03
1	0.37	0.09	0.30	0.04	0.053	0.024	0.23	0.02	0.36	0.03

S3.2 ^{1}H nuclear magnetic resonance analysis of polymers

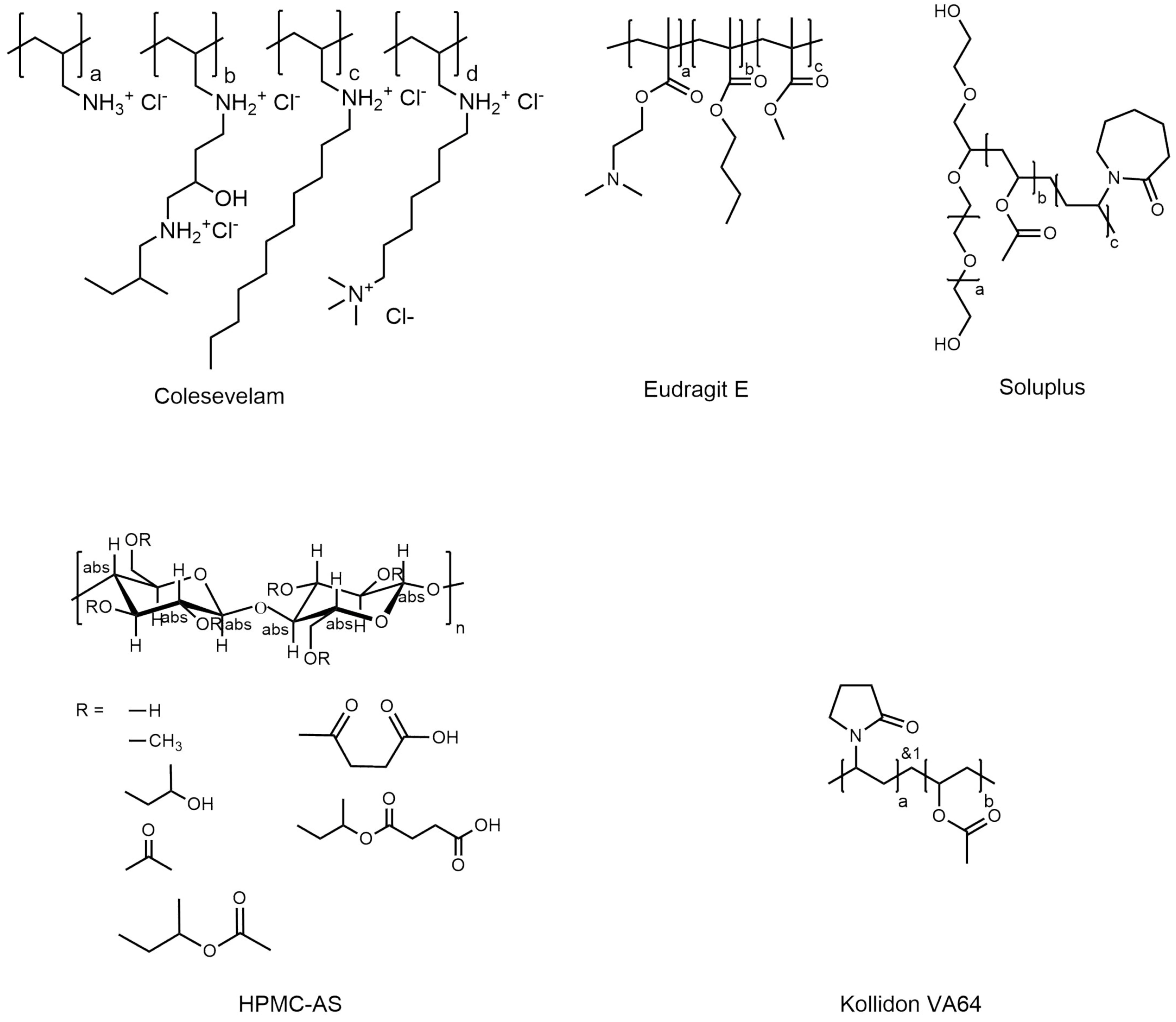

Figure S10: Chemical structures of used polymers.

S3.2.1 Colesevelam in PBS

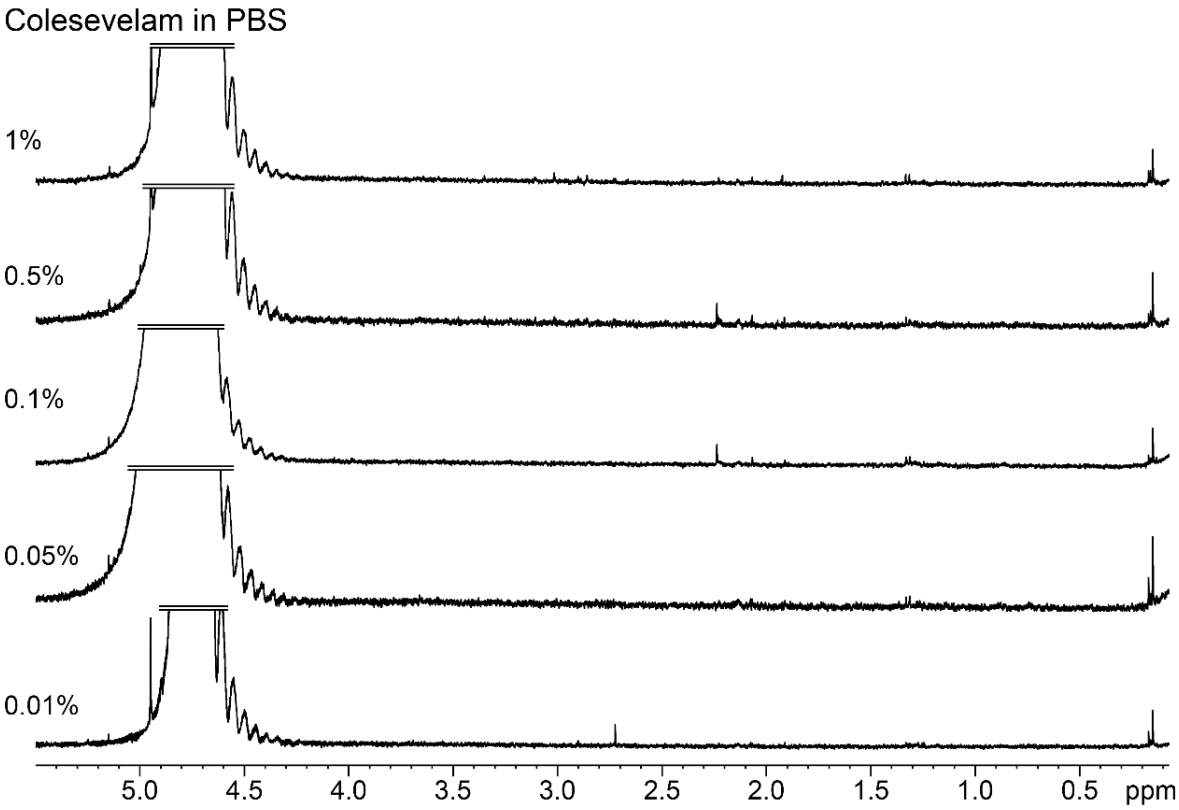

Figure S11: ^{1}H NMR spectra of Colesevelam at 0.01, 0.05, 0.1, 0.5, and 1% in PBS. No Colesevelam signals were detected.

S3.2.2 Colesevelam in TC/L in PBS

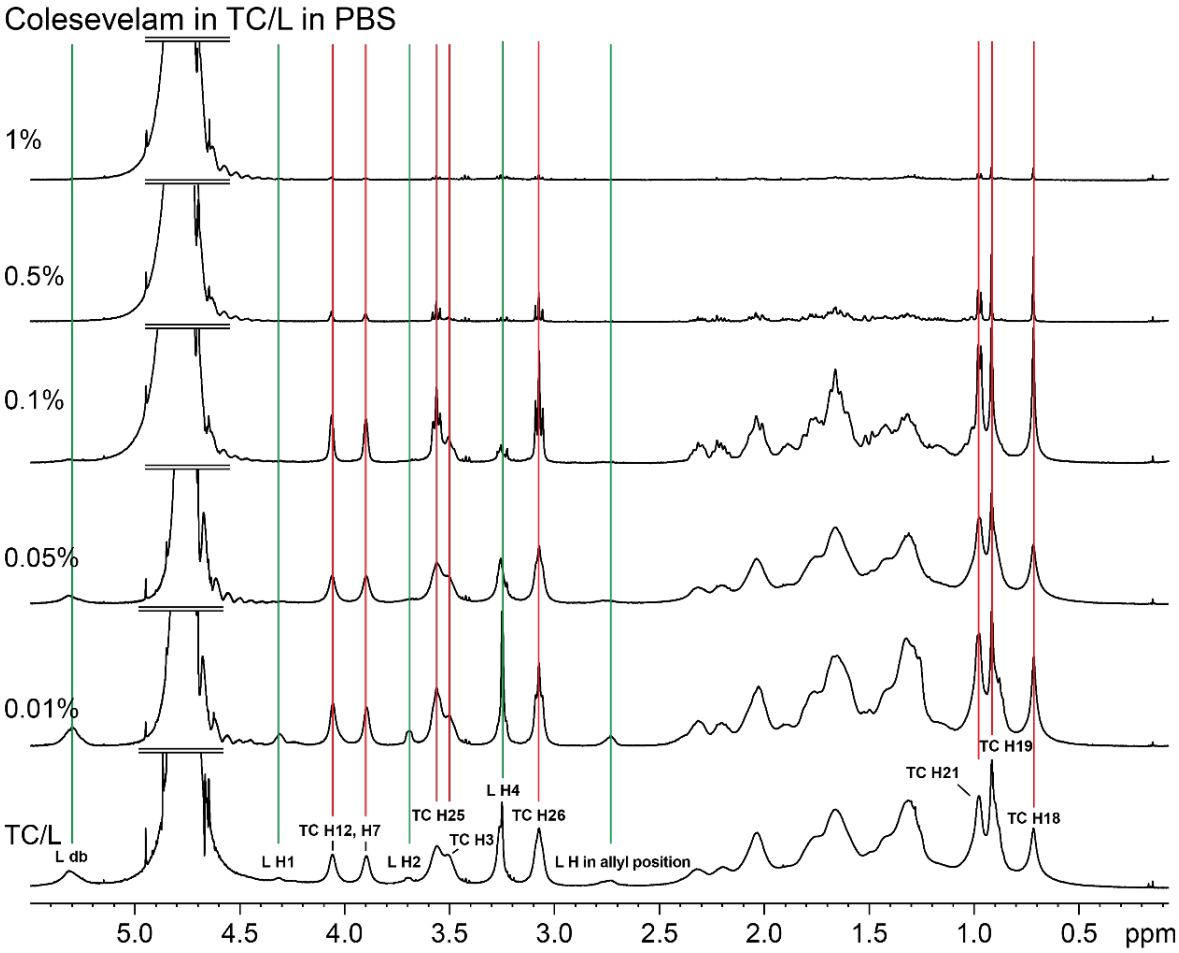

Figure S12: ^{1}H NMR spectra of Colesevelam at 0.01, 0.05, 0.1, 0.5, and 1% in TC/L in PBS indicated as (L) green lines and (TC) red lines. TC/L reference spectrum is shown (bottom). TC/L signal intensities decreased as a function of Colesevelam concentration. At ≥0.1% signals sharpened (e.g., TC H25 and H26). At ≥0.5 sharp TC signals with low intensity were found indicating precipitation of TC/L. Few TC remains in solution, but does not aggregate.

S3.2.3 Eudragit E in PBS

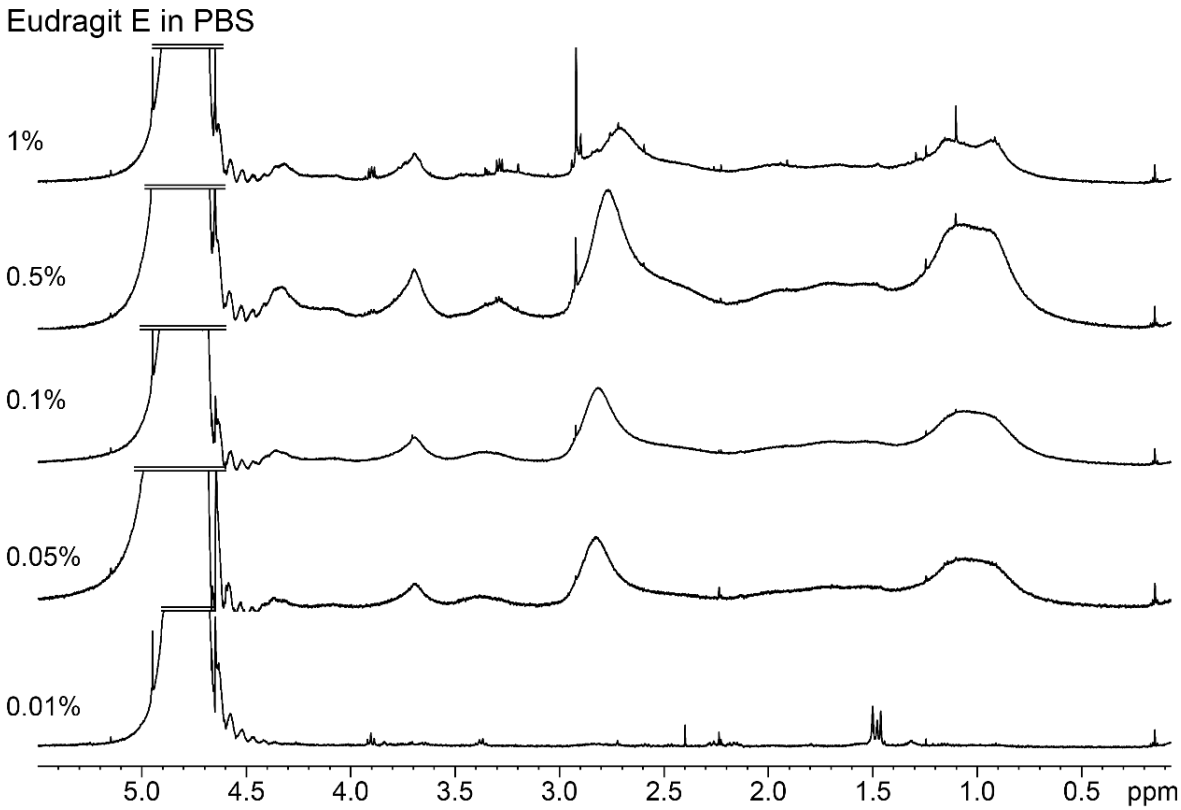

Figure S13: ^{1}H NMR spectra of Eudragit E at 0.01, 0.05, 0.1, 0.5, and 1% in PBS. Sharp signals with low intensity were detected at 0.01%. At ≥0.05%, broad Eudragit E signals were observed. Some sharp signals shifted to lower ppm dependent on concentration (e.g., at 2.8 ppm).

S3.2.4 Eudragit E in TC/L in PBS

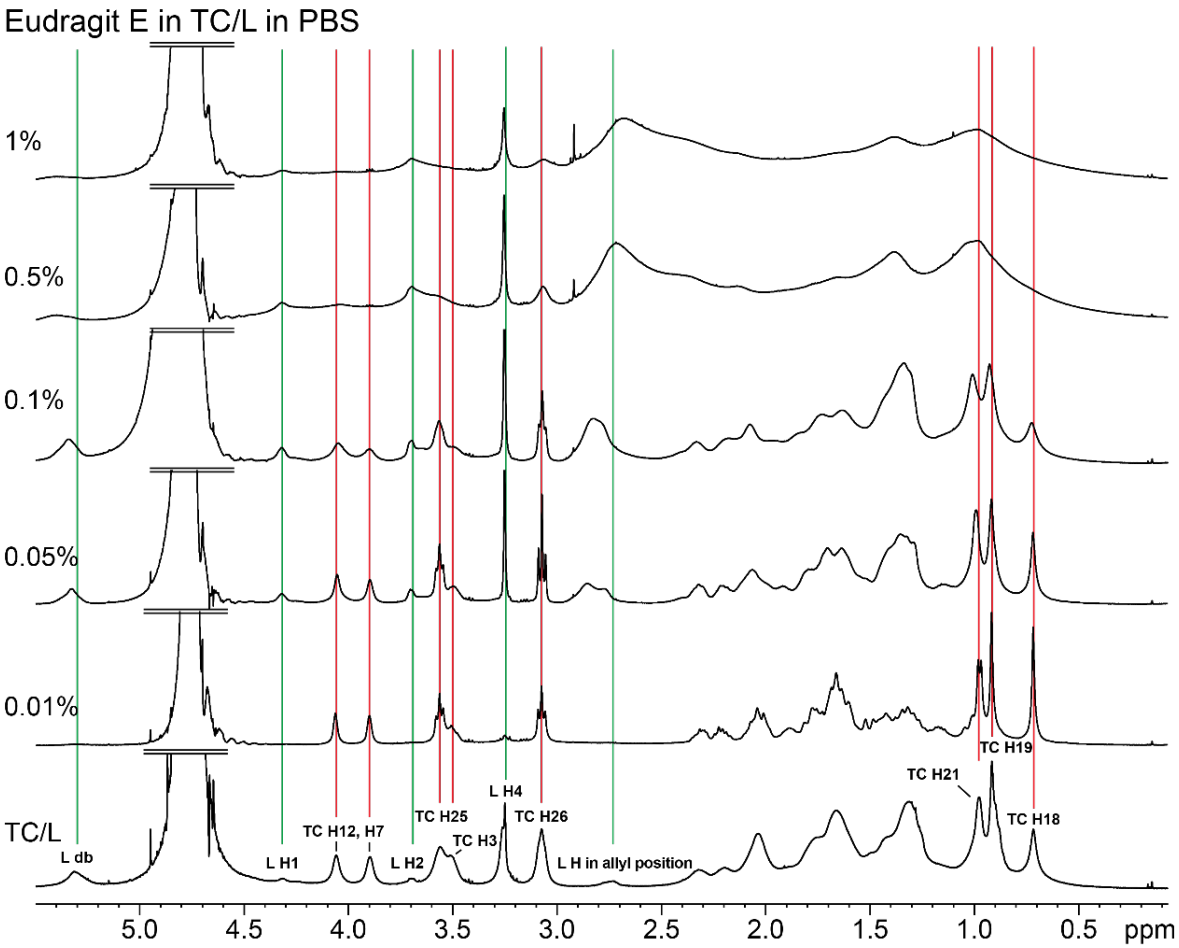

Figure S14: ^{1}H NMR spectra of Eudragit E at 0.01, 0.05, 0.1, 0.5, and 1% in TC/L in PBS indicated as (L) green lines and (TC) red lines. TC/L reference spectrum is shown (bottom). At 0.01% L signals disappeared, while TC signals sharpened. At ≥0.05% L signals reappeared. At ≥0.1% some TC/L signals shifted and at ≥0.5% disappeared (e.g., TC H21, H19, and 18). Other signals did not disappear, but intensity decreased along with signal broadening (e.g., L H4, TC H26).

S3.2.5 Soluplus in PBS

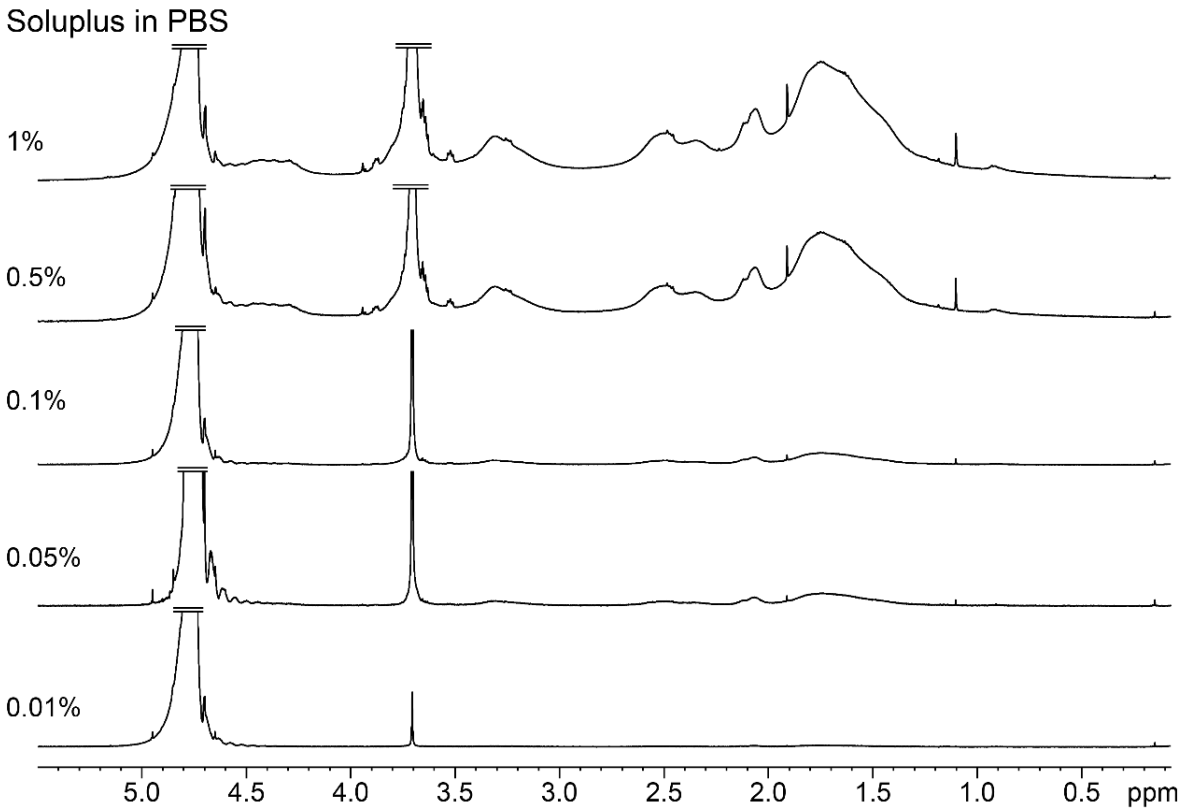

Figure S15: ^{1}H NMR spectra of Soluplus at 0.01, 0.05, 0.1, 0.5 and 1% in PBS. Signal intensity increased as a function of concentration. Broad signals (e.g., at 1.3-2.6 ppm) and sharp signals (e.g., at 1.1 and 1.9 ppm) were detected in parallel.

S3.2.6 Soluplus in TC/L in PBS

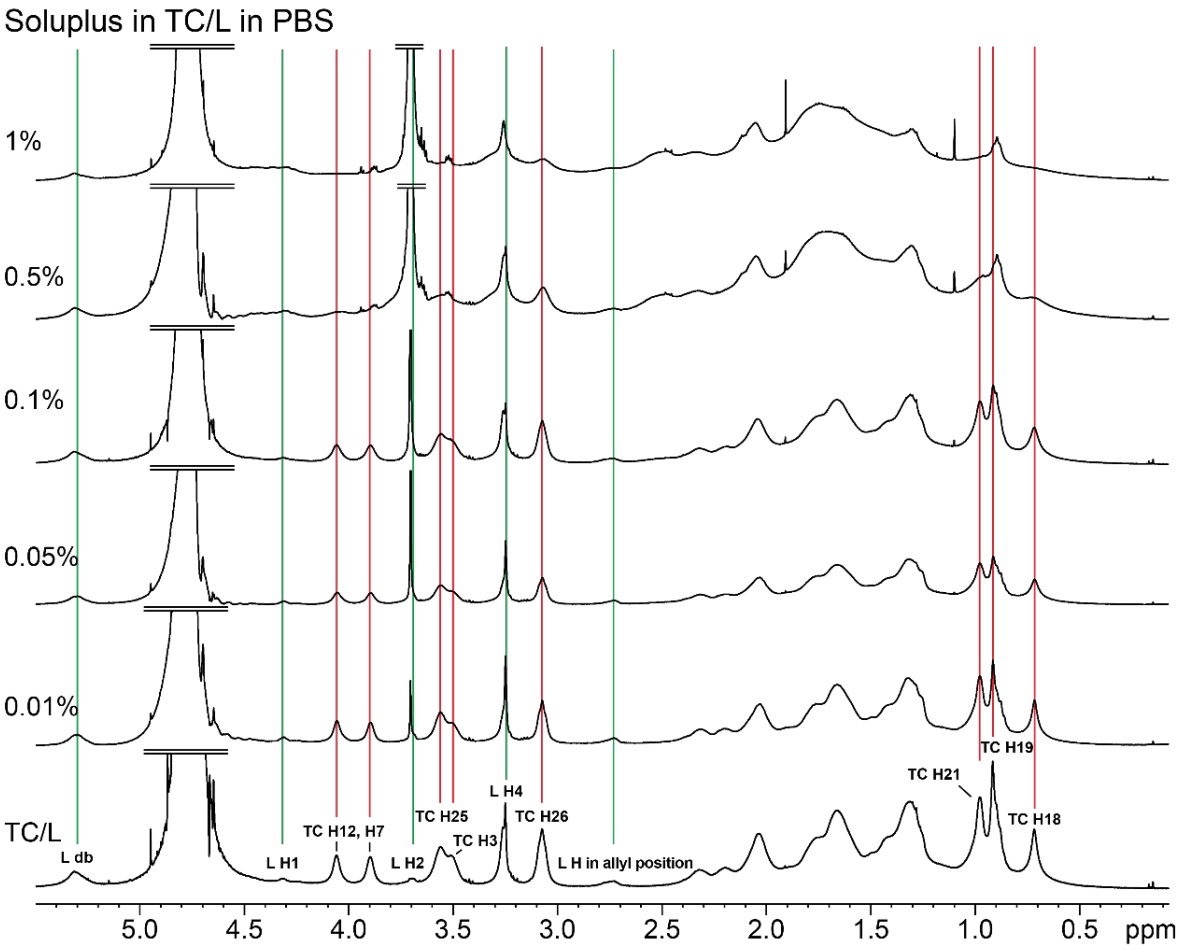

Figure S16: ^{1}H NMR spectra of Soluplus at 0.01, 0.05, 0.1, 0.5 and 1% in TC/L in PBS indicated as (L) green lines and (TC) red lines. TC/L reference spectrum is shown (bottom). At 1% some TC signals appeared very broad (e.g., TC H12, H7, H25, H3, H21, H19, and H18). Other signals were still observed (e.g., all L and TC H26).

S3.2.7 Kollidon VA 64 in PBS

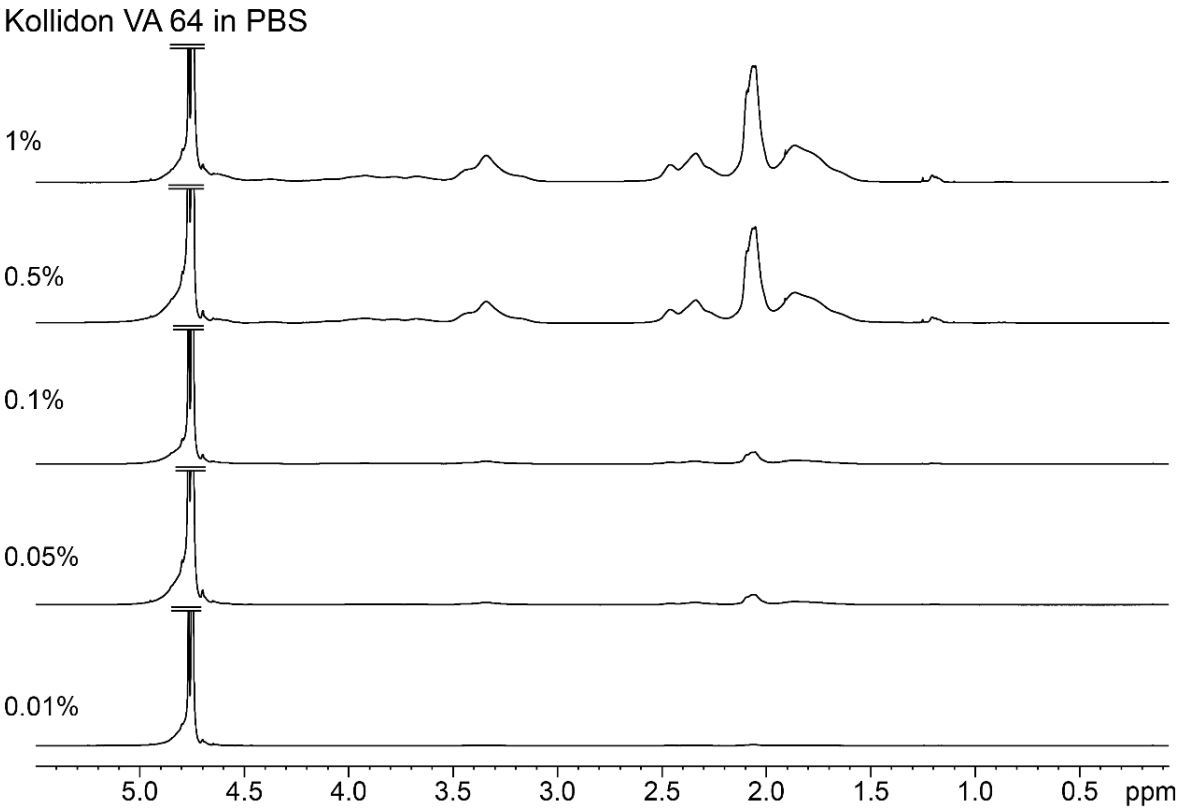

Figure S17: ^{1}H NMR spectra of Kollidon VA 64 at 0.01, 0.05, 0.1, 0.5 and 1% in PBS. Signal intensity increased as a function of concentration. Broad signals (e.g., at 1.6-2.5 ppm) were detected.

S3.2.8 Kollidon VA 64 in TC/L in PBS

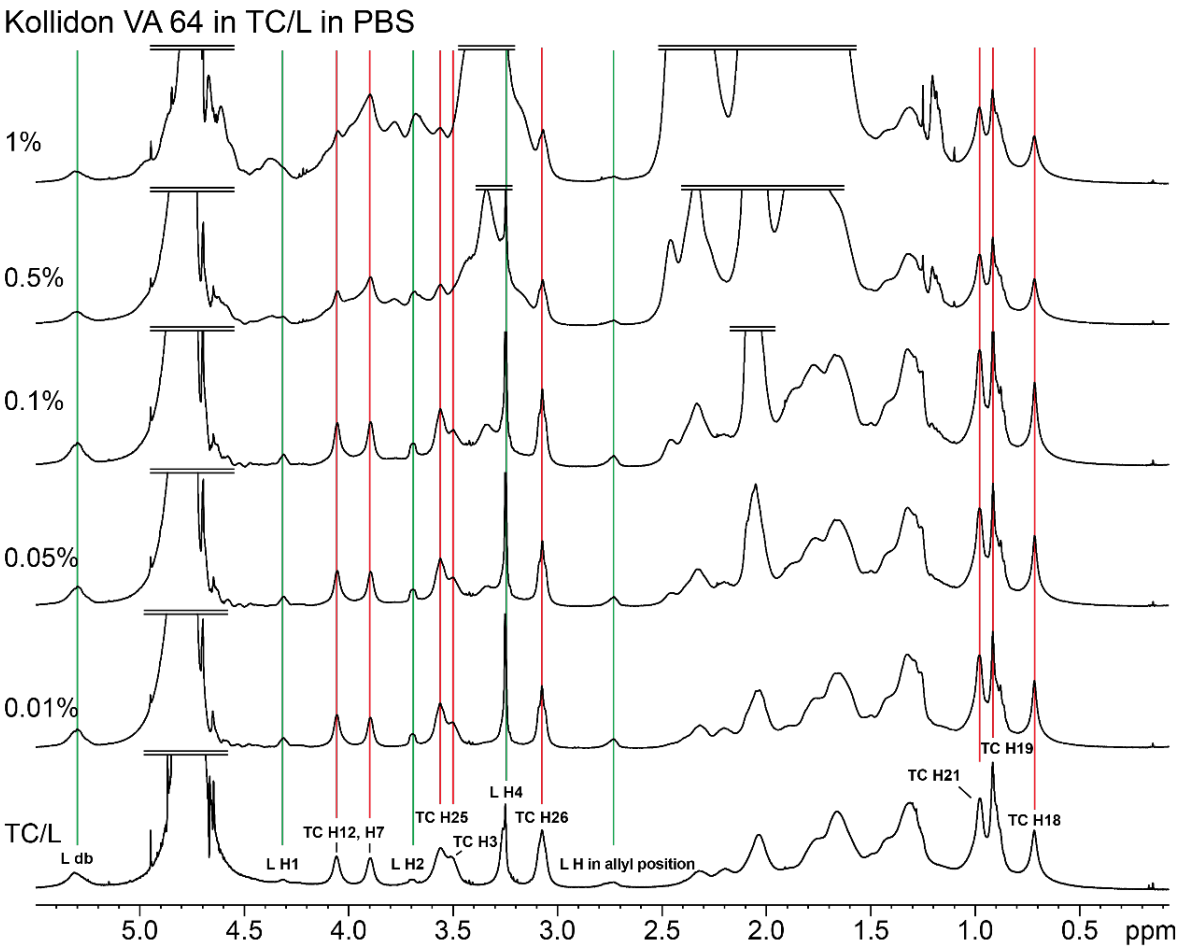

Figure S18: [1]H NMR spectra of Kollidon VA 64 at 0.01, 0.05, 0.1, 0.5 and 1% in TC/L in PBS indicated as (L) green lines and (TC) red lines. TC/L reference spectrum is shown (bottom). TC/L signals did not change. Kollidon VA 64 signals increased as a function of concentration overlapping with TC/L signals.

S3.2.9 HPMC-AS in PBS

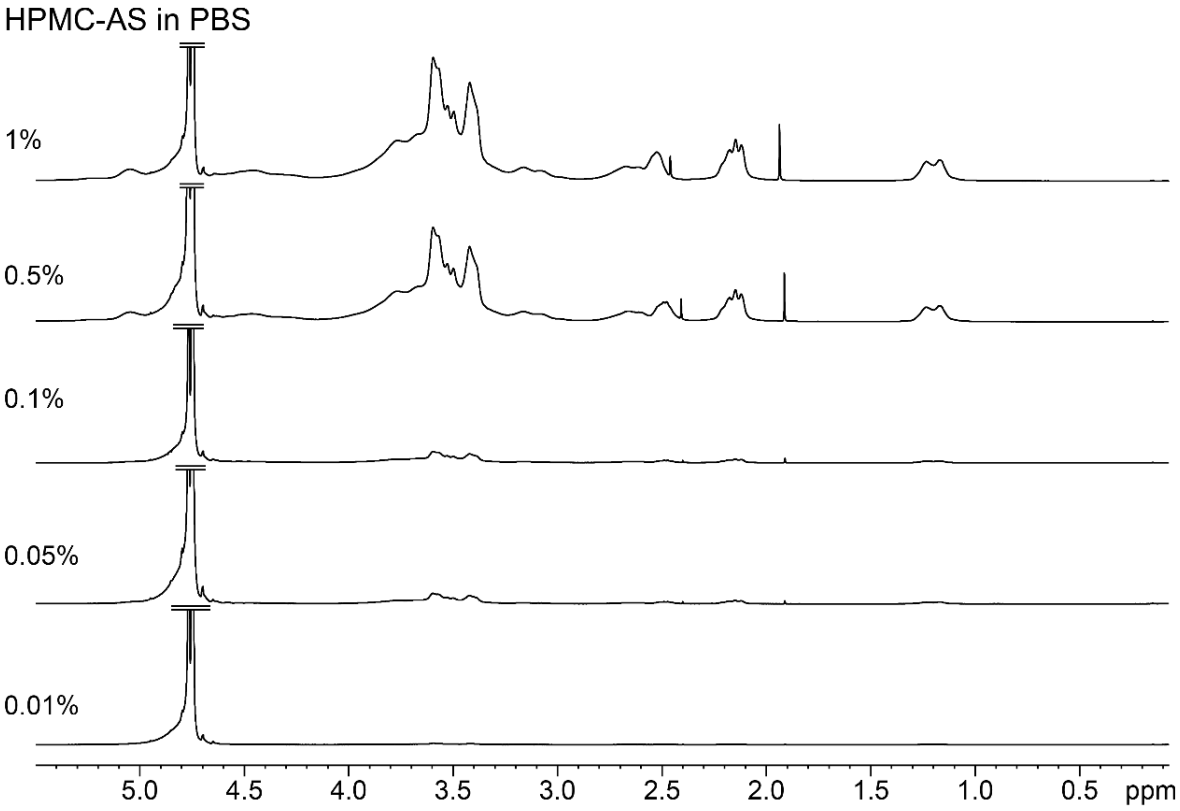

Figure S19: ^{1}H NMR spectra of HPMC-AS at 0.01, 0.05, 0.1, 0.5 and 1% in PBS. Signal intensity increased as a function of concentration. Broad signals (e.g., at 3.0-4.0 ppm) were detected along with sharp signals (e.g., at 1.9 and 2.4 ppm).

S3.2.10 HPMC-AS in TC/L in PBS

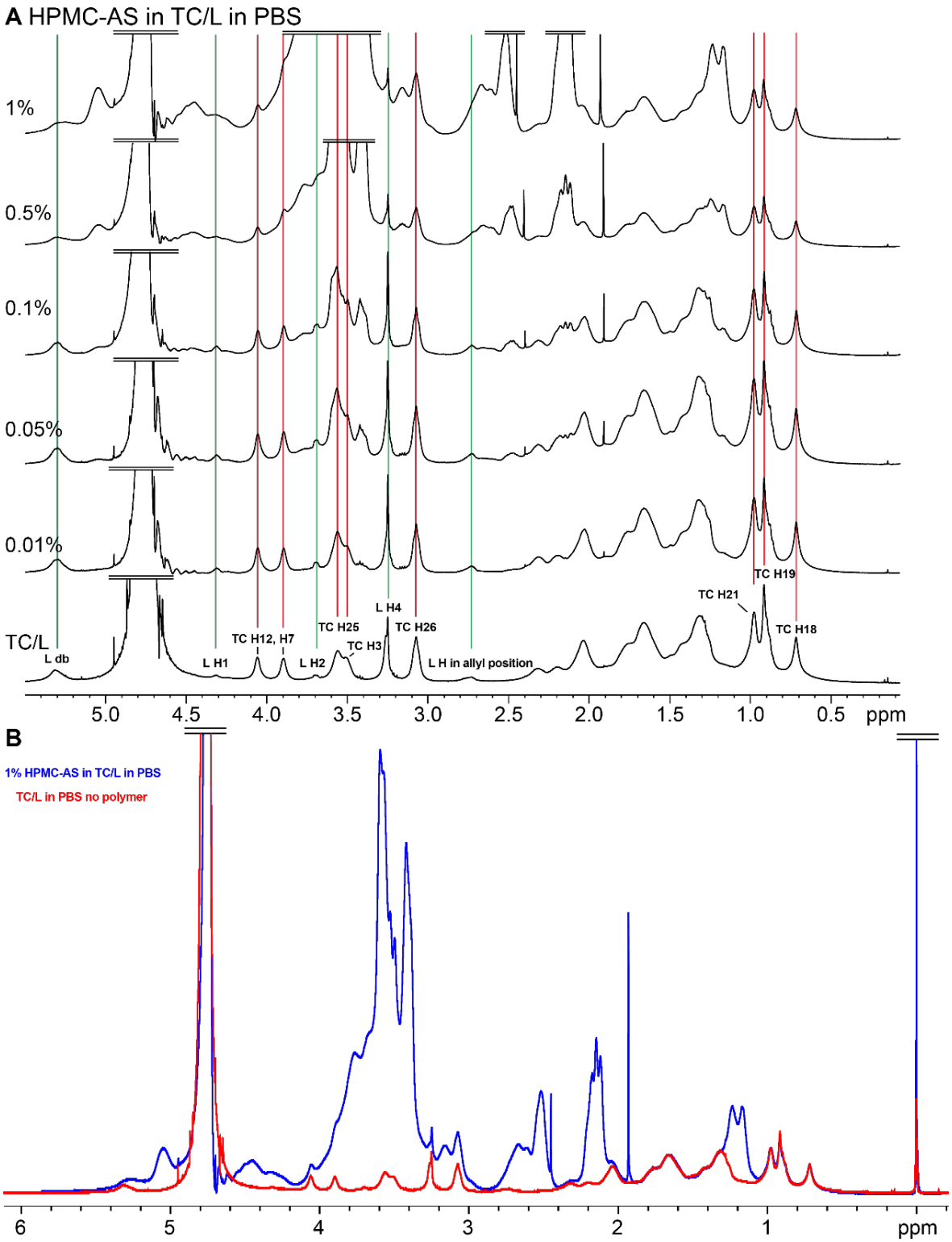

Figure S20: (A) ^{1}H NMR spectra of HPMC-AS at 0.01, 0.05, 0.1, 0.5 and 1% in TC/L in PBS indicated as (L) green lines and (TC) red lines. TC/L reference spectrum is shown (bottom). (B) Overlay of 1% HPMC-AS with TC/L and TC/L reference spectrum (B). TC/L signals did not change. HPMC-AS signals increased as a function of concentration and overlapped TC/L signals.

S3.2.11 Complete ^{1}H nuclear magnetic resonance spectra

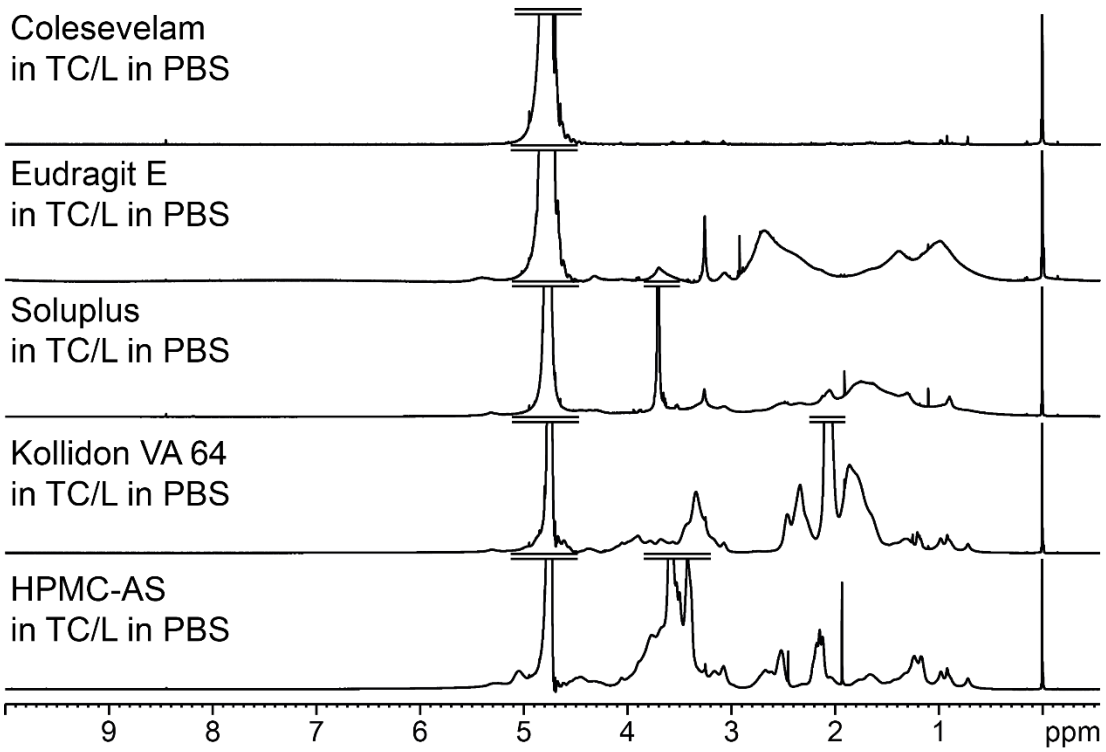

Figure S21: ^{1}H NMR spectra of 1% Colesevelam, Eudragit E, Soluplus, Kollidon VA 64, and HPMC-AS in TC/L in PBS.

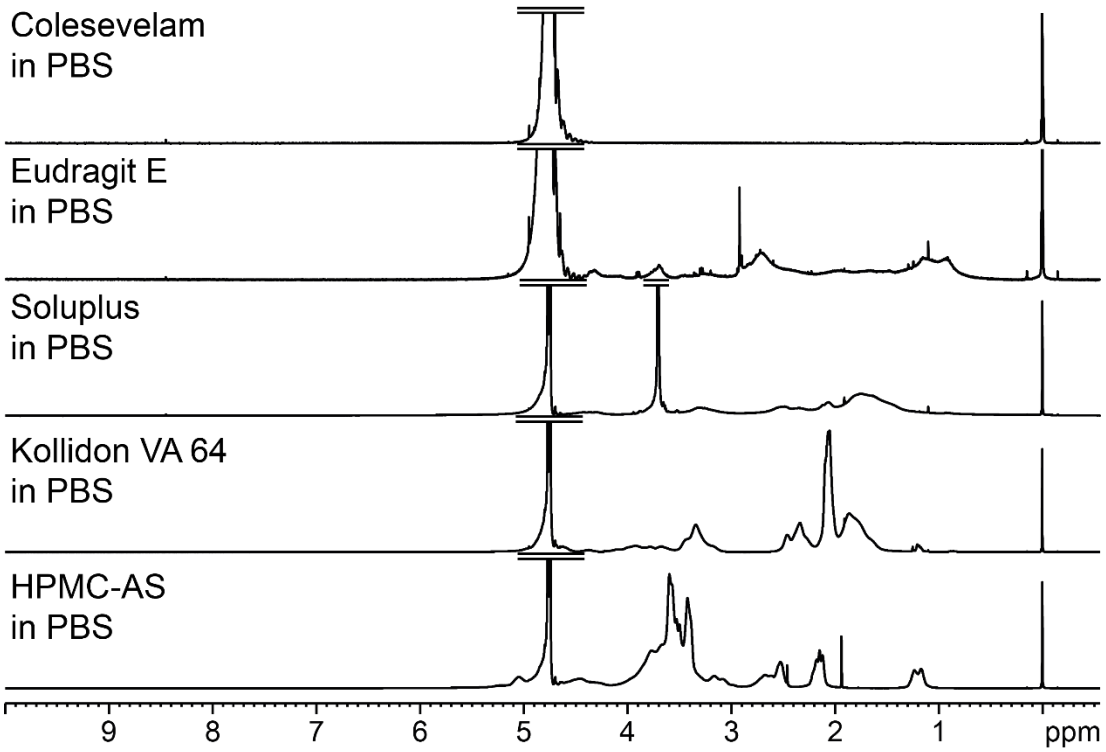

Figure S22: Complete ^{1}H NMR spectra of 1% Colesevelam, Eudragit E, Soluplus, Kollidon VA 64, and HPMC-AS in PBS.

S4 Polymer impact on free drug

S4.1 Perphenazine ^{1}H nuclear magnetic resonance analysis

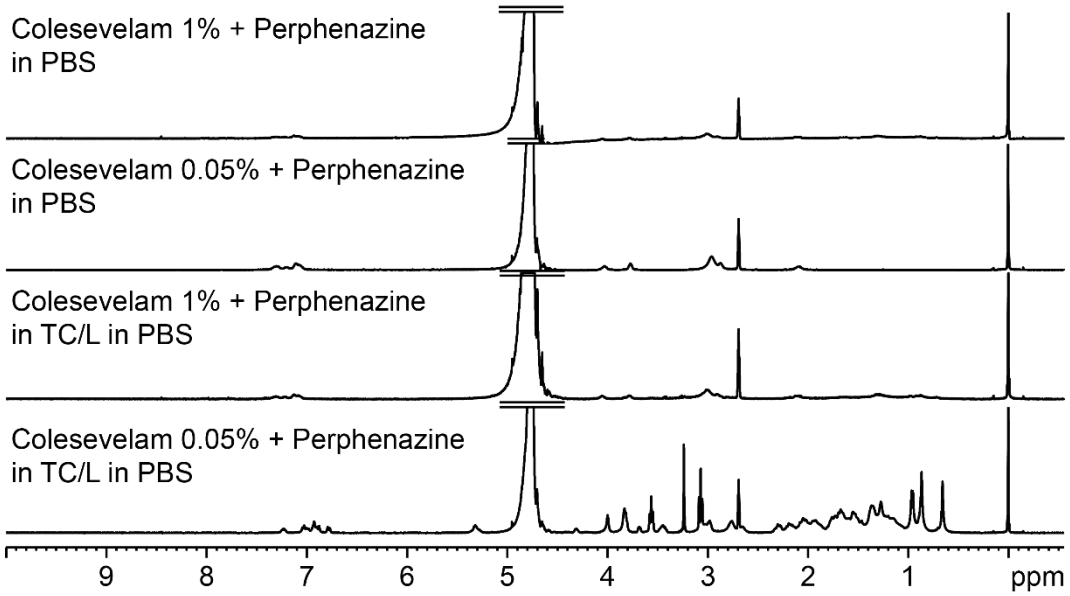

Figure S23: Complete ^{1}H NMR spectra of Colesevelam with Perphenazine in TC/L in PBS and in PBS.

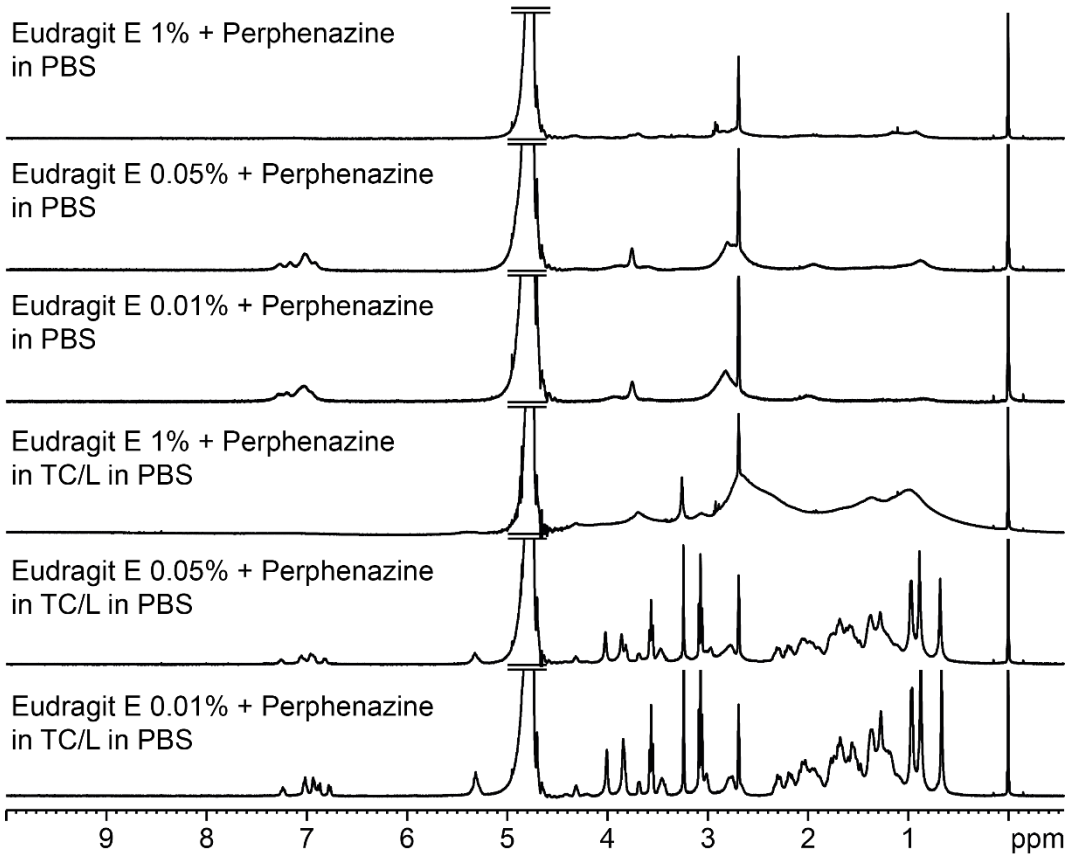

Figure S24: Complete ^{1}H NMR spectra of Eudragit E with Perphenazine in PBS in TC/L and in PBS

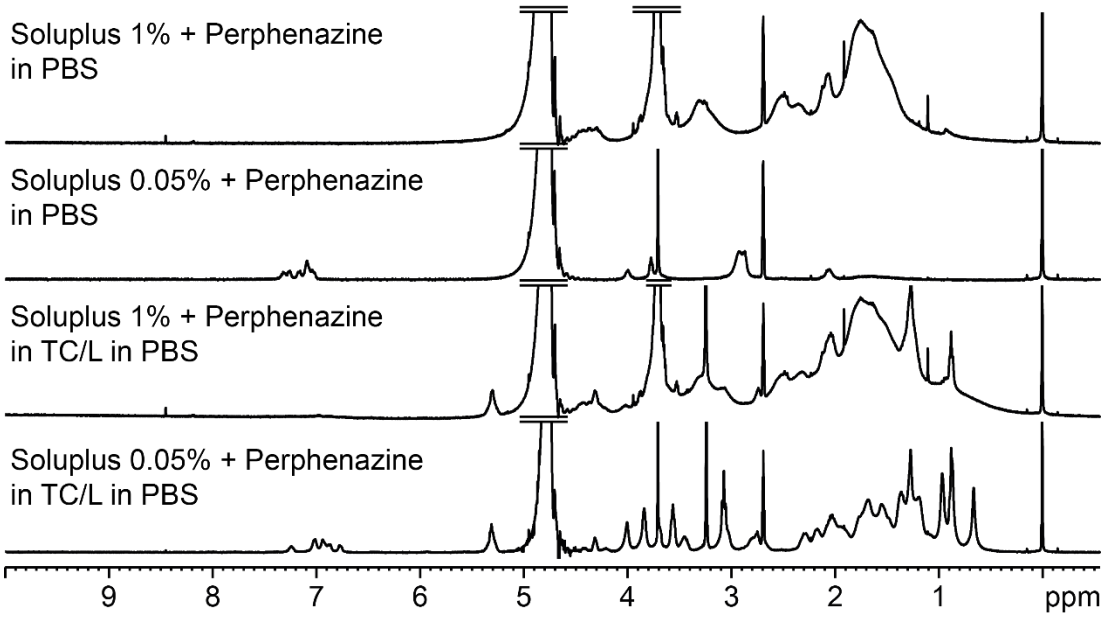

Figure S25: Complete ^{1}H NMR spectra of Soluplus with Perphenazine in PBS in TC/L and in PBS.

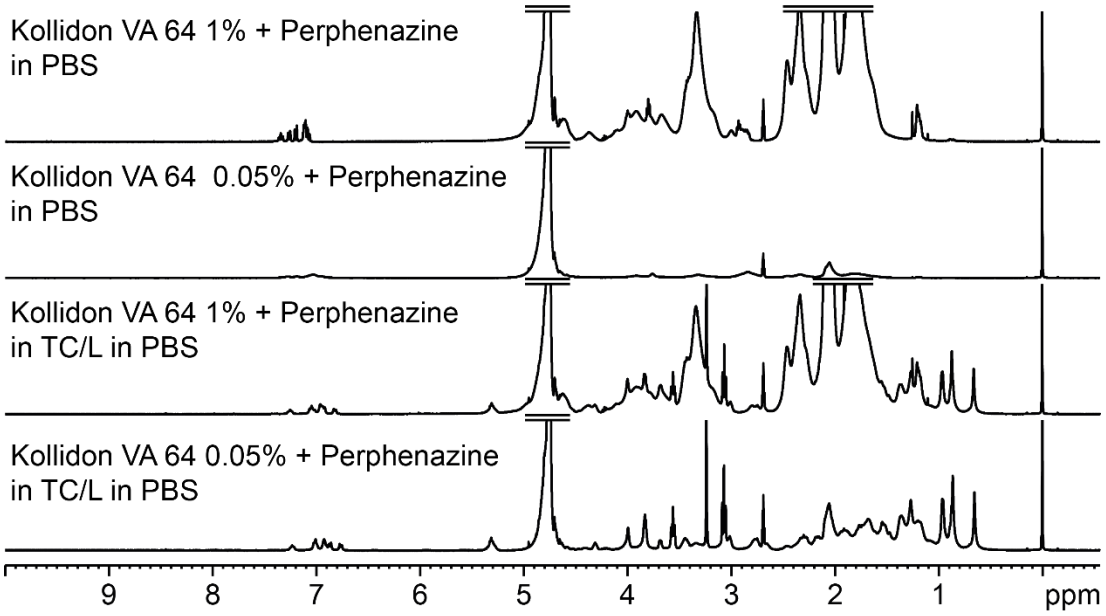

Figure S26: Complete ^{1}H NMR spectra of Kollidon VA 64 with Perphenazine in PBS in TC/L and in PBS.

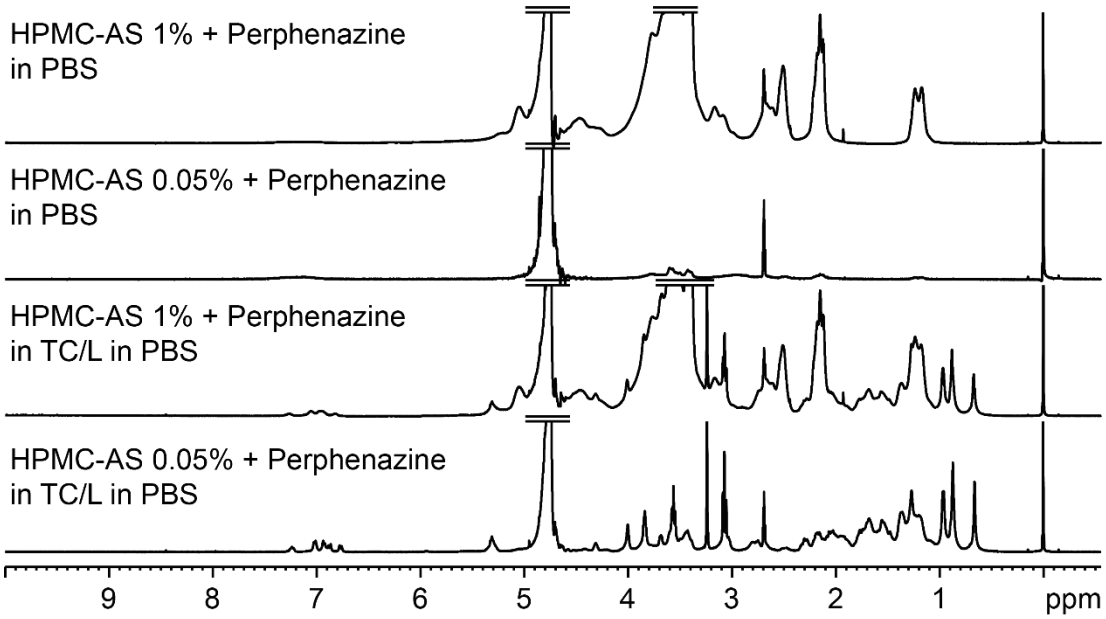

Figure S27: Complete ^{1}H NMR spectra of HPMC-AS with Perphenazine in PBS in TC/L and in PBS.

S4.2 Imatinib ^{1}H nuclear magnetic resonance analysis

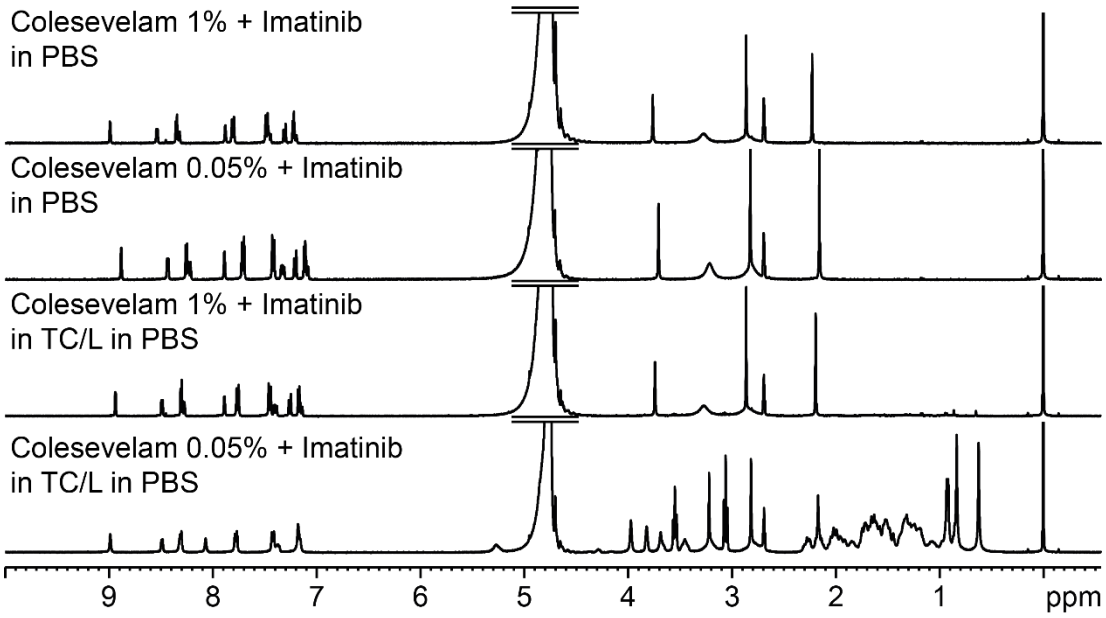

Figure S28: Complete ^{1}H NMR spectra of Colesevelam with Imatinib in PBS in TC/L and in PBS.

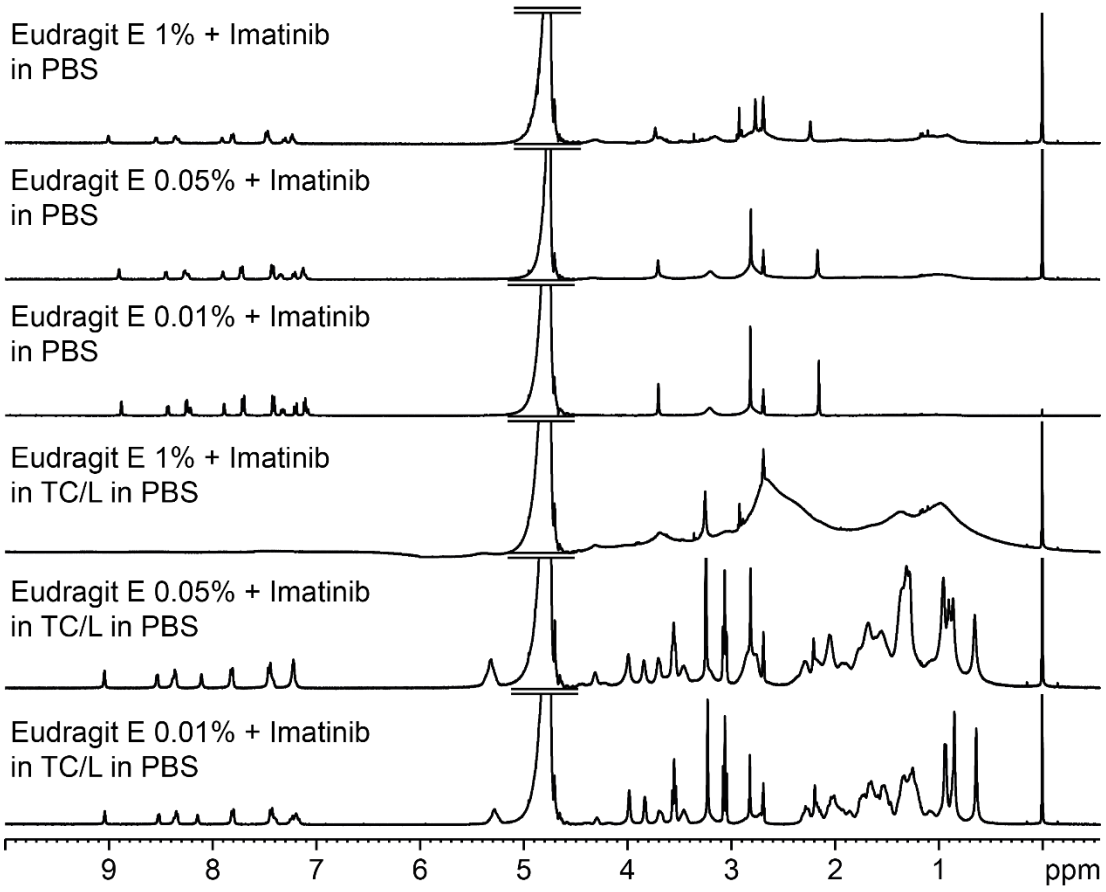

Figure S29: Complete ^{1}H NMR spectra of Eudragit E with Imatinib in PBS in TC/L and in PBS.

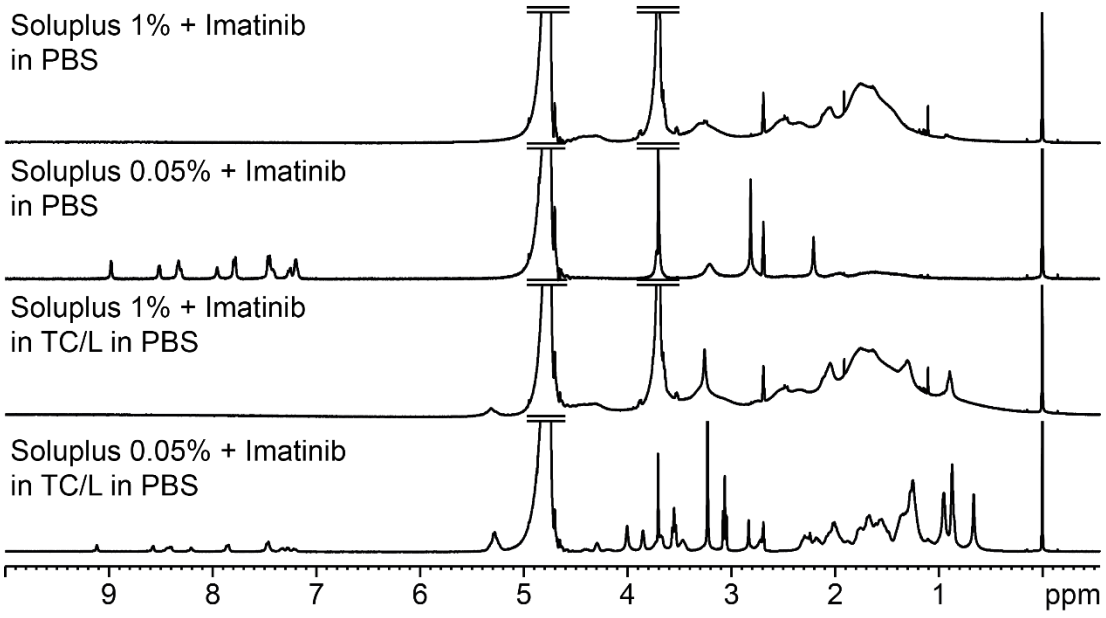

Figure S30: Complete ^{1}H NMR spectra of Soluplus with Imatinib in PBS in TC/L and in PBS.

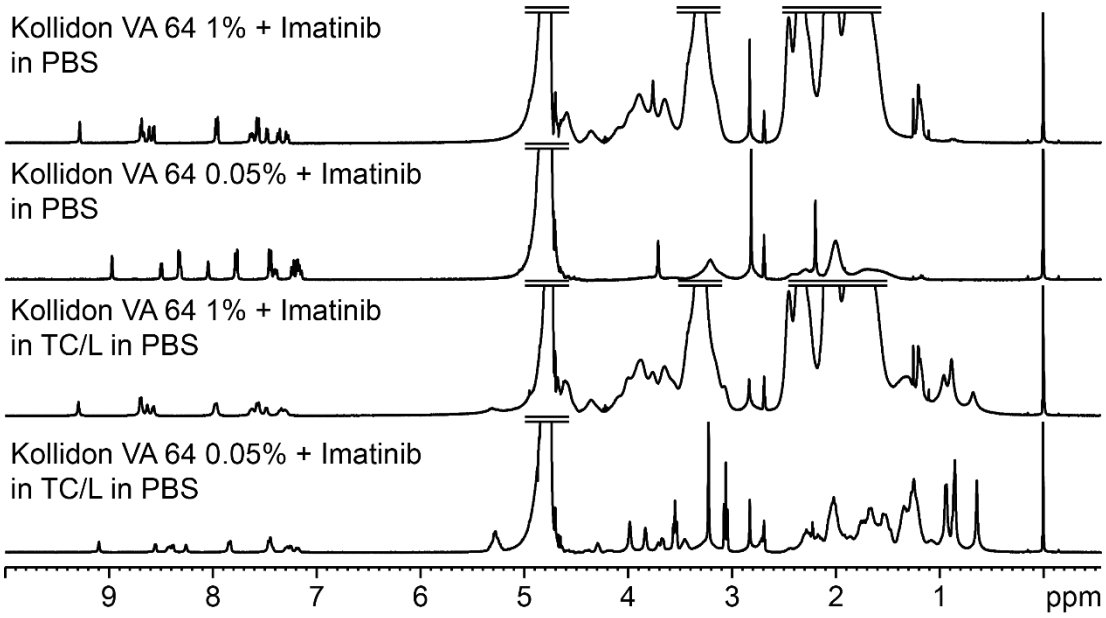

Figure S31: Complete ^{1}H NMR spectra of Kollidon VA 64 with Imatinib in PBS in TC/L and in PBS.

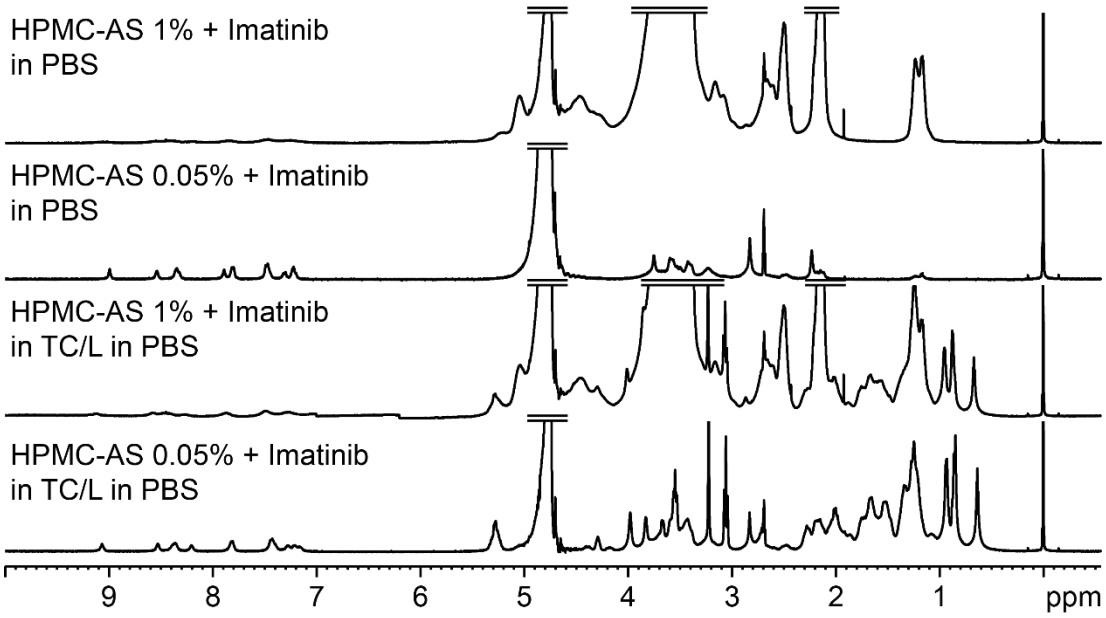

Figure S32: Complete ^{1}H NMR spectra of HPMC-AS with Imatinib in PBS in TC/L and in PBS.

S4.3 Metoprolol ^{1}H nuclear magnetic resonance analysis

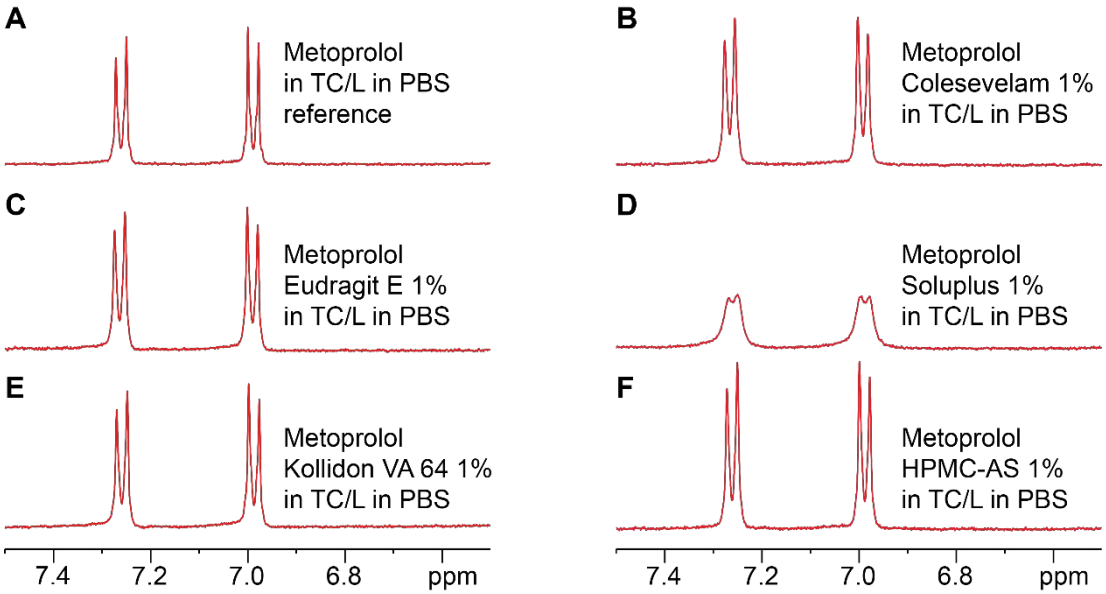

Figure S33: Metoprolol ^{1}H NMR aryl-proton spectra (A) in TC/L in PBS and with 1% respective polymer in TC/L in PBS (B-F). Metoprolol aryl-proton signals were not impacted by (B) Colesevelam, (C) Eudragit E, (E) Kollidon VA 64, and (F) HPMC-AS at 1% in TC/L in PBS. (D) Signal decreased in intensity and broadened by Soluplus.

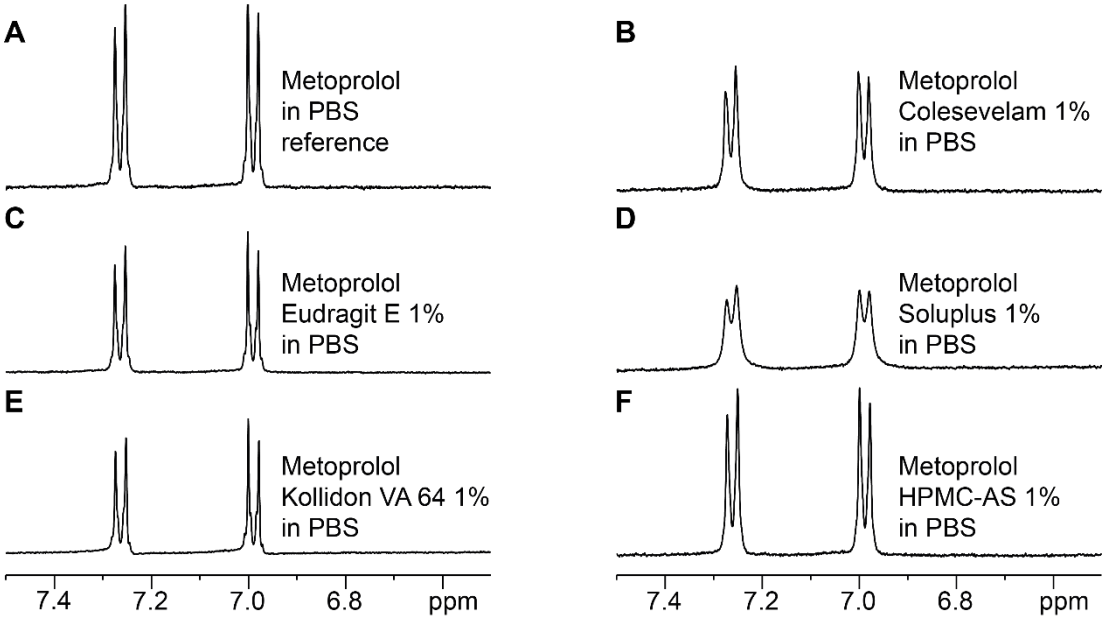

Figure S34: Metoprolol ^{1}H NMR aryl-proton spectra (A) in PBS and with 1% respective polymer in PBS (B-F). (B) Colesevelam, (C) Eudragit E, (D) Soluplus and (E) Kollidon VA 64 decreased signal intensity in PBS. (D) Soluplus broadened signals. (F) Signals were not impacted by 1% HPMC-AS in PBS.

S5 Polymer impact on HDO diffusivity

Table S4: HDO diffusion coefficients (D in m²/s) for polymers in TC/L in PBS with Perphenazine at 4.703 ppm.

Concentration [%]	Colesevelam		Eudragit E		Soluplus		Kollidon VA 64		HPMC-AS	
	D $*10^{-9}$	Error by fit $*10^{-11}$	D $*10^{-9}$	Error by fit $*10^{-11}$	D $*10^{-9}$	Error by fit $*10^{-11}$	D $*10^{-9}$	Error by fit $*10^{-11}$	D $*10^{-9}$	Error by fit $*10^{-11}$
0.01	N/A	N/A	2.60	0.597	N/A	N/A	N/A	N/A	N/A	N/A
0.05	2.61	9.9	2.56	1.74	2.57	0.745	2.60	0.948	2.60	0.626
1	2.62	0.624	2.58	0.864	2.55	0.318	2.47	3.19	2.52	0.717
0	$2.60*10^{-9}$ Error by fit: $2.70*10^{-12}$									

Table S5: Perphenazine aryl-proton diffusion coefficients (D in m²/s) for polymers (0.05%) in TC/L in PBS at 7.2 and 6.7 ppm. Preliminary data set as signal decay did not reach < 10 % of initial intensity.

Concentration, signal	Colesevelam		Eudragit E		Soluplus		Kollidon VA 64		HPMC-AS	
	D $*10^{-10}$	Error by fit $*10^{-11}$	D $*10^{-10}$	Error by fit $*10^{-11}$	D $*10^{-10}$	Error by fit $*10^{-11}$	D $*10^{-10}$	Error by fit $*10^{-11}$	D $*10^{-10}$	Error by fit $*10^{-11}$
0.05% 7.2ppm	1.55	2.92	1.12	6.00	0.782	4.46	1.23	2.49	1.22	2.40
0.05% 6.7ppm	1.62	3.09	1.12	4.94	0.538	4.72	1.31	3.04	1.02	2.37
0% 7.2ppm	$1.16*10^{-10}$Error by fit: $2.10*10^{-11}$									
0% 6.7ppm	$1.35*10^{-10}$ Error by fit: $2.57*10^{-11}$									

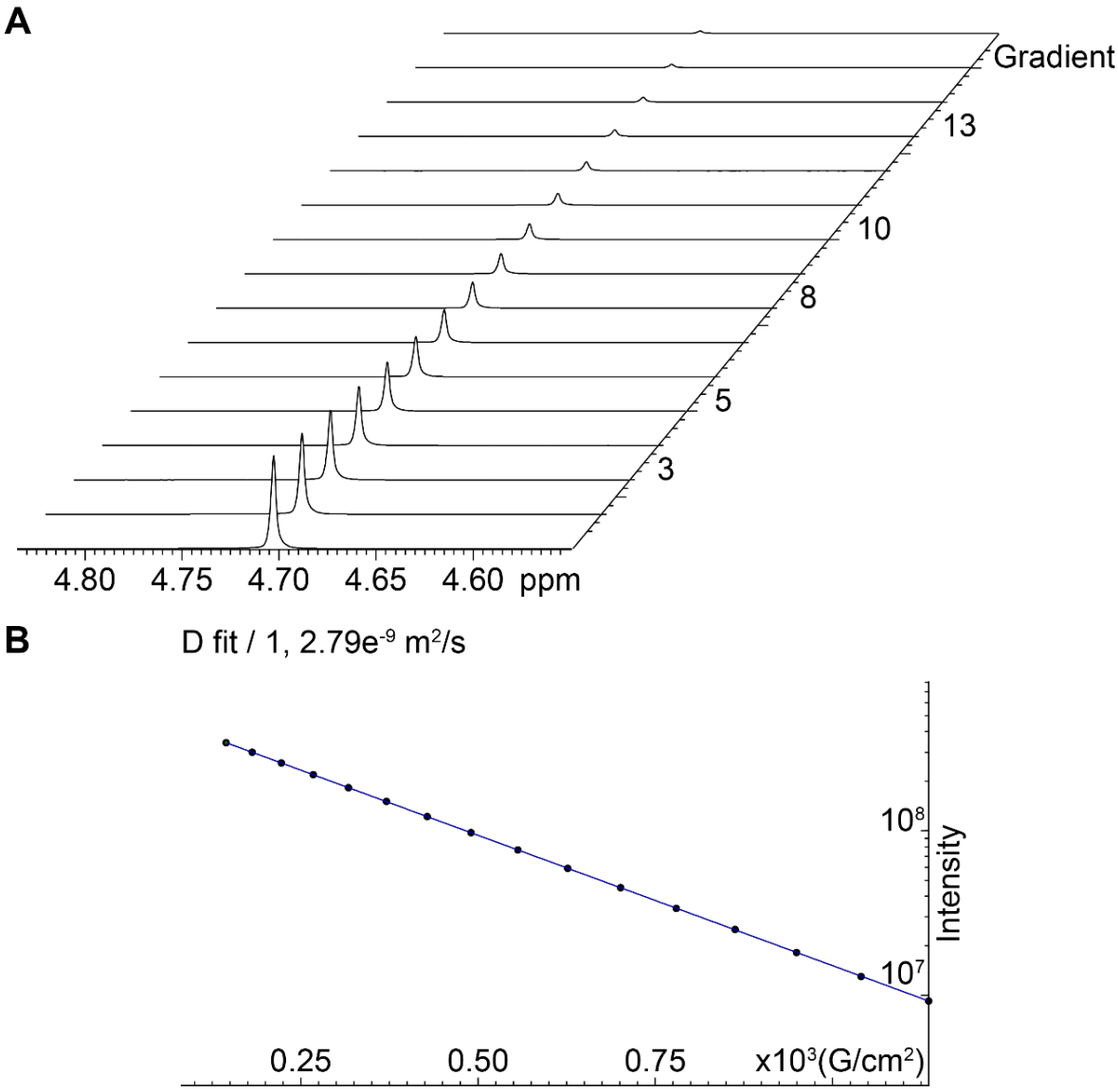

Figure S35: DOSY analysis: (A) HDO (4.703 ppm) signal attenuation with increased gradient strength and (B) fitted curve of experimental intensity decay as a function of the gradient strength for Perphenazine in TC/L in PBS (without polymer).

S6 Excipient concentration under physiological conditions

The fluid volume in the fasted small intestine varies between 45 and 319 ml (mean: 107 ± 72 ml), unevenly distributed in roughly four fluid pockets with a median volume of 12 ml.[2] An average oral dosage form contains 280 mg excipients.[3] Hence, dissolving 280 mg excipient in a fluid pocket with a volume of 12 ml results in a mass concentration of 2.33%. For tablet coating, few milligrams of glazing agent are required.[4] Assuming 2 mg coating mass results in a concentration of 0.017%. A tablet is usually composed of more than one excipient, consequently the concentration for one respective excipient is <2.33%. Therefore, our tested polymer concentrations ranging from 0.01-1% reflects the physiological situation.

S7 Flux evaluation

S7.1 Flux at different TC/L concentrations

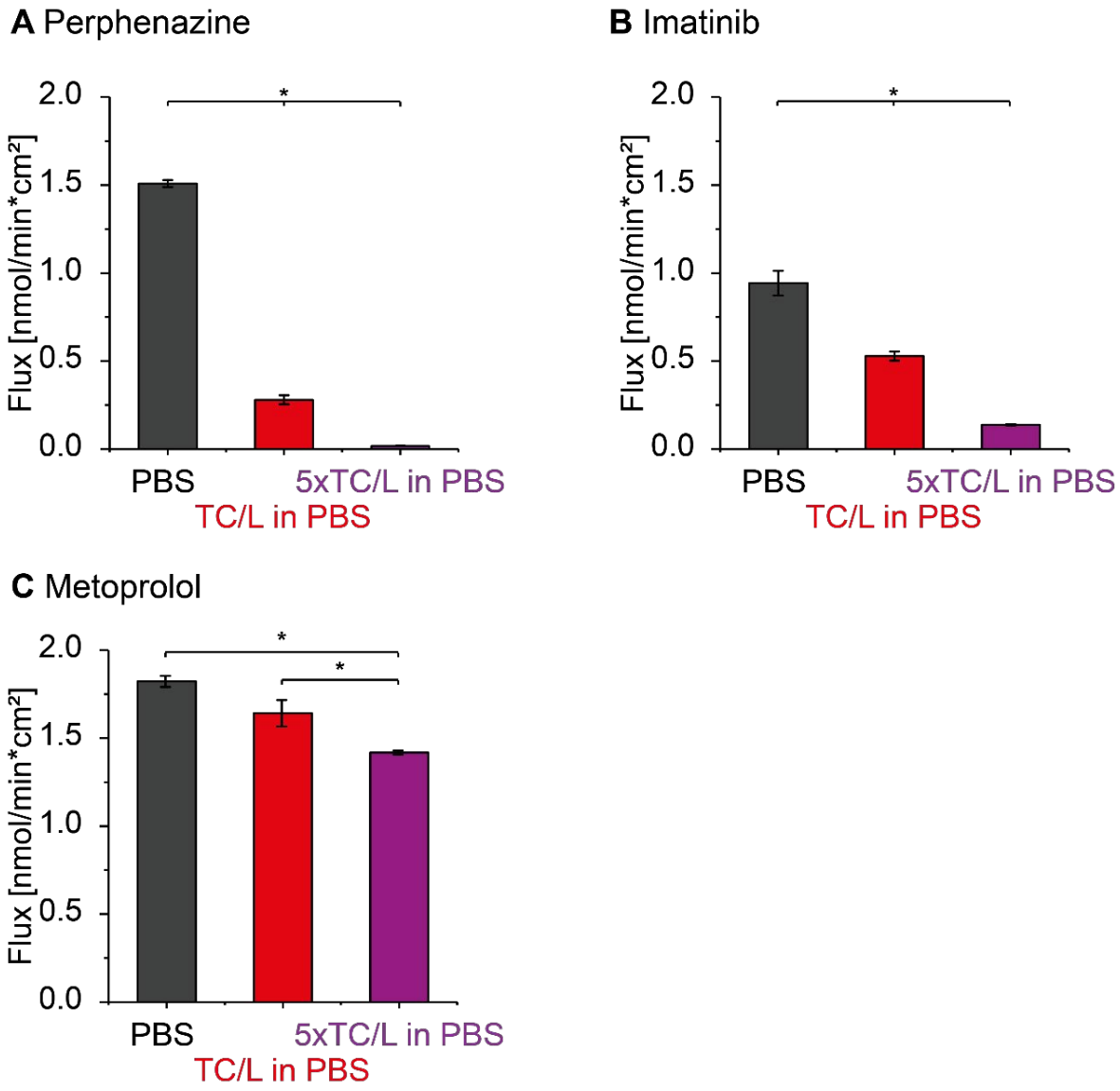

Figure S36: Flux of (A) Perphenazine, (B) Imatinib, and (C) Metoprolol (each at 1000 µmol/l) in PBS (black), in TC/L in PBS (red; simulating a fasted state and known as FaSSIF V1),[5] and in TC/L at fivefold concentration in PBS as compared to FaSSIF V1 (purple; simulating a fed state and known as FeSSIF V1).[5] Flux was significantly reduced for Perphenazine and Imatinib in TC/L in PBS and in 5xTC/L in PBS. Metoprolol flux was not significantly reduced in TC/L in PBS compared to PBS, but in 5xTC/L in PBS. Data shown as mean ± SD, ANOVA considering $p \leq 0.05$ as statistically significant followed by Games-Howell *post-hoc* test for pairwise comparison as the criteria of variance homogeneity was not fulfilled (significant differences are shown by asterisks).

S7.2 Flux at different drug starting concentrations

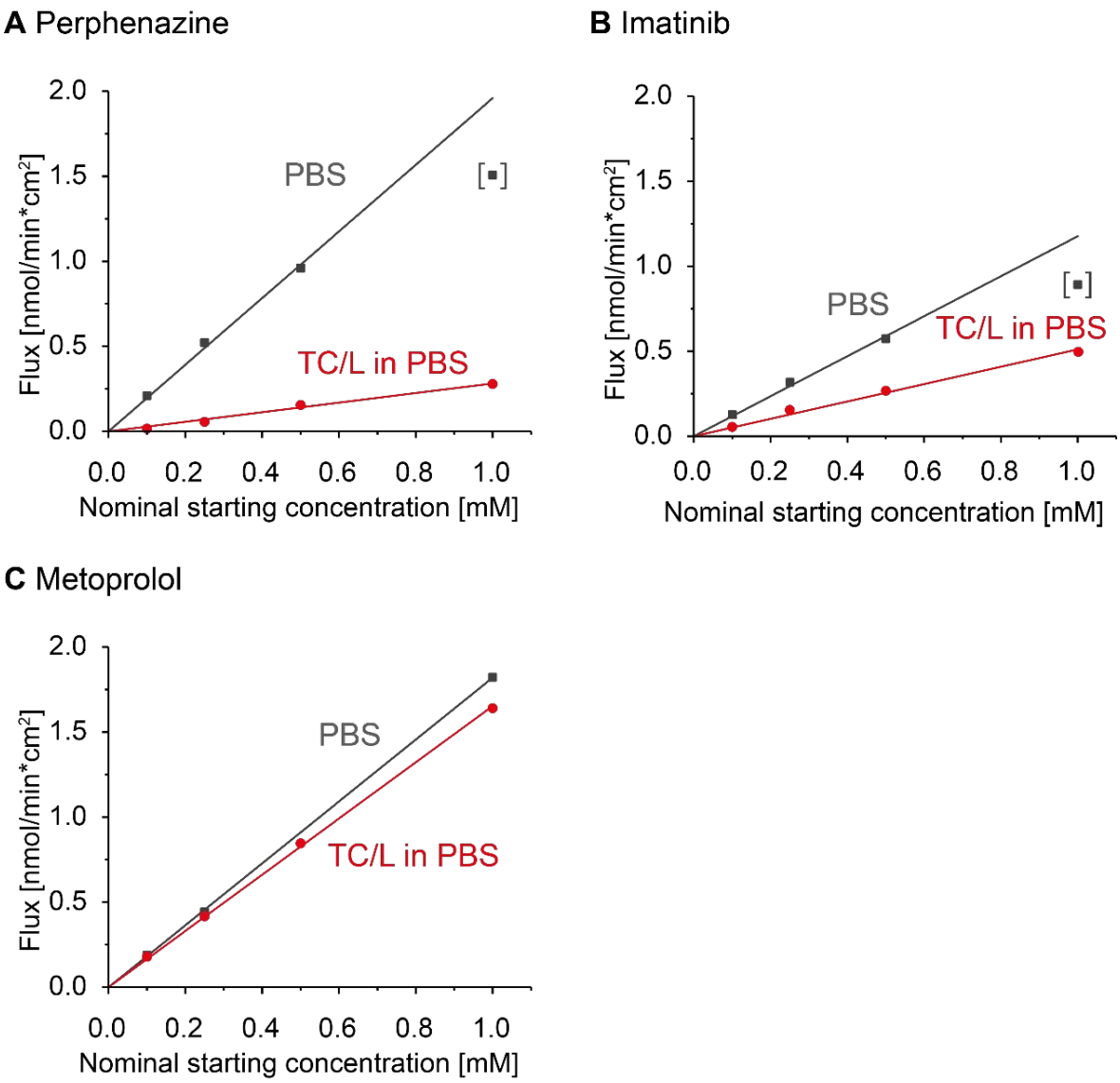

Figure S37: Flux of (A) Perphenazine, (B) Imatinib, and (C) Metoprolol at different starting concentrations (100, 250, 500, and 1000 µmol/l) in PBS (black) and in TC/L in PBS (red). Flux increased linearly over concentration in all cases in TC/L in PBS. In PBS at 1000 µM flux for (A) Perphenazine and (B) Imatinib did not follow the linear trend of measurements at low concentrations (data point in brackets). Nevertheless, flux was stable over time for this concentration (**Figure S37**). Data shown as a single point measurement.

S7.3 Drug concentration over time

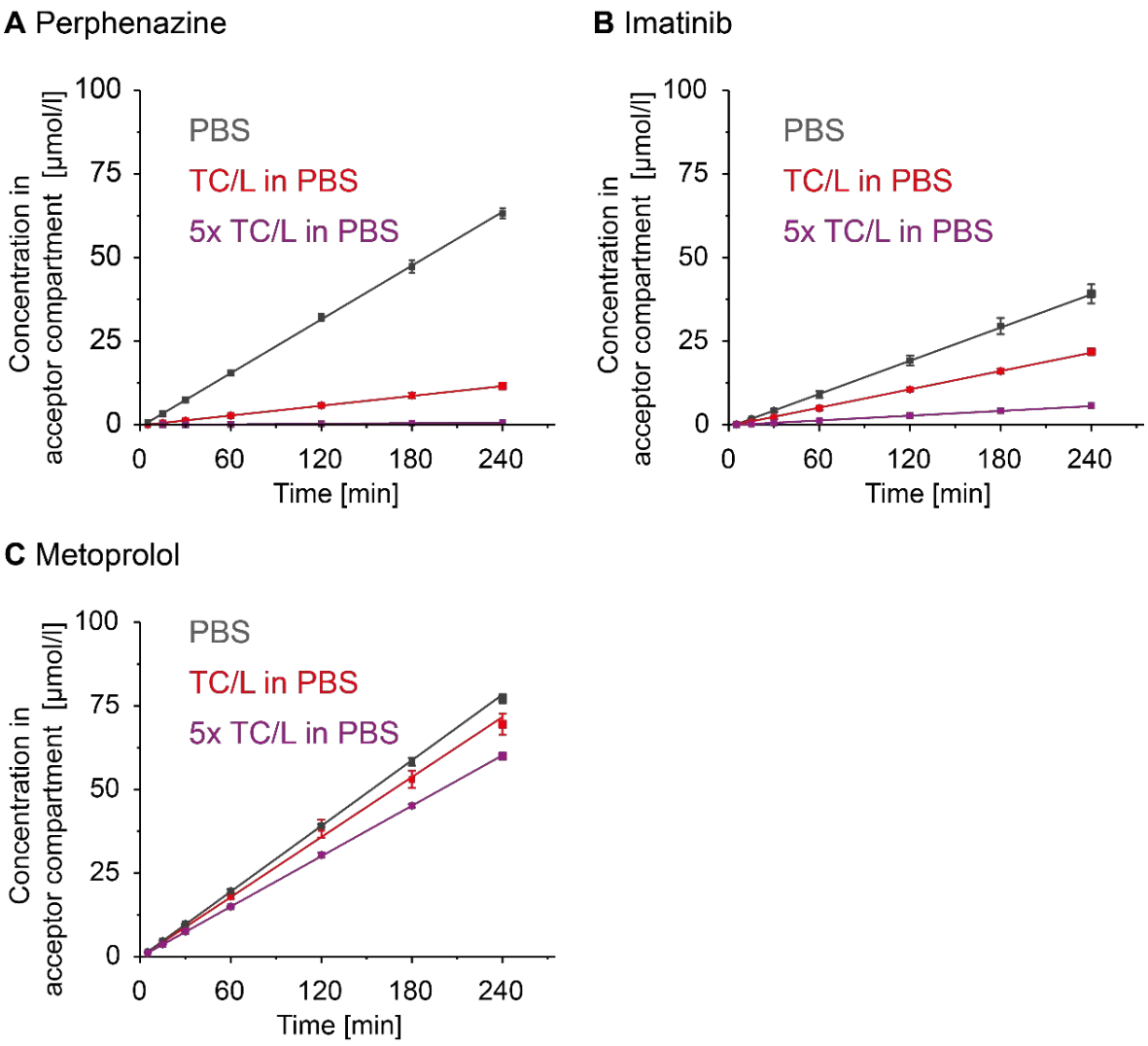

Figure S38: (A) Perphenazine, (B) Imatinib, and (C) Metoprolol concentration [µmol/l] in the flux acceptor compartment in PBS (black), in TC/L in PBS (simulating fasted state/FaSSIF V1; red), and with TC/L at fivefold concentration in PBS as compared to FaSSIF V1 (simulating fed state; FeSSIF V1; purple) over time at a starting concentration of 1000 µmol/l in the donor compartment. Concentration increased linearly over time in all cases indicating stable experimental conditions. Data shown as mean ± SD.

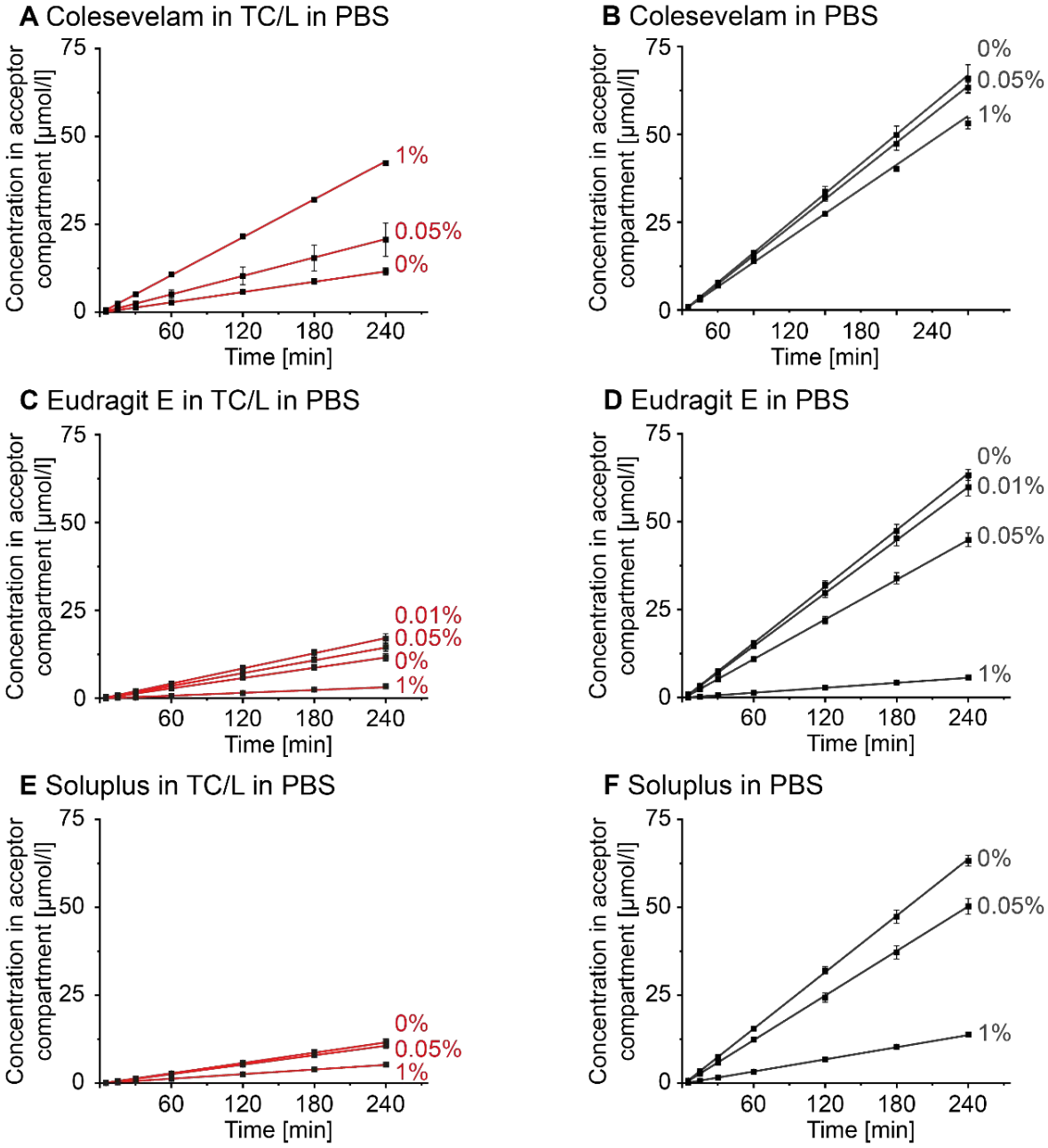

Figure S39: Perphenazine concentration [µmol/l] in the flux acceptor compartment over time with (A, B) Colesevelam, (C, D) Eudragit E, (E, F) Soluplus in TC/L in PBS (respective left panel) and in PBS (respective right panel) at concentrations as indicated. Data at 0% polymer concentration are identical for all panels and given for comparison.

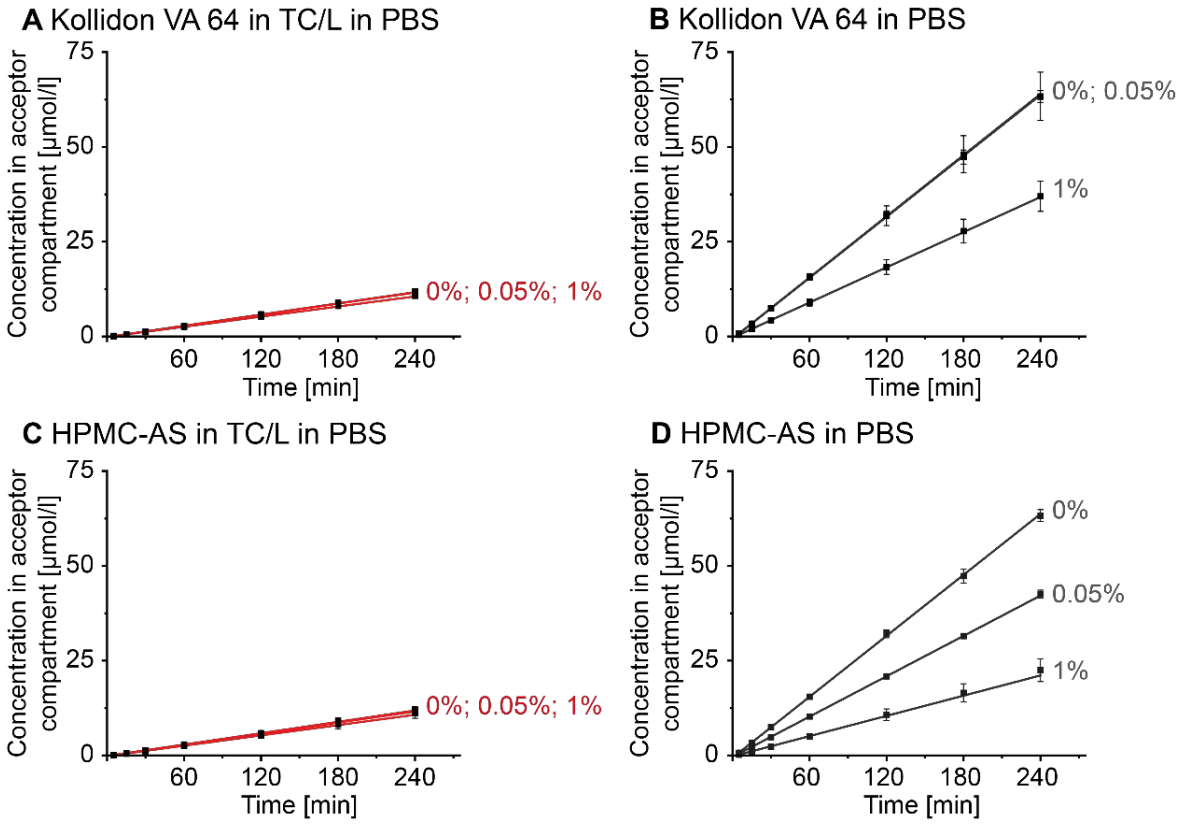

Figure S40: Perphenazine concentration [µmol/l] in the flux acceptor compartment over time with (A, B) Kollidon VA 64, (C, D) HPMCAS in TC/L in PBS (respective left panel) and in PBS (respective right panel) at concentrations as indicated. Data at 0% polymer concentration are identical for all panels and given for comparison.

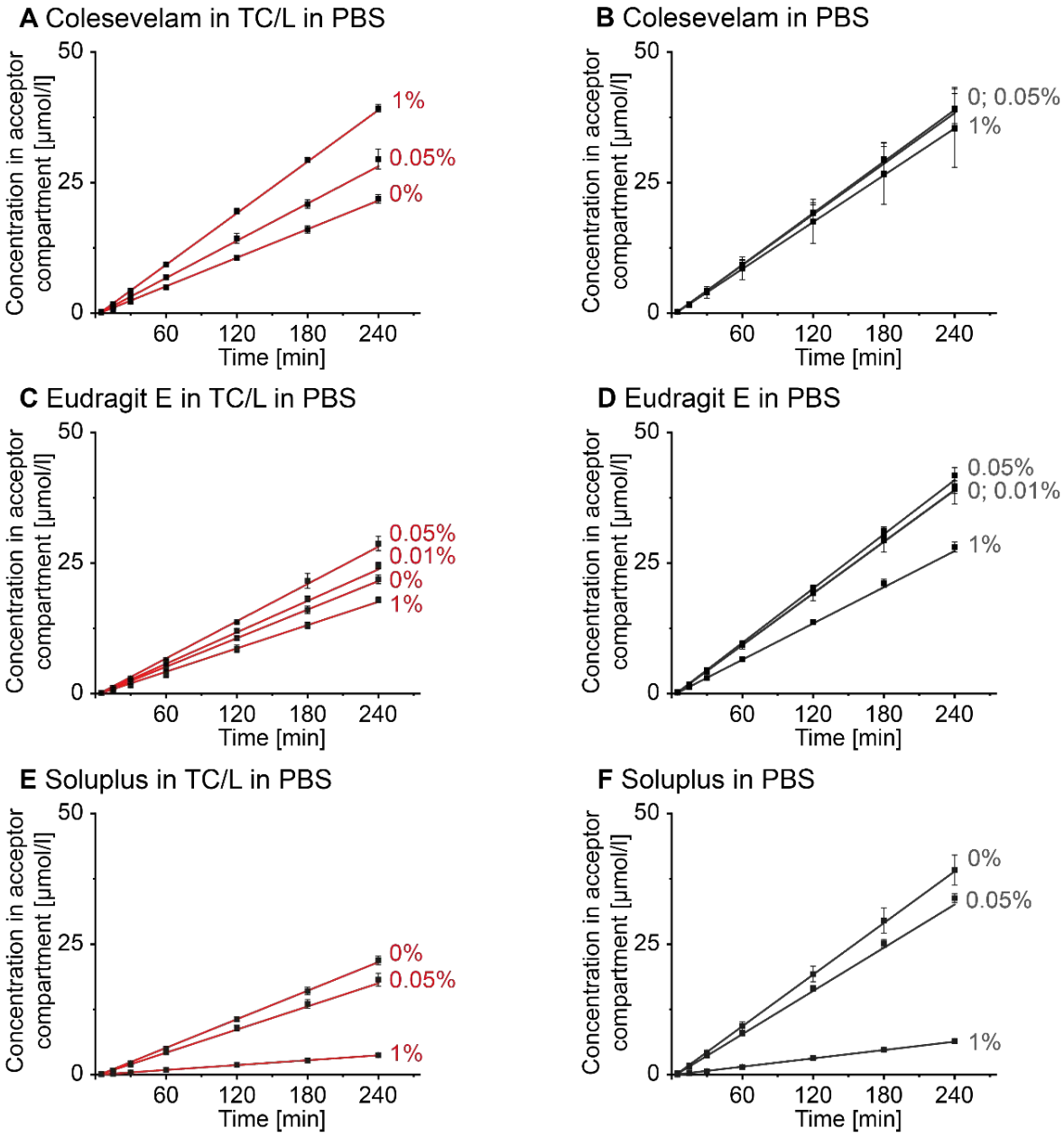

Figure S41: Imatinib concentration [µmol/l] in the flux acceptor compartment over time with (A, B) Colesevelam, (C, D) Eudragit E, (E, F) Soluplus in TC/L in PBS (respective left panel) and in PBS (respective right panel) at concentrations as indicated. Data at 0% polymer concentration are identical for all panels and given for comparison.

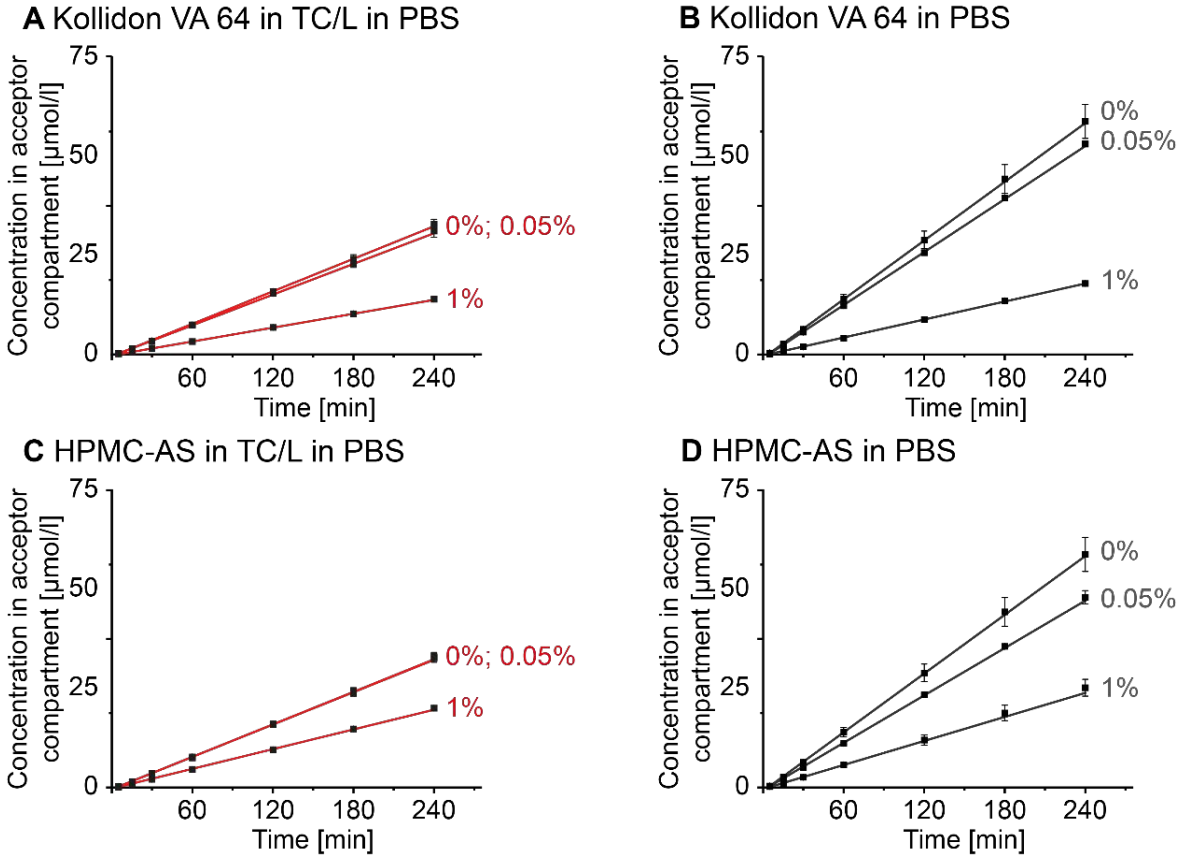

Figure S42: Imatinib concentration [µmol/l] in the flux acceptor compartment over time with (A, B) Kollidon VA 64, (C, D) HPMCAS in TC/L in PBS (respective left panel) and in PBS (respective right panel) at concentrations as indicated. Data at 0% polymer concentration are identical for all panels and given for comparison.

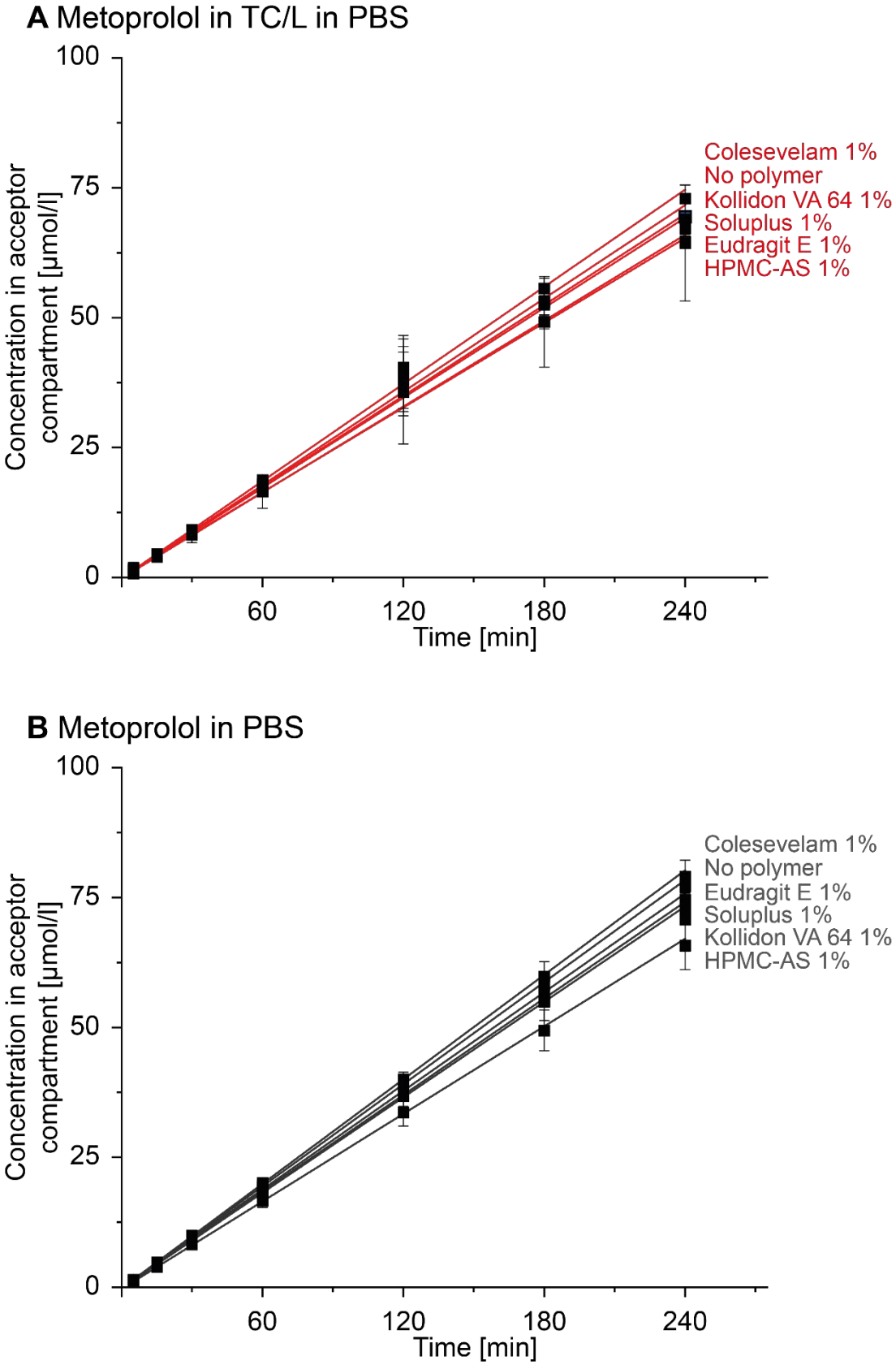

Figure S43: Metoprolol concentration [µmol/l] in the flux acceptor compartment over time with polymers as indicated (A) in TC/L in PBS and (B) in PBS at 1% polymer concentration. Data at 0% polymer concentration are provided in each panel.

S7.4 Flux lag time

S7.4.1 Lag time Perphenazine

Initial experiments were conducted at n = 3, thereby not allowing reasonable outlier testing. For the four groups with larger standard deviation as outlined in the table below, three additional experiments were conducted and outlier tests were performed. Subsequently, the lag time of these groups were evaluated (**Table S6**). One lag time observation for Perphenazine in PBS was categorized as an outlier based on a double-sided Grubb's outlier test and consequently excluded from the statistical analysis (**Figure S44**).

Table S6: Double-sided Grubb's outlier test for lag time of Perphenazine in PBS, in TC/L in PBS, in TC/L in PBS with 1% Eudragit E, and in TC/L in PBS with 1% HPMC-AS with a significance level of 0.05. One outcome was excluded as highlighted in bold/italic numbers.

Number	Lag time Perphenazine in PBS [min]	Lag time Perphenazine in TC/L in PBS [min]	Lag time Perphenazine in TC/L in PBS with 1% Eudragit E [min]	Lag time Perphenazine in TC/L in PBS with 1% HPMC-AS [min]
1	3,05	3,75	13,98	5,63
2	2,70	3,06	13,49	9,90
3	***-0,13***	1,81	16,66	5,50
4	2,84	5,93	8,57	7,76
5	2,24	5,62	12,21	7,29
6	2,60	5,77	8,73	7,52
Result from Grubb's-test	Outlier (-0,13)	No Outlier	No Outlier	No Outlier

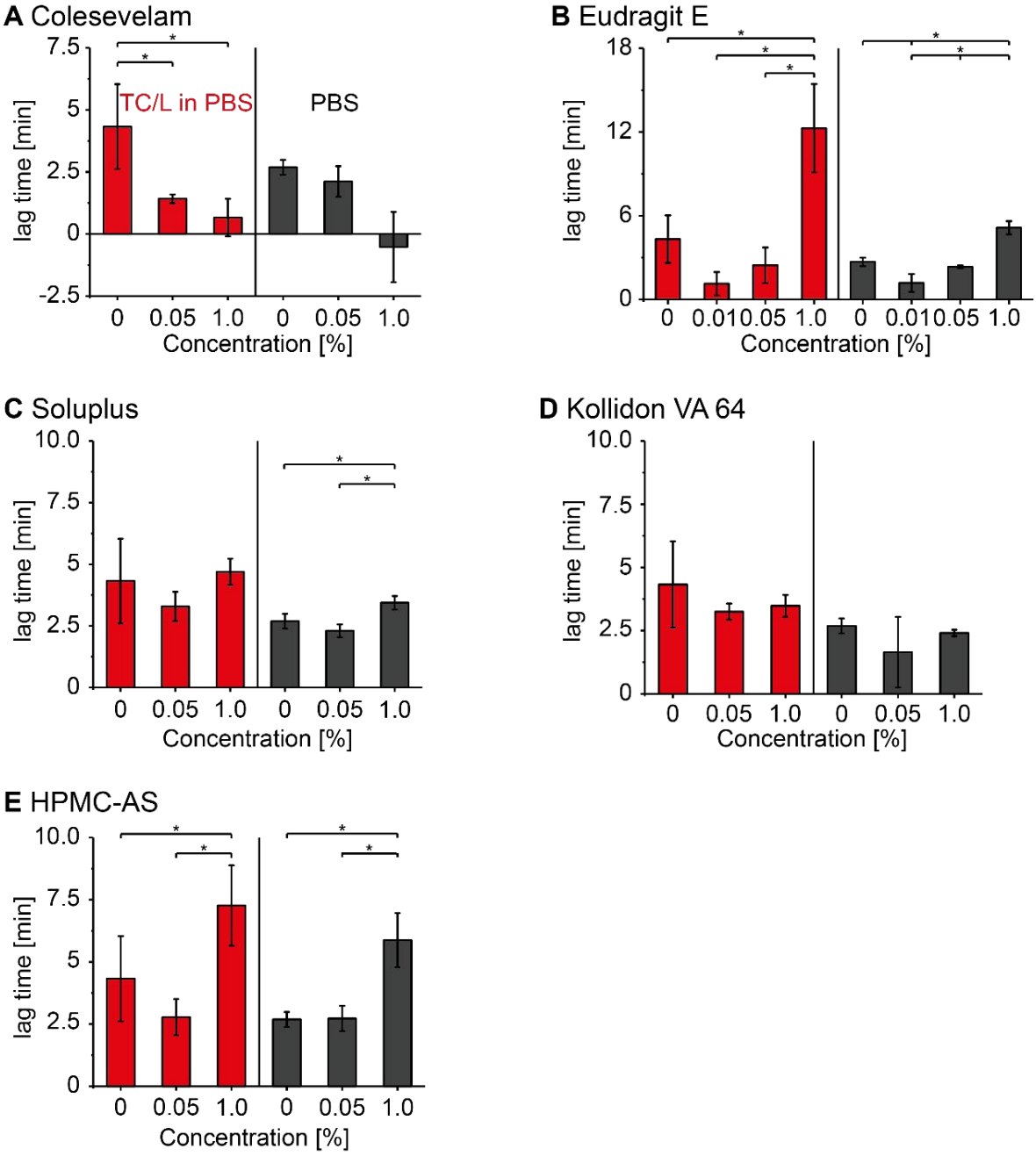

Figure S44: Lag time of Perphenazine with (A) Colesevelam, (B) Eudragit E, (C) Soluplus, (D) Kollidon VA 64, and (E) HPMC-AS in TC/L in PBS (red) and in PBS (black) at concentrations as indicated. The data reported at 0% are identical for all panels and given for comparison. Data for (B) Eudragit E is also shown in Figure 6 in the manuscript. Lag time was calculated by time axis intersect of the extrapolated linear part (**Figure S36**). Data shown as mean ± SD, ANOVA considering $p \leq 0.05$ as statistically significant followed by Tukey post-hoc test for pairwise comparison (significant differences are shown by asterisks).

S7.4.2 Lag time Imatinib

Due to a very high lag time standard deviation of some samples, outlier tests were performed. Lag time of Imatinib in TC/L in PBS, in TC/L in PBS with 1% Eudragit E, in TC/L in PBS with 1% Soluplus, and in TC/L in PBS with 1% HPMC-AS was reevaluated with three additional experimental repetitions (**Table S7**). As a result, one lag time data point for Imatinib in TC/L in PBS was removed from further statistical analysis (**Figure S45**).

Table S7: double-sided Grubb's outlier test for lag time of Imatinib in TC/L in PBS, in TC/L in PBS with 1% Eudragit E, in TC/L in PBS with 1% Soluplus, and in TC/L in PBS with 1% HPMC-AS with a significance level of 0.05. One outcome was excluded as highlighted in bold/italic numbers.

Number	Lag time Imatinib in TC/L in PBS [min]	Lag time Imatinib in TC/L in PBS with 1% Eudragit E [min]	Lag time Imatinib in TC/L in PBS with 1% Soluplus [min]	Lag time Imatinib in TC/L in PBS with 1% HPMC-AS [min]
1	3,32	8,33	4,02	6,99
2	3,68	5,10	1,23	2,34
3	***12,16***	14,74	2,46	6,16
4	5,11	6,45	6,15	8,56
5	5,54	8,62	6,63	6,22
6	5,03	8,88	5,33	8,49
Result from Grubb's-test	Outlier (12,16)	No Outlier	No Outlier	No Outlier

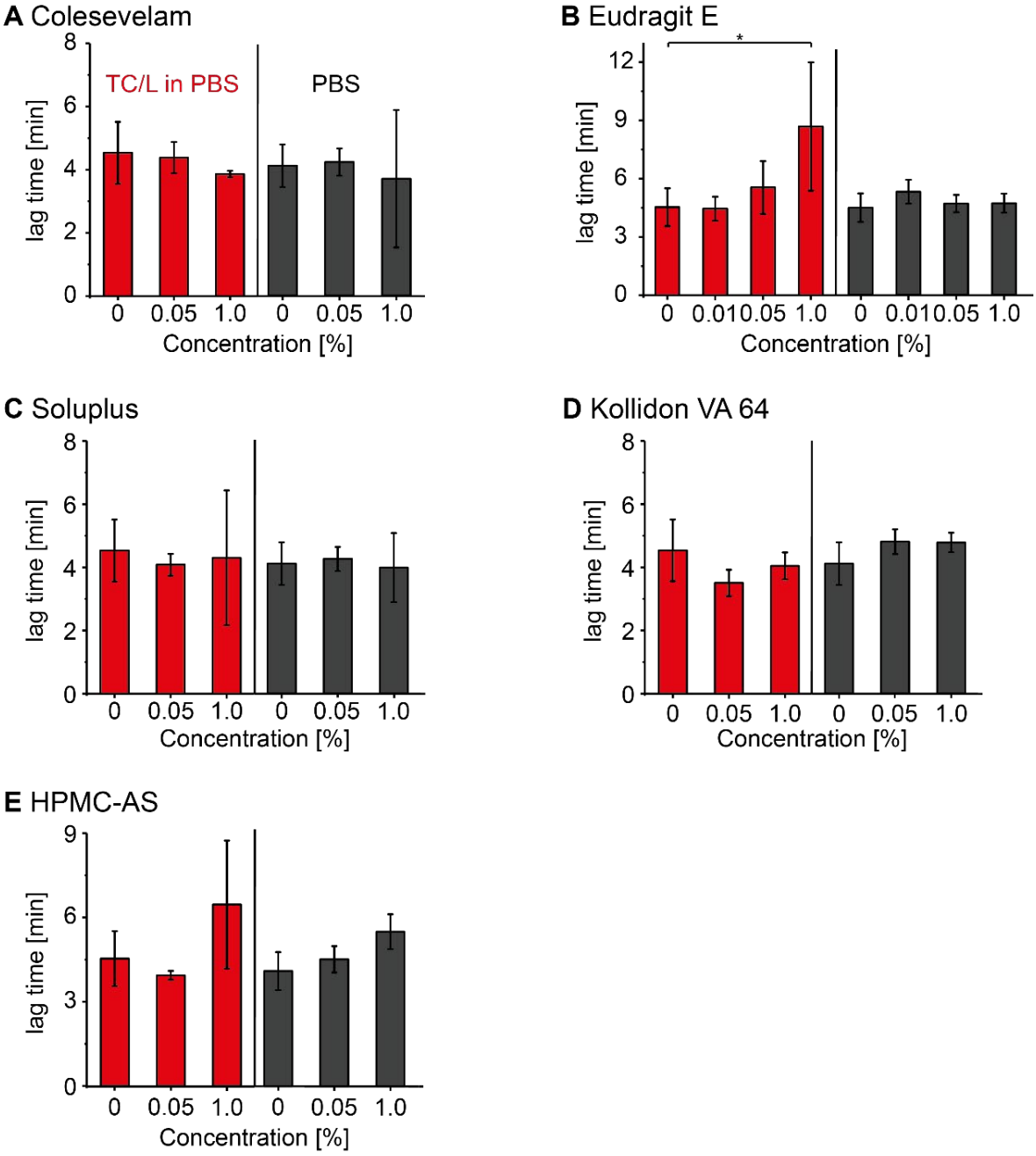

Figure S45: Lag time of Imatinib with (A) Colesevelam, (B) Eudragit E, (C) Soluplus, (D) Kollidon VA 64, and (E) HPMC-AS in TC/L in PBS (red) and in PBS (black) at concentrations as indicated. The first bars 0% are identical for all panels and for comparison. Data for (B) Eudragit E is also shown in Figure 6 in the manuscript. Lag time was calculated by time axis intersect of linear concentration over time extrapolation (**Figure S36**). Data shown as mean ± SD, ANOVA considering $p \leq 0.05$ as statistically significant followed by Tukey post-hoc test for pairwise comparison (significant differences are shown by asterisks).

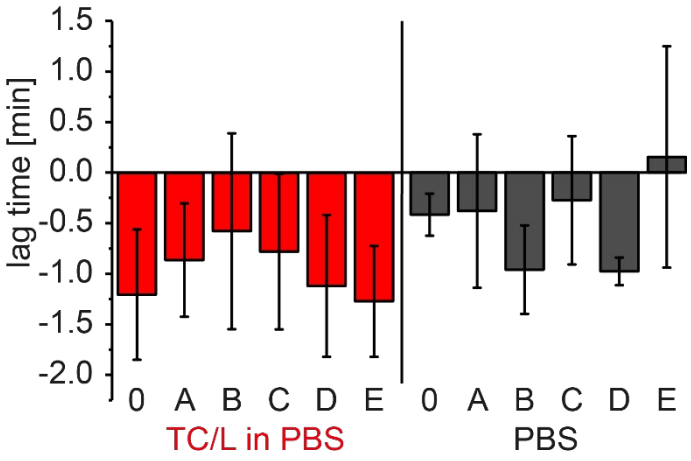

Figure S46: Metoprolol lag time (0) in absence of polymer, with 1% (A) Colesevelam, (B) Eudragit E, (C) Soluplus, (D) Kollidon VA 64, and (E) HPMC-AS in TC/L in PBS (red) and in PBS (black). No difference in lag time between the groups was observed.

S8 Imatinib flux reduction by polymer presence

Flux reduction was calculated at 1% polymer concentration as follows (Eq.1).

$$\text{Flux reduction [\%]} = \left(1 - \frac{Flux_{1\%\ polymer\ in\ TC/L\ in\ PBS}}{Flux_{1\%\ polymer\ in\ PBS}}\right) * 100 \qquad \text{Eq. 1}$$

Imatinib flux in Kollidon VA 64 and HPMC-AS presence was decreased by 23.0% and 20.8%, respectively. In contrast, Eudragit E and Soluplus decreased flux by 35.2% and 42.0%, respectively. This indicated higher affinity of Imatinib to TC/L/polymer MIM than to coexisting species.

References

1. Wiest, J.; Saedtler, M.; Böttcher, B.; Grüne, M.; Reggane, M.; Galli, B.; Holzgrabe, U.; Meinel, L., Geometrical and Structural Dynamics of Imatinib within Biorelevant Colloids. *Mol. Pharmaceutics* **2018**, 15 (10), 4470-4480.
2. Schiller, C.; Fröhlich, C. P.; Giessmann, T.; Siegmund, W.; Monnikes, H.; Hosten, N.; Weitschies, W., Intestinal fluid volumes and transit of dosage forms as assessed by magnetic resonance imaging. *Aliment. Pharmacol. Ther.* **2005**, 22 (10), 971-9.
3. Reker, D.; Blum, S. M.; Steiger, C.; Anger, K. E.; Sommer, J. M.; Fanikos, J.; Traverso, G., "Inactive" ingredients in oral medications. *Sci. Transl. Med.* **2019**, 11 (483).
4. Evonik Nutrition and Care GmbH, Eudragit Polymers for immediate release. https://healthcare.evonik.com/product/health-care/en/products/pharmaceutical-excipients/immediate-release/, **2020** (accessed 01 April 2020).
5. Boni, J. E.; Brickl, R. S.; Dressman, J.; Pfefferle, M. L., Instant FaSSIF and FeSSIF—Biorelevance Meets Practicality. *Dissolut. Technol.* **2009**, 16 (3), 41-45.

Chapter III: Bile and excipient interactions directing drug pharmacokinetics in rats

Jonas Schlauersbach[1], Simon Hanio[1], Martina Raschig[1], Bettina Lenz[1], Oliver Scherf-Clavel[1], Lorenz Meinel[1,2,*]

[1] Institute for Pharmacy and Food Chemistry, University of Wuerzburg, Am Hubland, DE-97074 Wuerzburg, Germany

[2] Helmholtz Institute for RNA-based Infection Biology (HIRI), Josef-Schneider-Straße 2/D15, DE-97080 Wuerzburg, Germany

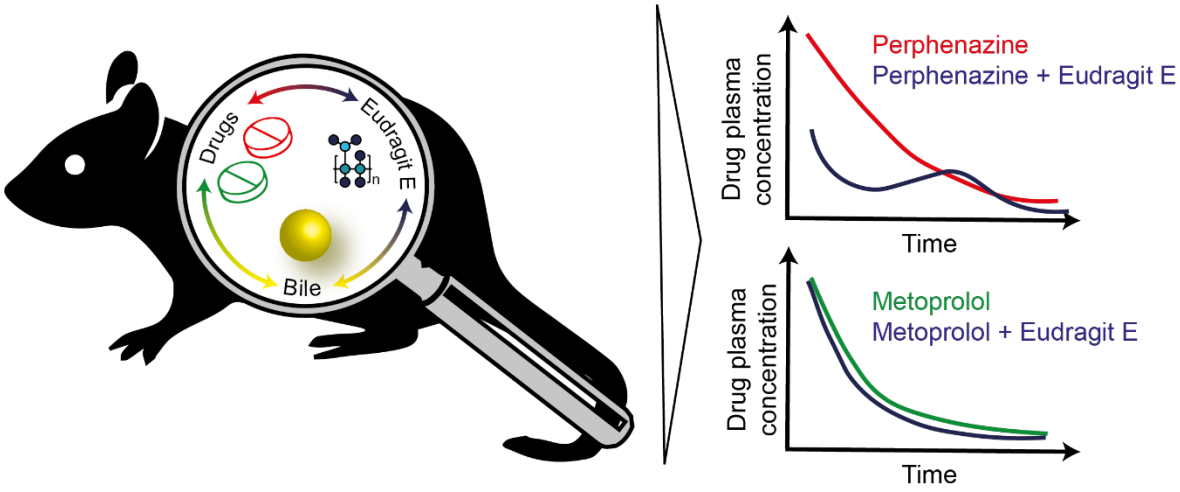

This chapter was originally published in European Journal of Pharmaceutics and Biopharmaceutics. Reprinted with permission from Schlauersbach J., et al. Journal of Pharmaceutics and Biopharmaceutics, "Bile and excipient interactions directing drug pharmacokinetics in rats"; vol. 178, pp. 65-68, 2022, DOI: 10.1016/j.ejpb.2022.07.016. Copyright © (2022) Elsevier. This manuscript version is made available under the CC-BY-NC-ND 4.0 license.

https://creativecommons.org/licenses/by-nc-nd/4.0/

*Corresponding author: Prof. Dr. Dr. Lorenz Meinel, Institute for Pharmacy and Food Chemistry, University of Wuerzburg, Am Hubland, DE-97074 Wuerzburg, Germany, E-Mail: lorenz.meinel@uni-wuerzburg.de

Abstract

Bile solubilization plays a major role in the absorption of poorly water-soluble drugs. Excipients used in oral drug formulations impact bile-colloidal properties and their molecular interactions. Polymer-induced changes of bile colloids, e.g., by Eudragit E, reduced the flux of the bile interacting drug Perphenazine whereas bile non-interacting Metoprolol was not impacted. This study corroborates these *in vitro* findings in rats. Eudragit E significantly reduced systemic availability of Perphenazine but not Metoprolol compared to the oral administrations without polymer. This study confirms the necessity to carefully select polymers for bile interacting drugs whereas non-bile interacting drugs are more robust in terms of excipient choice for formulation. The perspective of bile interaction may introduce interesting biopharmaceutical leverage for better performing oral formulations of tomorrow.

Introduction

Bile plays a key role in the lipid digestion of vertebrates.[1] Furthermore, poorly water-soluble drug**s** may be solubilized by bile, thereby enhancing their bioavailability.[2] Bile is essential for the absorption of drugs interacting with bile.[2] Nevertheless, some polymers used in oral drug formulations impact bile colloids. In fact, this polymer interaction with bile *in vitro* may reduce the flux of bile interacting drugs. The resulting hypothesis, bile interacting drugs may be preferentially formulated with bile-inert polymers whereas bile-non interacting drugs are more robust in terms of polymer choice, is now addressed *in vivo* in rats. For that, we focus on the pharmacokinetic profiles of Perphenazine (bile interacting) or Metoprolol (bile non-interacting), administered with and without (bile interacting) Eudragit E.[3] The *in vivo* study conditions were selected in light of previously published *in vitro* conditions.[3] We also integrated another arm by applying a mixture of Eudragit E and Colesevelam, as Colesevelam is a therapeutic agent designed to bind bile acids thereby serving as a positive control. Plasma concentrations were determined by liquid chromatography-tandem mass spectrometry (LC-MS/MS).

Materials and methods

Materials

Eudragit E PO was gifted from Evonik Nutrition and Care GmbH (Essen, Germany). Colesevelam hydrochloride was acquired from BOC Sciences (Shirley, NY, USA). Perphenazine, Metoprolol tartrate, Metoprolol-d_7 tartrate, and Omeprazole were purchased from Sigma-Aldrich (Schnelldorf, Germany). Perphenazine-$^{13}C3$ was in-house synthesized and purified.

Methods

Media preparation

Modified phosphate-buffered saline (PBS) pH 6.5 was prepared as reported.[3] For Colesevelam treatment groups, the PBS was adjusted with sodium hydroxide to neutralize acidic valency of the hydrochloride. Ionic strengths were kept constant in all treatment groups by adding sodium chloride if necessary.

Pharmacokinetic study in rats

A comparative **p**harmaco**k**inetic (**PK**) study in male wistar rats (Toxi Coop zrt., Budapest, Hungary) was conducted in compliance with the animal welfare directive 2010/63/EU at ATRC Aurigon Toxicological Research Center Ltd. (Dunakeszi, Hungary). 6 different treatment groups with 5 animals per group were included in this study (**Table 1**). The animals fasted overnight before application. Colesevelam and Eudragit E were equilibrated with respective PBS. Approximately 2 hours before administration, rats received 20 mg/kg Omeprazole in PBS to minimize pH effects.[4] Metoprolol or Perphenazine was added as a DMSO stock solution to excipient/medium mixtures right before administration resulting in a drug concentration of 2 mmol/l. The amount of DMSO in applied solutions was 1% V/V. Sampling time points were selected from previous reports.[5, 6] Perphenazine and Metoprolol concentrations were selected to ensure a dissolved state throughout the gastrointestinal passage. Perphenazine did not precipitate in any medium for at least four hours (data not shown). Rats received solutions orally by gavage with an administered volume of 5 ml/kg. Perphenazine and Metoprolol-tartrate doses were 10 µmol/kg (4.04 and 3.42 mg/kg, respectively). The Eudragit E concentration was 2% w/V and Colesevelam 10% w/V.

Table 1: Study treatment groups and dose regime.

Group name	Drug [10 µmol/kg]	Colesevelam [mg/kg]	Eudragit E [mg/kg]
Perphenazine control	Perphenazine	-	-
Perphenazine + Eudragit E	Perphenazine	-	100
Perphenazine + Colesevelam + Eudragit E	Perphenazine	500	100
Metoprolol control	Metoprolol	-	-
Metoprolol + Eudragit E	Metoprolol	-	100
Metoprolol + Colesevelam + Eudragit E	Metoprolol	500	100

A Colesevelam concentration 10 times higher compared to *in vitro* experiments was chosen, as rats have roughly a tenfold higher basal intestinal bile salt concentration compared to humans.[7] Roughly 200 µl blood was withdrawn from, e.g., tail, or sublingual vein, into lithium heparin tubes at 6 time points (1h, 2h, 3h, 5h, 10h, and 24h for Perphenazine; 15 min, 30 min, 45 min, 60 min, 120 min, and 270 min for Metoprolol), plasma was obtained by centrifugation (3000 g at room temperature for 10 min), and frozen until analysis. Animals were sacrificed after the last blood sampling.

Liquid chromatography-tandem mass spectrometry analysis

For liquid chromatography-tandem mass spectrometry (LC-MS/MS) analysis, plasma was extracted with ice-cold Acetonitrile including internal standard, and vortexed. Samples were centrifuged for 15 min at 4 °C and 24,900 g (Universal 320 R, Andreas Hettich GmbH & Co. Kg, Tuttlingen, Germany). The supernatant was diluted with the respective mobile phase, vortexed and centrifuged again. Ultra-high performance liquid chromatography (UHPLC) was performed on an Agilent 1200 Series HPLC system (Agilent Technologies, Waldbronn, Germany) equipped with a XBridge C18 3.5 µm 2.1 x 50 mm (Waters Corporation, Milford, MA) column. The column compartment temperature was set to 20 °C and the injection volume was 5 µl. Mobile phase A was 10 mM NH_4HCO_3 in water/methanol 90/10 (V/V). Mobile phase B was 10 mM NH_4HCO_3 in 90/10 (V/V) methanol/water. The flow rate was set to 0.6 mL/min. The UHPLC effluent was channeled to an Agilent 6460 triple quadrupole operating with an electrospray ionization interface, in multiple reaction monitoring and positive ion mode. Mass spectra were acquired using a transition of 404 to 143 m/z for Perphenazine and 407 m/z to 174.1 m/z for -Perphenazine $^{13}C3$ with a collision energy of 28 and 24 eV, respectively. For Metoprolol transitions from 268.1 to 159 m/z and 279.1 to 123 m/z for Metoprolol-d_7 with a collision energy of 17 and 20 eV were applied, respectively. Signal-to-noise ratios of 3 and 10 were used to estimate the limit of detection and limit of quantification, respectively.[8] The limit of detection and quantification was 0.53 nmol/l and 1.8 nmol/l for Perphenazine and 0.95 nmol/l and 3.15 nmol/l for Metoprolol, respectively. Drugs were quantified with respective internal standard pairing using calibration curves. Individual noncompartmental PK analysis was applied to plasma concentrations using R version 4.0.5 (R Foundation for Statistical Computing, Vienna, Austria) using the package 'NonCompart' version 0.4.9 (Kyun-Seop Bae). Area under the curve to last nonzero concentration using the linear up and down method was calculated (AUC_{last}). Rat number 41 (Perphenazine control) and 15 (Perphenazine + Eudragit E) were excluded from the analysis. Rat number 41 was not pretreated with Omeprazole and the 1 h plasma value of rat 15 was considered as an outlier.

Statistical Analysis

A double-sided Grubb's test was used for outlier testing. One-way ANOVA followed by *a post hoc* Tukey test was performed. Data were considered statistically significant at $p \leq 0.05$.

OriginPro 2020 (OriginLab Corporation, Northampton, MA, USA) was used for statistical analysis.

Results and discussion

Previously reported outcomes demonstrated the interaction of Eudragit E with taurocholate and lecithin in bile colloids (**Figure 1**; modified from [3]), and these interactions might impact drug solubilization, release rates, and ultimately bioavailability. For example, bile-solubilized Perphenazine had a reduced flux across cellulose membranes in presence of Eudragit E (**Figure 1A**; modified from [3]). Colesevelam, a polymeric bile acid sequestrant, increased Perphenazine flux. Metoprolol flux across cellulose membranes, a drug substance that is not relevantly solubilized by bile, was not affected by any of these conditions (**Figure 1B**). The *in vitro* study from which this data is shown[3] is now supplemented with in vivo pharmacokinetics in rats.

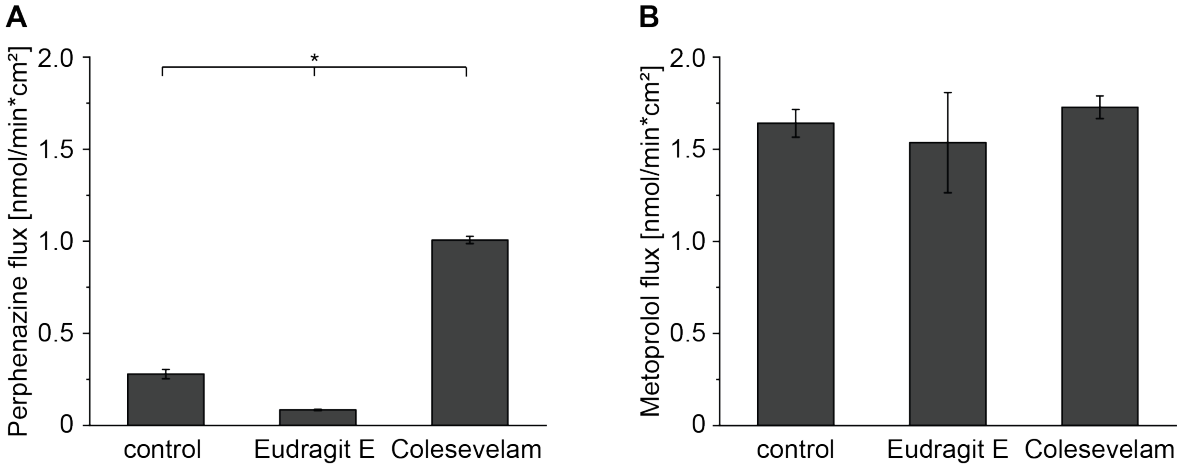

Figure 1: (A) Perphenazine and (B) Metoprolol flux over cellulose membrane in fasted state simulated intestinal fluid V1 (control) and with Eudragit E or Colesevelam. Data shown as mean ± SD, ANOVA considering $p \leq 0.05$ as statistically significant followed by Tukey post-hoc test for pairwise comparison (significant differences are shown by asterisks). The data was previously published: Schlauersbach et. al. "Leveraging bile solubilization of poorly water-soluble drugs by rational polymer selection", J. Control. Release, 330 (2021) 36-48 © Elsevier, 2020. Reprinted with license from Elsevier (license number: 5324180742375)

The plasma concentration profiles of Perphenazine (bile interacting[9]) were biphasic with an initial absorption and subsequent elimination phase (**Figure 2A**). Co-administration of Eudragit E particularly impacted the absorption phase (**Figure 2B**). Exposure to both, Eudragit E and Colesevelam further flattened the plasma-concentration profile (**Figure 2C**).

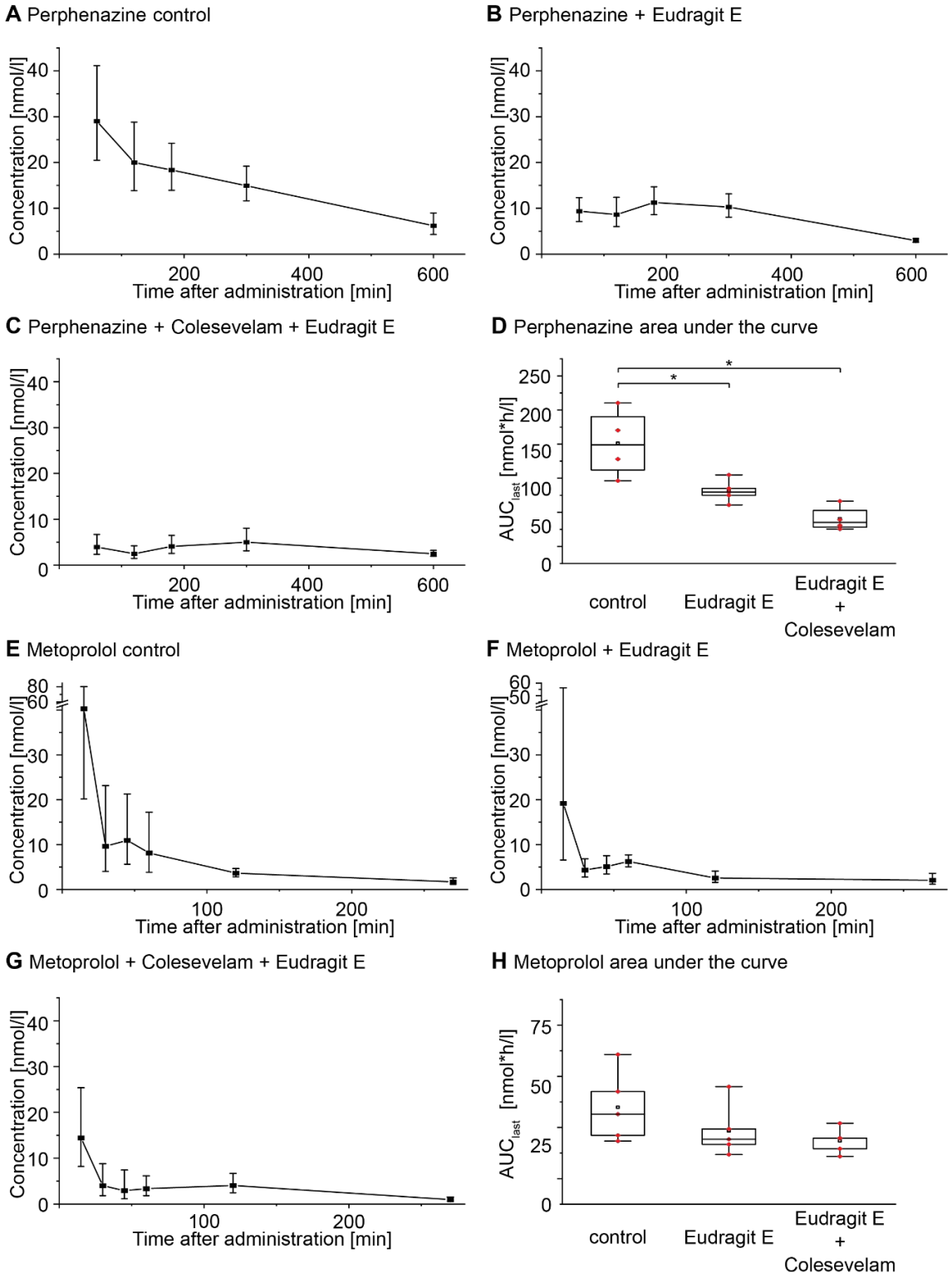

Figure 2: (A-C) Perphenazine and (E-G) Metoprolol plasma concentration over time (geometric mean ± geometric standard deviation) in rats (A, C n=4; B, E-G, n=5) after oral administration of 10 µmol/kg drug (A, E) in PBS, (B, F) with Eudragit E, and (C, G) Eudragit E and Colesevelam. Lines between points were linearly interpolated. AUC_{last} for (D) Perphenazine and (H) Metoprolol treatment groups. Data shown as red diamonds, boxplot in with mean as black dot, median as line, interquartile range from 25th percentile to 75th percentile as box, and range within minimum to maximum value as line. ANOVA considering $p \leq 0.05$ as statistically significant followed by Tukey *post-hoc* test for pairwise comparison (asterisks show significant differences).

Overall, the Perphenazine **a**rea **u**nder the **c**urve (**AUC**) was significantly reduced in presence of Eudragit E and for both polymers (**Figure 2D, Table 2**). Metoprolol plasma concentration declined faster compared to Perphenazine (**Figure 2E-G**). Metoprolol (not interacting with bile[3]) plasma profiles and the AUC were neither impacted by Eudragit E nor Eudragit E/Colesevelam (**Figure 2H**). T_{max} was increased for Perphenazine groups with Eudragit E, which might reflect a release of drug in more distal parts of the gastrointestinal system (**Table 2**) as reported in the context of colonic drug delivery.[10]

Taken together, Eudragit E induced changes to bile that significantly reduced flux and bioavailability of bile interacting Perphenazine. From our in vitro experiments, one might have expected higher perphenazine exposure in the presence of Colesevelam and Eudragit E since flux increased in the presence of Colesevelam. However, the reduction in exposure to Eudragit E was still dominant. Colesevelam was thus unable to release Perphenazine from the strong interaction with Eudragit E and bile. In contrast, bile non-interacting Metoprolol's flux and bioavailability were not impacted.

In conclusion, Eudragit E and Eudragit E with Colesevelam critically impacted Perphenazine absorption, but not Metoprolol. The *in vivo* data shown here corroborates previous *in vitro* data sets (shown again in part in **Figure 1**) and statements. Polymer selection for the formulation of bile interacting drug substances might be critical to preserving the solubilization capacity of bile.[3]

Table 2: Perphenazine and Metoprolol non-compartmental PK analysis for control, Eudragit E, and Colesevelam + Eudragit E treatment. T_{max} is shown as median and range in brackets. Data shown as mean ± SD. For Perphenazine groups with Eudragit E, no parameters dependent on λ_z could be calculated, as observed excretion period was too short.

Treatment	c_{max} [nmol/l]	T_{max} [h]	AUC_{last} [h*mg/l]	λ_z [1/h]	CL/F [l/h]
Perphenazine control	30.8 ± 12.1	1 (1-1)	151 ± 50	0.16 ± 0.02	57 ± 22
Perphenazine + Eudragit E	13.3 ± 3.1	3 (1-5)	81 ± 19	N/A	N/A
Perphenazine + Colesevelam + Eudragit E	5.8 ± 3.1	5 (3-10)	41 ± 18	N/A	N/A
Metoprolol control	50.3 ± 34.2	0.25 (0.25)	35 ± 17	0.48 ± 0.28	272 ± 90
Metoprolol + Eudragit E	35.3 ± 46.6	0.25 (0.25)	23 ± 13	0.29 ± 0.17	338 ± 144
Metoprolol + Colesevelam + Eudragit E	17.2 ± 10.4	0.25 (0.25 - 2)	18 ± 6	0.44 ± 0.22	511 ± 189

Acknowledgments

We gratefully acknowledge the financial support by Novartis Pharma AG for JS.

References

1. Hofmann, A. F.; Hagey, L. R.; Krasowski, M. D., Bile salts of vertebrates: structural variation and possible evolutionary significance. *J Lipid Res* **2010,** *51* (2), 226-46.
2. Sugano, K.; Kataoka, M.; Mathews Cda, C.; Yamashita, S., Prediction of food effect by bile micelles on oral drug absorption considering free fraction in intestinal fluid. *Eur. J. Pharm. Sci.* **2010,** *40* (2), 118-24.
3. Schlauersbach, J.; Hanio, S.; Lenz, B.; Vemulapalli, S. P. B.; Griesinger, C.; Poppler, A. C.; Harlacher, C.; Galli, B.; Meinel, L., Leveraging bile solubilization of poorly water-soluble drugs by rational polymer selection. *J. Control. Release* **2021,** *330*, 36-48.
4. Segawa, K.; Nakazawa, S.; Tsukamoto, Y.; Chujoh, C.; Yamao, K.; Hase, S., Effect of omeprazole on gastric acid secretion in rat: evaluation of dose, duration of effect, and route of administration. *Gastroenterol. Jpn.* **1987,** *22* (4), 413-8.
5. Mohammadi, P.; Mahjub, R.; Mohammadi, M.; Derakhshandeh, K.; Ghaleiha, A.; Mahboobian, M. M., Pharmacokinetics and brain distribution studies of perphenazine-loaded solid lipid nanoparticles. *Drug Dev. Ind. Pharm.* **2020**, 1-7.
6. Yoon, I. S.; Choi, M. K.; Kim, J. S.; Shim, C. K.; Chung, S. J.; Kim, D. D., Pharmacokinetics and first-pass elimination of metoprolol in rats: contribution of intestinal first-pass extraction to low bioavailability of metoprolol. *Xenobiotica* **2011,** *41* (3), 243-51.
7. Christfort, J. F.; Strindberg, S.; Plum, J.; Hall-Andersen, J.; Janfelt, C.; Nielsen, L. H.; Müllertz, A., Developing a predictive in vitro dissolution model based on gastrointestinal fluid characterisation in rats. *Eur. J. Pharm. Biopharm.* **2019,** *142*, 307-314.
8. Vial, J.; Jardy, A., Experimental Comparison of the Different Approaches To Estimate LOD and LOQ of an HPLC Method. *Anal. Chem.* **1999,** *71* (14), 2672-2677.
9. Hanio, S.; Schlauersbach, J.; Lenz, B.; Spiegel, F.; Bockmann, R. A.; Schweins, R.; Nischang, I.; Schubert, U. S.; Endres, S.; Poppler, A. C.; Brandl, F. P.; Smit, T. M.; Kolter, K.; Meinel, L., Drug-Induced Dynamics of Bile Colloids. *Langmuir* **2021,** *37* (8), 2543-2551.
10. Moustafine, R. I.; Salachova, A. R.; Frolova, E. S.; Kemenova, V. A.; Van den Mooter, G., Interpolyelectrolyte complexes of Eudragit E PO with sodium alginate as potential carriers for colonic drug delivery: monitoring of structural transformation and composition changes during swellability and release evaluating. *Drug Dev. Ind. Pharm.* **2009,** *35* (12), 1439-51.

Chapter IV: Harnessing bile for drug absorption through rational excipient selection

Jonas Schlauersbach[1], Dominic Werthmüller[2], Bruno Galli[2], Simon Hanio[1], Bettina Lenz[1], Sebastian Endres[3], Ann-Christin Pöppler[3], Oliver Scherf-Clavel[1], Lorenz Meinel[1,4], Cornelius Harlacher[2,] *

[1] Institute for Pharmacy and Food Chemistry, University of Wuerzburg, Am Hubland, DE-97074 Wuerzburg, Germany

[2] Novartis Pharma AG, Lichtstrasse 35, CH-4056 Basel, Switzerland

[3] Institute of Organic Chemistry, University of Wuerzburg, Am Hubland, DE-97074 Wuerzburg, Germany

[4] Helmholtz Institute for RNA-based Infection Biology (HIRI), Josef-Schneider-Straße 2/D15, DE-97080 Wuerzburg, Germany

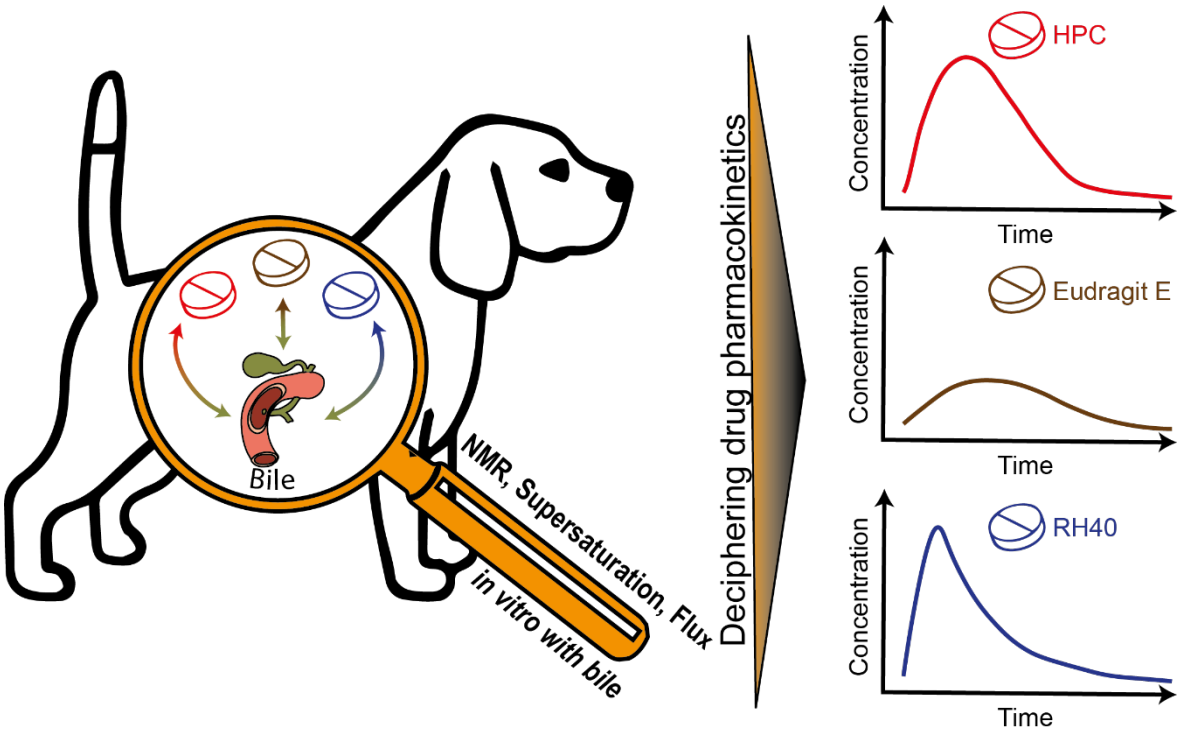

Keywords: *in vitro-in vivo* relationship; pharmacokinetics; flux; bile; excipient; NMR; dog study

unpublished manuscript

*Corresponding author: Dr. Cornelius Harlacher, Novartis Pharma AG, Lichtstrasse 35, CH-4056 Basel, Switzerland, E-Mail: cornelius.harlacher@novartis.com

Abstract

Bile solubilization and apparent solubility at resorption sites critically affect the bioavailability of orally administered and **p**oorly **w**ater-**s**oluble **d**rugs (**PWSD**s). Therefore, identification of drug-bile interaction may critically determine the overall formulation success. For the case of the drug candidate Naporafenib, drug in solution at phase separation onset significantly improved with polyethylene glycol-40 hydrogenated castor oil (**RH40**) and amino methacrylate copolymer (**Eudragit E**) but not **h**ydroxy**p**ropyl **c**ellulose (**HPC**) in both **p**hosphate-**b**uffered **s**aline (**PBS**) and PBS supplemented with bile components. Naporafenib interacted with bile as determined by ^{1}H, 2D ^{1}H-^{1}H nuclear magnetic resonance spectroscopy, and so did Eudragit E and RH40 but not HPC. Flux across artificial membranes was reduced in presence of Eudragit E. RH40 reduced Naporafenib supersaturation duration. HPC on the other side stabilized Naporafenib's supersaturation and did not impact flux. These insights on bile interaction correlated with pharmacokinetics in beagle dogs. HPC preserved Naporafenib bile solubilization in contrast to Eudragit E and RH40, resulting in favorable pharmacokinetics.

Introduction

Many **a**ctive **p**harmaceutical **i**ngredients (**API**) are **p**oorly **w**ater-**s**oluble **d**rug**s** (**PWSDs**) with good permeability across epithelial barriers in the **g**astro**i**ntestinal **t**ract (**GIT**) referred to as class II APIs within the biopharmaceutic classification system.[1-5] Consequently, pharmaceutical strategies for these PWSDs generally aim at improving the amount of the dissolved drug at resorption sites [6-8], including salt design,[9-12] use of lipid-based delivery systems,[13-15] or **a**morphous **s**olid **d**ispersion**s** (**ASDs**)[16-19] among others.[20] However, in addition to *in vitro* solubility considerations, biopharmaceutical solubilization may contribute to the availability of dissolved API at resorption sites. Biopharmaceutical solubilization can be studied *in vitro* in biorelevant media, using, e.g., **fa**sted and **fe**d **s**tate **s**imulated **i**ntestinal **f**luids (**FaSSIF/FeSSIF**).[21] FaSSIF/FeSSIF contain sodium **t**auro**c**holate (**TC**) as representative bile salt and **l**ecithin (**L**) reflecting intestinal phospholipids.[22, 23] Solubilization dynamics expand from isolated API-bile component interactions studied *in vitro* to multiple confounding players found *in vivo*, among them food ingredients or the presence of pharmaceutical excipients.[24, 25] Surprising outcomes may follow. For example, Eudragit E maximized the apparent solubility of a PWSD while decreasing bioavailability.[26] In another example, an API was better soluble in solutions mimicking a fed state rather than a fasted state (*in vitro*). Despite these findings, this did not affect the bioavailability in fed versus fasted animals.[22] These and other examples ask for advanced multi-parametric pharmaceutical strategies in development, extending beyond simple solubility applications.

Therefore, we are now integrating a biopharmaceutical-driven strategy using Naporafenib as a model PWSD.[27-29] Naporafenib interaction with TC/L and lipids was studied by ^{1}H and 2D ^{1}H-^{1}H **n**uclear **m**agnetic **r**esonance (**NMR**) spectroscopy, shake flask solubility, characterization of phase separation onset, and flux across artificial membranes in the presence of various pharmaceutically relevant excipients for oral drug delivery including the amino methacrylate copolymer Eudragit E, **h**ydroxy**p**ropyl **c**ellulose (**HPC**), and polyethylene glycol-40 hydrogenated castor oil (**RH40**). Finally, we correlated the molecular insights obtained *in vitro* with *in vivo* outcomes in beagle dogs.

Materials and methods

Materials

Deionized, purified water (Millipore) was from an in-house Millipore purification system from Merck KGaA (Darmstadt, Germany). Hexadeuterodimethyl sulfoxide (DMSO-d_6, 99.8% D) was purchased from Euriso-top (Saarbrücken, Germany) and deuterated water (D_2O, 99.9% D) from Deutero GmbH (Kastellaun, Germany). Eudragit E PO was from Evonik Nutrition and Care GmbH (Essen, Germany). Deuterated water (D_2O, 99.9% D) containing 0.05% 3-(trimethylsilyl) propionic-2,2,3,3-d_4 sodium salt (TSP-d_4), 40% sodium deuteroxide in deuterated water (NaOD, 99% D), 35% deuterium chloride in deuterated water (DCl, 99% D), sodium chloride (99%), monobasic sodium phosphate monohydrate (99%), were purchased from Sigma-Aldrich (Schnelldorf, Germany). Coaxial insert tubes and NMR tubes (5 mm, clear glass) were purchased from Norell (Landisville, PA, USA). FaSSIF/FeSSIF V1 and FeSSIF V2 powders were purchased from biorelevant.com (London, UK). Naporafenib monohydrate, Naporafenib tosylate, sodium **t**auro**c**holate (**TC**), polyethylene glycol-40 hydrogenated castor oil (**RH40**), and **h**ydroxy**p**ropyl **c**ellulose (**HPC**) were provided from Novartis Pharma AG (Basel, Switzerland). Ammonium acetate was from SERVA Electrophoresis GmbH (Heidelberg, Germany). **A**cceptor **s**ink **b**uffer (**ASB**) and lipid mixture (GIT-0 lipid solution) were from Pion Inc Ltd (Forest Row, United Kingdom). All other standard chemicals and laboratory consumables, if not stated otherwise, were purchased from either VWR International GmbH (Ismaning, Germany) or Sigma-Aldrich.

Methods

Media preparation

Modified **p**hosphate-**b**uffered **s**aline (**PBS**) pH 6.5 was prepared following the manufacturer's protocol (biorelevant.com). This buffer, from now on referred to as PBS, was used for biorelevant media preparation (**Table 1**). A 1.5-fold higher concentration for FeSSIF-V2 than described by the manufacturer was chosen to align the TC concentration between FeSSIF-V1 and FeSSIF-V2. In addition, 15 mmol/l TC was dissolved in PBS. For 1H NMR measurements, deuterated solvents were applied. In deuterated water, a correction factor was used, adjusting pD to 6.91 using DCl and NaOD.[30]

Table 1: Composition of simulated intestinal media

Component [mmol/l]	Purpose	FaSSIF-V1 "TC/L"	FeSSIF-V1 "5x TC/L"	FeSSIF-V2 "5x TC/L with lipids"
sodium taurocholate	natural bile salt	3	15	15
lecithin	phospholipids	0.75	3.75	3
sodium oleate	digestive product (lipid)	-	-	1.2
glycerol monooleate	digestive product (lipid)	-	-	6.5

Solubility

Solubility of Naporafenib in PBS and simulated intestinal fluids and in the presence of individual excipients at a concentration of 0.1% (% means the weight per weight unless stated otherwise; excipients were applied at a concentration of 0.1% if not stated otherwise) was determined by shake flask approach. An excess amount (10 mg/ml) of Naporafenib as tosylate salt or crystalline monohydrate was given into a 2 ml tube and shaken for 48 h at 25 °C and 750 rpm on a Thermomixer F1.5 (Eppendorf AG, Hamburg, Germany). The samples were centrifuged for 15 min on a MiniSpin centrifuge (Eppendorf AG) at 13000 rpm. The first supernatant was transferred into a new tube and centrifuged again. Then, the second supernatant was diluted with mobile phase (20% v/v **Ac**eto**n**itrile (ACN) in MilliQ with 0.1% **t**ri**f**luoroacetic **a**cid (**TFA**)) at a ratio of at least 1:2 and analyzed by **H**igh-**P**ressure **L**iquid **C**hromatography (**HPLC**) as mentioned below. Solubility experiments were carried out as triplicates.

Phase separation onset determination

Drug **p**hase **s**eparation **o**nset (**PSO**), representing liquid-liquid or liquid-glass phase separation, was determined by a Sirius T3 instrument (Pion Inc., Forest Row, UK). Excipient/medium mixtures without drug were shaken on an orbital shaker Reax 20 (Heidolph GmbH, Schwabach, Germany) for 2 hours at room temperature. 20 ml of medium or excipient/medium mixture was filled into a glass vessel and placed on alternated titration. Naporafenib stock solution in DMSO with medium dependent concentrations was gradually added, and light scattering at 401 nm was measured with the in-build UV-dip probe. The stirring speed was set to 4800 rpm. Experiments were conducted at room temperature. Every 20 s, a UV-spectrum was recorded, and 10 µL of Naporafenib stock solution was added. Each run consisted of 20 data points. PSO was determined by the tangent intersection point method using the respective baseline at 401 nm. PSO experiments were carried out as triplicates.

^{1}H nuclear magnetic resonance spectroscopy

Naporafenib in DMSO-d_6 was added to the deuterated medium or excipient/medium mixtures, subsequently shaking for two hours, at 25 °C, and 750 rpm on a Thermomixer F1.5 (Eppendorf). The amount of DMSO never exceeded 1% v/v. The Naporafenib concentration for ^{1}H **d**iffusion-**o**rdered **s**pectroscop**y** (DOSY) and ^{1}H-^{1}H **n**uclear **O**verhauser **e**ffect **s**pectroscop**y** (**NOESY**) was adjusted to 90% of the media-dependent phase separation onset (**Table S1**). ^{1}H NMR spectra were recorded on a Bruker Avance 400 MHz spectrometer (Bruker BioSpin GmbH, Karlsruhe, Germany) operating at 400.13 MHz with a BBI BB-H 5 mm probe and at a temperature of 300 K. Acquisition parameters were set as previously reported.[24] An exponential line broadening window function of 2 Hz was used with automatic baseline correction and manual phasing. The chemical shifts were referenced to the external standard of 0.05% 3-(trimethylsilyl) propionic-2,2,3,3-d_4 sodium salt (TSP-d_4) in D_2O filled in a coaxial insert tube. ^{1}H DOSY and ^{1}H-^{1}H NOESY data were recorded on a Bruker Avance III HD spectrometer (Bruker BioSpin) operating at 600.13 MHz equipped with a 5 mm BBFO probe or a 5 mm DCH cryo-probe. Both probes had a z-gradient and a temperature control unit set to 300K. Before and after DOSY and NOESY experiments, an ^{1}H NMR spectrum was acquired to verify sample integrity. Pulse-field-gradient NMR spectra (**DOSY**) were recorded using the ledbgp2s[31] or the dstebpgp3s[32, 33] pulse sequences without spinning as described earlier.[34] In brief, the dstebpgp3s pulse sequence was applied when the cryo-probe was used, avoiding convection effects with a maximum gradient strength of 57 G/cm. For the BBFO probe, the ledbgp2s pulse sequence with a gradient strength of 50 G/cm was used. Gradients were linearly incremented in 32 steps from 2 to 98%. The diffusion time (d20) was set to 100 ms, and the gradient pulse length (p30) was adjusted, achieving signal decay to 1% of the initial intensity. The attenuation curves were monoexponentially fitted by OriginPro 2020 (OriginLab Corporation, Northampton, MA) using equation 1.

$$I(G) = I_0 \cdot e^{-\gamma^2 \cdot G^2 \cdot \delta^2 \cdot (\Delta - \frac{\delta}{3}) \cdot D} \quad \text{(Eq.1)}$$

Where *I(G)* is the gradient strength-dependent signal intensity, I_0 initial signal intensity, γ gyromagnetic ratio of protons (4258 Hz/Gauss), *G* gradient strength, δ gradient pulse length, Δ diffusion time, and *D* diffusion coefficient.

Two dimensional ^{1}H-^{1}H NOESY spectra were acquired using the noesygpphpp sequence as described.[34] A recycle delay of > 3.5 s was used. The NOESY was recorded with three different mixing times (d8) of 20 ms, 40 ms, and 60 ms to check the linear increase of off-diagonal intensities. The signal assignment was done using ^{13}C, ^{1}H-^{1}H **co**rrelated **s**pectroscop**y** (**COSY**), and the edited ^{1}H-^{13}C **h**eteronuclear **s**ingle **q**uantum **c**oherence (**HSQC**) spectra as described before.[34, 35] All NMR data was processed using TopSpin 4.0.6 (Bruker BioSpin).

Flux across cellulose-based membranes

As described earlier, a side-by-side diffusion cell (PermeGear Inc., Hellertown, USA) setup was used.[24] In short, the donor and receiver compartment (containing 10 ml) were separated by a regenerated cellulose membrane (innoME GmbH, Espelkamp, Germany). The orifice with a diameter of 15 mm resulted in a surface area of 1.77 cm². Excipients in their respective medium were equilibrated for at least two hours on an orbital shaker at room temperature. The medium or excipient/medium mixture was transferred to the donor chamber. The receiver compartment was filled with PBS containing 0.2% Vitamin E TPGS. The maximum drug concentration in the receiver compartment was less than one-tenth of the equilibrium solubility of Naporafenib in 0.2% Vitamin E TPGS (**Table S2**). The temperature was held at 298 K by a Haake Fisons C1 water circulator (Thermo Fisher Scientific Inc., Karlsruhe, Germany) with a DLK 1002 cooling unit (FRYKA GmbH, Esslingen, Germany). A continuous stirring speed of 500 rpm was accomplished by an H9-CB-02 stirring apparatus (SES GmbH, Bechenheim, Germany). At the beginning of the flux experiment respective amount of a 0.2, 0.1, or 0.01 mol/l Naporafenib stock solution in DMSO was added to achieve the individual nominal donor concentration. The total amount of DMSO never exceeded 1% (v/v). After 15, 30, 45, 60, 75 or 90, 120, 180, and 240 min, aliquots of 100 µl were drawn from the acceptor chamber and replaced with fresh Vitamin E TPGS 0.2% in PBS. In the case of a rapid decline in flux, samples were drawn every 10 minutes to ensure at least four data points for linear regression modeling. Afterward, the samples were diluted with 25 µl of **ac**eto**n**itrile (**ACN**) containing 0.1% **t**ri**f**luoro**a**cetic acid (**TFA**), vortexed for at least 30 seconds (VTX-3000L, LMSCO. LTD., Tokyo, Japan), and centrifuged with a MiniSpin centrifuge (Eppendorf AG) at 13000 rpm for 10 minutes. Experiments were carried out as triplicates.

Flux across lipid-based membranes

For lipid-based flux, a µFlux (Pion) setup was applied using a gastrointestinal-mimicking artificial membrane and acceptor sink buffer in the acceptor chamber.[36, 37] The filling volume of the donor and receiver chamber was 22 ml, and the membrane surface area was 1.54 cm². The **p**oly**v**inylidene **dif**luoride (**PVDF**) membrane wetted with phospholipids in a volatile solvent (GIT-0 lipid) was prepared following the manufacturer's instructions. Experiments were conducted at 298 K. The excipients were dissolved into PBS with TC/L using a magnet stirrer (RET basic, IKA GmbH& Co. KG, Staufen, Germany) at 300 rpm until a clear solution was obtained. Naporafenib was added by DMSO stock solution, and mixtures were stirred for 30 min. They were transferred into the donor chamber. Magnetic stirrer agitation at 100 rpm in donor and acceptor chamber was controlled by AuPro Software (V5.1.7.0, AuPro GmbH, Buetzow, Germany). After 15, 30, 45, 60, 90, 120, 180, and 240 min after adding mixtures to donor cells, aliquots of 150 µl were drawn from the acceptor chamber and directly diluted with 150 µl isopropanol. Experiments were carried out as quadruplicates.

High-pressure liquid chromatography analysis

High-**P**ressure **L**iquid **C**hromatography (**HPLC**) was used to determine the concentration of Naporafenib in withdrawn samples. The flux in pmol/min/cm² was obtained from the slope of the resulting concentration versus time profile using linear regression and normalized to membrane area. Samples at the University of Wuerzburg were analyzed by an Agilent 1260 infinity II HPLC (Agilent Technologies Inc., Waldbronn, Germany) using a Synergi™ 4 µm Hydro-RP18 80 Å 150 x 4.6 mm LC column (Phenomenex LTD, Aschaffenburg, Germany). The device was equipped with a variable wavelength detector (G7114A, Agilent), an automatic vial sampler (G7129C, Agilent), flexible Pump (G7104C, Agilent), and multicolumn oven (G7116A, Agilent). Mobile phase A was 0.1% (V/V) TFA in Millipore water. Mobile phase B was ACN with 0.1% (V/V) TFA, the flow was set to 1 ml/min, injection volume was 50 µl, and the detector's wavelength was set to λ = 304 nm. The gradient started at 20% B, increasing to 100% within 6 minutes, held for 4 minutes, then back to 20% B within 1 minute, and held for 4 minutes. Quantification was done by a calibration curve using Agilent OpenLAB CDS ChemStation (Agilent). Samples from lipid-based flux membrane setup were analyzed by a Waters Classic Acquity LC system (Waters AG, Baden-Dättwil, Switzerland) equipped with a binary pump, photodiode array detector, a 2.7 µm CORTECS C18+ 90 Å 2.1 x 50 mm column (Waters), and an Acquity QDa **s**ingle

quadrupole mass spectrum detector (Waters). The mobile phase A was water (HPLC plus grade) with 4.76% (V/V) isopropanol, 0.05% (V/V) formic acid, and 3.75 mmol/l ammonium acetate. Mobile phase B consisted of isopropanol with 0.05% (V/V) formic acid. The gradient with a 1 ml/min flow rate was 1% B to 50% B within 1.4 min, followed by 50% to 98% B in 0.3 min. 98% B was held for 0.1 min, and then the gradient was set back to 1% B within 0.1 min and equilibrated for 2 min. The injection volume was either 2 or 5 µl, and the detector wavelength was set to 250 nm.). Naporafenib was quantified by a photodiode array signal using logarithmic calibration curves generated within a run.

Pharmacokinetic study in beagle dogs

A cross-over **p**harmaco**k**inetic (**PK**) comparative animal study in beagle dogs (male non-naïve, Marshall BioResources, North Rose, NY, USA) was conducted at Labcorp Early Development Laboratories Ltd. (Huntingdon, United Kingdom) under Novartis IACUC approved protocol in compliance Animal Welfare Act regulations and the Guide for the Care and Use of Laboratory Animals. The six healthy dogs were 12-15 months old and weighed 7.4-11.7 kg. The animals were fasted overnight before drug administration and offered food 4 hours post-dose. On the remaining sampling days, animals were fed with a 2025C pelleted dog maintenance diet following blood collection. Dogs received Naporafenib at a dose of 59.7 µmol/kg (30 mg/kg). Animals were treated on three consecutive weeks by oral gavage with a suspension of nominal 19.9 mmol/l Naporafenib as tosylate salt in 10 mg/ml (1% m/v) Eudragit E, HPC, or RH40 in **p**hosphate **c**itrate **b**uffer (**PCB**) pH 2.6 containing 0.2 mol/l Na_2HPO_4 and 0.1 mol/l citric acid, respectively. The dose formulations were administered to conscious dogs within 15 to 30 min after formulation preparation with a 3 ml/kg volume, followed by a gavage line flush with water at 2 ml/kg. Blood samples were drawn by collecting approximately 500 µl of blood from the jugular vein. The time points for sampling were set as follows: Pre-dose, 0.25, 0.5, 1, 2, 4, 7, 24, 48, 72, and 96 h post-dose. For **l**iquid **c**hromatography with coupled **m**ass **s**pectrometry (**LC-MS/MS**) analysis, plasma was obtained from K_2EDTA blood by centrifugation (2000 g, 4°C, 10 min) and kept frozen until analysis. The quantification of Naporafenib by LC-MS/MS in dog plasma samples was performed by Covance Laboratories Ltd. (Harrogate, UK). Proteins were precipitated by ACN including isotopically labeled internal standard. Samples were centrifuged and the supernatant was diluted. Quantification of Naporafenib was achieved by a Waters Aqcuity UPLC system using a C-18 column and a Sciex API 6500 Triple-Quad

using positive mode (AB SCIEX LLC., Framingham, MA, USA). Signal integration and noise correction were performed by Analyst Software (SCIEX). Naporafenib was quantified with internal standard pairing using linear calibration curves. The **l**imit **o**f **q**uantification (**LOQ**) was 1.0 ng/ml.

Individual noncompartmental PK analysis was applied to Naporafenib concentration data in dog plasma using R version 4.0.5 (R Foundation for Statistical Computing, Vienna, Austria) using the package 'NonCompart' version 0.4.9 (Kyun-Seop Bae). For each individuum and treatment, the first value below the limit of quantification was censored as the half of 0 and the limit of quantification. Later plasma concentration data points were excluded from the analysis. The maximum plasma concentration (**C_{max}**, mg/ml), time of C_{max} (**T_{max}**), estimated terminal rate constant (**λ_z**), Area under the curve to last nonzero concentration using linear up and down method (**AUC_{last}**), AUC to infinity using λ_z (**AUC_{inf}**, referred to as AUC), oral clearance calculated from observed last measurable plasma concentration (**Cl/F**), mean residual time to last nonzero concentration (**MRT_{last}**), MRT to infinity using λ_z (**MRT_{inf}**), and apparent volume of distribution by F (**V_Z/F**) were calculated. λ_z was calculated using the last three measurable plasma concentration data points by uniform log-linear regression. Monolix 2020R1 (Lixoft, Antony, France) was used to perform a compartmental analysis using an oral one-compartment model with first-order absorption and linear elimination. Peroral (**p.o.**) plasma concentration-time data for HPC, Eudragit E, and RH40 treatment was deconvoluted using previously published PK data with **i**ntra**v**ascular (**i.v.**) applied Naporafenib at a dose of 0.2 mg/kg.[3] A compartment and model-independent deconvolution method were applied after administration with a 10 h time frame.[38] Data was deconvoluted hourly, and missing time points were interpolated with a log-linear regression to align i.v. and p.o. data.

Statistical analysis

For PSO, flux, and solubility determination, pairwise comparisons of all groups were made by one-way ANOVA followed by *a post hoc* Tukey test. In the case of PK parameter analysis, one-way repeated measures ANOVA was performed. A Levene-test tested homogeneity of variance. A games-Howell post hoc test was performed if variance homogeneity was not fulfilled. A double-sided Grubb's test was used for outlier testing. Data were considered statistically significant at $p \leq 0.05$. OriginPro 2020 (OriginLab Corporation) and Minitab (Minitab GmbH, München, Germany) were used for statistical analysis.

Results

Phase separation and solubility

TC/L increased Naporafenib's apparent solubility and **p**hase **s**eparation **o**nset (**PSO**) compared to PBS (**Figure 1, Figure S1, Table S1**). In PBS, apparent solubility increased with HPC, Eudragit E, particularly with RH40 (**Figure 1A**). Naporafenib's PSO did not change when HPC was added to PBS, while it increased with Eudragit E and RH40 (**Figure 1B**). In the presence of TC/L, none of these excipients impacted apparent solubility (**Figure 1C, Table S2**). The PSO did not change with HPC but increased slightly with Eudragit E and more intensely with RH40 (**Figure 1D**).

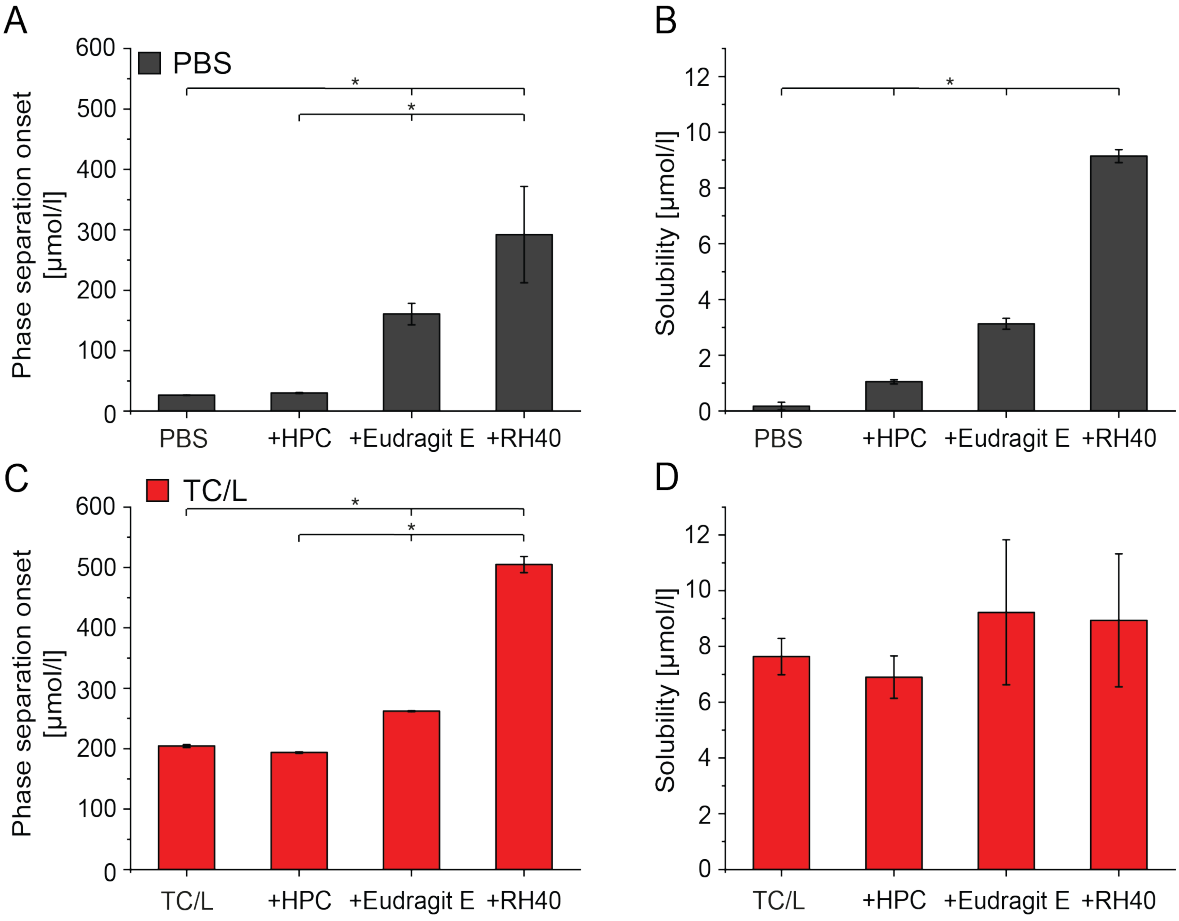

Figure 1: (A, C) Naporafenib monohydrate solubility after 48 h and Naporafenib phase separation onset (B, D) in (A, B) PBS with HPC, Eudragit E, or RH40 and (C, D) TC/L with HPC, Eudragit E, or RH40. Data are shown as mean ± SD, ANOVA considering $p \leq 0.05$ as statistically significant, followed by Tukey *post-hoc* test for pairwise comparison (asterisks indicate significant differences).

Naporafenib interaction with taurocholate and taurocholate/lecithin

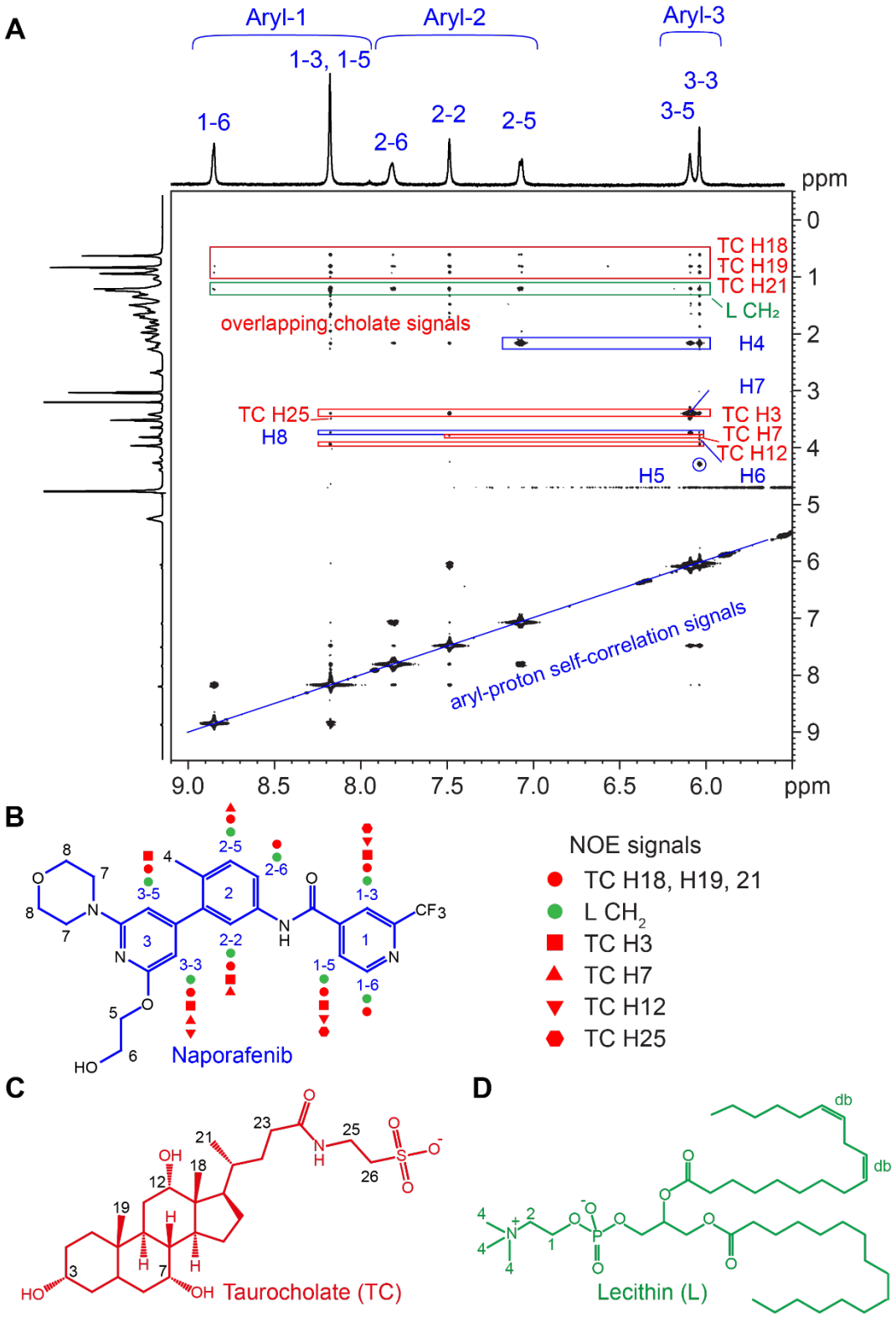

Figure 2: (A) Excerpt from a ^{1}H-^{1}H NOESY spectrum of Naporafenib (blue) in PBS with taurocholate (TC, red) with lecithin (L, green). The mixing time was 60 ms. (B) NOE-signals of Naporafenib aryl-protons between Naporafenib, (C) TC, and (D) L (green). Naporafenib signals were assigned using 1D and 2D NMR spectroscopy.

Naporafenib, TC, and L signals were assigned using 1D and 2D NMR spectra (**Figure 2**).[34] Naporafenib ^{1}H aryl-proton signals increased and shifted in the presence of TC/L (**Figure S2**) and *vice versa* (**Figure S3-8**). These results were confirmed with five-fold concentrated TC/L as detailed by ^{1}H-^{1}H NOESY spectra at Naporafenib concentration of 90% PSO (977 µmol/l). NOE signals were observed for the CH_2 protons of L's aliphatic side chain and additionally for TC's H18, H19, and H21 with all Naporafenib's aryl-protons, respectively (**Figure 2, S9; Table S1**). Additionally, selected interactions were seen between the aryl-protons 1-3 as well as 1-5 with TC H3, TC H25, and TC H12, aryl-protons 2-2 with TC H3, and TC H7, 2-5 with TC H7, and Naporafenib signal 3-3 with TC H3, TC H7, and TC H12 as well as 3-5 with TC H3 (**Figure 2B**). Furthermore, Naporafenib interacted with itself and with TC in the absence of L (**Figure S10, 11**). DOSY indicated that Naporafenib diffusion substantially decreased in TC and L compared to in PBS (**Figure 3, S12, 13**), whereas TC and L diffusion did not change in the presence of Naporafenib (**Table S3**).

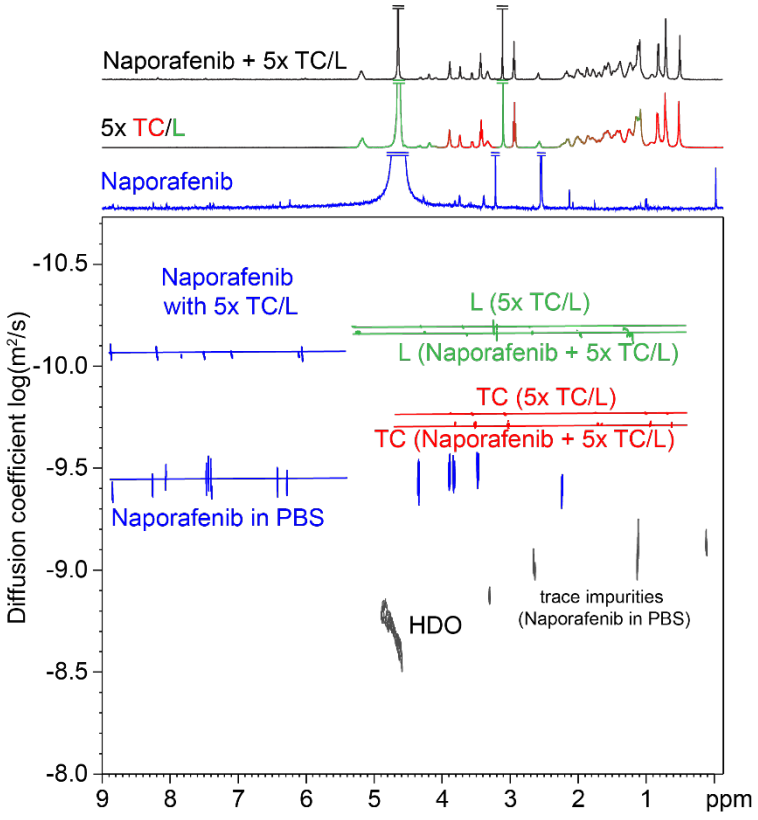

Figure 3: DOSY pseudo 2D plot of Naporafenib with 5x TC/L, Naporafenib in PBS, 5x TC/L without Naporafenib. The respective ^{1}H NMR spectra are shown on top.

Excipient-Naporafenib interaction

Sharp, small-intensity Naporafenib aryl-proton signals were observed in PBS (**Figure 4A, S14**). Phase separation was visually observed at 2 mmol/l Naporafenib concentration. Occurring phase separation did not impact Naporafenib signal intensity or shape compared to concentrations below PSO (**Figure S3, 4**). Naporafenib signals barely shifted or changed in intensity with HPC (**Figure 4B**). In contrast, nearly complete loss of signals resulted with Eudragit E (**Figure 4C**), while or RH40 caused signal intensity increase, broadening, and shifts (**Figure 4D**), respectively. In the presence of TC/L, Naporafenib aryl-protons signals broadened and shifted (**Figure 4E, S15**). The observations in the presence of the excipients were generally comparable to those in the absence of TC/L (**Figure 4F-H**).

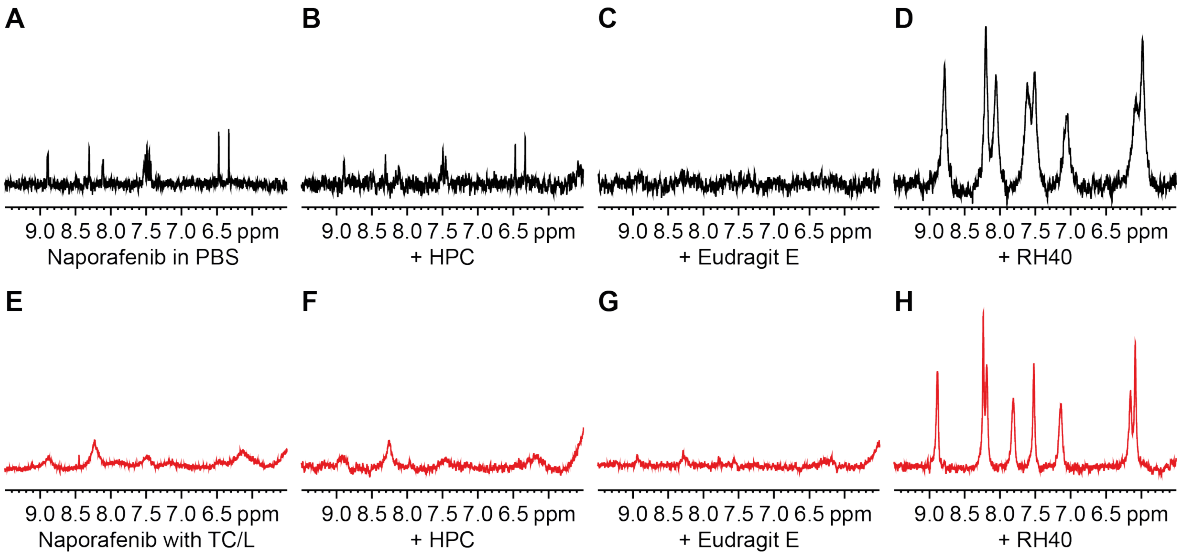

Figure 4: Aryl-proton region of the ^{1}H NMR spectra of Naporafenib in (A) PBS with (B) HPC, (C) Eudragit E, or (D) RH40. Analogous spectra in the presence of (E) TC/L with (F) HPC, (G) Eudragit E, or (H) RH40.

Flux

Naporafenib flux increased linearly to PSO concentrations and plateaued after reaching PSO (**Figure S16, 17, Table S1**). Naporafenib flux was highest with 5x TC/L and lowest in the absence of TC/L and significantly reduced by lipids at concentrations above ¼ PSO. The stirring rate in the donor compartment had no impact on flux in the presence of TC/L, but in the absence (**Figure S18**). Flux experiments across cellulose membranes detailed that Naporafenib flux at 2,000 µmol/l donor concentration with TC/L (2,000 µmol/l is beyond two-fold PSO in all cases, **Table S1**) was not impacted by HPC or RH40 but reduced by Eudragit E. All fluxes were constant throughout the experiment lasting for 4 hours (**Figure 5A, B**). This outcome was qualitatively confirmed at lower Naporafenib concentrations

(concentration = ½ x PSO; **Figure S19**). Experiments in which the (hydrophilic) cellulose membrane was replaced by (lipophilic) PVDF membranes confirmed the impact of the excipients on Naporafenib flux in TC/L. However, overall flux was higher (about 100-fold), and the flux was non-linear over time for RH40 (**Figure 5C, D**). These discriminative effects of the excipients could not be observed in the absence of TC/L (**Figure S20**).

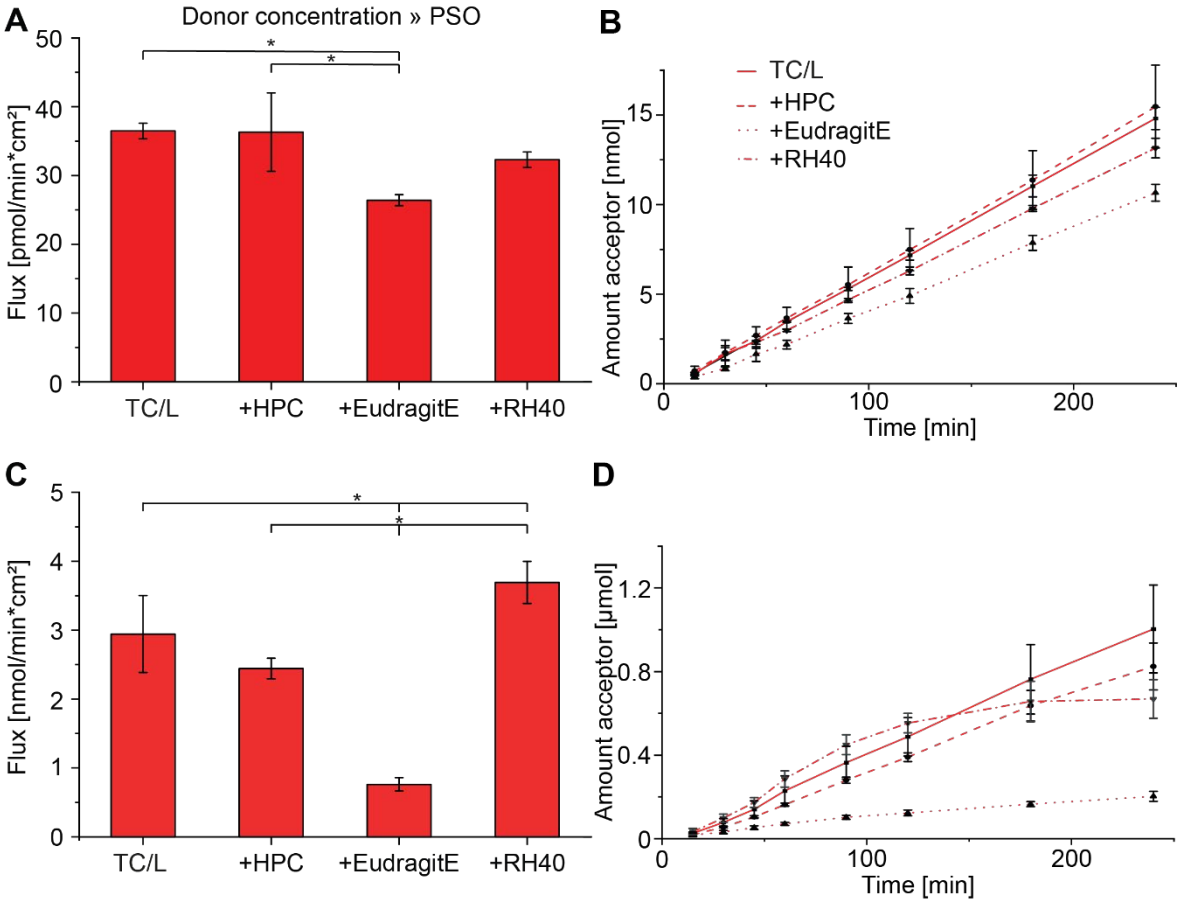

Figure 5: Naporafenib flux and amount in acceptor over time with TC/L in the presence of HPC (dashed lines), Eudragit E (dotted lines), RH40 (dashed-dotted lines), and without excipient (continuous line) using (A, B) cellulose-based membranes and (C, D) lipid-based membranes. Lines were linearly interpolated between two adjacent points. Naporafenib donor concentration was 2,000 µmol/, exceeding phase separation onset in all cases. Data are shown as mean ± SD, ANOVA considering $p \leq 0.05$ as statistically significant, followed by Tukey *post-hoc* test for pairwise comparison (asterisks indicate significant differences).

Pharmacokinetics

Eudragit E significantly reduced Naporafenib C_{max} and AUC in beagle dogs compared to treatment with either HPC or RH40 and as determined by non-compartmental **p**harmaco**k**inetic (**PK**) analysis (**Table 2, S4, S5**). Dog 2 was considered as an outlier and excluded from analysis (**Table S4**). The Naporafenib plasma concentration profiles over time were different for HPC, Eudragit E, and RH40 (**Figure 6A-C**).

Table 2: Naporafenib non-compartmental PK analysis (n=5, dog 2 was considered as outlier) for HPC, Eudragit E, and RH40. T_{max} is shown as median and range in brackets. Data shown as mean ± SD, differences were calculated by repeated-measures ANOVA considering $p \leq 0.05$ as statistically significant followed by Tukey post-hoc test for pairwise comparison (bold numbers with asterisks show significant differences compared to the other groups).

Treatment	C_{max} [mg/ml]	T_{max} [h]	λ_z [1/h]	AUC_{inf} [h*mg/l]	CL/F [l/h]
HPC	0.44	2	0.05	5.32	57.4
	±0.16	(1-4)	±0.03	±0.77	±7.8
Eudragit E	**0.13**	2	0.10	**2.05**	**200**
	±0.04*	(2-24)	±0.03	**±1.32***	**±115***
RH40	0.52	1	0.05	4.07	75.8
	±0.10	(0.5-2)	±0.03	±0.70	±16.2

The mean absorption coefficient *ka*, derived from modeling by compartmental population-based PK, was significantly increased for RH40 and reduced for Eudragit E (**Figure 6D, S21, 22**).

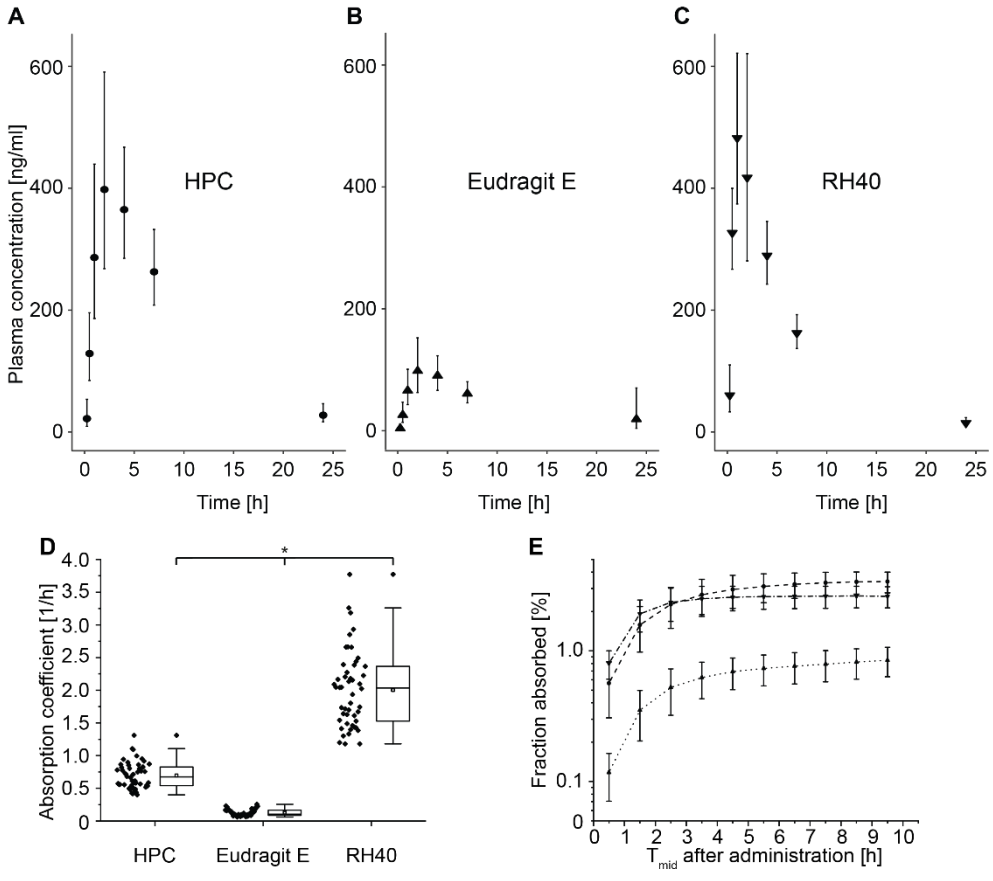

Figure 6: Naporafenib plasma concentration over time (geometric mean ± geometric standard deviation) in beagle dogs (n=5) after oral administration of 30 mg/kg Naporafenib with (A) HPC, (B) Eudragit E, and (C) RH40. (D) Absorption coefficient k_a derived from compartmental analysis using samples from the conditional distributions and (E) fraction absorbed assessed by deconvolution in the presence of HPC (dashed lines), Eudragit E (dotted lines), and RH40 (dashed-dotted lines). ANOVA considering $p \leq 0.05$ as statistically significant followed by games-Howell *post-hoc* test for pairwise comparison (asterisks show significant differences).

As calculated by deconvolution, the cumulative fraction absorbed was reduced for Eudragit E compared to all other groups (**Figure 6E**). The relative bioavailability (based on AUC) was 40 ± 26% and 77 ± 9% for Eudragit E and RH40 treatment, respectively, compared to HPC (**Table S6**).

Discussion

Naporafenib's **p**hase **s**eparation **o**nset (**PSO**) representing a kinetic solubility parameter and apparent solubility (representing a thermodynamic solubility parameter) increased with increasing TC/L and lipid concentration (**Figure 1, Figure S1**). The Naporafenib aryl-protons were close to the hydrophobic parts of the cholate structure, as well as to the hydrophobic aliphatic L chain (**Figure 2**). Similar observations have been published for other PWSD.[35, 39-41] Naporafenib accumulated particularly in hydrophobic parts within the colloids without distinct molecular arrangement (**Figure 2, 3, Figure S2, S7, S13, Table S2**).[24, 34, 35, 41] Similar to a previous study with other PWSDs and polymers, HPC did not interact with TC/L and stabilized Naporafenib supersaturation (**Figure 4, 5**),[24] contrasting Eudragit E and RH40 which interacted with TC/L colloids.[24] Bioavailability and absorption coefficients decreased with Eudragit E (**Figure 6, Table 2**). AUC was similar while the absorption coefficient increased with RH40 compared to HPC, respectively (**Figure 6**).

The outcome from the *in vitro* flux experiments correlated qualitatively with the respective *in vivo* AUC and with the absorption coefficients, *ka* (**Figure 5, 6, 7**). Flux was sensitive to the choice of the membrane - with a higher flux observed with lipid membranes as compared to cellulose membranes - reflecting the diffusion barrier of hydrophilic cellulose membranes for lipophilic Naporafenib. Therefore, flux using lipidic membranes was the most predictive method for the observed absorption coefficient *ka* (**Figure 7A**). A high lipidic flux qualitatively correlated with observed *ka*. Flux using cellulose membranes could not predict higher *ka* in presence of RH40 (**Figure 7B**). Solubility studies were unable to predict any difference (**Figure 7C**) and PSO would have overestimated *ka* in presence of Eudragit E (**Figure 7D**). Naporafenib dissolution rate and solubility increased with increasing TC/L concentration (**Figure 1, Table S1**,**Figure S23**).[42, 43] Furthermore, diffusion was also sensitive to the presence of TC/L (**Figure 3, S13, Table S3**).[44] Previous contributions support these findings and detail the thinning of the **u**nstirred **w**ater **l**ayer (**UWL**) in the presence of TC/L.[45-48] Other studies suggested that drugs with such features may be better

absorbed with food.[42] Naporafenib permeation is UWL limited in absence of TC/L, as demonstrated by stirring experiments on flux (**Figure S18**). Furthermore, increasing TC/L increased Naporafenib's flux, which at least in part might reflect TC/L driven UWL thinning as outlined above (**Figure S16, 17**). This effect might be entitled as a bile colloid mediated additive flux through UWL. These results indicated that flux experiments in the presence of TC/L (but not in the absence of TC/L; **Figure 5, S20)** are instrumental in categorizing the impact of excipients on both bioavailability and absorption.[49-51]

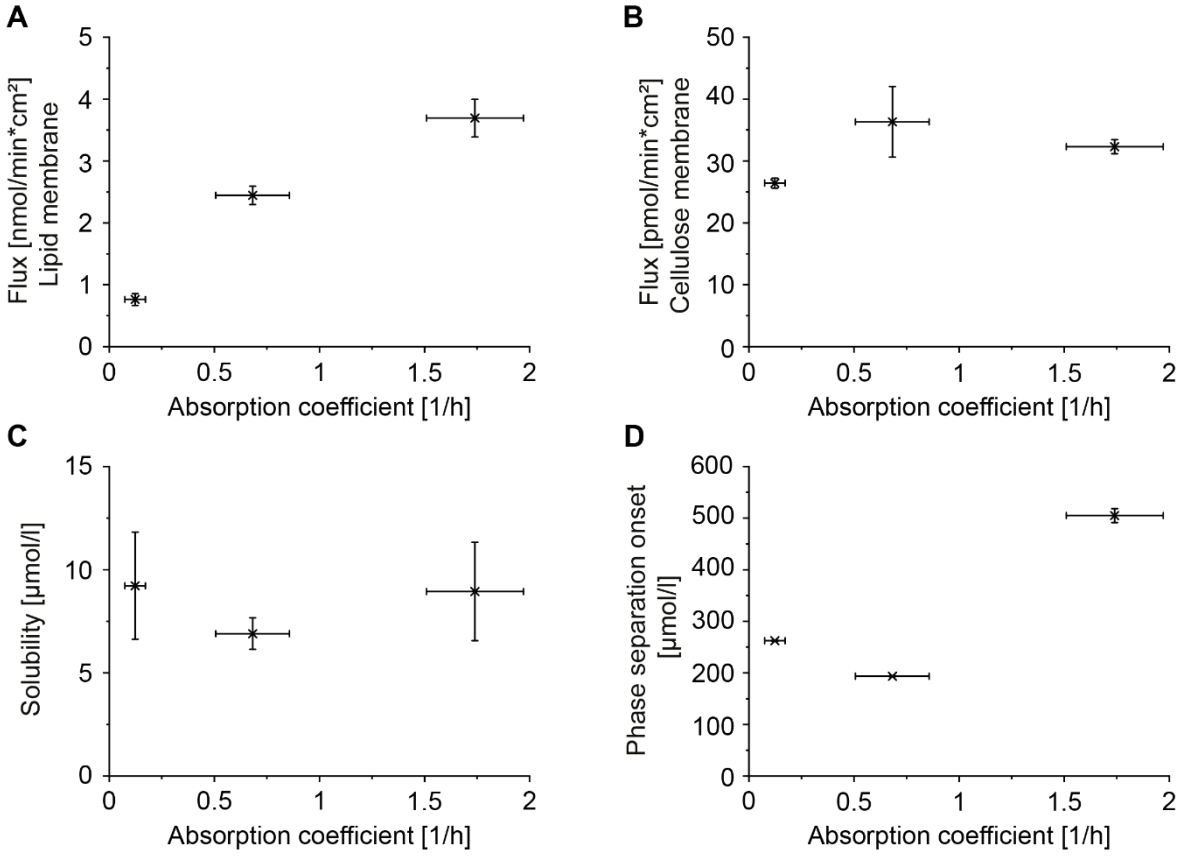

Figure 7: Correlation of absorption coefficient *ka* with (A) flux using lipidic membrane, (B) flux using cellulose membrane, (C) solubility, and (D) phase separation onset in presence of TC/L, respectively. Flux using lipid membrane correlated with *ka* in contrast to other methods.

Another generally occurring question revolves around the PWSD concentration at which flux experiments for excipient selection are reasonably conducted. Quite frequently, supersaturated solutions are used for *in vitro* studies. Consequently, extrapolating from *in vitro* to *in vivo* performances might be particularly challenging in cases in which low drug doses are tested orally. Other factors might also become rate-limiting for overall bioavailability such as drug dissolution. We solved this caveat by using excess amounts of Naporafenib-tosylate suspensions, which can be supposed to generate supersaturated and

phase-separated solutions/suspensions in both *in vitro* and *in vivo* (**Table S1, S7, Section S4**).[52, 53] However, selecting supersaturated states drives another critical consideration, the PSO. Previous studies, e.g., using telaprevir, nifedipine, or felodipine, suggested that interaction studies and flux studies with TC/L are preferentially conducted below PSO.[54, 55] Our findings expand these considerations for excipient selection. Firstly, measurements above the PSO support excipient selection, as do measurements below the PSO for Naporafenib (**Figure 5, S19**). However, TC/L is essential for excipient selection, and higher TC/L amounts may further increase flux of PWSDs (**Figure S16, 17, S20**). Therefore, the predictive screening of excipients for a new PWSD for oral delivery might at least require (i) selecting proper membranes to minimize barrier function (lipophilic ones were more favorable compared to hydrophilic cellulose in our case), (ii) PWSD concentrations below and above the PSO, and studies in the absence and the presence of (iii) TC/L. The excipient concentration may be studied at concentrations approximating *in vivo* conditions as used here within (**Section S4**).

Previous reports and this study aim at detailing the impact of different excipients on the excipient-drug-bile interplay and correlate outcome with drug absorption.[24] Superior outcome resulted from HPC, combining the stabilization of Naporafenib supersaturation and intact solubilization by bile. Mechanistically, the excipient may have maximized Naporafenib presentation to the TC/L colloids and subsequent solubilization, a hypothesis that requires further confirmatory structural studies. Furthermore, HPC was also reported to effectively delay drug crystallization from supersaturated solutions.[56] These features translate into the best pharmacokinetics regarding reproducibility, sustained absorption and bioavailability among the excipients tested here (**Figure 1, 4-6**). Eudragit E patterns were somehow deceiving. Simplified selection criteria focusing on apparent solubility outcome would lead one astray, as seen here and pointed out by others.[26, 57, 58] *Prima facie*, Eudragit E looked promising. The polymer prolonged supersaturation and increased apparent solubility in PBS (**Figure 5, S20**). Already alarming patterns were observed in the presence of TC/L (**Figure 1, 4, 5**) and pointing to unfortunate *in vivo* outcomes (**Figure 6**). PWSDs interacting with TC/L – including Naporafenib – should not necessarily be formulated with excipients (strongly) interacting with TC/L (such as Eudragit E), as the excipient might negatively impact bile and secondarily drug solubilization.[24] In addition, Eudragit E appeared to bind efficiently Naporafenib in the GIT and reduced its bioavailability. The associated NMR aryl-proton signal loss in Eudragit E with TC/L indicates substantially

reduced mobility hence strong association or 'entrapment' of Naporafenib (**Figure 4**) like previous findings for Ketoconazole or mefenamic acid.[58, 59] Reduced flux echoed these molecular interactions (**Figure 5**). RH40, interestingly, maximized absorption kinetics (*ka*; **Figure 6**). This finding may be solubility-related as Naporafenib's apparent solubility was higher in RH40 compared to Eudragit E (**Figure 1, Table S1**). Moreover, supersaturation with RH40 (PSO and buffer used to administer dogs) was substantially higher compared to Eudragit E (**Table S7**). Previous studies linked high supersaturation ratios to fast drug precipitation.[9, 11, 60] Arguably, such events may occur in vivo and may explain the comparable AUC for RH40 and HPC. Another interesting hypothesis that should be addressed in future might be facilitated colloidal-escape dynamics. These dynamics in the presence of RH40 might be even faster than rates seen with (pure) bile as compartmental analysis outcome suggested accelerated kinetics for (TC/L-interacting) RH40 as compared to (TC/L-non-interacting) HPC (**Figure 6**). In other words, the system with RH40 has a larger kinetic drug solubilization capacity than the system with HPC, but it is more unstable. Hence, RH40 interacted with TC/L and accelerated drug release from colloids. Further experiments might be deploying this exciting hypothesis. For Naporafenib as well as for previously reported itraconazole, however, RH40 was unable to stabilize supersaturation.[61]

Conclusion

Excipient selection from isolated drug solubility studies would have led to wrong decisions for Naporafenib. HPC would have been deprioritized versus RH40 and Eudragit E being pushed forward. Pharmacokinetics outcome, however, impressively ranked HPC first, followed by RH40 with some interesting PK features by itself and, far behind, Eudragit E. Therefore, more confidence is required for excipient selection. An expanded experimental scheme starts off categorizing drugs as bile interacting or non-interacting.[24] Frontrunner studies may further select the membrane type for the flux studies. The concentrations approximating expected *in vivo* conditions are calculated for the drug and the excipients (**Section S4**). Bile interacting drugs and excipients are tested at these concentrations in the presence of TC/L. In cases where a drug phase separates, additional concentration levels should be tested, for example, at half the concentration at which phase separation onset was seen. All our results indicate that sophisticated permeation experiments should be used in the development of rational drug formulations.

Acknowledgements

We acknowledge the financial support by Novartis Pharma AG for JS. DW and CH are, BG and LM were full-time associates of Novartis, respectively.

References

1. Lipinski, C., Poor aqueous solubility—an industry wide problem in drug discovery. *Am. Pharm. Rev.* **2002,** *5* (3), 82-85.
2. van Hoogevest, P.; Liu, X.; Fahr, A., Drug delivery strategies for poorly water-soluble drugs: the industrial perspective. *Expert Opin. Drug Delivery* **2011,** *8* (11), 1481-500.
3. Ramurthy, S.; Taft, B. R.; Aversa, R. J.; Barsanti, P. A.; Burger, M. T.; Lou, Y.; Nishiguchi, G. A.; Rico, A.; Setti, L.; Smith, A.; Subramanian, S.; Tamez, V.; Tanner, H.; Wan, L.; Hu, C.; Appleton, B. A.; Mamo, M.; Tandeske, L.; Tellew, J. E.; Huang, S.; Yue, Q.; Chaudhary, A.; Tian, H.; Iyer, R.; Hassan, A. Q.; Mathews Griner, L. A.; La Bonte, L. R.; Cooke, V. G.; Van Abbema, A.; Merritt, H.; Gampa, K.; Feng, F.; Yuan, J.; Mishina, Y.; Wang, Y.; Haling, J. R.; Vaziri, S.; Hekmat-Nejad, M.; Polyakov, V.; Zang, R.; Sethuraman, V.; Amiri, P.; Singh, M.; Sellers, W. R.; Lees, E.; Shao, W.; Dillon, M. P.; Stuart, D. D., Design and Discovery of N-(3-(2-(2-Hydroxyethoxy)-6-morpholinopyridin-4-yl)-4-methylphenyl)-2-(trifluorom ethyl)isonicotinamide, a Selective, Efficacious, and Well-Tolerated RAF Inhibitor Targeting RAS Mutant Cancers: The Path to the Clinic. *J. Med. Chem.* **2020,** *63* (5), 2013-2027.
4. Leeson, P. D., Molecular inflation, attrition and the rule of five. *Adv. Drug Delivery Rev.* **2016,** *101*, 22-33.
5. Waring, M. J.; Arrowsmith, J.; Leach, A. R.; Leeson, P. D.; Mandrell, S.; Owen, R. M.; Pairaudeau, G.; Pennie, W. D.; Pickett, S. D.; Wang, J.; Wallace, O.; Weir, A., An analysis of the attrition of drug candidates from four major pharmaceutical companies. *Nat. Rev. Drug Discov.* **2015,** *14* (7), 475-86.
6. Linn, M.; Collnot, E. M.; Djuric, D.; Hempel, K.; Fabian, E.; Kolter, K.; Lehr, C. M., Soluplus(R) as an effective absorption enhancer of poorly soluble drugs in vitro and in vivo. *Eur. J. Pharm. Sci.* **2012,** *45* (3), 336-43.
7. Guzman, H. R.; Tawa, M.; Zhang, Z.; Ratanabanangkoon, P.; Shaw, P.; Gardner, C. R.; Chen, H.; Moreau, J. P.; Almarsson, O.; Remenar, J. F., Combined use of crystalline salt forms and precipitation inhibitors to improve oral absorption of celecoxib from solid oral formulations. *J. Pharm. Sci.* **2007,** *96* (10), 2686-702.
8. Overhoff, K. A.; McConville, J. T.; Yang, W.; Johnston, K. P.; Peters, J. I.; Williams, R. O., 3rd, Effect of stabilizer on the maximum degree and extent of supersaturation and oral absorption of tacrolimus made by ultra-rapid freezing. *Pharm. Res.* **2008,** *25* (1), 167-75.
9. Reggane, M.; Wiest, J.; Saedtler, M.; Harlacher, C.; Gutmann, M.; Zottnick, S. H.; Piechon, P.; Dix, I.; Muller-Buschbaum, K.; Holzgrabe, U.; Meinel, L.; Galli, B., Bioinspired co-crystals of Imatinib providing enhanced kinetic solubility. *Eur. J. Pharm. Biopharm.* **2018,** *128*, 290-299.
10. Balk, A.; Holzgrabe, U.; Meinel, L., 'Pro et contra' ionic liquid drugs - Challenges and opportunities for pharmaceutical translation. *Eur. J. Pharm. Biopharm.* **2015,** *94*, 291-304.
11. Balk, A.; Wiest, J.; Widmer, T.; Galli, B.; Holzgrabe, U.; Meinel, L., Transformation of acidic poorly water soluble drugs into ionic liquids. *Eur. J. Pharm. Biopharm.* **2015,** *94*, 73-82.
12. Güntzel, P.; Schilling, K.; Hanio, S.; Schlauersbach, J.; Schollmayer, C.; Meinel, L.; Holzgrabe, U., Bioinspired Ion Pairs Transforming Papaverine into a Protic Ionic Liquid and Salts. *ACS Omega* **2020,** *5* (30), 19202-19209.

13. Pouton, C. W., Formulation of self-emulsifying drug delivery systems. *Adv. Drug Delivery Rev.* **1997,** *25* (1), 47-58.
14. Kalepu, S.; Manthina, M.; Padavala, V., Oral lipid-based drug delivery systems – an overview. *Acta Pharm. Sin. B* **2013,** *3* (6), 361-372.
15. Porter, C. J.; Pouton, C. W.; Cuine, J. F.; Charman, W. N., Enhancing intestinal drug solubilisation using lipid-based delivery systems. *Adv. Drug Delivery Rev.* **2008,** *60* (6), 673-91.
16. Pöppler, A. C.; Lübtow, M. M.; Schlauersbach, J.; Wiest, J.; Meinel, L.; Luxenhofer, R., Loading-Dependent Structural Model of Polymeric Micelles Encapsulating Curcumin by Solid-State NMR Spectroscopy. *Angew. Chem. Int. Ed. Engl.* **2019,** *58* (51), 18540-18546.
17. Baghel, S.; Cathcart, H.; O'Reilly, N. J., Polymeric Amorphous Solid Dispersions: A Review of Amorphization, Crystallization, Stabilization, Solid-State Characterization, and Aqueous Solubilization of Biopharmaceutical Classification System Class II Drugs. *J. Pharm. Sci.* **2016,** *105* (9), 2527-2544.
18. Schittny, A.; Huwyler, J.; Puchkov, M., Mechanisms of increased bioavailability through amorphous solid dispersions: a review. *Drug Delivery* **2020,** *27* (1), 110-127.
19. Iyer, R.; Petrovska Jovanovska, V.; Berginc, K.; Jaklic, M.; Fabiani, F.; Harlacher, C.; Huzjak, T.; Sanchez-Felix, M. V., Amorphous Solid Dispersions (ASDs): The Influence of Material Properties, Manufacturing Processes and Analytical Technologies in Drug Product Development. *Pharmaceutics* **2021,** *13* (10).
20. Lipinski, C. A.; Lombardo, F.; Dominy, B. W.; Feeney, P. J., Experimental and computational approaches to estimate solubility and permeability in drug discovery and development settings. *Adv. Drug Delivery Rev.* **1997,** *23* (1-3), 3-25.
21. Riethorst, D.; Mols, R.; Duchateau, G.; Tack, J.; Brouwers, J.; Augustijns, P., Characterization of Human Duodenal Fluids in Fasted and Fed State Conditions. *J. Pharm. Sci.* **2016,** *105* (2), 673-681.
22. Dahlgren, D.; Venczel, M.; Ridoux, J. P.; Skjold, C.; Mullertz, A.; Holm, R.; Augustijns, P.; Hellstrom, P. M.; Lennernas, H., Fasted and fed state human duodenal fluids: Characterization, drug solubility, and comparison to simulated fluids and with human bioavailability. *Eur. J. Pharm. Biopharm.* **2021,** *163*, 240-251.
23. Hanio, S.; Schlauersbach, J.; Lenz, B.; Spiegel, F.; Bockmann, R. A.; Schweins, R.; Nischang, I.; Schubert, U. S.; Endres, S.; Poppler, A. C.; Brandl, F. P.; Smit, T. M.; Kolter, K.; Meinel, L., Drug-Induced Dynamics of Bile Colloids. *Langmuir* **2021,** *37* (8), 2543-2551.
24. Schlauersbach, J.; Hanio, S.; Lenz, B.; Vemulapalli, S. P. B.; Griesinger, C.; Poppler, A. C.; Harlacher, C.; Galli, B.; Meinel, L., Leveraging bile solubilization of poorly water-soluble drugs by rational polymer selection. *J. Control. Release* **2021,** *330*, 36-48.
25. Brouwers, J.; Brewster, M. E.; Augustijns, P., Supersaturating drug delivery systems: the answer to solubility-limited oral bioavailability? *J. Pharm. Sci.* **2009,** *98* (8), 2549-72.
26. Saal, W.; Wyttenbach, N.; Alsenz, J.; Kuentz, M., Interactions of dimethylaminoethyl methacrylate copolymer with non-acidic drugs demonstrated high solubilization in vitro and pronounced sustained release in vivo. *Eur. J. Pharm. Biopharm.* **2018,** *125*, 68-75.
27. Janku, F.; Iyer, G.; Spreafico, A.; Yamamoto, N.; Bang, Y.-J.; Elez, E.; De Jonge, M. J.; Groen, H. J. M.; Marmé, F.; Gollmer, K.; St-Pierre, A.; Melendez, M.; Mais, A.; Nauwelaerts, H.; Stammberger, U. M.; Dummer, R., A phase I study of LXH254 in patients (pts) with advanced solid tumors harboring MAPK pathway alterations. *J. Clin. Oncol.* **2018,** *36* (15_suppl), 2586-2586.
28. Monaco, K. A.; Delach, S.; Yuan, J.; Mishina, Y.; Fordjour, P.; Labrot, E.; McKay, D.; Guo, R.; Higgins, S.; Wang, H. Q.; Liang, J.; Bui, K.; Green, J.; Aspesi, P.; Ambrose, J.; Mapa, F.; Griner, L.; Jaskelioff, M.; Fuller, J.; Crawford, K.; Pardee, G.; Widger, S.; Hammerman, P. S.; Engelman, J. A.; Stuart, D. D.; Cooke, V. G.; Caponigro, G., LXH254, a Potent and Selective ARAF-Sparing Inhibitor of BRAF and CRAF for the Treatment of MAPK-Driven Tumors. *Clin. Cancer Res.* **2021,** *27* (7), 2061-2073.

29. Novartis Pharmaceuticals, Identifier: NCT04417621, A Randomized, Open-label, Multi-arm, Two-part, Phase II Study to Assess Efficacy and Safety of Multiple LXH254 Combinations in Patients With Previously Treated Unresectable or Metastatic BRAFV600 or NRAS Mutant Melanoma. ClinicalTrials.gov [Internet]. Bethesda (MD): National Library of Medicine (US): 2020.
30. Baucke, F. G. K., Further Insight into the Dissociation Mechanism of Glass Electrodes. The Response in Heavy Water. *J. Phys. Chem. B* **1998,** *102* (24), 4835-4841.
31. Wu, D. H.; Chen, A. D.; Johnson, C. S., An Improved Diffusion-Ordered Spectroscopy Experiment Incorporating Bipolar-Gradient Pulses. *J. Magn. Reson. A* **1995,** *115* (2), 260-264.
32. Jerschow, A.; Müller, N., 3D Diffusion-Ordered TOCSY for Slowly Diffusing Molecules. *J. Magn. Reson.* **1996,** *123* (2), 222-225.
33. Jerschow, A.; Müller, N., Suppression of Convection Artifacts in Stimulated-Echo Diffusion Experiments. Double-Stimulated-Echo Experiments. *J. Magn. Reson.* **1997,** *125* (2), 372-375.
34. Endres, S.; Karaev, E.; Hanio, S.; Schlauersbach, J.; Kraft, C.; Rasmussen, T.; Luxenhofer, R.; Bottcher, B.; Meinel, L.; Poppler, A. C., Concentration and composition dependent aggregation of Pluronic- and Poly-(2-oxazolin)-Efavirenz formulations in biorelevant media. *J. Colloid Interface Sci.* **2022,** *606* (Pt 2), 1179-1192.
35. Wiest, J.; Saedtler, M.; Böttcher, B.; Grüne, M.; Reggane, M.; Galli, B.; Holzgrabe, U.; Meinel, L., Geometrical and Structural Dynamics of Imatinib within Biorelevant Colloids. *Mol. Pharmaceutics* **2018,** *15* (10), 4470-4480.
36. Tsinman, K.; Tsinman, O.; Riebesehl, B.; Grandeury, A.; Juhnke, M., In situ method for monitoring free drug concentration released from nanoparticles. *Poster Present AAPS Annu Meet Expo Oct* **2012**, 14-18.
37. Avdeef, A.; Tsinman, O., PAMPA—a drug absorption in vitro model: 13. Chemical selectivity due to membrane hydrogen bonding: in combo comparisons of HDM-, DOPC-, and DS-PAMPA models. *Eur. J. Pharm. Sci.* **2006,** *28* (1-2), 43-50.
38. Chiou, W. L., New compartment- and model-independent method for rapid calculation of drug absorption rates. *J. Pharm. Sci.* **1980,** *69* (1), 57-62.
39. Li, G.; McGown, L. B., A new approach to polydispersity studies of sodium taurocholate and sodium taurodeoxycholate aggregates using dynamic fluorescence anisotropy. *J. Phys. Chem.* **2002,** *97* (25), 6745-6752.
40. Li, G.; McGown, L. B., Model for Bile Salt Micellization and Solubilization from Studies of a "Polydisperse" Array of Fluorescent Probes and Molecular Modeling. *J. Phys. Chem.* **2002,** *98* (51), 13711-13719.
41. Vogtherr, M.; Marx, A.; Mieden, A. C.; Saal, C., Investigation of solubilising effects of bile salts on an active pharmaceutical ingredient with unusual pH dependent solubility by NMR spectroscopy. *Eur. J. Pharm. Biopharm.* **2015,** *92*, 32-41.
42. Sugano, K.; Kataoka, M.; Mathews Cda, C.; Yamashita, S., Prediction of food effect by bile micelles on oral drug absorption considering free fraction in intestinal fluid. *Eur. J. Pharm. Sci.* **2010,** *40* (2), 118-24.
43. Shekunov, B.; Montgomery, E. R., Theoretical Analysis of Drug Dissolution: I. Solubility and Intrinsic Dissolution Rate. *J. Pharm. Sci.* **2016,** *105* (9), 2685-2697.
44. Yano, K.; Masaoka, Y.; Kataoka, M.; Sakuma, S.; Yamashita, S., Mechanisms of membrane transport of poorly soluble drugs: role of micelles in oral absorption processes. *J. Pharm. Sci.* **2010,** *99* (3), 1336-45.
45. Wils, P.; Warnery, A.; Phung-Ba, V.; Legrain, S.; Scherman, D., High lipophilicity decreases drug transport across intestinal epithelial cells. *J. Pharmacol. Exp. Ther.* **1994,** *269* (2), 654-658.
46. Sugano, K., Estimation of effective intestinal membrane permeability considering bile micelle solubilisation. *Int. J. Pharm.* **2009,** *368* (1-2), 116-22.

47. Eriksen, J. B.; Jacobsen, A. C.; Christensen, K. T.; Bauer-Brandl, A.; Brandl, M., 'Stirred not Shaken!' Comparing Agitation Methods for Permeability Studies Using a Novel Type of 96-Well Sandwich-Plates. *J. Pharm. Sci.* **2021**.
48. Miller, J. M.; Beig, A.; Krieg, B. J.; Carr, R. A.; Borchardt, T. B.; Amidon, G. E.; Amidon, G. L.; Dahan, A., The solubility-permeability interplay: mechanistic modeling and predictive application of the impact of micellar solubilization on intestinal permeation. *Mol. Pharmaceutics* **2011,** *8* (5), 1848-56.
49. Lakshman, D.; Chegireddy, M.; Hanegave, G. K.; Sree, K. N.; Kumar, N.; Lewis, S. A.; Dengale, S. J., Investigation of drug-polymer miscibility, biorelevant dissolution, and bioavailability improvement of Dolutegravir-polyvinyl caprolactam-polyvinyl acetate-polyethylene glycol graft copolymer solid dispersions. *Eur. J. Pharm. Sci.* **2020,** *142*, 105137.
50. Borbas, E.; Kadar, S.; Tsinman, K.; Tsinman, O.; Csicsak, D.; Takacs-Novak, K.; Volgyi, G.; Sinko, B.; Pataki, H., Prediction of Bioequivalence and Food Effect Using Flux- and Solubility-Based Methods. *Mol. Pharmaceutics* **2019,** *16* (10), 4121-4130.
51. Borbas, E.; Nagy, Z. K.; Nagy, B.; Balogh, A.; Farkas, B.; Tsinman, O.; Tsinman, K.; Sinko, B., The effect of formulation additives on in vitro dissolution-absorption profile and in vivo bioavailability of telmisartan from brand and generic formulations. *Eur. J. Pharm. Sci.* **2018,** *114*, 310-317.
52. Almeida e Sousa, L.; Reutzel-Edens, S. M.; Stephenson, G. A.; Taylor, L. S., Supersaturation Potential of Salt, Co-Crystal, and Amorphous Forms of a Model Weak Base. *Cryst. Growth Des.* **2016,** *16* (2), 737-748.
53. Hsieh, Y. L.; Ilevbare, G. A.; Van Eerdenbrugh, B.; Box, K. J.; Sanchez-Felix, M. V.; Taylor, L. S., pH-Induced precipitation behavior of weakly basic compounds: determination of extent and duration of supersaturation using potentiometric titration and correlation to solid state properties. *Pharm. Res.* **2012,** *29* (10), 2738-53.
54. Raina, S. A.; Zhang, G. G.; Alonzo, D. E.; Wu, J.; Zhu, D.; Catron, N. D.; Gao, Y.; Taylor, L. S., Impact of Solubilizing Additives on Supersaturation and Membrane Transport of Drugs. *Pharm. Res.* **2015,** *32* (10), 3350-64.
55. Mosquera-Giraldo, L. I.; Taylor, L. S., Glass-liquid phase separation in highly supersaturated aqueous solutions of telaprevir. *Mol. Pharmaceutics* **2015,** *12* (2), 496-503.
56. Bachmaier, R. D.; Monschke, M.; Faber, T.; Krome, A. K.; Pellequer, Y.; Stoyanov, E.; Lamprecht, A.; Wagner, K. G., In vitro and in vivo assessment of hydroxypropyl cellulose as functional additive for enabling formulations containing itraconazole. *Int. J. Pharm. X* **2021,** *3*, 100076.
57. Yoshida, T.; Kurimoto, I.; Umejima, H.; Watanabe, S.; Sako, K.; Kikuchi, A., Effects of dissolved state of aminoalkyl methacrylate copolymer E/HCl on solubility enhancement effect for poorly water-soluble drugs. *Colloid Polym. Sci.* **2012,** *291* (5), 1191-1199.
58. Fine-Shamir, N.; Dahan, A., Methacrylate-Copolymer Eudragit EPO as a Solubility-Enabling Excipient for Anionic Drugs: Investigation of Drug Solubility, Intestinal Permeability, and Their Interplay. *Mol. Pharmaceutics* **2019,** *16* (7), 2884-2891.
59. Mistry, P.; Mohapatra, S.; Gopinath, T.; Vogt, F. G.; Suryanarayanan, R., Role of the Strength of Drug-Polymer Interactions on the Molecular Mobility and Crystallization Inhibition in Ketoconazole Solid Dispersions. *Mol. Pharmaceutics* **2015,** *12* (9), 3339-50.
60. Balk, A.; Widmer, T.; Wiest, J.; Bruhn, H.; Rybak, J. C.; Matthes, P.; Muller-Buschbaum, K.; Sakalis, A.; Luhmann, T.; Berghausen, J.; Holzgrabe, U.; Galli, B.; Meinel, L., Ionic liquid versus prodrug strategy to address formulation challenges. *Pharm. Res.* **2015,** *32* (6), 2154-67.
61. Brewster, M. E.; Vandecruys, R.; Peeters, J.; Neeskens, P.; Verreck, G.; Loftsson, T., Comparative interaction of 2-hydroxypropyl-beta-cyclodextrin and sulfobutylether-beta-cyclodextrin with itraconazole: phase-solubility behavior and stabilization of supersaturated drug solutions. *Eur. J. Pharm. Sci.* **2008,** *34* (2-3), 94-103.

Supporting Information

S1 Naporafenib solubility and phase separation onset

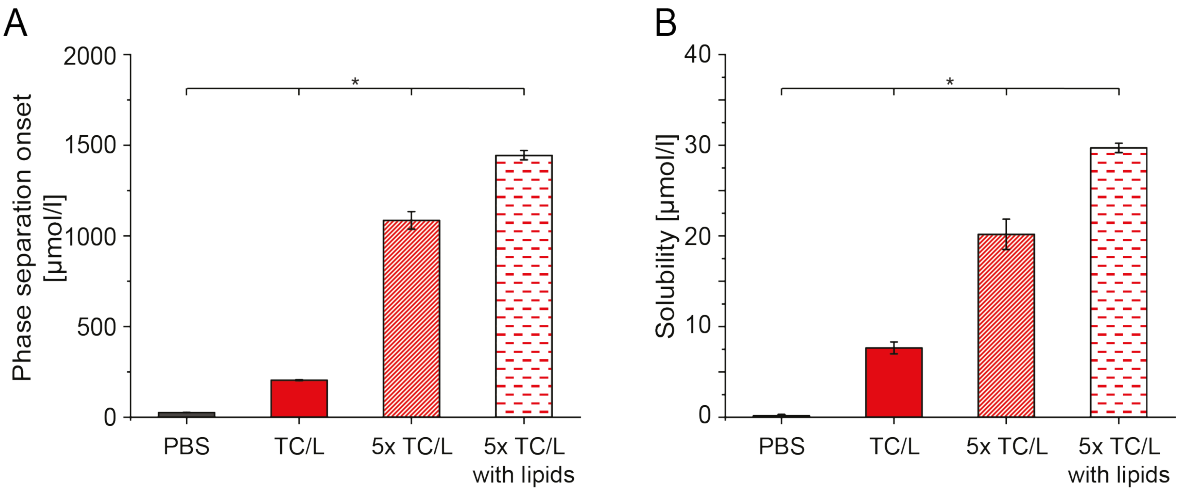

Figure S1: (A) Naporafenib phase separation onset and (B) Naporafenib monohydrate solubility after 48 h in PBS (grey), with TC/L (red), with 5x TC/L (hatched red lines), and with 5x TC/L and lipids (hatched red dashed lines). PBS and TC/L values are the same as shown in figure 1. Data shown as mean ± SD, ANOVA considering $p \leq 0.05$ as statistically significant followed by Tukey *post-hoc* test for pairwise comparison (significant differences are shown by asterisks).

Table S1: Naporafenib **p**hase **s**eparation **o**nset (**PSO**) and applied concentrations based on PSO.

Medium	**phase separation onset, average [µmol/l] ± standard deviation**	**concentration applied for DOSY/ NOESY [µmol/l]**	**donor concentration applied for flux [µmol/l]**		
% c of phase separation onset	**1x PSO**	**0.9x PSO**	**¼ PSO**	**½ PSO**	**2x PSO**
PBS	26.5 ± 0.2	24	7	13	53
TC/L	204.5 ± 2.6	-	51	102	409
15 mmol/l TC	464.8 ± 2.5	418	-	-	-
5x TC/L	1085 ± 49	977	271	543	2171
5x TC/L with lipids	1445 ± 26	1300	361	722	2889
PBS + HPC	30.1 ± 0.9	-	-	15	-
PBS + Eudragit E	161 ± 18	-	-	81	-
PBS + RH40	292 ± 80	-	-	146	-
TC/L + HPC	193.6 ± 1.1	-	-	97	-
TC/L + Eudragit E	262.3 ± 0.9	-	-	131	-
TC/L + RH40	505 ± 13	-	-	252	-

Table S2: Naporafenib monohydrate thermodynamic solubility after 48 h at 25 °C.

Time	thermodynamic solubility [µmol/l] ± standard deviation
PBS	0.18 ± 0.14
TC/L in PBS	7.6 ± 0.7
5x TC/L in PBS	20.8 ± 1.7
5x TC/L with lipids	29.7 ± 0.5
PBS + HPC	1.05 ± 0.08
PBS + Eudragit E	3.13 ± 0.20
PBS + RH40	9.15 ± 0.23
TC/L in PBS + HPC	6.9 ± 0.8
TC/L in PBS + Eudragit E	9.2 ± 2.6
TC/L in PBS + RH40	8.9 ± 2.4
PBS + Vitamin E TPGS 0.2%	32.5 ± 3.6

S2 ^{1}H nuclear magnetic resonance spectroscopy

S2.1 ^{1}H nuclear magnetic resonance spectra of Naporafenib in biorelevant media

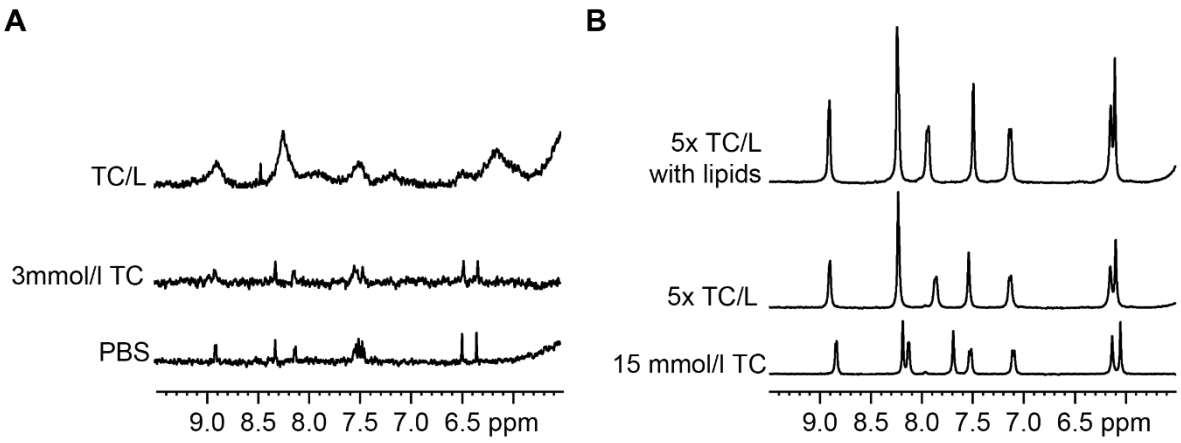

Figure S2: Aryl proton region of the ^{1}H NMR spectra of Naporafenib in fasted state simulating media (A) and fed state simulating media (B) at a concentration of 2 mmol/l added by DMSO stock solution. Panel A and B are scaled differently for better overview.

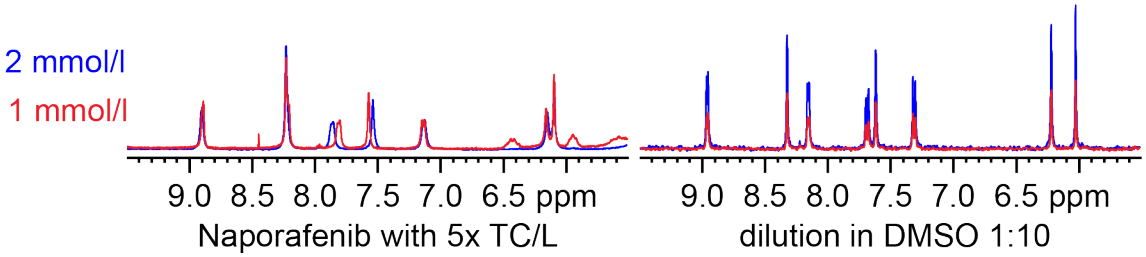

Figure S3: Aryl proton region of the ^{1}H NMR spectra of Naporafenib with 5x TC/L at a concentration of 1 mmol/l (red) and 2 mmol/l (blue) added by DMSO stock solution. Left panel shows signal shifts indicated by blue lines, but no signal intensity increase. Direct dilution of samples in DMSO destroying all kind of aggregates revealed higher Naporafenib amount in solution by increased signal intensity. Exceeding amorphous drug solubility had no significant impact on signal appearance (left panel).

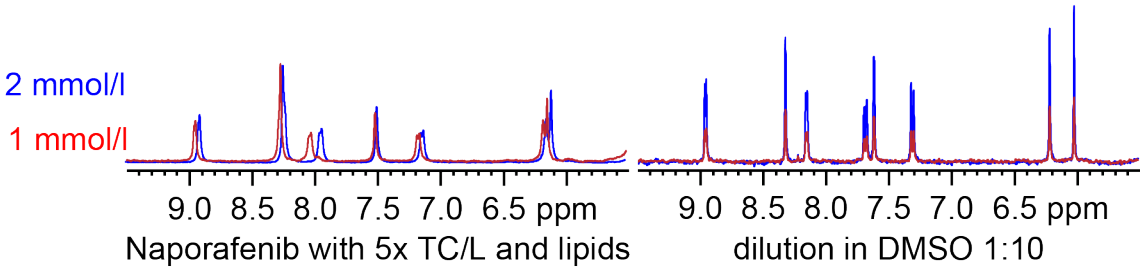

Figure S4: Aryl proton region of the ^{1}H NMR spectra of Naporafenib with 5x TC/L with lipids at a concentration of 1 mmol/l (red) and 2 mmol/l (blue) added by DMSO stock solution. Left panel shows signal shifts indicated by blue lines, but no signal intensity increase. Direct dilution of samples in DMSO destroying all kind of aggregates revealed higher Naporafenib amount in solution by increased signal intensity. Exceeding amorphous drug solubility had no significant impact on signal appearance (left panel).

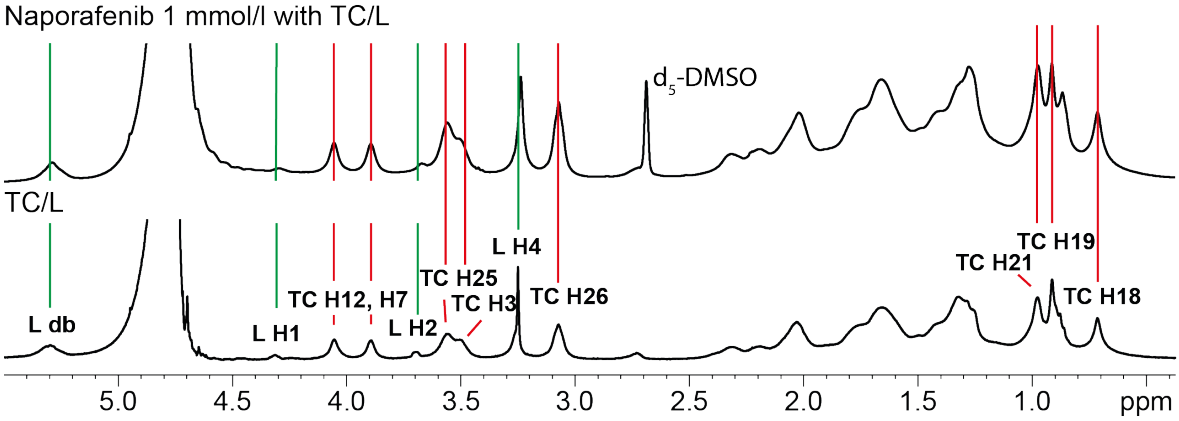

Figure S5: Extracts from ^{1}H NMR spectra of 1 mmol/l Naporafenib with TC/L (top) and TC/L reference (bottom). Chemical shifts of TC/L protons are indicated with red lines for TC and green lines for L protons, respectively.

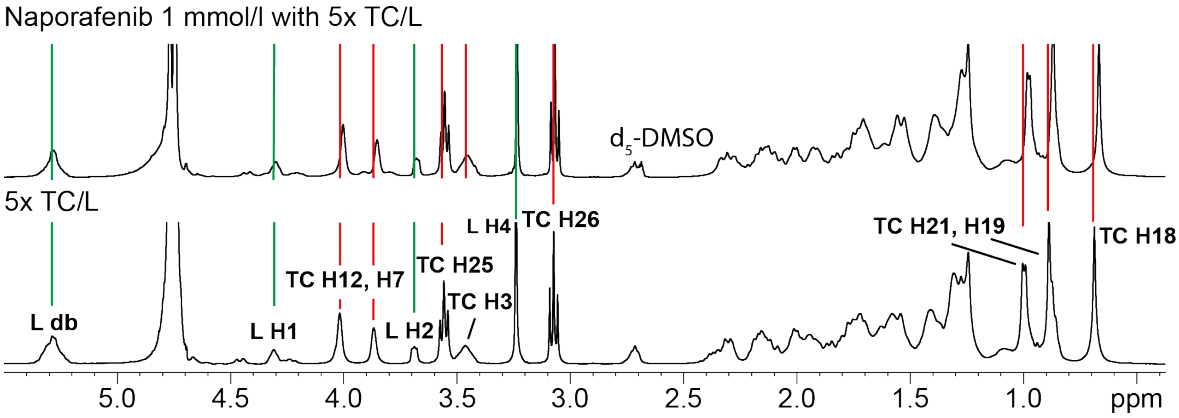

Figure S6: Extracts from ^{1}H NMR spectra of 1 mmol/l Naporafenib with 5x TC/L (top) and 5x TC/L reference (bottom). Chemical shifts of TC/L protons are indicated with red lines for TC and green lines for L protons, respectively.

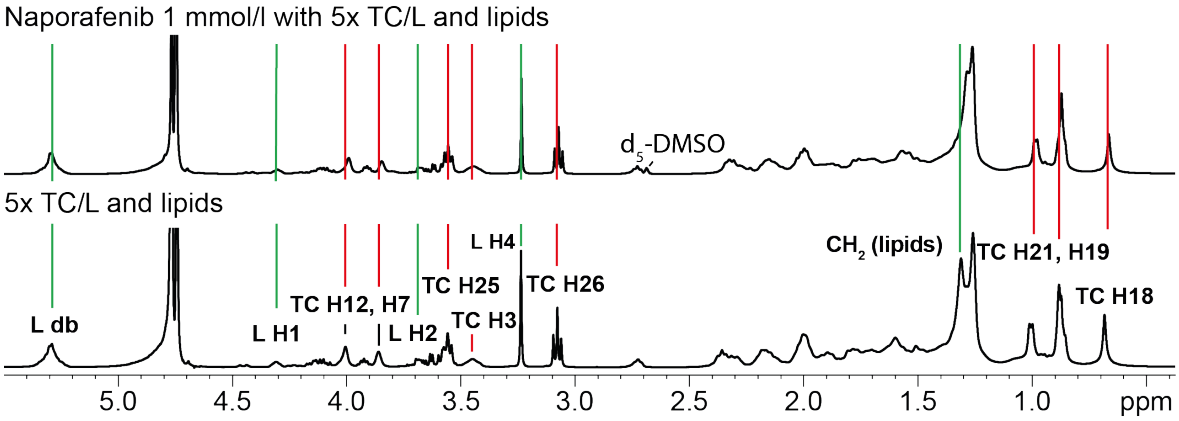

Figure S7: Extracts from ^{1}H NMR spectra of 1 mmol/l Naporafenib with 5x TC/L and lipids (top) and 5x TC/L and lipids reference (bottom). Chemical shifts of TC/L protons are indicated with red lines for TC and green lines for L with lipid protons, respectively.

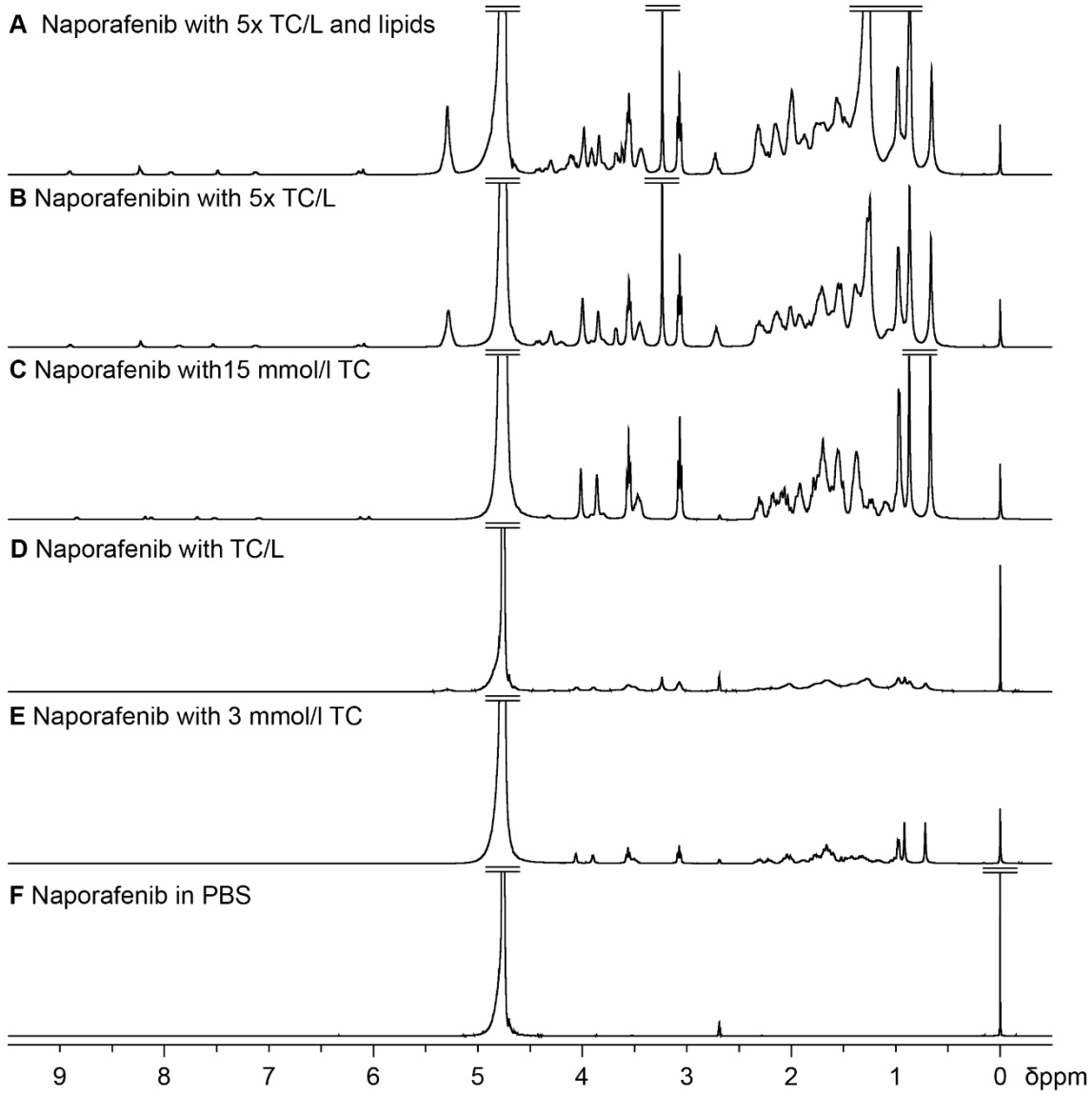

Figure S8: Full ^{1}H NMR spectra of 1 mmol/l Naporafenib with 5x TC/L and lipids (A), with 5x TC/L (B), in 15 mmol/l TC (C), with TC/L (D), in 3 mmol/L TC (E), and in PBS (F). Scaling is equal across all panels.

S2.2 Naporafenib, taurocholate, and lecithin ^{1}H-^{1}H nuclear Overhauser effect spectroscopy and diffusion ordered spectroscopy measurements

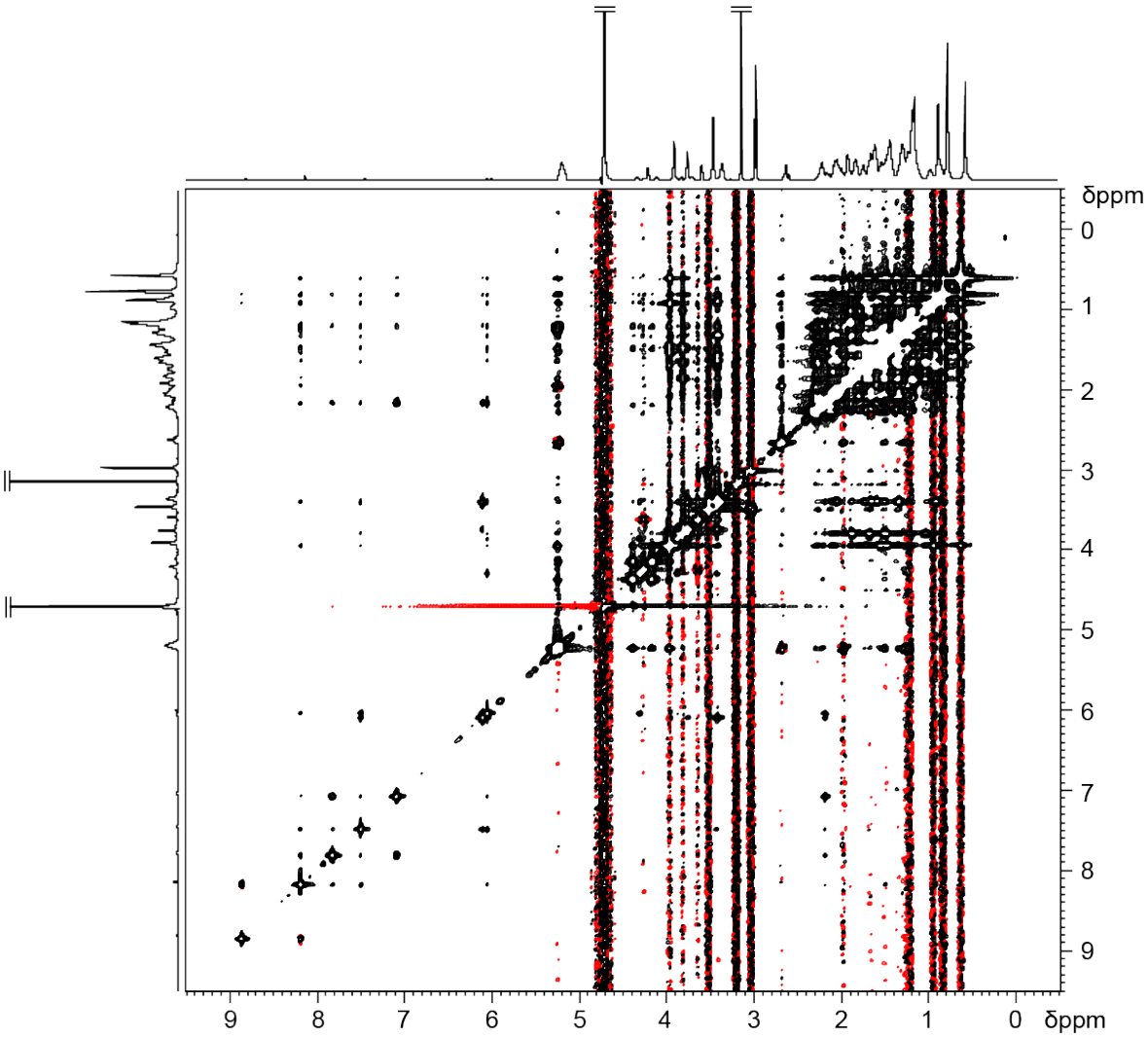

Figure S9: ^{1}H-^{1}H NOESY spectrum of 977 µmol/l Naporafenib with 5x TC/L (90% PSO). The spectrum was acquired with a mixing time of 60 ms, 24 co-added transients and 512 t_1 FIDs using a cryoprobe at 300 K and 14.1 T. Naporafenib-TC-L proton cross-signals exhibit the same phase as the diagonal, which was chosen to be positive (black). Negative resonances are shown in red.

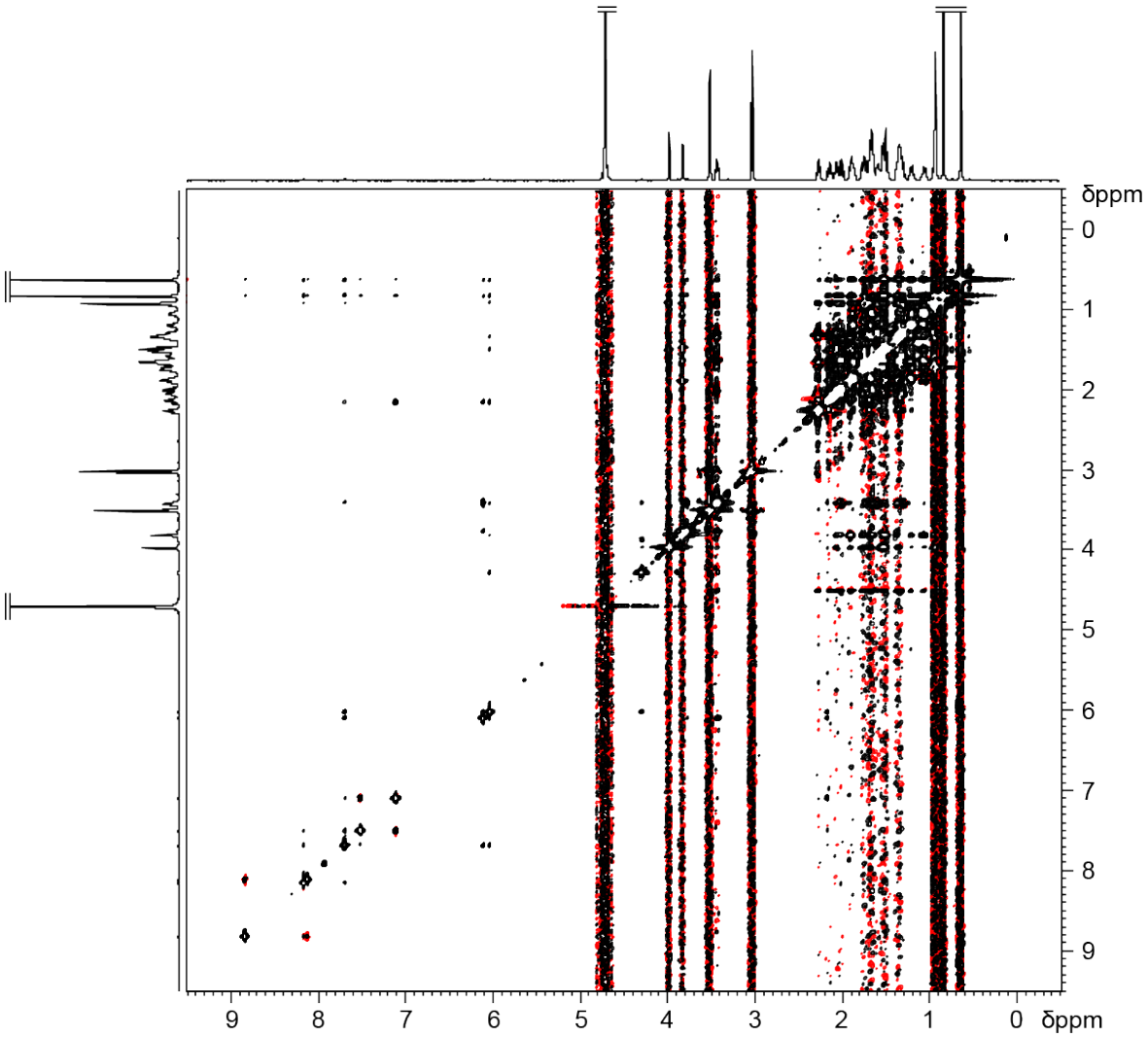

Figure S10: ^{1}H-^{1}H NOESY spectrum of 418 µmol/l Naporafenib in 15 mmol/l TC in PBS (90% PSO). The spectrum was acquired with a mixing time of 80 ms, 24 co-added transients and 512 t_1 FIDs using a cryoprobe at 300 K and 14.1 T. Naporafenib-TC proton cross-signals exhibit the same phase as the diagonal, which was chosen to be positive (black). Negative resonances are shown in red.

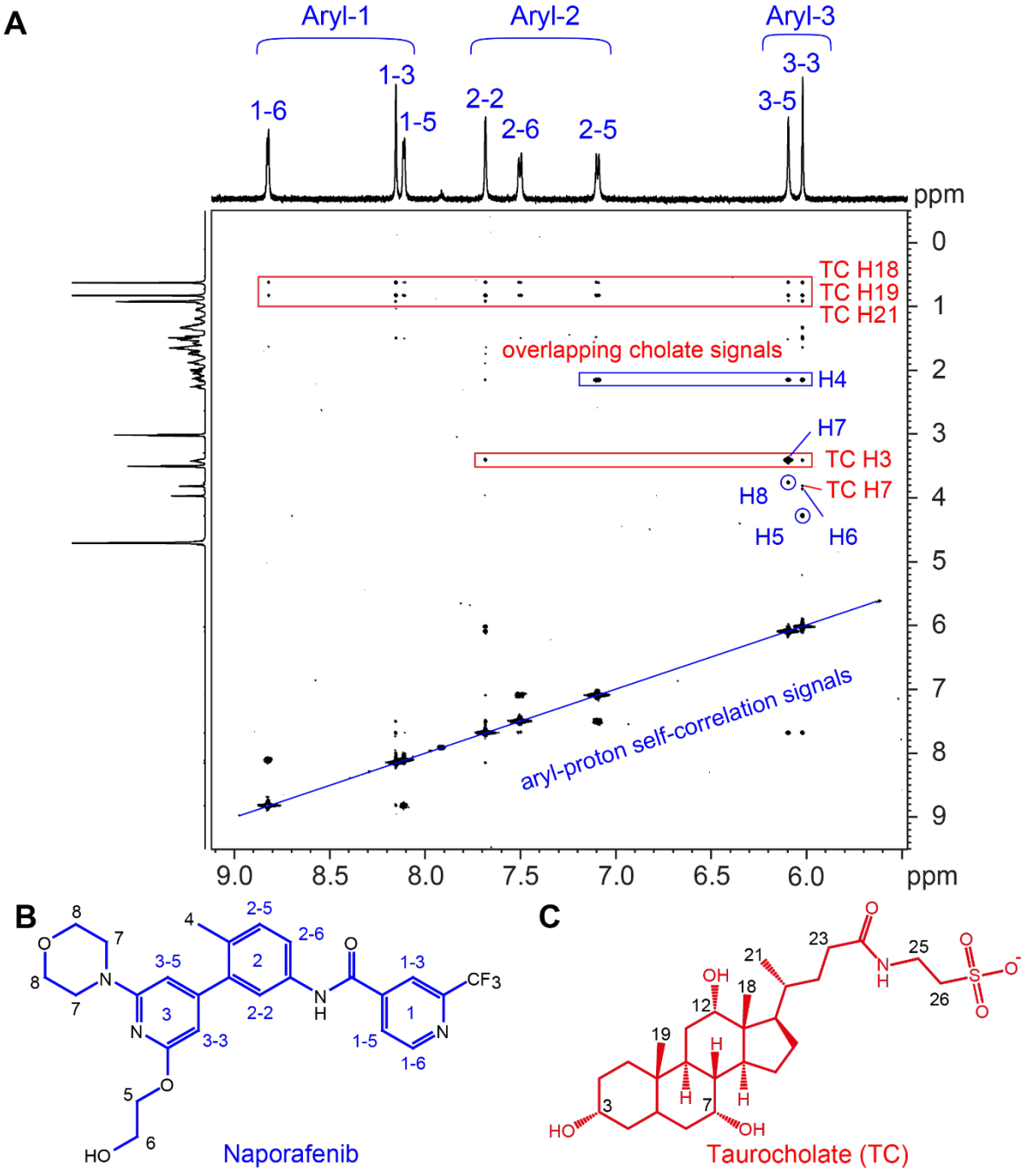

Figure S11: (A) Extract from an ^{1}H-^{1}H NOESY spectrum of Naporafenib (B, blue) in TC (C, red) in PBS. Mixing time was 80 ms.

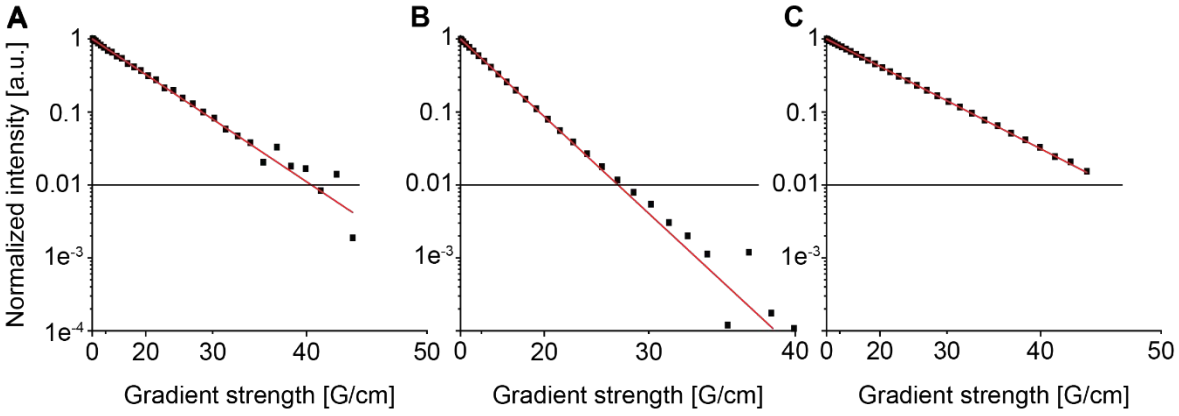

Figure S12: Exemplary normalized and linearized DOSY attenuation curves of Naporafenib aryl-proton 1-2 (A), TC H26 (B) and lecithin double bond (C) in 977 µmol/l Naporafenib with 5x TC/L. Little delta was 9.8ms, big delta was 49.9 ms. A mono-exponential model (red lines) was used to describe the signal decay.

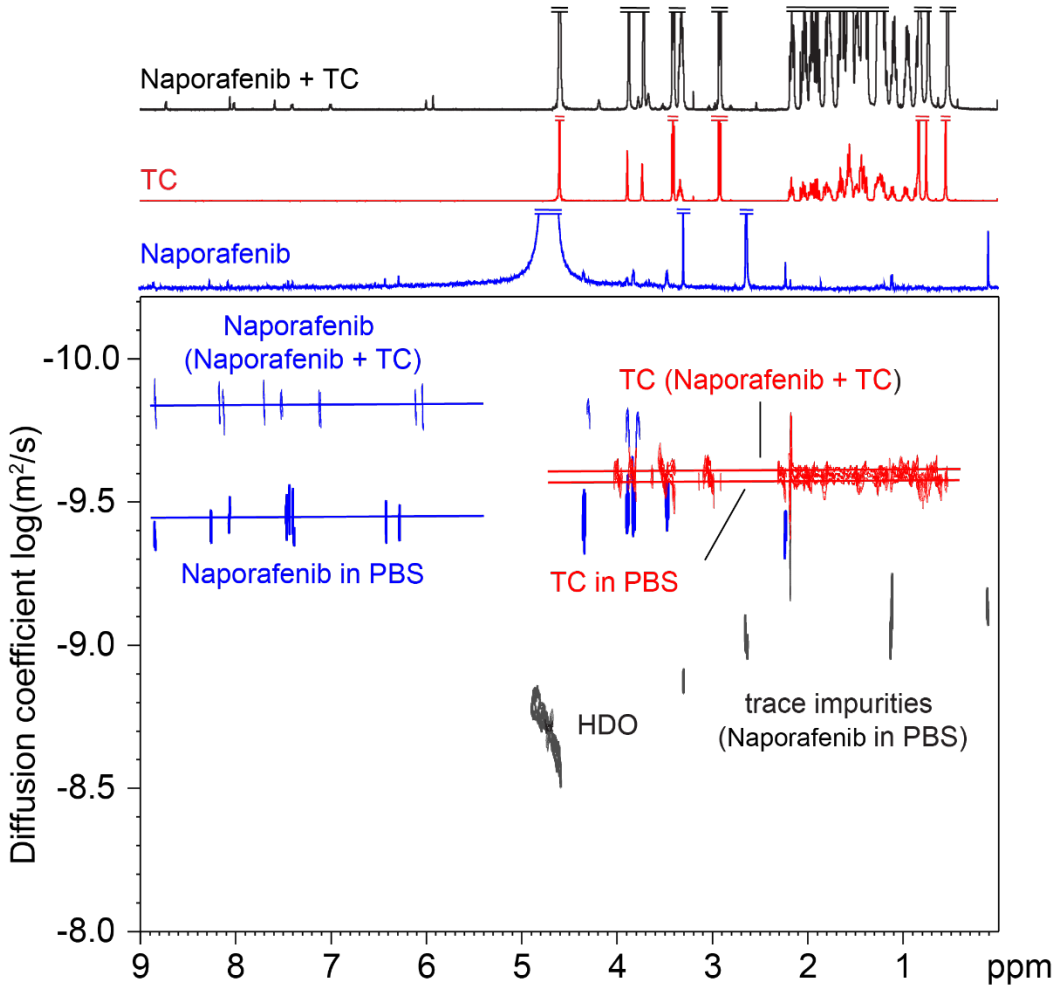

Figure S13: ^{1}H-DOSY pseudo 2D plot of Naporafenib with TC, Naporafenib in PBS, and TC without Naporafenib. The respective ^{1}H NMR spectra are shown on top.

Table S3: Diffusion coefficients (D) of Naporafenib, TC, and L in different media. D are shown as [m^2/s] * 10^{-10} ± standard error. Non-overlapping signals were used for D analysis. In case of overlapping or shifting signals for Naporafenib (NPF), the signal with the chemical shift to higher ppm was chosen for analysis. D with a signal decay between 1 and 10% are in italic.

Proton	Chemical shift NPF with 5x TC/L [ppm]	NPF in PBS	15 mmol/l TC in PBS	NPF in 15 mmol/l TC in PBS	5x TC/L in PBS	NPF with 5x TC/L	NPF with 5x TC/L with lipids
NPF 3-3	8.86	4.66 ± 0.43		1.48 ± 0.02		0.868 ± 0.008	*0.791 ± 0.022*
NPF 3-1 or 3-2	8.19	3.63 ± 0.40		1.45 ± 0.01		0.871 ± 0.004	*0.783 ± 0.014*
NPF 2-2 or 2-3	7.83	4.46 ± 0.43		1.51 ± 0.02		0.893 ± 0.010	*0.837 ± 0.027*
NPF 2-1	7.09	3.86 ± 0.50		1.56 ± 0.03		0.889 ± 0.009	*0.799 ± 0.037*
NPF 1-1 or 1-2	6.11	*4.17 ± 0.37*		1.50 ± 0.02		0.878 ± 0.007	*0.826 ± 0.022*
Mean D NPF		4.15 ± 0.47		1.50 ± 0.02		0.880 ± 0.008	*0.807 ± 0.024*
TC H25	3.51		2.57 ± 0.003	2.47 ± 0.001	1.70 ± 0.001	1.91 ± 0.002	1.27 ± 0.010
TC H26	3.02		2.58 ± 0.004	2.47 ± 0.001	1.70 ± 0.002	1.91 ± 0.002	1.45 ± 0.002
TC H21	0.93		2.57 ± 0.003	2.47 ± 0.001	1.69 ± 0.002	1.83 ± 0.007	1.41 ± 0.003
TC H18	0.62		2.58 ± 0.006	2.47 ± 0.001	1.69 ± 0.001	1.92 ± 0.003	1.43 ± 0.003
Mean D TC			2.57 ± 0.004	2.47 ± 0.004	1.69 ± 0.001	1.89 ± 0.003	1.39 ± 0.004
L Hdb	5.24				*0.640 ± 0.002*	*0.676 ± 0.001*	*0.607 ± 0.001*
L H4	3.19				*0.634 ± 0.001*	*0.674 ± 0.001*	*0.601 ± 0.001*
L H next to db	2.67				*0.644 ± 0.002*	*0.689 ± 0.003*	*0.604 ± 0.002*
Mean D L					*0.639 ± 0.001*	*0.680 ± 0.002*	*0.604 ± 0.001*

S2.3 ^{1}H nuclear magnetic resonance spectra of Naporafenib with excipients in PBS and in TC/L in PBS

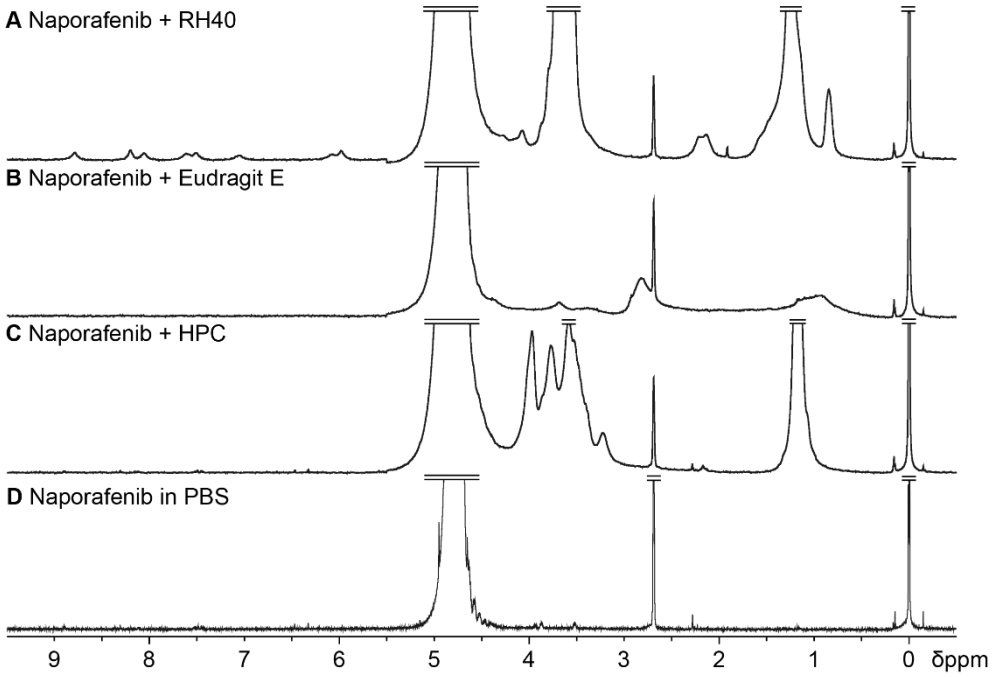

Figure S14: Full ^{1}H NMR spectra of 2 mmol/l Naporafenib in PBS with (A) RH40, (B) Eudragit E, (C) HPC, and reference (D).

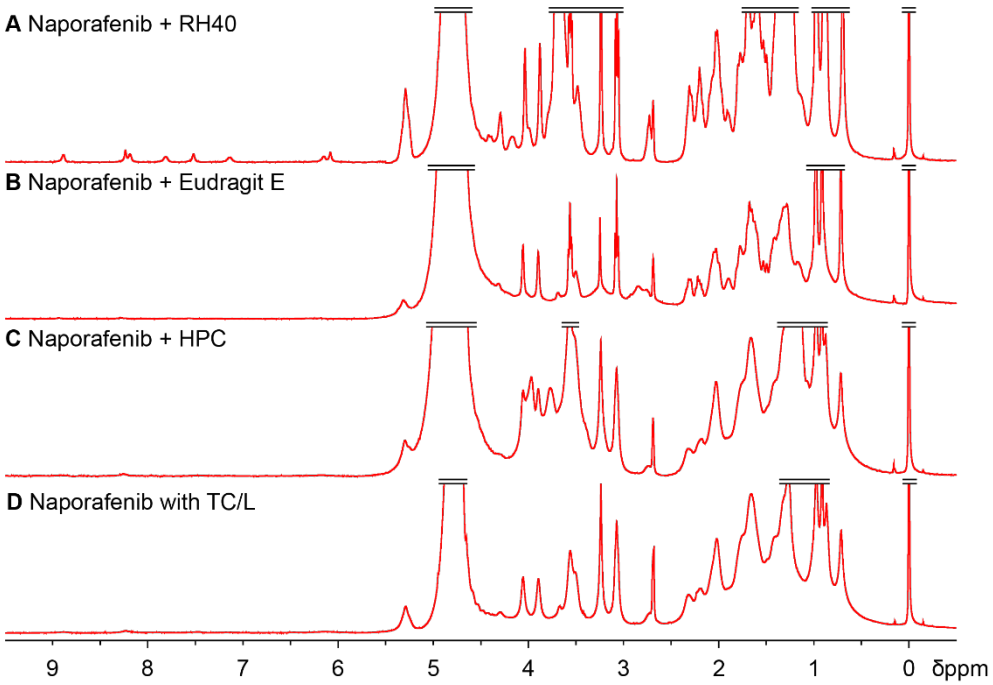

Figure S15: Full ^{1}H NMR spectra of 2 mmol/l Naporafenib in TC/L with (A) RH40, (B) Eudragit E, (C) HPC, and reference (D).

S3 Naporafenib flux across artificial membranes

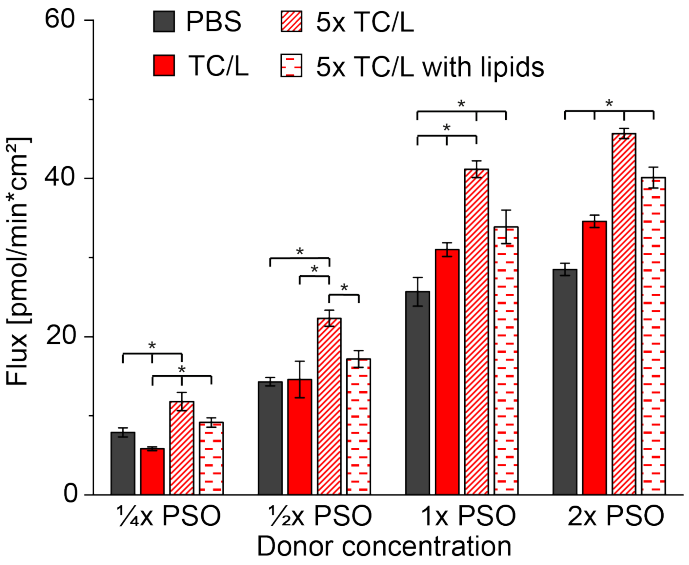

Figure S16: Naporafenib flux at ¼, ½, 1-fold, and 2-fold of the respective PSO donor concentration in PBS (grey), with TC/L (red), with 5x TC/L (hatched red lines), and with 5x TC/L and lipids (hatched red dashed lines). Data shown as mean ± SD, ANOVA considering $p \leq 0.05$ as statistically significant followed by Tukey *post-hoc* test for pairwise comparison (significant differences are shown by asterisks).

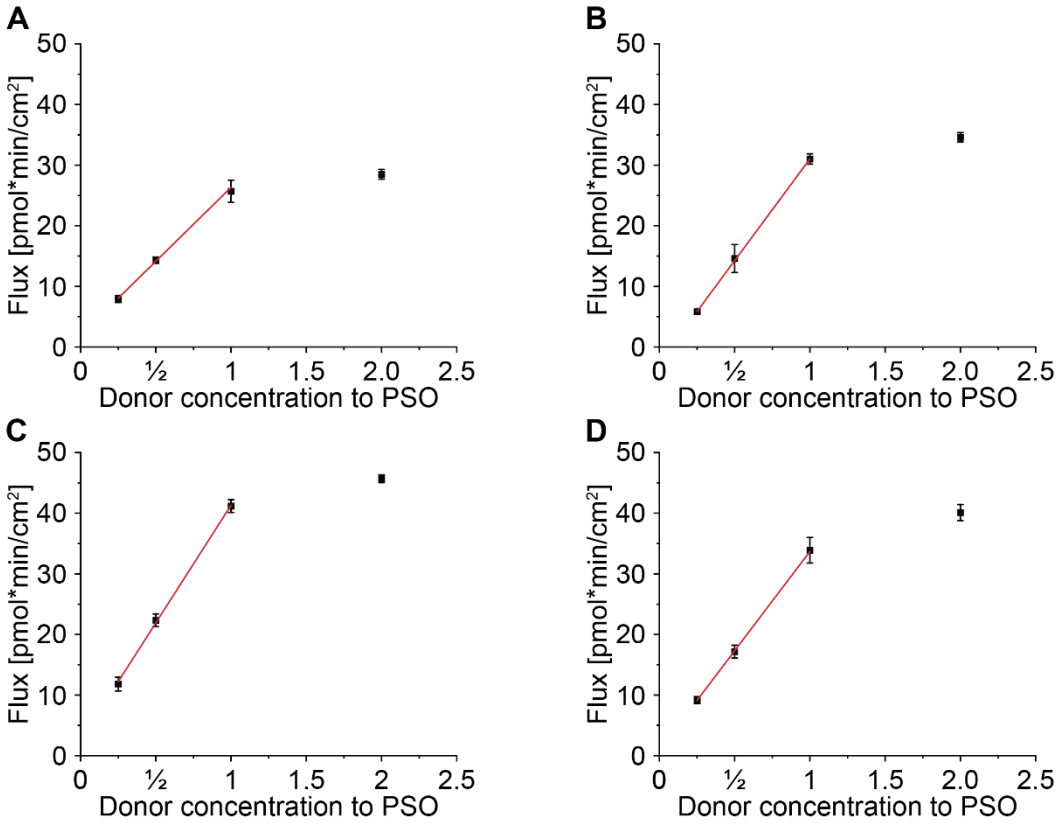

Figure S17: Naporafenib flux ¼, ½, 1-fold, and 2-fold of respective PSO adjusted donor concentration in (A) PBS, (B) with TC/L, (C) with 5x TC/L (D) with 5x TC/L and lipids. Linear regression converged for 1/4, 1/2, and 1-fold, but not for 2-fold. Data from figure S16.

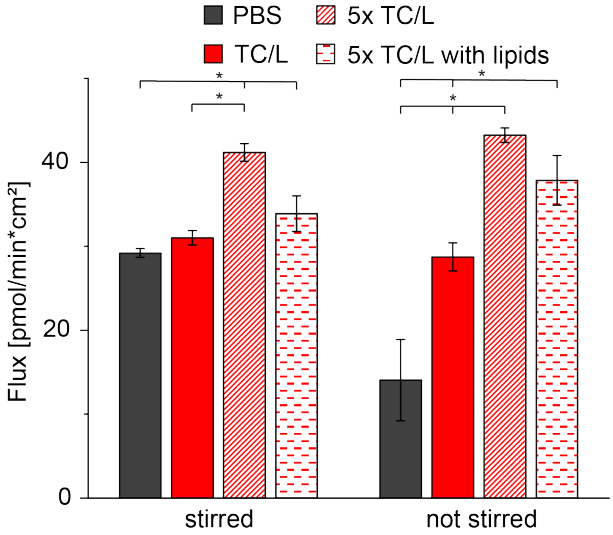

Figure S18: Naporafenib flux at 1x PSO donor concentration in PBS (grey), with TC/L (red), with 5x TC/L (hatched red lines), and with 5x TC/L and lipids (hatched red dashed lines) with stir bar (same data as figure 5) and without stir bar in the donor cell after initial equilibration time of 5 min. PBS was supplemented with 0.1% HPC to avoid fast de-supersaturation. Data shown as mean ± SD, ANOVA considering $p \leq 0.05$ as statistically significant followed by Tukey *post-hoc* test for pairwise comparison between stirred and non-stirred groups (significant differences are shown by asterisks).

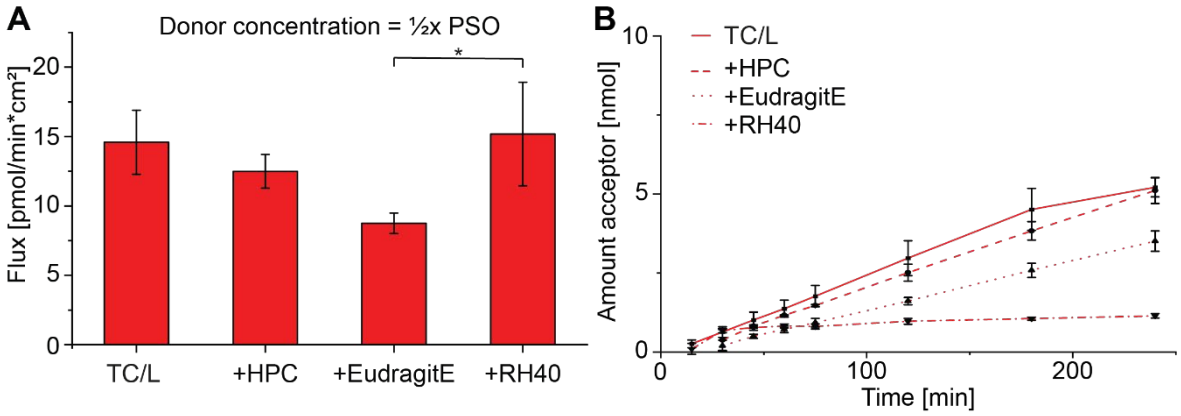

Figure S19: Naporafenib (A) flux and (B) amount in acceptor over time in cellulose-based membrane flux setup with TC/L in presence of HPC (dashed lines), Eudragit E (dotted lines), RH40 (dashed dotted lines), and medium without excipient (continuous line). Lines were linearly interpolated between two adjacent points. Naporafenib donor concentration was adjusted to ½x PSO. (A) Data shown as mean ± SD, ANOVA considering $p \leq 0.05$ as statistically significant followed by Tukey *post-hoc* test for pairwise comparison (significant differences are shown by asterisks).

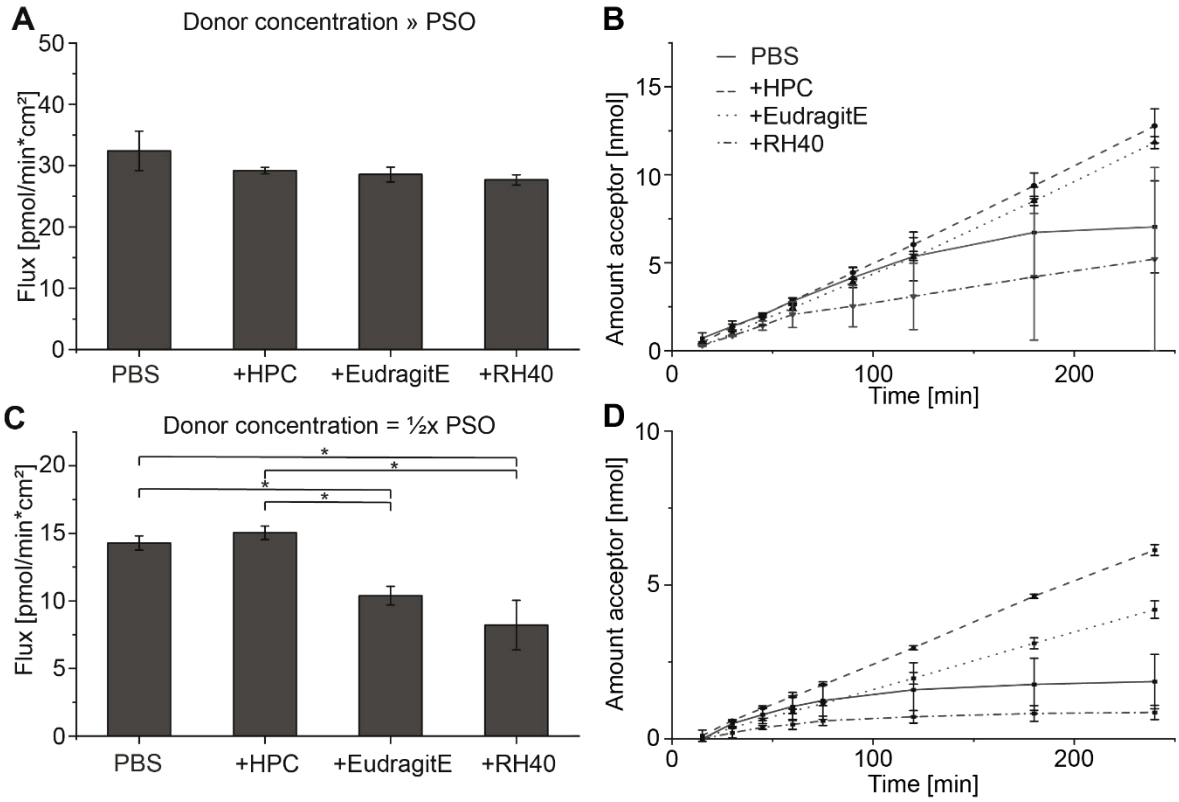

Figure S20: Naporafenib (A, C) flux and (B, D) amount in acceptor over time in cellulose-based membrane flux setup in PBS in presence of HPC (dashed lines), Eudragit E (dotted lines), RH40 (dashed dotted lines), and medium without excipient (continuous line). Lines were linearly interpolated between two adjacent points. (A, B) Naporafenib donor concentration was 2,000 µmol/l. (C, D) Naporafenib donor concentration was adjusted to ½x PSO. (A) Data shown as mean ± SD, ANOVA considering $p \leq 0.05$ as statistically significant followed by Tukey *post-hoc* test for pairwise comparison (significant differences are shown by asterisks).

S4 Naporafenib exposure in beagle dogs

S4.1 Correlation of in vivo physiology with in vitro conditions

Here, we explain the rationale for comparing *in vitro* to *in vivo* dog conditions. The dogs received a nominal dose of 30 mg/kg Naporafenib (40.3 mg/kg Naporafenib tosylate) with excipients at 30 mg/kg, administered at a volume of 3 ml/kg, followed by a gavage line flush with water (2 ml/kg). Assuming a beagle dog's weight to 10 kg, absolute dose was roughly 300 mg in 50 ml administered buffer (drug as well as excipients). Although there were to date no studies addressing the canine basal gastric volume, the stomach capacity is comparable to humans.[1] Basal duodenal bile salt concentration in dogs was reported to be generally higher than in humans.[2] It can be approximated from studies in humans, that the solution is further diluted in stomach and small intestine within 10 to 50 ml.[3] Therefore, the concentration in the gastrointestinal system is assumed to be around 3 mg/ml (6 mmol/l), which is far above the **p**hase **s**eparation **o**nset (**PSO**) of Naporafenib even if more bile salts

compared to humans might be present. Due to further dilution within the gastrointestinal system, at the absorption site concentrations near 1-2 mg/ml can be considered as realistic. Hence *in vitro* studies were conducted at 2 mmol/l (1 mg/ml) Naporafenib (above the PSO) and 1 mg/ml excipient concentrations.

S4.2 Pharmacokinetic analysis

Table S4: Individual noncompartmental pharmacokinetic analysis data. Outlier identified by Grub's test at 0.05 level are highlighted and in italic. Dog 2 was identified as an outlier and was excluded from further analysis. Vz/F value for dog 4 was excluded from calculation.

Dog	Treatment	c_{max} [mg/ml]	T_{max} [h]	λz [1/h]	AUC_{last} [h*mg/ml]	AUC_{inf} [h*mg/ml]	CL/F [l/h]	MRT_{last} [h]	MRT_{inf} [h]	Vz/F [l]
1	Eudragit E	0.14	*24*	0.065	4.30	4.31	60.38	21.53	21.69	932
2	Eudragit E	*0.412*	2	0.062	3.81	3.82	57.50	6.51	6.68	934
3	Eudragit E	0.101	4	0.114	1.68	1.68	190.36	13.86	13.97	1671
4	Eudragit E	0.0775	2	0.110	0.93	0.93	376.20	8.70	8.94	3418
5	Eudragit E	0.156	2	0.118	1.39	1.40	221.62	7.35	7.49	1877
6	Eudragit E	0.164	2	0.068	1.90	1.91	152.01	9.33	9.63	2229
1	HPC	0.321	4	0.067	5.27	5.27	47.43	12.16	12.30	712
2	HPC	0.587	2	0.068	5.65	5.66	37.13	6.10	6.20	545
3	HPC	0.661	2	0.026	5.73	5.75	53.90	6.80	7.23	2075
4	HPC	0.469	2	0.028	6.32	6.34	55.24	8.10	8.44	1948
5	HPC	0.514	1	0.026	4.84	4.88	63.53	8.24	9.37	2449
6	HPC	0.258	4	0.097	4.33	4.33	66.84	8.20	8.29	686
1	RH40	0.507	2	0.038	4.77	4.79	52.18	7.93	8.25	1388
2	RH40	*1.91*	2	0.006	*15.96*	*16.40*	12.79	6.41	13.24	2063
3	RH40	0.663	1	0.038	4.23	4.26	72.74	5.59	6.25	1933
4	RH40	0.546	2	0.002	3.97	4.49	75.72	7.00	66.59	*32679*
5	RH40	0.477	1	0.071	3.81	3.82	81.21	8.13	8.32	1146
6	RH40	0.399	0.5	0.086	2.97	2.98	97.16	7.47	7.77	1125

Table S5: Naporafenib non-compartmental pharmacokinetic analysis results after HPC, Eudragit E, and RH40 application. T_{max} shown as median and range in brackets. Data shown as mean ± SD, repeated measures ANOVA considering $p \leq 0.05$ as statistically significant followed by Tukey *post-hoc* test for pairwise comparison (asterisks show significant differences compared to both other treatment groups).

Treatment	c_{max} [mg/ml]	T_{max} [h]	λ_Z [1/h]	AUC_{last} [h*mg/l]	AUC_{inf} [h*mg/l]	CL/F [l/h]	MRT_{last} [h]	MRT_{inf} [h]	V_Z/F [l]
HPC	0.44 ± 0.16	2.0 (1-4)	0.05 ± 0.03	5.30 ± 0.77	5.32 ± 0.77	57.4 ± 7.8	8.70 ± 2.02	9.13 ± 1.93	1574 ± 820
Eudragit E	**0.13 ± 0.04***	2.0 (2-24)	0.10 ± 0.03	**2.04 ± 1.32***	**2.05 ± 1.32***	**200 ± 115***	12.2 ± 5.8	12.4 ± 5.8	2025 ± 911
RH40	0.52 ± 0.10	1.0 (0.5-2)	0.05 ± 0.03	3.95 ± 0.66	4.07 ± 0.70	75.8 ± 16.2	7.23 ± 1.01	19.4 ± 26.4	1398 ± 376

Table S6: Relative bioavailability calculation using individual data from non-compartmental PK analysis referring to HPC treatment.

Dog No.	Treatment	Relative bioavailability $\frac{\text{AUCinf treatment}}{\text{AUCinf treatment (HPC)}}$*100%
1	HPC	-
3	HPC	-
4	HPC	-
5	HPC	-
6	HPC	-
	Mean ± SD	-
1	Eudragit E	81.69%
3	Eudragit E	29.26%
4	Eudragit E	14.66%
5	Eudragit E	28.66%
6	Eudragit E	44.00%
	Mean ± SD	39.7 ± 25.7%
1	RH40	90.78%
3	RH40	74.13%
4	RH40	70.75%
5	RH40	78.23%
6	RH40	68.80%
	Mean ± SD	76.5 ± 8.7%

Table S7: Naporafenib concentration in respective media [µmol/l] after 30 min, 24h, and 48h determined by shake flask approach using Naporafenib tosylate salt (10 mg/ml). The 30 min concentration may reflect the situation of suspensions applied to dogs. The excipient concentration was 1% (m/v).

Time	30 min	24 h	48 h
Average Concentration ± standard deviation [µmol/l]			
PCB pH2.6	29.9 ± 2.0	38 ± 10	1.1 ± 0.5
PCB pH2.6 + HPC	27.1 ± 3.1	31.4 ± 4.2	17.5 ± 3.3
PCB pH2.6 + Eudragit E	367 ± 54	754 ± 73	835 ± 88
PCB pH2.6 + RH40	2164 ± 76	1116 ± 283	172.3 ± 8.0

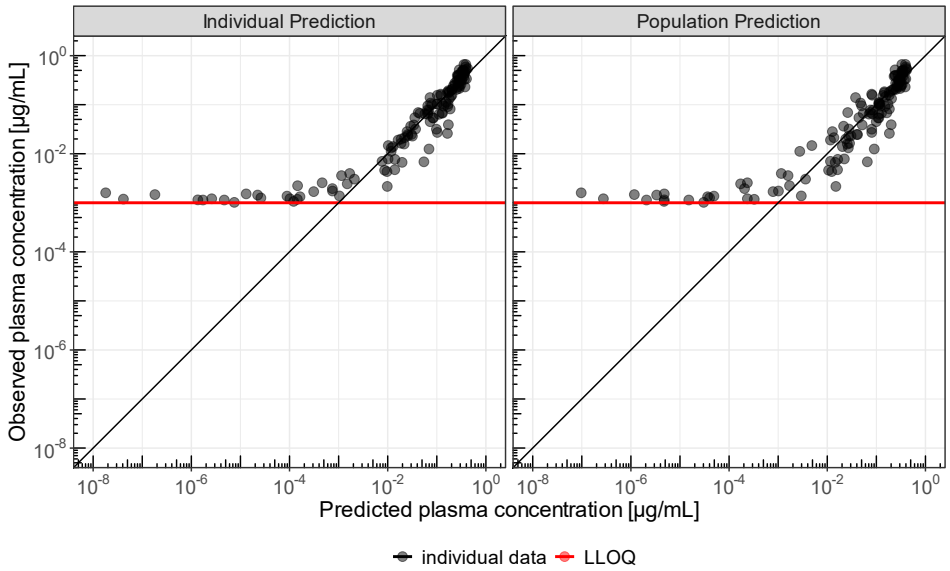

Figure S21: Observed Naporafenib dog plasma concentrations vs. model predicted concentrations. LLOQ: lower limit of quantification (1 ng/mL). This plot shows that high plasma concentrations were sufficiently described by the one-compartmental modeling by Monolix. Concentrations close to the LLOQ (red line) showed higher deviations. Nevertheless, modeling was estimated as sufficient.

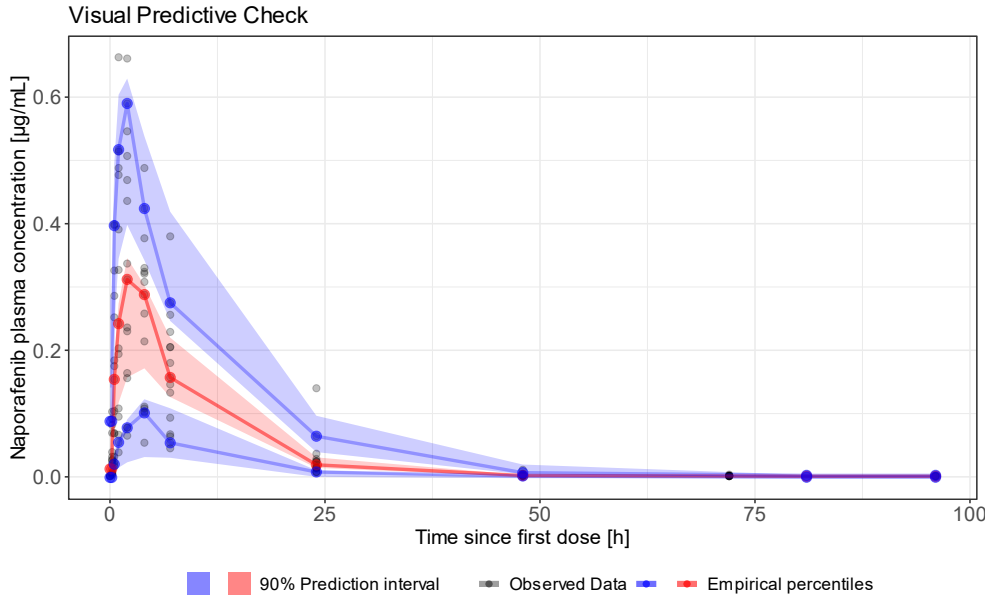

Figure S22: Visual predictive check of population-based PK analysis. The solid lines represent the 5th (lower blue), 50th (red), and 95th (upper blue) percentiles of the observed data. Shaded regions represent the 90% confidence intervals surrounding the 5th, 50th, and 95th percentiles from the predicted data. Overall, the plot demonstrates that the model predictions captured the majority of observed Naporafenib concentrations within the 5th and 95th percentiles of the simulated values.

S5 Dissolution rate of Naporafenib tosylate

The dissolution rate of Naporafenib in media was measured by a Sirius T3 instrument (Pion) as previously described.[4] Tablets discs were prepared by compression of 3–10 mg of each sample under a weight of 1.8 tons (25.2 x 10^6 Pa) for 5 min with a manual hydraulic tablet press (Paul Weber, Stuttgart, Germany). The release of drug substance from the tablet discs allowed data collection with a standardized surface area of 0.07 cm^2 to calculate dissolution rates.[5] Dissolution rates were determined photometrically at room temperature in PBS, TC/L in PBS, and with 5x TC/L at a stirring speed of 4800 rpm at alternate titration position with 20 ml media filling volume following manufacturer's instructions (**Figure S23**). The amount of dissolved Naporafenib was calculated by the Beer-Lambert law using the spectroscopic data obtained by a fibre optic dip probe connected to a diode array detector. The linear part of the release profile was used for calculation of the dissolution rate (dissolved substance per time and surface area). Experiments were carried out as triplicates.

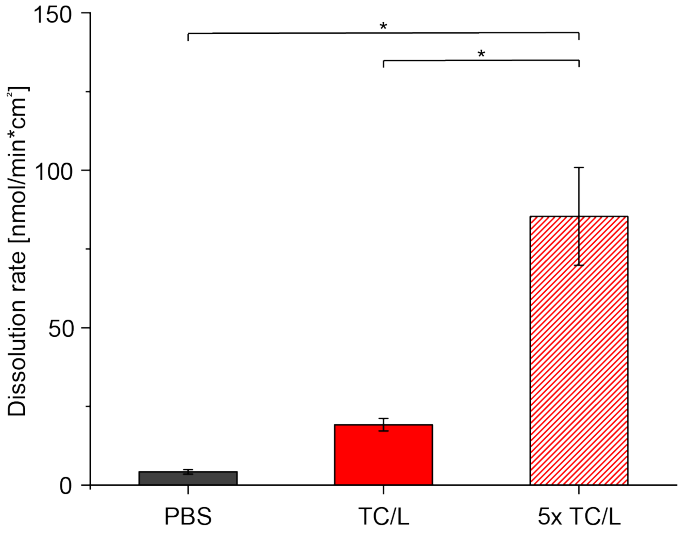

Figure S23: Surface normalized dissolution rate of Naporafenib tosylate in in PBS (grey), with TC/L (red), and with 5x TC/L (hatched red lines). Data shown as mean ± SD, ANOVA considering $p \leq 0.05$ as statistically significant followed by Tukey post-hoc test for pairwise comparison (significant differences are shown by asterisks).

References

1. Kararli, T. T., Comparison of the gastrointestinal anatomy, physiology, and biochemistry of humans and commonly used laboratory animals. *Biopharm. Drug. Dispos.* **1995,** *16* (5), 351-80.
2. Arndt, M.; Chokshi, H.; Tang, K.; Parrott, N. J.; Reppas, C.; Dressman, J. B., Dissolution media simulating the proximal canine gastrointestinal tract in the fasted state. *Eur. J. Pharm. Biopharm.* **2013,** *84* (3), 633-41.
3. Schiller, C.; Fröhlich, C. P.; Giessmann, T.; Siegmund, W.; Monnikes, H.; Hosten, N.; Weitschies, W., Intestinal fluid volumes and transit of dosage forms as assessed by magnetic resonance imaging. *Aliment. Pharmacol. Ther.* **2005,** *22* (10), 971-9.
4. Pöppler, A. C.; Lübtow, M. M.; Schlauersbach, J.; Wiest, J.; Meinel, L.; Luxenhofer, R., Loading-Dependent Structural Model of Polymeric Micelles Encapsulating Curcumin by Solid-State NMR Spectroscopy. *Angew. Chem. Int. Ed. Engl.* **2019,** *58* (51), 18540-18546.
5. Gravestock, T.; Box, K.; Comer, J.; Frake, E.; Judge, S.; Ruiz, R., The " dissolution" method: a low volume, in vitro apparatus for assessing the dissolution/precipitation behaviour of an active pharmaceutical ingredient under biorelevant conditions. *Anal. Methods* **2011,** *3* (3), 560-567.

Appendix: Step by step guide for excipient screening with simulated intestinal fluids for drug substances

Jonas Schlauersbach, Simon Hanio, Lena Scheller, Lorenz Meinel

Institute for Pharmacy and Food Chemistry, University of Wuerzburg, Am Hubland, DE-97074 Wuerzburg, Germany

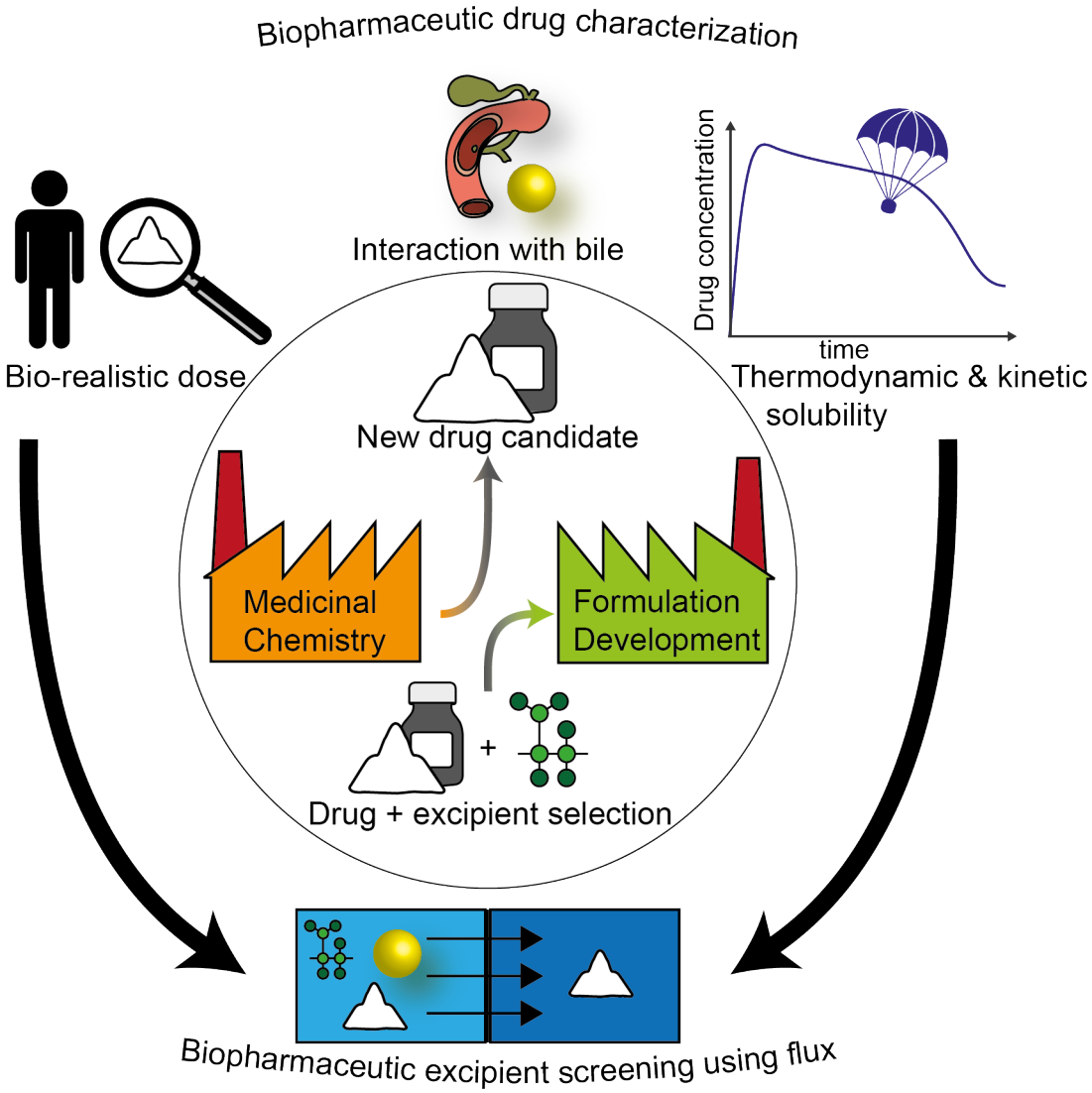

unpublished manuscript

Abstract

This protocol provides step-by-step guidance to select polymers for poorly water-soluble, orally administered drugs from a biopharmaceutical perspective. This commences with calculations on the amount of drug required at the absorption site and continues with the preparation and conduct of studies using simulated intestinal fluids, including the quantification by HPLC. The workflow further includes bile-drug interaction studies with ^{1}H nuclear magnetic resonance spectroscopy and, if not readily available, provides predictive algorithms. The set of studies also includes the assessment of thermodynamic and kinetic drug solubility and of cell-free permeation/flux studies, respectively. The resulting data set fuels a decision tree, facilitating rational polymer selection for poorly water-soluble drug substances from a biopharmaceutical perspective.

Introduction

In the past, trial and error approach dominated early drug formulation development for orally applied **p**oorly **w**ater-**s**oluble **d**rugs (**PWSD**s). These have been largely replaced by standardized research processes[1, 2], which are mainly driven by solubility/dissolution rate considerations,[3, 4] including the use of **s**imulated **i**ntestinal **f**luids (**SIF**) supposed to mimic the gastrointestinal environment.[5, 6] These studies guide physical adaptations (e.g., amorphization, salt design, or nano milling) and the selection of functional excipients. This selection was based on shelf-life stability of the dosage forms,[7, 8] and improvements in apparent drug solubility.[9-11] In the past, excipient interactions with biological processes were arguably underestimated (excipients are still referred to as bio-inert molecules),[12] a perhaps regulatory motivated euphemism neglecting the complex interplays. For example, drug-excipient interactions may increase a drug's solubility *in vitro*, but these excipients fail to mediate bioavailability increases.[13] This randomly selected example illustrates that polymer selection based on solubility/dissolution rate considerations alone may occasionally be insufficient. For example, polymers may interfere with bile colloids/solubilization. In cases in which poorly water-soluble drugs benefit from bile interaction, a bile-interacting polymer might impair drugs solubilization and reduce bioavailability (possibly despite a potential benefit seen for apparent solubility).[14-16] It is precisely for these, more recently communicated insights, why we compiled this series of protocols. The entry point is an identified stable drug form (e.g., salt, free base, or most stable polymorph has been found). At first, calculations are exemplarily given gating bio-realistic drug and excipient concentrations at the absorption site. These assessments are essential for screening within relevant concentration ranges. Next, the drug is characterized for its interaction with SIFs, we then provide a brief section about proper handling of SIFs and a guide how to build a **h**igh-**p**erformance liquid **c**hromatography (**HPLC**) method for drug quantification. **^{1}H n**uclear **m**agnetic **r**esonance spectroscopy (**^{1}H NMR**), thermodynamic and kinetic solubility protocols are described for drug/SIF interaction qualification and quantification. We furthermore refer to an algorithm for bile interaction prediction (**manuscript in preparation**). Secondly, biopharmaceutic excipient screening is detailed. Flux studies across artificial membranes are described to check the interaction potential of excipients with drugs. Excipients ensuring fast and stable permeation of drugs through membranes should be considered as promising candidates for formulation development. This protocol might be

integrated into existing decision trees to rationally aid the formulation development of orally administered PWSDs.

Materials

Reagents and supplies

- **Ac**eto**n**itrile (**ACN**) HPLC-gradient grade (Sigma-Aldrich, Schnelldorf, Germany; cat. no. 34851)
- Deuterium chloride in deuterium oxide 35% m/v (Sigma-Aldrich; cat. no. 543047)
- Deuterium oxide (Euroiso-top, Saarbrücken, Germany; cat. no. D214H)
- Deuterium oxide (D_2O, 99.9% D) containing 0.05% 3(trimethylsilyl)-propionic-2,2,3,3-d_4 sodium salt (TSP-d_4) (Sigma-Aldrich; cat. no. 450510)
- D-α-tocopherole-polyethylenglycol-1000-succinat, Vitamin E TPGS (Sigma-Aldrich; cat. no. 57668)
- Excipients e.g., Kollidon VA 64 (BASF SE, Ludwigshafen, Germany), Soluplus (BASF), Cellulose derivates (HPC, HPMC, HPMC-AS; Shin-Etsu Chemical Co Ltd., Tokyo, Japan), Eudragit (E PO, L; Evonik, Essen, Germany), polyethylene glycol-40 hydrogenated castor oil (RH40, BASF), Polysorbate 80 (Sigma-Aldrich; 59924)
- Fasted state simulating intestinal fluid powder (Biorelevant ltd., London, United Kingdom; cat. no. FFF02)
- GIT-0 lipid solution (Pion Inc Ltd., East Sussex, United Kingdom; cat. no. 110669)
- Hexadeuterodimethyl sulfoxide (Euroiso-top; cat. no. D010B)
- HPLC glass inserts 0.1 ml, 5x31 mm (VWR, Darmstadt, Germany; cat. no. 548-0308)
- HPLC screwcaps 5.5x1.3 mm (VWR; cat. no. 548-0024)
- HPLC vials 1.5 ml 11.632 mm (VWR; cat. no. 548-0387)
- Hydrochloric acid (Sigma-Aldrich; cat. no. 320331)
- Methanol HPLC-gradient grade (Sigma-Aldrich; cat. no. 34885-M)
- MicroFLUX **p**oly**v**inylidene **di**f**l**uoride (PVDF) membrane (Pion Inc Ltd.; cat. no. 120875)
- Monobasic sodium phosphate monohydrate (Sigma-Aldrich; cat. no. S9638)
- NMR coaxial inserts (Norell, Landisville, PA, USA; cat. no. NI5CCI-B)

- NMR tubes 5mm clear glass (Norell; cat. no. S-5-400-7)
- Purified water (Milli-Q) from in-house purification system (Merck KGaA, Darmstadt, Germany; cat. no. C85358)
- Reaction tubes: 1.5 ml + 2 ml (Sarstedt, Nümbrecht, Germany; cat. no. 72.698 + cat. no. 72.691)
- Regenerated cellulose membranes Permeaplain 25 mm (innoME GmbH, Espelkamp, Germany; cat. no. 300410)
- Screw cap tube (falcon tubes): 15 ml + 50 ml (Sarstedt; cat. no. 62.554.502 + cat. no. 62.559)
- Sodium chloride (Sigma-Aldrich; cat. no. S9888)
- Sodium deuteroxide in deuterium oxide 40% m/v (Sigma-Aldrich; cat. no. 176788)
- Sodium hydroxide pellets (Sigma-Aldrich; cat. no. 221465)
- **T**ri**f**luoroacetic **a**cid (**TFA**) suitable for HPLC (Sigma-Aldrich; cat. no. 302031)

Equipment

- Agilent Infinity II 1260 HPLC system (Agilent Technologies Germany GmbH & Co. KG, Waldbronn, Germany) equipped with a flexible pump (G7104C) vial sampler (G7129C), column oven (G7116A), and VWD (G7114A)
- Bruker Avance 400 MHz spectrometer (Bruker BioSpin GmbH, Karlsruhe, Germany)
- DLK 1002 cooling unit (FRYKA GmbH, Esslingen, Germany)
- H9-CB-02 stirring apparatus (SES GmbH, Bechenheim, Germany)
- Haake Fisons C1 water circulator (Thermo Fisher Scientific Inc., Karlsruhe, Germany)
- Orbital shaker Reax 20 (Heidolph GmbH, Schwabach, Germany)
- pH electrode pHenomenal 221 + bench pH meter pH 1100L (VWR; 662-1657)
- Side-by-side diffusion cells with metal clamps, stir bars and stoppers (PermeGear Inc., Hellertown, USA)
- Sirius T3 instrument (Pion Inc.)
- UV-spectrometer evolution 201 (Thermo Fisher Scientific Inc.)
- **General:** magnetic stir plate (RET basic, IKA GmbH& Co. KG, Staufen, Germany), research pipettes (Transferpette S Brand, Wertheim, Germany; 1−10 µl, 10−100 µl, 100− 1000 µl), centrifuge MiniSpin (Eppendorf SE, Hamburg, Germany),

Thermomixer F1.5 (Eppendorf), vortex VTX-3000L (LMSCO. LTD., Tokyo, Japan), freezer (−20 °C and −80 °C), ZORBAX Eclipse 5 µm XDB-C18 80 Å 150 x 4.6 mm LC column (Agilent), standard laboratory glassware, stopwatch, stirring bar retriever

Procedures

Estimation of drug/excipient concentrations in the small intestine

At first, the desired amount of drug delivered to the absorption site is to be estimated. in early stages, dose is often still unknown.[2] In this case, our procedure may be helpful to identify the drug dose maximum deliverable. Bio-realistic drug concentrations in the intestine are set as the benchmark for formulation design from a biopharmaceutic view. Concentration of excipients in the intestine are estimated analogously. Approximating human fasted conditions might be the overarching approach for most considerations. The fluid volume in the human small intestine (mean 107 ± 7 ml) is unevenly distributed in fluid pockets with a median volume of 12 ml.[17] An average dosage form contains 100-300 mg excipients.[12] Hence, dissolving 100 mg excipient in a fluid pocket with a volume of 10 ml results in a mass concentration of 1%. A tablet is usually swallowed with a glass of water (200 ml), so the initial excipient concentration might be lower. Water absorption is completed after 75-120 min (half-life 11-13 min).[18] Excipients for coatings only weigh about few milligrams, which would theoretically result in a concentration of roughly 0.01%. Interspecies differences must be considered when designing animal studies. Fasted state simulating intestinal fluids for rat,[19, 20] dog,[21, 22] as well as pig[23] have been described. When designing pharmacokinetic studies in rats one must consider the low intestinal fluid volume of roughly 1 ml and high species-specific metabolism.[24] Comparison between laboratory animal gastrointestinal physiology and human intestinal physiology was also described in literature.[25, 26]

Preparation of simulated intestinal fluids and medium/excipient mixtures

Unproper storage of SIF powder can be detrimental for experimental outcome.[27] For best robustness, we recommend using one batch of SIF powder for all experiments. It was further proposed to use up one bottle of SIF powder after six months.[27] The powder must be kept well sealed and refrigerated to 4°C. Moreover, SIF powder is hygroscopic. Opening the SIF bottle after taking it out from the fridge can lead to significant moisture entry. One option to

reduce moisture entry is to equilibrate SIF bottles in a desiccator to room temperature before powder withdrawal. Water can accelerate hydrolyzation of esters in lecithin.[28] Sticky SIF powder should be discarded in general. Right handling of SIFs and SIF powder is obligatory to obtain comparable experimental output. **Fa**sted **s**tate **SIF** (**FaSSIF-V1**) needs an equilibration time of 2 h after preparation. SIFs may be used for 96 h after preparation when stored at room temperature.[29] Modified **p**hosphate **b**uffered **s**aline (**PBS**) as described for FaSSIF-V1 was also used **fe**d **s**tate **SIF** (**FeSSIF-V1**) preparation to avoid misleading effects from the usage of different buffers with differing ionic strength, ingredients, and pH values. Hereinafter we refer to this modified FeSSIF-V1. A calculation tool for buffer preparation is available on the SIFs manufacturer's website (biorelevant.com). When preparing excipient medium mixtures, we recommend an equilibration time of at least 2 h before using them in an assay.

Note: For preparation of deuterated PBS, use deuterium oxide (D_2O) instead of deionized water, 40% sodium deuteroxide in deuterium oxide, and 35% deuterium chloride in deuterium oxide for preparation. Adjust pD to 6.91.[30] Use 50 ml falcon tubes for preparation, add required amount D_2O with volumetric glass pipette.

1. Phosphate buffered saline preparation (1 l)
    a. Weigh into a 1 l beaker: 0.42 g sodium hydroxide, 3.95 g sodium phosphate monobasic monohydrate, 6.19 g sodium chloride.
    b. Fill beaker to roughly 90% with purified water.
    c. Stir beaker on a magnetic stirrer and wait for ingredients to dissolve.
    d. Check pH with pH meter.
    e. Adjust to pH 6.5 ± 0.05, if necessary, with dropwise addition of sodium hydroxide (1 mol/l in deionized water) or hydrochloric acid (1 mol/l in deionized water).
    f. Fill buffer quantitatively into 1 l volumetric flask, fill up to line, seal, and shake.
    g. Store buffer up to one week at 4 °C, let buffer equilibrate to room temperature before use.
2. FaSSIF-V1/FeSSIF-V1 preparation (100 ml)
    a. Take SIF powder out of fridge. Put bottle into a desiccator, equilibrate bottle to room temperature for 15 min.

b. Take bottle out of desiccator, weigh 224 mg (FaSSIF-V1)/1.12 g (FeSSIF-V1) into a 100 ml volumetric flask. Seal bottle tightly and put it back to the fridge.
c. Fill up volumetric flasks with PBS to 90% of volume and shake.
d. Wait until bubbles vanish and fill up to 100 ml.
e. For FaSSIF-V1 wait 2 h until use.

3. Medium/excipient mixture preparation (10-15 ml)
    a. Weigh respective excipient amount (3.1) in a 15 ml falcon tube (for higher amounts use volumetric flasks)
    b. Fill up with respective medium to desired volume
    c. Shake mixtures at least 2 h at room temperature on orbital shaker Reax 20.

Drug quantification

An integral part for all following steps is the establishment of a reliable method for drug quantification. When using SIFs, we recommend chromatographic methods over direct measurements like UV as composition of investigated fluids or crystallization events might compromise direct measurements.[31] If direct light-based measurements within SIFs are desired, one must always calibrate for the respective media (and excipients) as absorption maxima might shift. For most PWSDs, **r**eversed **p**hase **HPLC** (**RP-HPLC**) with UV-detection offers an easy and widely accessible platform. HPLC chromatography is compound specific. Therefore, the choice of columns, detector, and mobile phases cannot be generalized. For ionizable compounds, we recommend the use of acids (e.g., TFA) within the mobile phase to convert the drug into one ionization state improving chromatographic resolution. The organic mobile phase should be chosen based on drug solubility in the respective solvents (e.g., ACN, methanol, or isopropanol). For drug with weak absorbing chromophores, detection by an evaporative light scattering detector might be a promising alternative.

Note: This workflow was optimized for an Agilent 1260 infinity II HPLC (Agilent Technologies Inc., Waldbronn, Germany) using a ZORBAX Eclipse 5 µm XDB-C18 80 Å 150 x 4.6 mm LC column (Agilent). The device was equipped with a variable wavelength detector (G7114A), an automatic vial sampler (G7129A), flexible Pump (G7104A), and multicolumn oven (G7116A). Mobile phase A was 0.1% (V/V) TFA in Millipore water.

Mobile phase B was ACN with 0.1% (V/V) TFA, the flow was set to 1 ml/min. This workflow is meant to guarantee a fast and robust method for drug quantification.

RP-HPLC calibration:

1. Drug-specific wavelength identification
    a. Prepare mobile phases by adding 1 ml TFA to 1000 ml purified water (mobile phase A) and ACN (mobile phase B), respectively.
    b. Mix 5 ml mobile phase A with 5 ml mobile phase B (test mixture).
    c. Dissolve roughly 0.5 mg drug in 0.5 ml mobile phase B (drug solution).
    d. Dilute drug solution 1:100 and 1:1000 in test mixture (10 µl drug solution + 990 µl test mixture; 1 µl drug solution + 999 µl test mixture).
    e. Fill dilutions in quartz-cuvettes.
    f. Scan dilutions by UV spectrometer, identify maxima.

Note: If drug precipitates, use higher amount of mobile phase B for test mixture. Further dilutions might be necessary if detector is saturated. Choose a wavelength above the TFA induced UV cutoff of 210 nm for quantification.[32] For RP HPLC pilot experiments use dilutions.

2. RP-HPLC sample preparation
    a. Draw 100 µl of sample, transfer sample to 1.5 ml reaction tube.
    b. Centrifuge sample for 15 min at 13000 rpm with MiniSpin centrifuge.
    c. Dilute supernatant with mixture of mobile phase A and B resulting in an amount of organic solvent in sample matching respective HPLC method start gradient.
    d. Vortex sample.
    e. Transfer 75 µl of sample to HPLC vials with glass inserts, seal them.
    f. Put samples into sample HPLC drawer or freeze samples to -80 °C for later analysis.

Note: Dilution is dependent on substance specific properties and sample concentration. Long term storage must ensure temperature below - 50 °C, as ACN freeze point is around - 45 °C. Not aligning mobile phase B composition in samples can lead to double peaks especially at high column loading.

3. Prepare HPLC
    a. Apply mobile phase A and B to HPLC, purge channels for 5 min at 5 ml/min.
    b. Attach ZORBAX Eclipse XDB-C18 column to HPLC.

c. Wash column with mobile phase B for at least 5 column volumes.
d. Equilibrate column with start gradient for at least 5 column volumes (default: 10% mobile phase B).
e. Perform two blank runs before sample measurement. If no drug specific HPLC method has been developed, use default Method: gradient starting with 10% mobile phase B, increase gradient to 100% mobile phase B within 6 min, hold for 4 min, set back to start gradient within 1 min and equilibrate for 4 min. set column oven temperature to ambient temperature (22 °C).

4. Build HPLC Method
    a. For pilot experiments a gradient starting with 10% mobile phase B and injection volume of 5 µl should be chosen.
    b. Set detector wavelength to drug-specific wavelength (step 1).
    c. Load default method.
    d. Inject diluted drug solutions (step 1 and 2), dilute if detector saturation occurs.
    e. Adjust start gradient and gradient ramp to obtain a main peak retention time of 3 to 5 min.

Note: Use of UHPLC columns may shorten analysis time. If the drug elutes at mobile phase B composition over 90%, consider use of C8 or C4 based columns. In case of very broad peaks, a higher temperature might be applied following the column manufactures instructions.

5. Calibrate HPLC
    a. Define desired calibration range according to pilot experiments (step 4).
    b. Make at least 5 samples with different concentrations in this calibration range using a mixture of mobile phase A and B resembling drug specific start gradient.
    c. Prepare samples for measurement (step 2).
    d. Measure samples.
    e. Repeat three times.

Note: The calibrated area is drug dependent. For a very low soluble compound you need high injection volumes of 50 µl and your lowest calibrated concentration should approximate the limit of quantification (signal to noise ratio > 10).

6. Evaluate data

a. Manually integrate peak areas with ChemStation OpenLab software.
b. For calibration: perform weighted linear regression of peak area and respective concentration. A regression coefficient greater than 0.99 is acceptable.
c. For concentration determination: Calculate concentration using calibration curve. Factor in all dilution steps and chosen injection volume.

Note: The peak area for concentration determination must be within your calibrated range. For better results, use a narrow calibration range (not more than 3 log steps).

7. After analysis
    a. Wash column with TFA-free ACN for at least 5 column volumes
    b. Detach column
    c. Purge system with 50% Methanol/Milli-Q

Note: Please check which storage medium is suited for your column. ACN should not be allowed to stand in the HPLC system, as polymerization might occur and clog mixture capillaries. Store ACN cool and protected from light.

^{1}H nuclear magnetic resonance spectroscopy for drug/SIF interaction determination

^{1}H NMR spectroscopy offers a fast and easy method to qualify a drug's interaction with SIFs. Drug aryl-proton signal shifts and intensity alteration occur when a drug is interacting with SIFs. The interaction pattern of isolated drug signals (drug aryl-proton signals) resembles molecular interactions. FaSSIF-V1 forms bigger colloidal structures than FeSSIF-V1.[33, 34] Some drugs induce geometric colloidal transformation in FaSSIF-V1. Drugs integrated into big FaSSIF-V1 colloidal structures often result in weak and broad signals, and therefore use of PBS and FeSSIF-V1 is advised. Drug precipitation does not impair the NMR measurement, as precipitated drug is not detectable by this method. We developed an algorithm predicting the interaction probability of a drug with **t**auro**c**holate (**TC**) and **l**ecithin (**L**) (**Chapter I**). This algorithm based on calculation of readily available 2D molecular drug descriptors may be also used.

Note: This procedure uses a Bruker Avance 400 MHz spectrometer (Bruker BioSpin GmbH, Karlsruhe, Germany) operating at 400.13 MHz with a BBI BB-H 5 mm probe head and at a temperature of 300 K. Acquisition parameters were set to 256 scans, flip angle of 30°, a spectral width of 20.55 ppm, and transmitter offset of 6.175 ppm. The acquisition time was

3.985 seconds, followed by a relaxation delay of 1.0 seconds with collection of 64 000 data points at a sample spinning frequency of 20 Hz. One NMR measurement lasts 21 min.

1. Prepare PBS and FeSSIF-V1 in D_2O (3.2).
2. Prepare a 0.1 mol/l drug stock solution in DMSO-d_6.
3. Fill 594 µl of respective medium in a 1.5 ml reaction tube.
4. Add 6 µl of stock solution to media (resulting in a drug concentration of 1 µmol/l).
5. Vortex samples.
6. Fill 500 µl of sample into NMR tube with a coaxial insert containing 100 µl of 0.05% TSP-d_4 in D_2O, label tube.
7. Measure sample in spectrometer.
8. Process spectra in TopSpin:
    a. Manual phase spectrum.
    b. Apply automatic baseline correction.
    c. Reference spectrum to TSP-d_4 signal.
    d. Rescale spectra: Receiver gain: 128, 254 scans and 9 ms pulse length.
    e. Identify medium with highest signal intensity.
    f. Overlay spectra.
    g. Determine mean aryl-proton signal shifts from PBS to FeSSIF-V1.

NMR tube cleaning:

1. Remove coaxial inserts, empty tubes.
2. Clean inserts with 70% v/v ethanol in demineralized water.
3. Fill tubes with 70% v/v ethanol in demineralized water, place them in a high beaker, fill beaker with water, put beaker into sonification bath for at least 15 min.
4. Rinse tubes at least 3 times with 70% v/v ethanol.
5. Dry the outside of tubes with a wipe, check tube cleanliness and integrity.
6. Put tubes into vacuum drier at 60 °C for at least 12 h (horizontally).

Thermodynamic solubility

Thermodynamic solubility is addressed by shake flask method. This method is versatile regarding drug amount. Upscaling to 96-well plate is possible.[35] Shake flask solubility is dependent on solid drug state. Different polymorphs of a drug result in different thermodynamic solubilities.[36] Centrifugation instead of filtration was applied to separate insoluble particles, as filter material can interact with SIFs in a drug substance specific

manner.[37, 38] If syringe filters have to be used, glass microfiber filters or regenerated cellulose filters are recommended.[39] Glass microfiber syringes with an average diameter of 0.45 µm are recommended by the manufacturer of SIFs (Biorelevant.com). For solubility measurements and all following experiments temperature must kept constant. Therefore, we chose an operating temperature of 25 °C to ensure comparability with other methods described here.

Note: 2 ml reaction tubes are used, as mixing in Thermomixer is better compared to 1.5 ml tubes.

1. Weigh roughly 1 mg drug substance into reaction tube.
2. Fill up with 500 µl of respective medium.
3. Vortex samples.
4. Shake samples on Thermomixer at 25 °C, 750 rpm.
5. Visually check samples after 6h. Add more 5 mg of drug, if everything dissolved
6. After 24h, take samples put of mixer. Transfer 200 µl of supernatant to a fresh 1.5 ml reaction tube.
7. Analyze samples as described in 3.2.2.
8. Calculate FaSSIF-V1 dose number, use dose as defined in 3.1:
    a. $Dose\ number = \frac{Dose\ [mg]}{Solublity(FaSSIF)\left[\frac{mg}{ml}\right] \cdot 250}$
9. Calculate FaSSIF-V1 solubility ratio: $Solubility\ ratio\ FaSSIF = \frac{Solubility\ [FaSSIF]}{Solubility\ [PBS]}$
10. Calculate FeSSIF-V1 solubility ratio: $Solubility\ ratio\ FeSSIF = \frac{Solubility\ [FeSSIF]}{Solubility\ [FaSSIF]}$

Note: Dilution is dependent on the solubility and HPLC calibration. Pre-wet the pipette tip with sample before transferring to avoid unspecific binding of drug to pipette tip material or insufficient wetting in case of aggregating compounds or compounds with surface activity. Always use your mobile phase start gradient for sample dilution.

Kinetic solubility

Exceeding the maximum drug supersaturation leads to drug phase separation. This can appear as **l**iquid-**l**iquid **p**hase **s**eparation (**LLPS**), **l**iquid-**g**lasslike **p**hase **s**eparation (**LGPS**), amorphous precipitation, or even crystalline precipitation, which limits the maximum free drug concentration.[40, 41] These events together are here defined as **p**hase **s**eparation **o**nset (**PSO**). The separated phase might serve as a reservoir for drug absorption dependent on separated phase properties.[42] Bile salts, lecithin, as well as polymers potentially stabilize

drug supersaturation and elevate PSO, also by increasing a drug's thermodynamic solubility.[43-45]

Note: This procedure uses a Sirius T3 instrument (Pion Inc., Forest Row, UK). Alternatively, any device with turbidity sensor (e.g., UV spectrometers, dynamic light scattering devices) allowing simultaneous stirring and turbidity detection may be used.

1. Calibrate UV dip probe of Sirius T3.
2. Run clean up experiment using 2 ml 80% v/v methanol in demineralized water.
3. Prepare ca. 220 µl (required amount for one run) of drug stock solution in DMSO (or methanol if drug is not soluble in DMSO) in a 1.5 ml reaction tube.

Note: Drug stock solution concentration should be the 100-fold of the determined bio-realistic intestinal drug concentration (3.1).

4. Fill 20 ml of FaSSIF-V1 of FaSSIF-V1/excipient mixtures into a glass vessel and place it on alternate titration position.
5. Build up an GI dissolution experiment with following parameters:
    a. Alternate titration position (right upper side next to folder "use alternate")
    b. Fill in details about buffer (optional)
    c. Separate reference vial: no
    d. Number of pH values to collect at: 1
    e. Initial adjustment: None
    f. Stirring at a speed of -30% (4800 rpm, counterclockwise)
    g. Period between points at first pH: 20 Seconds
    h. Number of points at first pH: 21
    i. Collect spectra stirring at a speed of -30%
6. Start assay (red "play" symbol, upper left side), confirm position ("proceed") and fill of vessel ("done"), blank spectrum is taken. The titration arm will lift again.
7. Confirm "ready to lower arm". After first spectra taken (shutter noise) manually add with a micropipette 10 µl of drug stock solution to medium.
8. Repeat every 20 seconds for 19 times.
9. After experiment finished, titration arm will move to storage position. Right click on raw UV-spectra ("Absorbance") and copy x/y data.
10. Copy x/y data to an Excel sheet, copy row of a non-absorbing wavelength (e.g., 401 nm) and plot absorption against concentration (1 add is equal to a concentration rise

of 1/20 of defined bio-realistic concentration in the vessel, the first data point measured is equal to blank).

11. Estimate PSO by tangent intersection point method using respective baseline at the non-absorbing wavelength and scatter increase after PSO.
12. Adjust stock solution in the manner to achieve PSO after roughly 8-10 titrations.
13. Repeat experiment with adjusted stock solution 3 times.
14. Run clean up experiment, switch off UV-lamp.

Permeability assays

Free drug fraction is determined by permeability assays using artificial size-exclusion membranes (cell-free systems). Free drug fraction is associated with absorbed drug fraction *in vivo*.[46, 47] The donor medium has no impact on drug transport processes in cell free setups compared to cell-based permeation studies (e.g., sodium taurocholate inhibits P-gp efflux in Caco2 cell setups[48]). Excipients may impact a drug's bioavailability by interacting with bile or drug itself.[14, 49] Cell-free permeation assay allow the determination of free drug fraction and duration of drug supersaturation. Drug crystallization and concomitant loss of supersaturation decreases drug flux. Principally, two artificial membrane types can be differentiated. One membrane type represents a hydrophilic drug diffusion barrier (regenerated cellulose, cut-off 6-8 kDa, Permeaplain), the other a hydrophobic barrier (PVDF membrane impregnated with phospholipids in organic solvent, PAMPA).[50] Both membrane types are compared in this setup.

Note: This setup uses 12 side-by-side diffusion cells (PermeGear Inc., Hellertown, USA) with a filling volume of 10 ml and an orifice diameter of 15 mm (area: 1.77cm²). The temperature was held at 25 °C by a Haake Fisons C1 water circulator (for heating, Thermo Fisher Scientific Inc., Karlsruhe, Germany) with a DLK 1002 cooling unit (FRYKA GmbH, Esslingen, Germany). A continuous stirring speed of 500 rpm was accomplished by an H9-CB-02 stirring apparatus (SES GmbH, Bechenheim, Germany). Similar setups with different fillings or UV measurement with UV- dip probes are possible (µFlux, Pion).

1. Determine drug solubility in acceptor medium (default: 0.2% Vitamin E TPGS in PBS). Drug acceptor concentration must not exceed 1/10 of drug acceptor medium solubility (sink conditions).

Note: Surfactants like Vitamin E TPGS in the donor are necessary to avoid unspecific adsorption of drugs to cell material and to guarantee sink conditions. Other surfactants (like

sodium dodecyl sulfate) may also be applied, if drug solubility in Vitamin E TPGS is too low. Albumin is not recommended due to precipitation in presence of organic solvents during HPLC sample preparation. The acceptor and donor compartment must use the same buffer as solvent to avoid "false efflux" effects.[51]

2. Prepare drug stock solutions (section 3.5, step 2) resulting in a 100-fold concentration of the desired drug donor concentration.

Note: If no bio-realistic concentration could be defined in step 3.1, use the PSO as donor drug concentration as flux is expected to be maximal.[52]

3. Pre-wet PVDF membranes with 50 µl GIT-0 lipid solution as described by manufacturer (surface must appear transparent). Gently wipe off excess lipid solution. Regenerated cellulose membranes can be used without additional preparation.
4. Mount membranes between acceptor and donor cell using two polytetrafluorethylene sealings.
5. Insert cells into clamps, place them on the stirrer and connect cells to water circulation.
6. Fill circulating water system with demineralized water, switch on and set temperature to 25 °C.
7. Fill donor compartment with 9.9 ml of respective medium, fill receiver with 10 ml Vitamin E TPGS 0.2 % solution.
8. Add stir bars, switch on stirrer. Arrange them into the right position with a stirring bar retriever. Wait for 15 min for temperature equilibration. Plug cell openings.
9. Add 100 µl of drug stock solution to the first donor compartment. Start stopwatch. After 30 s add drug stock solution to the next donor compartment and proceed accordingly.

Note: If you use 12 cells and want to draw samples in less than 6 minutes apart from each other, you need two persons, as sample draw time points overlap.

10. After, e.g., 15, 30, 60, 120, 180, and 240 min draw 100 µl from the acceptor compartment into 1.5 ml reaction tube and replace missing volume with fresh acceptor medium.

Note: Sampling time points can be adjusted to drug specific properties (e.g., a fast-precipitating drug needs a steeper sampling steps). 240 min as last time point is bio-realistic, as main drug absorption takes place within this time frame.

11. Add organic solvent (determined in 3.3) to align HPLC gradient.
12. Vortex samples.
13. Centrifuge samples for 15 min at 13000 rpm with MiniSpin centrifuge.
14. Transfer 75 µl of sample to HPLC vials with glass inserts, seal them.
15. Put samples into sample HPLC drawer or freeze samples to -80 °C for later analysis.
16. Run HPLC analysis (3.3).
17. Plot drug donor concentration against time.
18. Calculate slope in linear section and correlate slope to orifice area (=flux) [nmol/(min/cm²)].

Cleaning of diffusion cells:

1. Turn of stirrer and water circulation.
2. Empty water from circulation system, detach cells from system.
3. Empty cells, detach cells, wash donor, receiver cells, and plugs + stirrer separately.
4. Rinse with demineralized water, and 70% v/v isopropanol.
5. Put cells into warm bath with detergents and soak them for several hours.
6. Rinse cells again with demineralized water. Check donor cells for residues.
7. Dry cells and equipment until next experiment.

Note: Donor cells must be carefully cleaned if drug precipitation happened during analysis. Do not use brushes for cell cleaning to avoid roughening of surfaces, which can accelerate drug crystallization.

Statistical analysis

We recommend to pairwise compare all groups of a test set by one-way ANOVA followed by *a post hoc* Tukey test if conditions are fulfilled. A double-sided Grubb's test may be used for outlier testing. Data is considered statistically significant at $p \leq 0.05$. We suggest OriginPro 2020 (OriginLab Corporation) and Minitab (Minitab GmbH, München, Germany) for statistical analysis.

Timing

The total timeline for all experiments is scaled to roughly 2-4 weeks. Time is estimated, as drug specific challenges (e.g., analytical challenges, unexpected stability problems, etc.) might prolong the process. Furthermore, the number of implemented excipients drive process duration. In the timeline presented here, we refer to 5 excipients.

Preparation:

- Estimation of drug/excipient concentrations in the small intestine (2-4 h)
- Preparation of SIFs and medium/excipient mixtures (3-4 h)
- Drug quantification (1-3 d; drug dependent)

Experiments:

- ^{1}H nuclear magnetic resonance spectroscopy for interaction determination (3-4 h)
- Thermodynamic solubility (2-3 d)
- Kinetic solubility (2 d)
- Permeability assays (1-3 weeks)

Anticipated results

We now detail the exact workflow and possible results for the described processes. The first part of the process is the biopharmaceutic characterization of a drug and flux membrane selection (**Figure 1**). At first, the bio-realistic drug concentration at absorption site must be determined. If it is impossible to define bio-realistic concentrations, the highest possible drug concentration for permeability assays should be anticipated. The first experiment qualifies a drug's interaction with SIFs by ^{1}H NMR. Following signal patterns can be derived from signal intensity and signal shift analysis (**Table 1**).

Table 1: Drug classification by ^{1}H NMR aryl-proton signal shift pattern analysis.

Pattern	Medium with highest signal intensity	Mean shift in FeSSIF-V1*	SIF interaction
1	PBS	<8 Hz	No
2	PBS	>8 Hz	Yes
3	FeSSIF-V1	-	Yes

*Compared to PBS

The threshold for signal qualification was referenced to the mean aryl-proton signal shift of metoprolol, a drug classified as not interacting with bile.[14] Drugs categorized into pattern 1 do not show sensitivity towards SIFs. Hence, formulation design is not dependent on SIFs and biopharmaceutic excipient screening is not necessary for those drugs. Still direct drug/excipient interactions must be considered and tested. Drugs categorized into pattern 2 show sensitivity towards SIFs. Nevertheless, signal intensity of those drugs is still highest in PBS correlating with high drug solubility or stable supersaturation in presence of TC/L. Solubility studies and dose number calculations are needed to determine, if biopharmaceutic excipient screening is necessary for those compounds. Drugs categorized into pattern 3 are

also sensitive to SIF and are expected to be PWSDs as signal intensity in absence of TC/L is lower compared to with TC/L (**Chapter I**). Thermodynamic solubilities in PBS, FaSSIF-V1, and FeSSIF-V1 are necessary to quantify the drug/SIF interaction. The dose number in FaSSIF-V1 values solubility results.[53] It helps to identify drugs with anticipated dose related intestinal solubility problems. A dose number greater than 1 means, that the drug dose will be not completely dissolved in the small intestine.

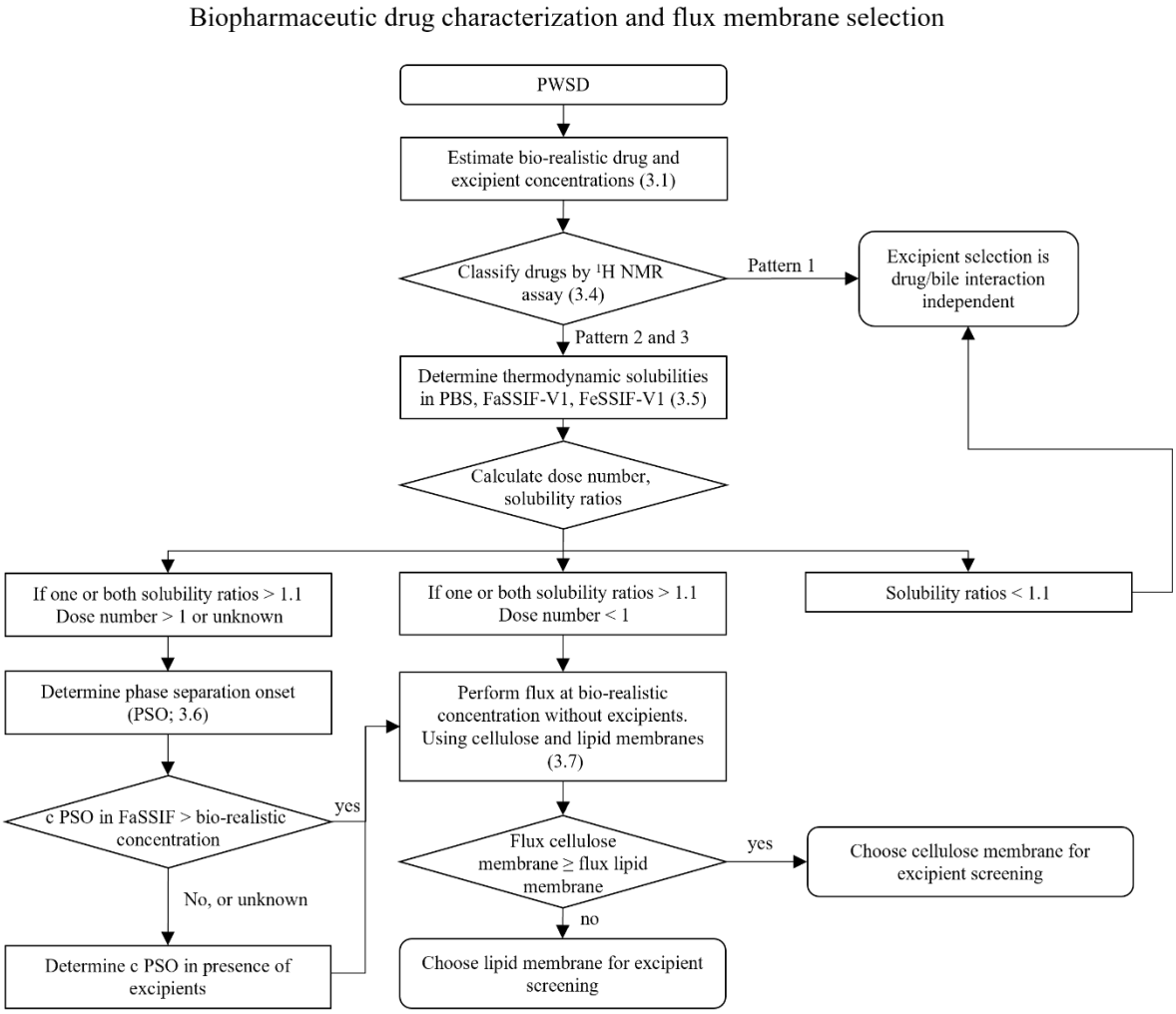

Figure 1: Flowchart of biopharmaceutic drug screening. First, bio-realistic drug concentrations and interaction with SIFs was defined by NMR and thermodynamic solubility. Drugs with a dose number greater than 1 must be checked for PSO in FaSSIF-V1 and in presence of desired excipients. The membrane type representing lowest permeation resistance must be evaluated before biopharmaceutic excipient screening.

The FaSSIF/PBS and FeSSIF/FaSSIF solubility ratio indicates a bile dependent solubility enhancement. Drugs with one solubility ratio greater than 1.1 and a dose number greater than 1 need to be included into the biopharmaceutic excipient screening. Drugs with a Dose number below 1 and one solubility ratio greater than 1.1 should be included into the excipient screening, but the kinetic drug solubility will not play a role for those drug substances (skip

part kinetic solubility). Drugs with no solubility enhancement by SIFs, may also be excluded from biopharmaceutic excipient screening. The threshold applied for critical dose number here is quite arbitrary. Similar decision trees in early phase drug development implementing dose number, for example at Boehringer Ingelheim, set the threshold to a dose number of 10 for enabling excipient screening.[3] They suggested that below this threshold physical drug modification is more important than choosing functional excipients.

PSO determination is necessary to define concentrations for permeation studies for drugs with a high or unknown dose number. If the PSO is above bio-realistic drug concentrations (3.1), use bio-realistic drug concentration for permeation studies. PSO will not occur during further experiments. The bio-realistic concentration is kinetically stabilized in this case. If PSO occurs below bio-realistic concentrations, PSO concentrations must be determined for FaSSIF-V1 and FaSSIF-V1/excipient mixtures. The **u**nstirred **w**ater **l**ayer (**UWL**) can impose the permeation rate limiting step especially for hydrophobic drugs.[54] Therefore, membrane type representing the least diffusion barrier should be identified prior to permeability assays with excipients. Withdraw the membrane representing the highest diffusion barrier from further experiments.

As mentioned above, permeation studies must be conducted at bio-realistic drug concentrations determined in 3.1 (**Figure 2**). If PSO concentration is above bio-realistic drug concentrations, permeation studies must be conducted at this concentration. Sometimes the bio-realistic drug concentration is unknown. Here, flux should be conducted at its maximum, represented by PSO concentration. If bio-realistic drug concentration is beyond the PSO, experiments must be conducted at drug concentrations over PSO and below PSO (e.g., ½ concentration of specific PSO) as biorelevant interactions might be veiled *in vitro* due to overcompensation effects.[52] Furthermore, supersaturation stabilization is a very important factor. If drug supersaturation is not maintained, the driving force for flux will immediately decline. The flux results can be interpreted as follows:

1. Flux with PSO ≥ bio-realistic concentration:
    a. Flux in presence of excipients can be lower, equal, or higher compared to control.
    b. Precipitation might occur reducing duration of stable flux.

Choose excipients with higher or equal flux compared to FaSSIF reference and a precipitation stabilization better or equal to control.

2. Flux PSO < bio-realistic concentration:
    a. Flux in presence of excipients can be lower, equal, or higher compared to control below PSO.
    b. Drug precipitation might occur reducing duration of stable flux above PSO.

Choose excipients with higher or equal flux compared to reference below PSO (no overcompensation effects anticipated) and a precipitation stabilization better than control at bio-realistic concentration above PSO (bio-realistic concentration for precipitation stabilization).

Excipients are either recommended for formulation design or not. Our study paves the way for efficient formulation design with a set of bio-compatible excipients. Further studies need to evaluate formulation principles and optimize excipient use.

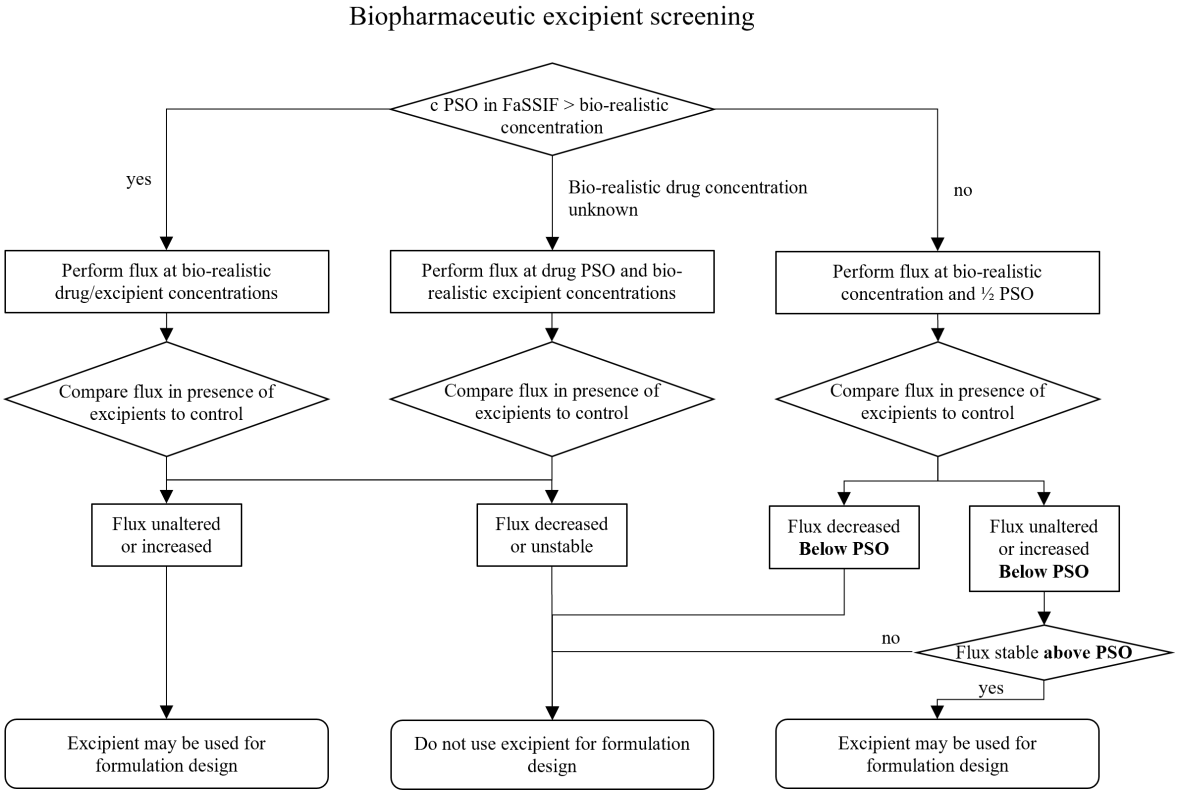

Figure 2: Flowchart of biopharmaceutic excipient screening. The bio-realistic concentration leverages the concentration flux experiments should be conducted. A decreased or instable flux leads to withdrawal of respective excipient, while excipients not impacting and stabilizing flux are desired for formulation design.

Summary

We provided a detailed protocol on the biopharmaceutic excipient screening process designed for PWSDs. In the first step, we profiled the drug interaction with SIFs. We showed how to qualify interaction by ^{1}H NMR and how to quantify interaction by thermodynamic solubility assays and calculation of dose number and bile related solubility enhancement. Biopharmaceutic excipient screening might be only relevant for drugs interacting with SIFs. PSO (= kinetic solubility) determination was described for drugs with high dose numbers and bile related solubility enhancement. Cell-free permeability assays were described. First, membrane representing the lowest resistance for permeation was evaluated. Next, biopharmaceutic excipient screening applying permeation studies was described dependent on a drug's bio-realistic concentration and PSO. With this decision trees, an excipient's suitability for formulation development may be assessed. Our approach can therefore narrow down the number of excipients to be further tested in the formulation development process of orally applied PWSDs.

Acknowledgements

We acknowledge the financial support by Novartis Pharma AG for JS.

References

1. Aungst, B. J., Optimizing Oral Bioavailability in Drug Discovery: An Overview of Design and Testing Strategies and Formulation Options. *J. Pharm. Sci.* **2017,** *106* (4), 921-929.
2. Palucki, M.; Higgins, J. D.; Kwong, E.; Templeton, A. C., Strategies at the interface of drug discovery and development: early optimization of the solid state phase and preclinical toxicology formulation for potential drug candidates. *J. Med. Chem.* **2010,** *53* (16), 5897-905.
3. Zane, P.; Gieschen, H.; Kersten, E.; Mathias, N.; Ollier, C.; Johansson, P.; Van den Bergh, A.; Van Hemelryck, S.; Reichel, A.; Rotgeri, A.; Schafer, K.; Mullertz, A.; Langguth, P., In vivo models and decision trees for formulation development in early drug development: A review of current practices and recommendations for biopharmaceutical development. *Eur. J. Pharm. Biopharm.* **2019,** *142*, 222-231.
4. Fridgeirsdottir, G. A.; Harris, R.; Fischer, P. M.; Roberts, C. J., Support Tools in Formulation Development for Poorly Soluble Drugs. *J. Pharm. Sci.* **2016,** *105* (8), 2260-9.
5. Dahlgren, D.; Venczel, M.; Ridoux, J. P.; Skjold, C.; Mullertz, A.; Holm, R.; Augustijns, P.; Hellstrom, P. M.; Lennernas, H., Fasted and fed state human duodenal fluids: Characterization, drug solubility, and comparison to simulated fluids and with human bioavailability. *Eur. J. Pharm. Biopharm.* **2021,** *163*, 240-251.
6. Flanagan, T.; Van Peer, A.; Lindahl, A., Use of physiologically relevant biopharmaceutics tools within the pharmaceutical industry and in regulatory sciences: Where are we now and what are the gaps? *Eur. J. Pharm. Sci.* **2016,** *91*, 84-90.

7. Chadha, R.; Bhandari, S., Drug-excipient compatibility screening--role of thermoanalytical and spectroscopic techniques. *J. Pharm. Biomed. Anal.* **2014,** *87*, 82-97.
8. Serajuddin, A. T.; Thakur, A. B.; Ghoshal, R. N.; Fakes, M. G.; Ranadive, S. A.; Morris, K. R.; Varia, S. A., Selection of solid dosage form composition through drug-excipient compatibility testing. *J. Pharm. Sci.* **1999,** *88* (7), 696-704.
9. Linn, M.; Collnot, E. M.; Djuric, D.; Hempel, K.; Fabian, E.; Kolter, K.; Lehr, C. M., Soluplus(R) as an effective absorption enhancer of poorly soluble drugs in vitro and in vivo. *Eur. J. Pharm. Sci.* **2012,** *45* (3), 336-43.
10. Overhoff, K. A.; McConville, J. T.; Yang, W.; Johnston, K. P.; Peters, J. I.; Williams, R. O., 3rd, Effect of stabilizer on the maximum degree and extent of supersaturation and oral absorption of tacrolimus made by ultra-rapid freezing. *Pharm. Res.* **2008,** *25* (1), 167-75.
11. Guzman, H. R.; Tawa, M.; Zhang, Z.; Ratanabanangkoon, P.; Shaw, P.; Gardner, C. R.; Chen, H.; Moreau, J. P.; Almarsson, O.; Remenar, J. F., Combined use of crystalline salt forms and precipitation inhibitors to improve oral absorption of celecoxib from solid oral formulations. *J. Pharm. Sci.* **2007,** *96* (10), 2686-702.
12. Reker, D.; Blum, S. M.; Steiger, C.; Anger, K. E.; Sommer, J. M.; Fanikos, J.; Traverso, G., "Inactive" ingredients in oral medications. *Sci. Transl. Med.* **2019,** *11* (483).
13. Fine-Shamir, N.; Dahan, A., Methacrylate-Copolymer Eudragit EPO as a Solubility-Enabling Excipient for Anionic Drugs: Investigation of Drug Solubility, Intestinal Permeability, and Their Interplay. *Mol. Pharmaceutics* **2019,** *16* (7), 2884-2891.
14. Schlauersbach, J.; Hanio, S.; Lenz, B.; Vemulapalli, S. P. B.; Griesinger, C.; Poppler, A. C.; Harlacher, C.; Galli, B.; Meinel, L., Leveraging bile solubilization of poorly water-soluble drugs by rational polymer selection. *J. Control. Release* **2021,** *330*, 36-48.
15. Saal, W.; Wyttenbach, N.; Alsenz, J.; Kuentz, M., Interactions of dimethylaminoethyl methacrylate copolymer with non-acidic drugs demonstrated high solubilization in vitro and pronounced sustained release in vivo. *Eur. J. Pharm. Biopharm.* **2018,** *125*, 68-75.
16. Pinto, J. M. O.; Rengifo, A. F. C.; Mendes, C.; Leao, A. F.; Parize, A. L.; Stulzer, H. K., Understanding the interaction between Soluplus(R) and biorelevant media components. *Colloids Surf. B* **2020,** *187*, 110673.
17. Schiller, C.; Fröhlich, C. P.; Giessmann, T.; Siegmund, W.; Monnikes, H.; Hosten, N.; Weitschies, W., Intestinal fluid volumes and transit of dosage forms as assessed by magnetic resonance imaging. *Aliment. Pharmacol. Ther.* **2005,** *22* (10), 971-9.
18. Peronnet, F.; Mignault, D.; du Souich, P.; Vergne, S.; Le Bellego, L.; Jimenez, L.; Rabasa-Lhoret, R., Pharmacokinetic analysis of absorption, distribution and disappearance of ingested water labeled with D(2)O in humans. *Eur. J. Appl. Physiol.* **2012,** *112* (6), 2213-22.
19. Christfort, J. F.; Strindberg, S.; Plum, J.; Hall-Andersen, J.; Janfelt, C.; Nielsen, L. H.; Müllertz, A., Developing a predictive in vitro dissolution model based on gastrointestinal fluid characterisation in rats. *Eur. J. Pharm. Biopharm.* **2019,** *142*, 307-314.
20. Uchida, K.; Okuno, I.; Takase, H.; Nomura, Y.; Kadowaki, M.; Takeuchi, N., Distribution of bile acids in rats. *Lipids* **1978,** *13* (1), 42-8.
21. Walsh, P. L.; Stellabott, J.; Nofsinger, R.; Xu, W.; Levorse, D.; Galipeau, K.; Kesisoglou, F., Comparing Dog and Human Intestinal Fluids: Implications on Solubility and Biopharmaceutical Risk Assessment. *AAPS PharmSciTech* **2017,** *18* (4), 1408-1416.
22. Arndt, M.; Chokshi, H.; Tang, K.; Parrott, N. J.; Reppas, C.; Dressman, J. B., Dissolution media simulating the proximal canine gastrointestinal tract in the fasted state. *Eur. J. Pharm. Biopharm.* **2013,** *84* (3), 633-41.
23. Henze, L. J.; Koehl, N. J.; Jansen, R.; Holm, R.; Vertzoni, M.; Whitfield, P. D.; Griffin, B. T., Development and evaluation of a biorelevant medium simulating porcine gastrointestinal fluids. *Eur. J. Pharm. Biopharm.* **2020,** *154*, 116-126.
24. McConnell, E. L.; Basit, A. W.; Murdan, S., Measurements of rat and mouse gastrointestinal pH, fluid and lymphoid tissue, and implications for in-vivo experiments. *J. Pharm. Pharmacol.* **2008,** *60* (1), 63-70.

25. Kararli, T. T., Comparison of the gastrointestinal anatomy, physiology, and biochemistry of humans and commonly used laboratory animals. *Biopharm. Drug. Dispos.* **1995,** *16* (5), 351-80.
26. Kambayashi, A.; Murano, M.; Imai, S.; Miyata, K.; Sugita, K.; Fujii, Y.; Kinoshita, M.; Nomura, A.; Kimoto, T.; Miyazaki, Y.; Sakakibara, H.; Kakuda, S.; Tsujimoto, T.; Fujita, Y.; Kano, M.; Nakamura, H.; Akaogi, S.; Honda, M.; Anraku, M.; Kamada, N.; Ohta, K.; Uchida, M.; Kataoka, M.; Kikuchi, H.; Yamashita, S.; Kondo, H., Interspecies differences in gastrointestinal physiology affecting the in vivo performance of oral pharmaceutical solid dosage forms. *J. Drug Delivery Sci. Technol.* **2022,** *67*.
27. Krollik, K.; Lehmann, A.; Wagner, C.; Kaidas, J.; Bulhoff, J.; Kubas, H.; Weitschies, W., Increasing the Robustness of Biopharmaceutical Precipitation Assays - Part II: Recommendations on the use of FaSSIF. *J. Pharm. Sci.* **2022,** *111* (1), 155-163.
28. Kloefer, B.; van Hoogevest, P.; Moloney, R.; Kuentz, M.; Leigh, M. L. S.; Dressman, J., Study of a Standardized Taurocholate– Lecithin Powder for Preparing the Biorelevant Media FeSSIF and FaSSIF. *Diss. Technol.* **2010,** *17* (3), 6-13.
29. Klumpp, L.; Nagasekar, K.; McCullough, O.; Seybert, A.; Ashtikar, M.; Dressman, J., Stability of Biorelevant Media Under Various Storage Conditions. *Diss. Technol.* **2019,** *26* (2), 6-18.
30. Baucke, F. G. K., Further Insight into the Dissociation Mechanism of Glass Electrodes. The Response in Heavy Water. *J. Phys. Chem. B* **1998,** *102* (24), 4835-4841.
31. Lehmann, A.; Krollik, K.; Beran, K.; Hirtreiter, C.; Kubas, H.; Wagner, C., Increasing the Robustness of Biopharmaceutical Precipitation Assays - Part I: Derivative UV Spectrophotometric Method Development for in-line Measurements. *J. Pharm. Sci.* **2022,** *111* (1), 146-154.
32. Winkler, G.; Wolschann, P.; Briza, P.; Heinz, F. X.; Kunz, C., Spectral properties of trifluoroacetic acid—acetonitrile gradient systems for separation of picomole quantities of peptides by reversed-phase high-performance liquid chromatography. *J. Chromatogr. A* **1985,** *347*, 83-88.
33. Hanio, S.; Schlauersbach, J.; Lenz, B.; Spiegel, F.; Bockmann, R. A.; Schweins, R.; Nischang, I.; Schubert, U. S.; Endres, S.; Poppler, A. C.; Brandl, F. P.; Smit, T. M.; Kolter, K.; Meinel, L., Drug-Induced Dynamics of Bile Colloids. *Langmuir* **2021,** *37* (8), 2543-2551.
34. Wiest, J.; Saedtler, M.; Böttcher, B.; Grüne, M.; Reggane, M.; Galli, B.; Holzgrabe, U.; Meinel, L., Geometrical and Structural Dynamics of Imatinib within Biorelevant Colloids. *Mol. Pharmaceutics* **2018,** *15* (10), 4470-4480.
35. Alsenz, J.; Meister, E.; Haenel, E., Development of a partially automated solubility screening (PASS) assay for early drug development. *J. Pharm. Sci.* **2007,** *96* (7), 1748-62.
36. Pudipeddi, M.; Serajuddin, A. T., Trends in solubility of polymorphs. *J. Pharm. Sci.* **2005,** *94* (5), 929-39.
37. Li, X.; Ding, X.; Bian, C.; Wu, S.; Chen, M.; Wang, W.; Wang, J.; Cheng, L., Hydrophobic drug adsorption loss to syringe filters from a perspective of drug delivery. *J. Pharmacol. Toxicol. Met.* **2019,** *95*, 79-85.
38. Kiehm, K.; Dressman, J. B., Evaluation of Drug Adsorption to Membrane Filters under Biowaiver Test Conditions. *Diss. Technol.* **2008,** *15* (4), 13-17.
39. Lindenberg, M.; Wiegand, C.; Dressman, J. B., Comparison of the Adsorption of Several Drugs to Typical Filter Materials. *Diss. Technol.* **2005,** *1* (1), 22-25.
40. Taylor, L. S.; Zhang, G. G. Z., Physical chemistry of supersaturated solutions and implications for oral absorption. *Adv. Drug Delivery Rev.* **2016,** *101*, 122-142.
41. Jackson, M. J.; Kestur, U. S.; Hussain, M. A.; Taylor, L. S., Dissolution of Danazol Amorphous Solid Dispersions: Supersaturation and Phase Behavior as a Function of Drug Loading and Polymer Type. *Mol. Pharmaceutics* **2016,** *13* (1), 223-31.
42. Wilson, V.; Lou, X.; Osterling, D. J.; Stolarik, D. F.; Jenkins, G.; Gao, W.; Zhang, G. G. Z.; Taylor, L. S., Relationship between amorphous solid dispersion in vivo absorption and

in vitro dissolution: phase behavior during dissolution, speciation, and membrane mass transport. *J. Control. Release* **2018,** *292*, 172-182.

43. Li, N.; Mosquera-Giraldo, L. I.; Borca, C. H.; Ormes, J. D.; Lowinger, M.; Higgins, J. D.; Slipchenko, L. V.; Taylor, L. S., A Comparison of the Crystallization Inhibition Properties of Bile Salts. *Cryst. Growth Des.* **2016,** *16* (12), 7286-7300.
44. Indulkar, A. S.; Gao, Y.; Raina, S. A.; Zhang, G. G. Z.; Taylor, L. S., Crystallization from Supersaturated Solutions: Role of Lecithin and Composite Simulated Intestinal Fluid. *Pharm. Res.* **2018,** *35* (8), 158.
45. Ashwathy, P.; Anto, A. T.; Sudheesh, M. S., A mechanistic review on the dissolution phase behavior and supersaturation stabilization of amorphous solid dispersions. *Drug Dev. Ind. Pharm.* **2021,** *47* (1), 1-11.
46. Berben, P.; Bauer-Brandl, A.; Brandl, M.; Faller, B.; Flaten, G. E.; Jacobsen, A. C.; Brouwers, J.; Augustijns, P., Drug permeability profiling using cell-free permeation tools: Overview and applications. *Eur. J. Pharm. Sci.* **2018,** *119*, 219-233.
47. Berben, P.; Brouwers, J.; Augustijns, P., The artificial membrane insert system as predictive tool for formulation performance evaluation. *Int. J. Pharm.* **2018,** *537* (1-2), 22-29.
48. Ingels, F.; Deferme, S.; Destexhe, E.; Oth, M.; Van den Mooter, G.; Augustijns, P., Simulated intestinal fluid as transport medium in the Caco-2 cell culture model. *Int. J. Pharm.* **2002,** *232* (1-2), 183-192.
49. Brouwers, J.; Brewster, M. E.; Augustijns, P., Supersaturating drug delivery systems: the answer to solubility-limited oral bioavailability? *J. Pharm. Sci.* **2009,** *98* (8), 2549-72.
50. O'Shea, J. P.; Augustijns, P.; Brandl, M.; Brayden, D. J.; Brouwers, J.; Griffin, B. T.; Holm, R.; Jacobsen, A. C.; Lennernas, H.; Vinarov, Z.; O'Driscoll, C. M., Best practices in current models mimicking drug permeability in the gastrointestinal tract - An UNGAP review. *Eur. J. Pharm. Sci.* **2022,** *170*, 106098.
51. Neuhoff, S.; Ungell, A. L.; Zamora, I.; Artursson, P., pH-dependent bidirectional transport of weakly basic drugs across Caco-2 monolayers: implications for drug-drug interactions. *Pharm. Res.* **2003,** *20* (8), 1141-8.
52. Elkhabaz, A.; Moseson, D. E.; Brouwers, J.; Augustijns, P.; Taylor, L. S., Interplay of Supersaturation and Solubilization: Lack of Correlation between Concentration-Based Supersaturation Measurements and Membrane Transport Rates in Simulated and Aspirated Human Fluids. *Mol. Pharmaceutics* **2019,** *16* (12), 5042-5053.
53. Wuelfing, W. P.; El Marrouni, A.; Lipert, M. P.; Daublain, P.; Kesisoglou, F.; Converso, A.; Templeton, A. C., Dose Number as a Tool to Guide Lead Optimization for Orally Bioavailable Compounds in Drug Discovery. *J. Med. Chem.* **2022,** *65* (3), 1685-1694.
54. Sugano, K.; Kataoka, M.; Mathews Cda, C.; Yamashita, S., Prediction of food effect by bile micelles on oral drug absorption considering free fraction in intestinal fluid. *Eur. J. Pharm. Sci.* **2010,** *40* (2), 118-24.

Conclusion and outlook

Most emerging new drug candidates can be categorized as **p**oorly **w**ater-**s**oluble **d**rugs (**PWSDs**).[1-3] Formulation development of orally applied PWSDs is time consuming and cost intensive compared to the development of water-soluble and highly permeable drugs.[4] The **b**iopharmaceutic **c**lassification **s**ystem (**BCS**) helps to identify critical drugs, prior to drug formulation development.[5-7] BCS class II drugs are poorly water-soluble, but highly permeable. BCS class IV drugs are poorly water-soluble and low permeable drugs. Formulation development of BCS class IV compounds is challenging as permeation properties can be hardly amended by formulation design.[8] On the other side, formulation scientists have a well filled toolbox to overcome poor water solubility of BCS class II drugs.[9] Decision trees effectively guide formulation scientists during formulation design.[10] Almost every pharmaceutical company established their own decision trees or formulation guidelines. Unfortunately, these decision trees are often restricted to company internal use. Summarized, their focus lies on physical drug state characterization as a base for formulation suggestions. Most available PWSD formulation strategies reach for maximization of a drug's apparent solubility.[11] This can be either achieved by modifying the physical state of a drug (nano-milling[12], salt design[13, 14]) and/or by excipient-based approaches (lipid-based delivery systems[15], **a**morphous **s**olid **d**ispersion**s** (**ASDs**)[16], solubility enhancers[17, 18]). Simulated intestinal fluids are already implemented at this development stage to predict the solubility of PWSDs in the gastrointestinal system.[19] Simulated intestinal fluids are composed of bile salts and lecithin mimicking bile.[20] Furthermore, various *in vitro* setups have been described to imitate biopharmaceutic drug permeability.[21] Not only PWSDs, but also excipients might interact with bile affecting overall drug bioavailability.[22, 23] Unfortunately, less effort has been put on mechanistical explanations regarding excipient/bile interactions.[24] Summarized, we hypothesized that bile/drug/excipient interplay can be evaluated with *in vitro* and *in silico* methods to predict bile dependent drug pharmacokinetics paving the way for rational drug formulation design of PWSDs.

This thesis detailed this interaction interplay between drugs, excipients, and bile on a molecular level. A ^{1}H NMR based algorithm was described for identifying bile interacting drugs *in silico*. Furthermore, *in vitro* methods like kinetic/thermodynamic solubility, dissolution rate, and flux were described to evaluate excipients regarding their biopharmaceutic compatibility for bile interacting drugs condensed into an applicable

decision tree. The *in vivo* relevance of this excipient screening process was confirmed by two animal studies.

We suggested that beyond the physical drug characterization in early drug formulation development processes, bile impact on drug related physicochemical parameters should be assessed. Bile is always present in the small intestine and a potential interaction partner.[25, 26] Some drugs benefit from solubilization by bile or by the stabilization of drug supersaturation.[27, 28] Therefore, it was anticipated that the positive food effect of PWSDs correlates with bile mediated solubility enhancement.[29, 30] The food effect of a drug is a substantial information for drug formulation development, especially for the design of clinical studies.[31, 32] Unfortunately, food effect has multiple reasons and remains challenging to predict, as not only bile, but other factors, such as prolonged gastrointestinal passage, enzymatic stability, food components, or transporter inhibition might outrank bile mediated solubility.[33-35] The benefit of intestinal solubilization does not always correlate with poor drug water solubility. Even PWSDs can be divided into bile interacting and bile non-interacting drugs (**Chapter I**). ^{1}H NMR was proposed as a potential tool for interaction characterization.[36, 37] Our study included 141 drugs, which were analyzed regarding aryl-proton signal shift in presence and absence of bile and lipids. The shift of the non-bile interacting, highly permeable and water-soluble drug Metoprolol was set as reference shift for studies. Metoprolol is furthermore listed by the FDA as a reference drug for the low/high permeability drug class boundary.[38] Drugs were classified as bile and lipid interacting or non-interacting by shift analysis. Structural property relationship analysis revealed that bile interaction correlated with drug polarizability and lipophilicity. Similar postulations were proposed elsewhere.[39-41] The predictive algorithm had a balanced accuracy of 0.8, which makes it a promising *in silico* screening tool. A high probability for bile interaction correlated in part with a positive food effect and was at least as predictive as solubility studies in simulated intestinal fluids.[30] Nevertheless, *in silico* prediction of drug specific food effect solely by calculated drug parameters remains a herculean challenge, which future studies might address.[42, 43]

Traditionally solubility studies are conducted at early phase of drug formulation development to predict the bio-performance of a drug formulation.[44, 45] Furthermore, dissolution rate,[46] kinetic drug solubility,[47] and drug permeability experiments[21] may be used to extrapolate drug performance *in vivo*.[48] We and others proposed that usage of simulated

intestinal fluids is mandatory for the *in vitro* to *in vivo* portability.[43, 49, 50] There are several examples available in literature were simulated intestinal fluids were not used for *in vitro* experiments which led to wrong decisions for *in vivo* formulations.[22, 51] Furthermore, we hypothesized that the impact of excipients on bile also impacted bile mediated drug solubility enhancement. We showed *in vitro* that interaction of excipients with simulated bile reduced the free drug fraction for the bile interacting Perphenazine and Imatinib but not for the bile non-interacting Metoprolol (**Chapter II**). Free drug fraction mainly determines passive drug absorption.[29] This impact was further evaluated in an animal model (**Chapter III**). *In vivo*, bile interacting excipients reduced bioavailability of Perphenazine, but not Metoprolol. We defined another recently developed drug, the MAP-kinase inhibitor Naporafenib[52], as bile interacting. A pharmacokinetic study in beagle dogs showed, that the usage of simulated intestinal fluids was mandatory to draw the right conclusions about biopharmaceutic excipient evaluation (**Chapter IV**). Superior outcome on drug absorption was predicted for the bile non interacting excipient, only when simulated intestinal fluids were applied *in vitro*. Nevertheless, the here presented interaction between drug excipients and bile resembles only a small part of drug formulation development.[44] Drug specific delivery challenges like poor enzymatic stability, dissolution rate, poor permeability, etc. might outline the importance of a biopharmaceutic excipient screening. However, the biopharmaceutic excipient screening is applicable for bile interacting drugs with low intestinal solubility.[53]

Therefore, an overarching approach for future rational formulation design would use large databases to identify the most critical drug property, formulation design must address. Our developed bile interaction algorithm might be integrated into existing *in silico* approaches. The molecular and mechanistical insight into the interplay of drugs, excipients, and bile fueled a step-by-step instruction for the biopharmaceutic excipient screening (**Chapter V**). It represents an applicable tool for early phase drug formulation development. Pre-selection of bio-pharmaceutically suited excipients is guided. This might serve as an additional tool for formulation scientists towards rational formulation design. It also narrows down the number of possible excipients for development. It accelerates the development process as e.g., less time-consuming stability tests for drug/excipient combinations must be screened.[54]

Conclusively, traditional trial and error approaches within drug formulation development are and will be more and more replaced by high complex and sophisticated decision trees and *in silico* tools. Unfortunately, most of this knowledge is generated in pharmaceutical industry

and knowledge is restricted to company internal use. Data transfer is often limited due to patent reasons. Academia struggles with limited experimental capability. Nevertheless, in this thesis we accumulated the state-of-the-art knowledge about the interaction screening between drugs excipients and bile, which might serve formulation scientists a blueprint for an implementable workflow within rational formulation design. Future studies may expand research towards *in silico*-driven formulation design approaches.

References

1. Waring, M. J.; Arrowsmith, J.; Leach, A. R.; Leeson, P. D.; Mandrell, S.; Owen, R. M.; Pairaudeau, G.; Pennie, W. D.; Pickett, S. D.; Wang, J.; Wallace, O.; Weir, A., An analysis of the attrition of drug candidates from four major pharmaceutical companies. *Nat. Rev. Drug Discovery* **2015,** *14* (7), 475-86.
2. van Hoogevest, P.; Liu, X.; Fahr, A., Drug delivery strategies for poorly water-soluble drugs: the industrial perspective. *Expert Opin. Drug Delivery* **2011,** *8* (11), 1481-500.
3. Vo, C. L.; Park, C.; Lee, B. J., Current trends and future perspectives of solid dispersions containing poorly water-soluble drugs. *Eur. J. Pharm. Biopharm.* **2013,** *85* (3 Pt B), 799-813.
4. Kawabata, Y.; Wada, K.; Nakatani, M.; Yamada, S.; Onoue, S., Formulation design for poorly water-soluble drugs based on biopharmaceutics classification system: basic approaches and practical applications. *Int. J. Pharm.* **2011,** *420* (1), 1-10.
5. Lipinski, C. A.; Lombardo, F.; Dominy, B. W.; Feeney, P. J., Experimental and computational approaches to estimate solubility and permeability in drug discovery and development settings. *Adv. Drug Delivery Rev.* **1997,** *23* (1-3), 3-25.
6. Chatzizacharia, K.; Hatziavramidis, D., New frames of reference for mapping drugs in the four classes of the BCS and BDDCS into regions with clear boundaries. *AIChE J.* **2015,** *61* (11), 3570-3579.
7. Fridgeirsdottir, G. A.; Harris, R.; Fischer, P. M.; Roberts, C. J., Support Tools in Formulation Development for Poorly Soluble Drugs. *J. Pharm. Sci.* **2016,** *105* (8), 2260-9.
8. Ghadi, R.; Dand, N., BCS class IV drugs: Highly notorious candidates for formulation development. *J. Control. Release* **2017,** *248*, 71-95.
9. K.P.R, C.; A, P. K., Recent Research on Formulation Development of BCS Class II Drugs – A Review. *Int. res. j. pharm. appl. sci.* **2013,** *3* (1), 173-181.
10. Zane, P.; Gieschen, H.; Kersten, E.; Mathias, N.; Ollier, C.; Johansson, P.; Van den Bergh, A.; Van Hemelryck, S.; Reichel, A.; Rotgeri, A.; Schafer, K.; Mullertz, A.; Langguth, P., In vivo models and decision trees for formulation development in early drug development: A review of current practices and recommendations for biopharmaceutical development. *Eur. J. Pharm. Biopharm.* **2019,** *142*, 222-231.
11. Li, P.; Zhao, L., Developing early formulations: practice and perspective. *Int. J. Pharm.* **2007,** *341* (1-2), 1-19.
12. Merisko-Liversidge, E.; Liversidge, G. G., Nanosizing for oral and parenteral drug delivery: a perspective on formulating poorly-water soluble compounds using wet media milling technology. *Adv. Drug Delivery Rev.* **2011,** *63* (6), 427-40.
13. Wiest, J.; Saedtler, M.; Balk, A.; Merget, B.; Widmer, T.; Bruhn, H.; Raccuglia, M.; Walid, E.; Picard, F.; Stopper, H.; Dekant, W.; Luhmann, T.; Sotriffer, C.; Galli, B.; Holzgrabe, U.; Meinel, L., Mapping the pharmaceutical design space by amorphous ionic liquid strategies. *J. Control. Release* **2017,** *268*, 314-322.
14. Reggane, M.; Wiest, J.; Saedtler, M.; Harlacher, C.; Gutmann, M.; Zottnick, S. H.; Piechon, P.; Dix, I.; Muller-Buschbaum, K.; Holzgrabe, U.; Meinel, L.; Galli, B.,

Bioinspired co-crystals of Imatinib providing enhanced kinetic solubility. *Eur. J. Pharm. Biopharm.* **2018,** *128*, 290-299.

15. Feeney, O. M.; Crum, M. F.; McEvoy, C. L.; Trevaskis, N. L.; Williams, H. D.; Pouton, C. W.; Charman, W. N.; Bergstrom, C. A. S.; Porter, C. J. H., 50years of oral lipid-based formulations: Provenance, progress and future perspectives. *Adv. Drug Delivery Rev.* **2016,** *101*, 167-194.
16. Baghel, S.; Cathcart, H.; O'Reilly, N. J., Polymeric Amorphous Solid Dispersions: A Review of Amorphization, Crystallization, Stabilization, Solid-State Characterization, and Aqueous Solubilization of Biopharmaceutical Classification System Class II Drugs. *J. Pharm. Sci.* **2016,** *105* (9), 2527-2544.
17. Linn, M.; Collnot, E. M.; Djuric, D.; Hempel, K.; Fabian, E.; Kolter, K.; Lehr, C. M., Soluplus(R) as an effective absorption enhancer of poorly soluble drugs in vitro and in vivo. *Eur. J. Pharm. Sci.* **2012,** *45* (3), 336-43.
18. Jansook, P.; Ogawa, N.; Loftsson, T., Cyclodextrins: structure, physicochemical properties and pharmaceutical applications. *Int. J. Pharm.* **2018,** *535* (1-2), 272-284.
19. Riethorst, D.; Mols, R.; Duchateau, G.; Tack, J.; Brouwers, J.; Augustijns, P., Characterization of Human Duodenal Fluids in Fasted and Fed State Conditions. *J. Pharm. Sci.* **2016,** *105* (2), 673-681.
20. Dahlgren, D.; Venczel, M.; Ridoux, J. P.; Skjold, C.; Mullertz, A.; Holm, R.; Augustijns, P.; Hellstrom, P. M.; Lennernas, H., Fasted and fed state human duodenal fluids: Characterization, drug solubility, and comparison to simulated fluids and with human bioavailability. *Eur. J. Pharm. Biopharm.* **2021,** *163*, 240-251.
21. O'Shea, J. P.; Augustijns, P.; Brandl, M.; Brayden, D. J.; Brouwers, J.; Griffin, B. T.; Holm, R.; Jacobsen, A. C.; Lennernas, H.; Vinarov, Z.; O'Driscoll, C. M., Best practices in current models mimicking drug permeability in the gastrointestinal tract - An UNGAP review. *Eur. J. Pharm. Sci.* **2022,** *170*, 106098.
22. Saal, W.; Wyttenbach, N.; Alsenz, J.; Kuentz, M., Interactions of dimethylaminoethyl methacrylate copolymer with non-acidic drugs demonstrated high solubilization in vitro and pronounced sustained release in vivo. *Eur. J. Pharm. Biopharm.* **2018,** *125*, 68-75.
23. Pinto, J. M. O.; Rengifo, A. F. C.; Mendes, C.; Leao, A. F.; Parize, A. L.; Stulzer, H. K., Understanding the interaction between Soluplus(R) and biorelevant media components. *Colloids Surf. B* **2020,** *187*, 110673.
24. Pigliacelli, C.; Belton, P.; Wilde, P.; Qi, S., Probing the molecular interactions between pharmaceutical polymeric carriers and bile salts in simulated gastrointestinal fluids using NMR spectroscopy. *J. Colloid Interface Sci.* **2019,** *551*, 147-154.
25. Wiest, J.; Saedtler, M.; Böttcher, B.; Grüne, M.; Reggane, M.; Galli, B.; Holzgrabe, U.; Meinel, L., Geometrical and Structural Dynamics of Imatinib within Biorelevant Colloids. *Mol. Pharmaceutics* **2018,** *15* (10), 4470-4480.
26. Vogtherr, M.; Marx, A.; Mieden, A. C.; Saal, C., Investigation of solubilising effects of bile salts on an active pharmaceutical ingredient with unusual pH dependent solubility by NMR spectroscopy. *Eur. J. Pharm. Biopharm.* **2015,** *92*, 32-41.
27. Indulkar, A. S.; Gao, Y.; Raina, S. A.; Zhang, G. G. Z.; Taylor, L. S., Crystallization from Supersaturated Solutions: Role of Lecithin and Composite Simulated Intestinal Fluid. *Pharm. Res.* **2018,** *35* (8), 158.
28. Pavlovic, N.; Golocorbin-Kon, S.; Danic, M.; Stanimirov, B.; Al-Salami, H.; Stankov, K.; Mikov, M., Bile Acids and Their Derivatives as Potential Modifiers of Drug Release and Pharmacokinetic Profiles. *Front. Pharmacol.* **2018,** *9*.
29. Sugano, K.; Kataoka, M.; Mathews Cda, C.; Yamashita, S., Prediction of food effect by bile micelles on oral drug absorption considering free fraction in intestinal fluid. *Eur. J. Pharm. Sci.* **2010,** *40* (2), 118-24.
30. Kawai, Y.; Fujii, Y.; Tabata, F.; Ito, J.; Metsugi, Y.; Kameda, A.; Akimoto, K.; Takahashi, M., Profiling and Trend Analysis of Food Effects on Oral Drug Absorption Considering Micelle Interaction and Solubilization by Bile Micelles. *Drug Metab. Pharmacokinet.* **2011,** *26* (2), 180-191.

31. Cheng, L.; Wong, H., Food Effects on Oral Drug Absorption: Application of Physiologically-Based Pharmacokinetic Modeling as a Predictive Tool. *Pharmaceutics* **2020,** *12* (7), 672.
32. Lentz, K. A., Current Methods for Predicting Human Food Effect. *AAPS J.* **2008,** *10* (2), 282-8.
33. Bennett-Lenane, H.; Griffin, B. T.; O'Shea, J. P., Machine learning methods for prediction of food effects on bioavailability: A comparison of support vector machines and artificial neural networks. *Eur. J. Pharm. Sci.* **2022,** *168*, 106018.
34. Deng, J.; Zhu, X.; Chen, Z.; Fan, C. H.; Kwan, H. S.; Wong, C. H.; Shek, K. Y.; Zuo, Z.; Lam, T. N., A Review of Food-Drug Interactions on Oral Drug Absorption. *Drugs* **2017,** *77* (17), 1833-1855.
35. Riedmaier, A. E.; DeMent, K.; Huckle, J.; Bransford, P.; Stillhart, C.; Lloyd, R.; Alluri, R.; Basu, S.; Chen, Y.; Dhamankar, V.; Dodd, S.; Kulkarni, P.; Olivares-Morales, A.; Peng, C. C.; Pepin, X.; Ren, X.; Tran, T.; Tistaert, C.; Heimbach, T.; Kesisoglou, F.; Wagner, C.; Parrott, N., Use of Physiologically Based Pharmacokinetic (PBPK) Modeling for Predicting Drug-Food Interactions: an Industry Perspective. *AAPS J.* **2020,** *22* (6), 123.
36. LaPlante, S. R.; Carson, R.; Gillard, J.; Aubry, N.; Coulombe, R.; Bordeleau, S.; Bonneau, P.; Little, M.; O'Meara, J.; Beaulieu, P. L., Compound aggregation in drug discovery: implementing a practical NMR assay for medicinal chemists. *J. Med. Chem.* **2013,** *56* (12), 5142-50.
37. Matsuoka, K.; Yamamoto, A., Study on Micelle Formation of Bile Salt Using Nuclear Magnetic Resonance Spectroscopy. *J. Oleo Sci.* **2017,** *66* (10), 1129-1137.
38. Dahan, A.; Miller, J. M.; Hilfinger, J. M.; Yamashita, S.; Yu, L. X.; Lennernas, H.; Amidon, G. L., High-permeability criterion for BCS classification: segmental/pH dependent permeability considerations. *Mol. Pharmaceutics* **2010,** *7* (5), 1827-34.
39. Ottaviani, G.; Gosling, D. J.; Patissier, C.; Rodde, S.; Zhou, L.; Faller, B., What is modulating solubility in simulated intestinal fluids? *Eur. J. Pharm. Sci.* **2010,** *41* (3-4), 452-7.
40. Fagerberg, J. H.; Karlsson, E.; Ulander, J.; Hanisch, G.; Bergstrom, C. A., Computational prediction of drug solubility in fasted simulated and aspirated human intestinal fluid. *Pharm. Res.* **2015,** *32* (2), 578-89.
41. Niederquell, A.; Kuentz, M., Biorelevant Drug Solubility Enhancement Modeled by a Linear Solvation Energy Relationship. *J. Pharm. Sci.* **2018,** *107* (1), 503-506.
42. Tistaert, C.; Heimbach, T.; Xia, B.; Parrott, N.; Samant, T. S.; Kesisoglou, F., Food Effect Projections via Physiologically Based Pharmacokinetic Modeling: Predictive Case Studies. *J. Pharm. Sci.* **2019,** *108* (1), 592-602.
43. Fagerberg, J. H.; Bergstrom, C. A., Intestinal solubility and absorption of poorly water soluble compounds: predictions, challenges and solutions. *Ther. Delivery* **2015,** *6* (8), 935-59.
44. Aungst, B. J., Optimizing Oral Bioavailability in Drug Discovery: An Overview of Design and Testing Strategies and Formulation Options. *J. Pharm. Sci.* **2017,** *106* (4), 921-929.
45. Palucki, M.; Higgins, J. D.; Kwong, E.; Templeton, A. C., Strategies at the interface of drug discovery and development: early optimization of the solid state phase and preclinical toxicology formulation for potential drug candidates. *J. Med. Chem.* **2010,** *53* (16), 5897-905.
46. Balk, A.; Holzgrabe, U.; Meinel, L., 'Pro et contra' ionic liquid drugs - Challenges and opportunities for pharmaceutical translation. *Eur. J. Pharm. Biopharm.* **2015,** *94*, 291-304.
47. Taylor, L. S.; Zhang, G. G. Z., Physical chemistry of supersaturated solutions and implications for oral absorption. *Adv. Drug Delivery Rev.* **2016,** *101*, 122-142.
48. Wilson, C. G.; Aarons, L.; Augustijns, P.; Brouwers, J.; Darwich, A. S.; De Waal, T.; Garbacz, G.; Hansmann, S.; Hoc, D.; Ivanova, A.; Koziolek, M.; Reppas, C.; Schick, P.; Vertzoni, M.; Garcia-Horsman, J. A., Integration of advanced methods and models to study drug absorption and related processes: An UNGAP perspective. *Eur. J. Pharm. Sci.* **2022,** *172*, 106100.

49. Abuhassan, Q.; Khadra, I.; Pyper, K.; Augustijns, P.; Brouwers, J.; Halbert, G. W., Fasted intestinal solubility limits and distributions applied to the biopharmaceutics and developability classification systems. *Eur. J. Pharm. Biopharm.* **2022,** *170*, 160-169.
50. Riethorst, D.; Brouwers, J.; Motmans, J.; Augustijns, P., Human intestinal fluid factors affecting intestinal drug permeation in vitro. *Eur. J. Pharm. Sci.* **2018,** *121*, 338-346.
51. Fine-Shamir, N.; Dahan, A., Methacrylate-Copolymer Eudragit EPO as a Solubility-Enabling Excipient for Anionic Drugs: Investigation of Drug Solubility, Intestinal Permeability, and Their Interplay. *Mol. Pharmaceutics* **2019,** *16* (7), 2884-2891.
52. Ramurthy, S.; Taft, B. R.; Aversa, R. J.; Barsanti, P. A.; Burger, M. T.; Lou, Y.; Nishiguchi, G. A.; Rico, A.; Setti, L.; Smith, A.; Subramanian, S.; Tamez, V.; Tanner, H.; Wan, L.; Hu, C.; Appleton, B. A.; Mamo, M.; Tandeske, L.; Tellew, J. E.; Huang, S.; Yue, Q.; Chaudhary, A.; Tian, H.; Iyer, R.; Hassan, A. Q.; Mathews Griner, L. A.; La Bonte, L. R.; Cooke, V. G.; Van Abbema, A.; Merritt, H.; Gampa, K.; Feng, F.; Yuan, J.; Mishina, Y.; Wang, Y.; Haling, J. R.; Vaziri, S.; Hekmat-Nejad, M.; Polyakov, V.; Zang, R.; Sethuraman, V.; Amiri, P.; Singh, M.; Sellers, W. R.; Lees, E.; Shao, W.; Dillon, M. P.; Stuart, D. D., Design and Discovery of N-(3-(2-(2-Hydroxyethoxy)-6-morpholinopyridin-4-yl)-4-methylphenyl)-2-(trifluorom ethyl)isonicotinamide, a Selective, Efficacious, and Well-Tolerated RAF Inhibitor Targeting RAS Mutant Cancers: The Path to the Clinic. *J. Med. Chem.* **2020,** *63* (5), 2013-2027.
53. Wuelfing, W. P.; El Marrouni, A.; Lipert, M. P.; Daublain, P.; Kesisoglou, F.; Converso, A.; Templeton, A. C., Dose Number as a Tool to Guide Lead Optimization for Orally Bioavailable Compounds in Drug Discovery. *J. Med. Chem.* **2022,** *65* (3), 1685-1694.
54. Chadha, R.; Bhandari, S., Drug-excipient compatibility screening--role of thermoanalytical and spectroscopic techniques. *J. Pharm. Biomed. Anal.* **2014,** *87*, 82-97.

Abbreviations

^{1}H NMR	^{1}H nuclear magnetic resonance
1D	One-dimensional
2D	Two-dimensional
ACN	Acetonitrile
API	Active pharmaceutical ingredient
ASB	Acceptor sink buffer
ASD	Amorphous solid dispersion
AUC	Area under the curve
AUC_{inf}	AUC to infinity using λz
AUC_{last}	Area under the curve to last nonzero concentration using linear up and down method
BAcc	Balanced accuracy
BCS	Biopharmaceutical classification system
Cl/F	Oral clearance calculated from observed last measurable plasma concentration
C_{max}	Maximum plasma concentration
Colesevelam	Modified polyallylamine
COSY	^{13}C, ^{1}H-^{1}H correlated spectroscopy
CV	Cross validation
D	Diffusion coefficient
Da	Dalton
DFG	Deutsche Forschungsgemeinschaft
DLS	Dynamic light scattering
DMSO	Hexadeuterodimethyl sulfoxide
DOSY	Diffusion-ordered spectroscopy
EFRE	Europäischer Fonds für regionale Entwicklung
ESI	Electrospray ionization
Eudragit E	Amino methacrylate copolymer
F	Fraction absorbed
FaSSIF-V1	Fasted state simulated intestinal fluid version 1
FDA	Food and Drug Administration

FeSSIF-V1	Fed state simulated intestinal fluid version 1
FeSSIF-V2	Fed state simulated intestinal fluid version 2
FS	Filtered set
GIT	Gastrointestinal
HIRI	Helmholtz Institute for RNA-based Infection Biology
HPC	Hydroxypropyl cellulose
HPLC	High pressure liquid chromatography
HPMC-AS	Hydroxypropyl methylcellulose acetate succinate
HS	Holdout set
HSQC	^{1}H-^{13}C heteronuclear single quantum coherence
i.v.	Intravascular
ka	Absorption kinetics
Kollidon VA 64	Vinylpyrrolidone-vinyl acetate copolymer
L	Lecithin
LC-MS/MS	Liquid chromatography with coupled mass spectrometry
LGPS	Liquid-glasslike phase separation
LLPS	Liquid-liquid phase separation
LOD	Limit of detection
LOQ	Limit of quantification
λ_z	Estimated terminal rate constant
MIM	Mixed micelles
MOE	Molecular operating environment
MRM	Multiple reaction monitoring
MRT_{inf}	Mean residual time to infinity using λ_z
MRT_{last}	Mean residual time to last nonzero concentration
NOESY	Nuclear Overhauser enhancement spectroscopy
NPF	Naporafenib
OD	Optical density
P	Perphenazine
p.o.	Peroral
PAMPA	Parallel artificial membrane permeability assay
PBS	Phosphate buffered saline

PCB	Phosphate citrate buffer
PDI	Polydispersity index
PK	Pharmacokinetic
PSO	Phase separation onset
PVDF	Polyvinylidene difluoride
PWSD	Poorly water-soluble drug
QSPR	Quantitative structure-property relationships
RFE	Recursive feature extraction
RH40	Polyethylene glycol-40 hydrogenated castor oil
RI	Refractive index
ROC	Receiver operating characteristic
RP	Reversed phase
S/N	Signal to noise
SIF	Simulated intestinal fluid
Soluplus	Polyvinyl caprolactam–polyvinyl acetate–polyethylene glycol graft copolymer
TC	Taurocholate
TFA	Trifluoroacetic acid
t_{max}	Time of maximum plasma concentration
TS	Training set
TSP-d_4	Trimethylsilyl-propionic-2,2,3,3-d_4 sodium salt
UHPLC	Ultra-high performance liquid chromatography
UWL	Unstirred water layer
V_Z/F	Apparent volume of distribution by fraction absorbed

Publications

Schlauersbach, J.; Hanio, S.; et al., Bile and excipient interactions directing drug pharmacokinetics in rats. *Eur. J. Pharm. Biopharm.* (2022), 178, 65-68

Schlauersbach, J.; Kehrein, J.; et. al., Predicting Bile and Lipid Interaction for Drug Substances. *Mol. Pharmaceutics* 2022, 19 (8), 2868-2876

Endres, S.; Karaev, E.; et al., Concentration and composition dependent aggregation of Pluronic- and Poly-(2-oxazolin)-Efavirenz formulations in biorelevant media. *J. Colloid Interface Sci.* 2022, 606 (Pt 2), 1179-1192.

Hanio, S.; Schlauersbach, J.; et al., Drug-Induced Dynamics of Bile Colloids. *Langmuir* 2021, 37 (8), 2543-2551.

Schlauersbach, J.; Hanio, S.; et al., Leveraging bile solubilization of poorly water-soluble drugs by rational polymer selection. *J. Controlled Release* 2021, 330, 36-48.

Güntzel, P.; Schilling, K.; et al., Bioinspired Ion Pairs Transforming Papaverine into a Protic Ionic Liquid and Salts. *ACS Omega* 2020, 5 (30), 19202-19209.

Chamberlain, R.; Schlauersbach, J.; et al., Freeze-drying in protective bags: Characterization of heat and mass transfer. *Eur. J. Pharm. Biopharm*. 2020, 154, 309-316.

Pöppler, A. C.; Lübtow, M. M.; et al., Loading-Dependent Structural Model of Polymeric Micelles Encapsulating Curcumin by Solid-State NMR Spectroscopy. *Angew. Chem. Int. Ed. Engl.* 2019, 58 (51), 18540-18546.

Posters/Presentations

Schlauersbach, J.; Wiest, J. Detecting compound aggregation in aqueous and biorelevant media by nuclear magnet resonance (NMR) spectroscopy. *qNMR Summit* 2018, Würzburg

Schlauersbach, J.; Wiest, J. Pharmaceutical profiling of Imatinib for bile interaction using ^{1}H-NMR spectroscopy. *3rd European Conference on Pharmaceutics* 2019, Bologna

Schlauersbach, J.; Hanio, S. Polymers in oral formulations – truly inert excipients? *24th CRS Annual meeting* 2020, Munich

Schlauersbach, J.; Hanio, S. Leveraging bile solubilization of poorly water-soluble drugs by rational polymer selection**.** *13th International Conference and Workshop on Biological Barriers* 2021, Saarbrücken (online)

Acknowledgements

I would like to thank Prof. Dr. Dr. Lorenz Meinel giving me the opportunity to join his research group on the excellent topic on poorly-water soluble drug and bile interaction working closely together with the PHAD CPP and DP department from Novartis, Basel, Switzerland. Thank you for providing the connection and accessibility to the vast number of methods used in here. I am grateful for all his helpful advice, ideas, and scientific training throughout the years.

Furthermore, I would like to thank Dr. Cornelius Harlacher, Dr. Bruno Galli, and Dominic Werthmüller from Novartis for providing valuable scientific input and sharing fruitful thoughts and discussions. This helped a lot to bring the topic to a contemporary relevance. Of course, I would like to thank Novartis for financially supporting our research.

Prof. Dr. Ann-Christin Pöppler from the institute of organic chemistry is gratefully acknowledged for giving best advice and support in the complex field of NMR measurements and co-refereeing this thesis. I thank Dr. Sebastian Endres, Theresa Zorn for their help on complex 2D-NMR measurements. My gratitude is also directed to Dr. Johannes Wiest for paving the way in my first year, Curd Schollmayer for introduction into NMR, Prof. Dr. Oliver Scherf-Clavel for teaching me pharmacokinetics, Sebastian Zimmermann for LC-MS/MS guidance, Prof. Dr. Sotriffer for modeling expertise, and Josef Kehrein for QSPR modeling.

I would like to thank my PhD colleagues for all their help and support in the lab. Special thanks are to Simon Hanio and Lena Scheller for extraordinary great teamwork and mischief, Bettina Lenz for her help in the daily routine, Christine Schneider for advanced management, and Marco Saedtler for introduction into Sirius. I thank Dr. Anke Ritter and Yvonne Portsch for keeping me as a part-time member at the Schloss-Apotheke Arnstadt.

Finally, I am truly grateful to my parents Harry and Gabi, my brother Robin, my best friend Sven, the Theater Dreieck, Franzi, Daniel, Katrin, Rainer, and all my other close friends for their emotional support and encouragement. I thank my wife Annika for being always at my side and sharing all moments in the past years with her heartily and supportive personality that makes life worth living.

Documentation of authorship

This section contains a list of the individual contribution for each author to the publications reprinted in this thesis. Unpublished manuscripts are handled, accordingly.

Julius-Maximilians-
UNIVERSITÄT
WÜRZBURG

Fakultät für
CHEMIE UND
PHARMAZIE

Erklärung zur Autorenschaft

Chapter I: "Predicting bile and lipid interaction for drug substances", Jonas Schlauersbach, Josef Kehrein, Simon Hanio, Bruno Galli, Cornelius Harlacher, Christopher Heidenreich, Bettina Lenz, Christoph Sotriffer, Lorenz Meinel; *Mol. Pharmaceutics* (2022), 19 (8), 2868-2876

Autor 1 (JS), Autor 2 (JK), Autor 3 (SH), Autor 4 (BG), Autor 5 (CH), Autor 6 (CH), Autorin 7 (BL), Autor 8 (CS), Autor 9 (LM)										
Autor	**A1**	**A2**	**A3**	**A4**	**A5**	**A6**	**A7**	**A8**	**A9**	**∑ in Prozent**
^{1}H nuclear magnetic resonance (NMR) spectroscopy	20%		2%			5%	2%			29%
Drug classification	5%									5%
Model Generation		20%								20%
BCS/Solubility literature research	5%									5%
Publication writing	11%	8%							9%	28%
Coordination and supervision			0.25%	0.25%	0.25%	0.25%		2%	10%	13%
Summe	41%	28%	2.25%	0.25%	0.25%	5.25%	2%	2%	19%	100%

Documentation of authorship

Julius-Maximilians-
UNIVERSITÄT
WÜRZBURG

Fakultät für
CHEMIE UND
PHARMAZIE

Erklärung zur Autorenschaft

Chapter II: "Leveraging bile solubilization of poorly water-soluble drugs by rational polymer selection", Jonas Schlauersbach, Simon Hanio, Bettina Lenz, Sahithya P. B. Vemulapalli, Christian Griesinger, Ann-Christin Pöppler, Cornelius Harlacher, Bruno Galli, Lorenz Meinel; *J. Controlled Release* 330 (2021) 36-48

Autor 1 (JS), Autor 2 (SH), Autorin 3 (BL), Autor 4 (SV), Autor 5 (GC), Autorin 6 (ACP), Autor 7 (CH), Autor 8 (BG), Autor 9 (LM)

Autor	**A1**	**A2**	**A3**	**A4**	**A5**	**A6**	**A7**	**A8**	**A9**	**∑ in Prozent**
Dynamic light scattering (DLS)	4%		1%							5%
^{1}H nuclear magnetic resonance (NMR) spectroscopy	8%	8%				2%				18%
^{1}H diffusion-ordered spectroscopy (DOSY)	2%	2%		4%						8%
Flux	8%	17%								25%
HPLC Analysis	3%	2%	1%							6%
Publication writing	10%	3%		1.5%		1.5%			9%	25%
Coordination and supervision				0.5%	2%		1%	1%	8.5%	13%
Summe	35%	32%	2%	6%	2%	3.5%	1%	1%	17.5%	100%

Julius-Maximilians-
UNIVERSITÄT
WÜRZBURG

Fakultät für
CHEMIE UND
PHARMAZIE

Erklärung zur Autorenschaft

Chapter III: "Bile and excipient interactions directing drug pharmacokinetics in rats", Jonas Schlauersbach, Simon Hanio, Martina Raschig, Bettina Lenz, Oliver Scherf-Clavel, Lorenz Meinel, *Eur. J. Pharm. Biopharm.* (2022), 178, 65-68

Autor 1 (JS), Autor 2 (SH), Autorin 3 (MR), Autorin 4 (BL), Autor 5 (OSC), Autor 6 (LM)							
Autor	**A1**	**A2**	**A3**	**A4**	**A5**	**A6**	**∑ in Prozent**
13C Perphenazine synthesis			3%			2%	5%
Buffer preparation	2%			3%			5%
Plasma extraction	15%						15%
LC MS/MS analysis	18%	5%			2%		25%
Pharmacokinetic analysis	3%				7%		10%
Publication writing	13%	2%			2%	10%	27%
Coordination		1%			1%	11%	13%
Summe	51%	8%	3%	3%	12%	23%	100%

Documentation of authorship

Julius-Maximilians-
UNIVERSITÄT
WÜRZBURG

Fakultät für
CHEMIE UND
PHARMAZIE

Erklärung zur Autorenschaft

Chapter IV: “Harnessing bile for drug absorption through rational excipient selection”, Jonas Schlauersbach, Dominic Werthmüller, Bruno Galli, Simon Hanio, Bettina Lenz, Sebastian Endres, Ann-Christin Pöppler, Oliver Scherf-Clavel, Lorenz Meinel, Cornelius Harlacher; (2022) unpublished manuscript

Autor 1 (JS), Autor 2 (DW), Autor 3 (BG), Autor 4 (SH), Autorin 5 (BL), Autor 6 (SE), Autorin 7 (ACP), Autor 8 (OSC), Autor 9 (LM), Autor 10 (CH)											
Autor	**A1**	**A2**	**A3**	**A4**	**A5**	**A6**	**A7**	**A8**	**A9**	**A10**	**∑ in Prozent**
Phase separation, solubility, and dissolution rate	8%			1%							9%
1H nuclear magnetic resonance (NMR) spectroscopy	8%			1%	1%						10%
1H diffusion-ordered spectroscopy and nuclearOverhauser effect spectroscopy (DOSY/NOESY)	3%					3%	2%				8%
Flux (cellulose membranes)	10%			1%	1%						12%
Flux (lipid membranes)		8%									8%
Design in vivo study (Conduction and analysis by Covance, Harrogate)	0.5%	1%							0.5%	6%	8%
Pharmacokinetic analysis	1%							2%			3%
Publication writing	11%	4%						1%	10%	2%	28%
Coordination			1%	0.25%			0.5%	0.25%	9%	3%	14%
Summe	41.5%	13%	1%	3.25%	2%	3%	2.5%	3.25%	19.5%	11%	100%

Julius-Maximilians-
UNIVERSITÄT
WÜRZBURG

Fakultät für
CHEMIE UND
PHARMAZIE

Erklärung zur Autorenschaft

Appendix: “Step by step guide for excipient selection with simulated intestinal fluids”, Jonas Schlauersbach, Simon Hanio, Lena Scheller, Lorenz Meinel; (2022) unpublished manuscript

Autor 1 (JS), Autor 2 (SH), Autorin 3 (LS), Autor 4 (LM)					
Autor	**A1**	**A2**	**A3**	**A4**	**∑ in Prozent**
Literature analysis, interpretation	20%				20%
Publication writing	45%			10%	55%
Coordination		5%	5%	15%	25%
Summe	65%	5%	5%	25%	100%

Erklärung zu den Eigenanteilen des Doktoranden sowie der weiteren Doktoranden als Koautoren an Publikationen und Zweitpublikationsrechten bei einer kumulativen Dissertation.

Für alle in dieser kumulativen Dissertation verwendeten Manuskripte liegen die notwendigen Genehmigungen der Verlage (‚reprint permission') für die Zweitpublikation vor, außer das betreffende Kapitel ist noch gar nicht publiziert. Dieser Umstand wird einerseits durch die genaue Angabe der Literaturstelle der Erstpublikation auf der ersten Seite des betreffenden Kapitels deutlich gemacht oder die bisherige Nichtveröffentlichung durch den Vermerk „unpublished" oder „nicht veröffentlicht" gekennzeichnet.

Die Mitautoren der in dieser kumulativen Dissertation verwendeten Manuskripte sind sowohl über die Nutzung als auch über die oben angegebenen Eigenanteile informiert.

Die Beiträge der Mitautoren an den Publikationen sind in den vorausgehenden Tabellen aufgeführt.

Prof. Dr. Dr. Lorenz Meinel Unterschrift

Jonas Schlauersbach Unterschrift